

**A molecular view of
membrane-related phenomenon:
Unravelling the secrets of G-protein
coupled receptors**

Thesis Submitted to AcSIR For the Award of
the Degree of
DOCTOR OF PHILOSOPHY
In Chemical Sciences



By

Xavier Prasanna

10CC11A26045

Under the guidance of

Dr. Pankaj Poddar and Dr. Durba Sengupta

CSIR - National Chemical Laboratory

Dr. Homi Bhabha Road

Pune - 411008, INDIA

October 2016

Certificate

This is to certify that the work incorporated in this Ph.D thesis entitled “**A molecular view of membrane-related phenomenon: Unravelling the secrets of G-protein coupled receptors**” submitted by Mr. Xavier Prasanna to Academy of Scientific and Innovative Research (AcSIR) in fulfilment of the requirements for the award of the degree of Doctor of Philosophy, embodies original research work carried out under our supervision. We further certify that this work has not been submitted to any other university or institution, in part or full, for the award of any degree or diploma. Research material obtained from other sources has been duly acknowledged in this thesis. Any text, illustration, table, figure *etc* used in the thesis from other sources, have been duly cited and acknowledged.

Place : Pune.....

Date : 3rd April 2017....



Xavier Prasanna
(Research Student)



Dr. Pankaj Poddar
(Supervisor)



Dr. Durba Sengupta
(Co-Supervisor)

Declaration of Authorship

I, Xavier Prasanna, hereby declare that this Ph.D thesis entitled “**A molecular view of membrane-related phenomenon: Unravelling the secrets of G-protein coupled receptors**” was carried out by me for the degree of Doctor of Philosophy in Chemical Sciences under the guidance and supervision of Dr. Durba Sengupta, CSIR-National Chemical Laboratory, Pune, INDIA.

I confirm that:

- this work was done wholly by me while in candidature for a research degree at this institution.
- no part of this thesis has previously been submitted for a degree or any other qualification at this institution or any other institution.
- the interpretations put forth are based on my reading and understanding of the original articles and all sources have been duly acknowledged.

Place :Pune.....

Date : ...3rd April 2017...



.....
Xavier Prasanna

Dedicated to
Margaret Reeta
my mother, my teacher

ಮನೆಯೇ ಮೊದಲ ಪಾಠಶಾಲೆ
ತಾಯಿಯೇ ಮೊದಲ ಗುರು
ನನ್ನ ಅಸ್ಥಿತ್ವ ನೆಲೆಸಿರುವುದು ನಿನ್ನಲ್ಲಿ
ಯಾವ ಎತ್ತರಕ್ಕೆ ನಾ ಬೆಳೆದರು

ತೋರಿದೆ ನೀ ಜ್ಞಾನದ ದಾರಿಯನ್ನು
ಕೈ ಹಿಡಿದು ನಡೆಸಿದೆ ಅದರಡೆ ನೀ ಎನ್ನ
ಕಂಡೆ ಎನ್ನಲಿ ಕಲಿಯುವ ಪ್ರತಿಭೆಯನ್ನು
ರೂಪಿಸಿದೆ ನಿನ್ನ ಶ್ರಮದಿಂದ ಅದನ್ನು

ಪ್ರತಿಯಾಗಿ ಏನನ್ನು ನಿನಗೆ ನಾ ನೀಡಲಿ
ನನ್ನಲಿರುವುದೆಲ್ಲ ನಿನ್ನಿಂದಲೇ, ಬೆರೇನು ಬೇಡಲಿ
ಶಿರಬಾಗಿ ಮಾಡುವೆ ನಿನಗೆ ನಾ ಈ ಅರ್ಪಣೆ
ಸ್ವೀಕರಿಸು, ಅಮ್ಮ, ನನ್ನ ರಚನೆಯ ಸಮರ್ಪಣೆ

Abstract

“There is no greater agony than bearing an untold story inside you.”

– Maya Angelou, *I Know Why the Caged Bird Sings*



-protein coupled receptors (GPCRs) represent a large, diverse family of transmembrane proteins. Their central role in regulating several physiological functions makes them a crucial target for pharmaceutical research. All GPCRs show high degree of structural similarity in their transmembrane segment, which consists of seven α -helices linked alternatively by loops in extracellular and intracellular region. Recent studies suggest that membrane lipids influence the structure, function and higher order organization in GPCRs. However, the molecular basis of the lipid-mediated modulation of GPCR association is not well characterized.

The research carried out in this thesis aims towards examining the molecular details of protein-lipid interaction, and its consequent effect on GPCR association. We have used coarse-grained molecular dynamics simulation as an approach for our investigation. Our work primarily focuses on the role of cholesterol in conjunction with other membrane lipid species in influencing GPCR organization. Two well known GPCR members: β_2 -adrenergic receptor and serotonin_{1A} receptor were chosen for our studies, as cholesterol has been shown to influence their structure, function and organization. Our results highlight the combined contribution of specific and non-specific lipid-mediated effects in modulating organizational conformation of the GPCR associated states. Cholesterol appears to influence the distribution and interaction of other membrane lipids around the receptor. Our results find importance in the context that GPCR oligomerization has implications in functional regulation and a molecular-level understanding of these conformers would be essential for development of effective and target-specific drugs.

Acknowledgments

“Anyone who ever gave you confidence, you owe them a lot.”

– Truman Capote, *Breakfast at Tiffany’s*



When I look back now on the path that I’ve treaded to reach here, I’m not reminded of the success that I cherished or the failures that I regreted. No, I see only memories each unique, each necessary. And it has only been made more special by the people who have walked along with me in this journey towards PhD.

My supervisor, Dr. Durba Sengupta. It was her scientific vision, passion and motivation that encouraged me to leave my comfort zone and pursue my PhD in computational biophysics at CSIR-National Chemical Laboratory (CSIR-NCL), Pune. Being one of the first student in her group, I had the privilege to gain experience in my research work directly from her. I’ve seen our group grow over the years: from its inception to becoming a established, well recognized and active contributor to the scientific community. The credit once again goes to Durba. She always makes it a point to give everyone the freedom to explore their research interest in a way that they feel comfortable with, while constantly providing valuable guidance and support at every step. I would never have made it this far in my scientific career if it wasn’t for her ever supportive nature, patience and trust in me. Thank you Durba. I owe you big time.

I would like to thank Dr. Pankaj Poddar for his immense support and encouragement in ensuring that my research work continued smoothly without any bureaucratic hassle. It is unfortunate that I could not gain much scientific experience from him due to several limitations. Nevertheless, I am privileged to have his constant and unlimited support throughout my research period at NCL. Thank you very much sir.

I would like to thank our collaborator, Prof. Amitabha Chattopadhyay, CSIR-Center for

Cellular and Molecular Biology (CSIR-CCMB), Hyderabad. His passion for research, from scientific and social perspective, has been an great source of inspiration to me. His humble character, friendly approach towards everyone, ever supportive and helpful nature always made me feel comfortable in his presence. Thank you sir for your trust, constant encouragement and guidance. Thank you also for making my visit to CCMB a memorable one every time. I extend my heartiest gratitude to members of Prof. Chattopadhyay's research group who share the same zeal towards science and life at large. Thank you Arunima for entrusting me with your work and constant support at every stage of our collaborative research. I would also like to thank Jafri for his guidance, comments and contribution for the sphingolipid story. Aditya, Sreetama, Sandeep, Suman, Hirak, Bhagyashree, Parijat, Thirupathi Reddy, Ranga Rao and Lakshmi. Thank you all for making me feel at home while at CCMB, for your encouragement and critical review of my research work.

I would like to express my sincere gratitude to members of my Doctoral Advisory Committee (Dr. Sudip Roy, Dr. Neelanjana Sengupta, Dr. Pankaj Doshi, Dr. Kiran Kulkarni and Dr. Rahul Banerjee) for taking time-out to critically review my research work and providing valuable suggestions for improvement. My thanks to course co-ordinators (Dr. Kumar Vanka, Dr. Ajit Kumar, Dr. Sarika Bhattacharyya, Dr. Sudip Roy, Dr. Kavita Joshi, Dr. Ashish Orpe and Dr. Leelavati Narlikar) for having enriched my knowledge in fundamental topics which I found very useful while pursuing my research work.

A very special thanks to KD Deshpande and the IT team at DIRC. Thank you sir for providing workspace for students at DIRC, prompt response to all technical/non-technical needs and ensuring a hassle-free work environment. I would also like to thank Sunny for his prompt and impeccable janitorial services.

Past members of our group: Praveen, Pallavi, Sneha, Chirag, Abhiram, Saket, Shivani, Ganesh and Vikas. Present members: Aiswarya, Aditi, Shalmali and Krushna. My fellow labmates (who share(d) the same labpace): Anju, Vaibhav, Ganesh Nainaru, Sunil, Arvind, Esha, Sanchit, Yogesh, Chinmayi, Monalisa, Pooja, Sanket, Deepthi, Rakhi and Divya. Thank you all for your help, support, counsel and especially for putting up with me. I know it was not easy sometimes, but nevertheless you did it (As if you had any other choice !!!). A special note of thanks to Srini. Thank you for your guidance and support. I got to learn so much from you during your brief stay at NCL. You've set standards in the group which none of us have

achieved yet. Thanks for the goodies that you've manage to get for us every year without fail and during your occasional visits to NCL.

Deepak Pandit: my friend, counsellor and well-wisher. You've been there for me from the beginning of my journey at NCL. Even after you've left it, you continue to help, guide, motivate and reason with me. You have always been a great source of inspiration for me. I don't believe I could have asked for a better friend than you. Thanks for being critical about my judgments and providing your suggestions. Thanks to Anita (Mrs. Deepak Pandit) for extending a warm welcome whenever I visited your home.

I would also like to thank Mr Poman for providing tasty home-cooked dinner every day (no matter how late I turned up at the mess), Mr Amaran and Mr Kakade for providing a roof over my head during my stay in Pune.

A special thanks to all my other friends and well wishers at NCL.

A strong body makes the mind strong. Thanks to all the trainers at Success Fitness Club: Prabhakar, Gopal, Prashanth, Sunil, Aditya and Sagar. Your constant motivation and guidance helped me stay fit and active. It was always a pleasure to work out at the gym with you guys around.

A home away from home. Members of the Loyola chapel community: The Jesuit fathers (Fr. Mario, Fr. Peter, Fr. Altrichter, Fr. Stanley, Fr. Bhaskar, Fr. Mariakumar, Fr. Bert, Fr. Nirdosh, Fr. Sushil, Fr. Robert, Fr. Nelton and Br. Malcolm), Sisters of convent of Mary and Jesus (Sr. Ida, Sr. Clarence, Sr. Columbiere, Sr. Richard, Sr. Florey, Sr. Laila, Late Sr. Lourdes), Sr. Susan, Sr. Teresa, Dorothy, Diana, Sandra, Punyakumar, Nalini, Gerald, Sheila, Anto, Christiano, Balaswamy, Merlyn, Oliver, Sarah, James, Joe, Brigida, Stella and Jimmy. Thank you all for giving me a new family and accepting me as one of your own.

A special thanks to my unofficial local guardian, Mrs. Ruby Patel. Thanks for always being there for me, for the wonderful discussions that we had, for your views and valuable suggestions on everything, for ferrying me around Pune, for inviting me over to your home, for helping me out whenever I was in need. My gratitude is the least that I can repay you with for everything that you have done for me.

And finally, I would like to thank my family for being their constant support, encouragement, trust, patience and prayers. I made it through my PhD at last.

List of Publications

“It is our choices. . . that show what we truly are, far more than our abilities.”

– Albus Dumbeldore, *J.K. Rowling’s “Harry Potter and the Chamber of Secrets”*

Articles

- X. Prasanna, Md. Jafurulla, D. Sengupta, A. Chattopadhyay, “The Ganglioside GM1 Interacts with the Serotonin_{1A} Receptor via the Sphingolipid Binding Domain”, *Biochim. Biophys. Acta*(2016), 1858, 2818-2826.
- *A. Chaudhuri, X. Prasanna, P. Agiru, H. Chakraborty, A. Rydström, J. C.S. Ho, C. Svanborg, D. Sengupta and A. Chattopadhyay, “Protein-dependent Membrane Interaction of a Partially Disordered Protein Complex with Oleic Acid: Implications in Cancer Lipidomics”, *Sci. Rep (In Press)*.
- X. Prasanna, D. Sengupta and A. Chattopadhyay, “Cholesterol-dependent Conformational Plasticity in GPCR dimers”, *Sci. Rep.*(2016), 6, 31858.
- *S. M. Patra, S. Chakraborty, G. Shahane, X. Prasanna, D. Sengupta, P. K. Maiti and A. Chattopadhyay, “Differential Dynamics of the Serotonin_{1A} Receptor in Membrane Bilayers of Varying Cholesterol Content Revealed by All Atom Molecular Dynamics Simulation”, *Mol. Membr. Biol.*(2015), 32, 127-137.
- X. Prasanna, A. Chattopadhyay and D. Sengupta, “Role of Lipid-mediated Effects in β_2 -Adrenergic Receptor Dimerization”, *Adv.Exp.Med.Biol.*(2015), 842, 247-261.
- X. Prasanna, A. Chattopadhyay and D. Sengupta, “Cholesterol Modulates the Dimer Interface of the β_2 -Adrenergic Receptor via Cholesterol Occupancy Sites”, *Biophys. J.*(2014), 106, 1290-1300.

- *X. Prasanna, P.J. Praveen and D. Sengupta, “Sequence Dependent Lipid-mediated Effects Modulate the Dimerization of ErbB2 and its Associative Mutants”, *Phys.Chem.Chem.Phys.* (2013), 15, 19031-19041.

Reviews

- A. B. Pawar, X. Prasanna and D. Sengupta, “Effect of Lipid Bilayer Composition on Membrane Protein Association”, *Advances in Planar Lipid Bilayers and Liposomes*(2015), 22, 43-63.
- *D. Sengupta, G. A. Kumar, X. Prasanna, and A. Chattopadhyay, “Experimental and Computational Approaches to Study Membranes and Lipid-protein Interactions” in *Computational Biophysics of Membrane Proteins* (Domene, C., Ed.), Royal Society of Chemistry, London (in press).

* These publications have not been included in the thesis

Contents

Abstract	i
Acknowledgments	iii
List of Publications	vii
1 Introduction	1
1.1 Cell membrane: Structure and composition	1
1.2 Membrane proteins	6
1.3 Lipid protein interaction	7
1.4 GPCRs: Structure, classification and function	8
1.5 Rhodopsin-like GPCRs	10
1.5.1 β_2 -adrenergic receptor	11
1.5.2 Serotonin _{1A} receptor	12
1.6 Higher order organization of GPCRs	12
1.6.1 Evidences for GPCR oligomerization	14
1.6.2 Interaction pattern observed in GPCR association	18
1.7 Factors regulating GPCR organization	24
1.8 Functional significance of GPCR oligomerization	24
1.9 “Molecular insights” into GPCR oligomerization	27
2 Methodology	31
2.1 Force field	32
2.1.1 Properties of a force field	34
2.2 Statistical mechanics	34

2.3	Molecular dynamics	36
2.3.1	Practical aspects of simulation	37
2.3.2	Steps involved in molecular dynamics simulation	45
2.4	Coarse-graining : The MARTINI model	46
2.4.1	Mapping scheme	47
2.4.2	Non-bonded interactions	48
2.4.3	Bonded interactions	51
2.4.4	Scaling factor for kinetic processes	52
2.4.5	Validation for MARTINI coarse-grained model	52
2.4.6	MARTINI based applications	53
2.4.7	Limitations of MARTINI coarse-grained model	53
3	Cholesterol Modulates Dimer Interface in β_2-AR	55
3.1	Introduction	55
3.2	Materials and methods	57
3.2.1	System setup	57
3.2.2	Simulation parameters	58
3.2.3	Analysis	59
3.3	Results	59
3.3.1	The β_2 -adrenergic receptor dimerizes in the membrane bilayer	59
3.3.2	Dimer interface of the β_2 -adrenergic receptor in the POPC bilayer	61
3.3.3	Cholesterol modulates helices involved at the dimer interface	62
3.3.4	Cholesterol occupancy at transmembrane helix IV restricts its involvement in the dimer interface	64
3.3.5	Cholesterol occupancy site at transmembrane helix IV	67
3.3.6	POPC binding site at the dimer interface	68
3.4	Discussion	69
3.4.1	Exploring the energy landscape by unbiased simulations	70
3.4.2	The dimer interface and comparison with experimental data	71
3.4.3	Structural plasticity of the dimeric interface	71
3.4.4	Cholesterol occupancy sites	73
3.4.5	Functional significance of cholesterol-mediated dimer interfaces	74

4	Role of Lipid-Mediated Effects in β_2-AR Dimerization	77
4.1	Introduction	77
4.2	Methods	78
4.2.1	System setup	78
4.2.2	Simulation parameters	79
4.2.3	Analysis	79
4.3	Results	80
4.3.1	Indirect effects: Hydrophobic mismatch around the receptor	80
4.3.2	Direct effects: Specific protein-lipid interactions	83
4.3.3	Characterization of the lipid site at helix I	85
4.3.4	Exploring the energetics of association	86
4.4	Discussion	87
5	Cholesterol-dependent Conformational Plasticity in GPCR Dimers	91
5.1	Introduction	91
5.2	Methods	93
5.2.1	System setup	93
5.2.2	Simulation parameters	94
5.2.3	Analysis	95
5.3	Results	97
5.3.1	Receptor association is dependent on cholesterol concentration	97
5.3.2	Cholesterol increases plasticity of dimer conformers	98
5.3.3	Cholesterol modulates the receptor dimer interface	100
5.3.4	Unfavorable dimer interfaces dissociate at ns to μ s time scale	102
5.3.5	Cholesterol modulates receptor dimerization through direct and indirect effects	104
5.3.6	Nonannular cholesterol contributes to dimer flexibility and plasticity	107
5.4	Discussion	110
6	Cholesterol Regulates Serotonin_{1A} Receptor Oligomerization	113
6.1	Introduction	113
6.2	Methods	115

6.2.1	System setup	115
6.2.2	Simulation parameters	116
6.2.3	Analysis	117
6.3	Results	117
6.3.1	Cholesterol inhibits higher order oligomerization in serotonin _{1A} receptor	118
6.3.2	Cholesterol modulates contact interface between receptors	119
6.3.3	Different contact interfaces are sampled during transient association between receptors	121
6.3.4	Cholesterol occupancy around transmembrane helices correlates with its involvement at contact interface	123
6.3.5	Protein-lipid interaction energetics regulates serotonin _{1A} receptor oligomerization	124
6.4	Discussion	125
7	GM1 Ganglioside Interacts with Serotonin_{1A} Receptor	131
7.1	Introduction	131
7.2	Methods	133
7.2.1	System setup	133
7.2.2	Simulation parameters	134
7.2.3	Analysis	134
7.3	Results	136
7.3.1	GM1 clusters interact with the serotonin _{1A} receptor	136
7.3.2	GM1 interacts with the extracellular loop 1 of the serotonin _{1A} receptor	138
7.3.3	Characterizing the sphingolipid binding domain at the extracellular loop	1140
7.3.4	GM1 stabilizes a ‘flip-out’ conformation of extracellular loop 1	143
7.3.5	Identifying the effect of serotonin _{1A} receptor on GM1 clusters	144
7.4	Discussion	146
8	Conclusion	153
8.1	Cholesterol regulates GPCR association	154
8.2	Membrane lipids show multiple binding sites around GPCR surface	154
8.3	Cholesterol modulates contact interface during GPCR association	156

8.4	Implications for GPCR oligomerization	156
8.4.1	Functional regulation	156
8.4.2	Drug research	158

List of Figures

1.1	Eukaryotic cell membrane	3
1.2	Common membrane lipid population	4
1.3	Protein-lipid interactions	7
1.4	GPCR crystal structure	9
1.5	GPCR signaling mechanism	10
1.6	GPCR heterodimerization	13
1.7	Experimental evidences for GPCR association	14
1.8	Functional significance of GPCR association	25
2.1	Force field	33
2.2	Molecular dynamics	36
2.3	MARTINI coarse-grained mapping	48
3.1	β_2 -adrenergic receptor: Initial system setup	58
3.2	Time vs distance plot between β_2 -adrenergic receptors	60
3.3	β_2 -adrenergic receptor dimer conformations at varying cholesterol concentrations	61
3.4	Quantitative estimation of dimer contact interfaces observed between the two β_2 -adrenergic receptor	62
3.5	POPC binds at β_2 -adrenergic receptor dimer interface	63
3.6	Cholesterol binds at β_2 -adrenergic receptor dimer interface	64
3.7	Spatial distribution of cholesterol around β_2 -adrenergic receptor	65
3.8	Cholesterol occupancy around β_2 -adrenergic receptor in monomer and dimer regime	66
3.9	Cholesterol binding sites on transmembrane helix IV of β_2 -adrenergic receptor .	68

3.10	POPC binding sites at dimer interface of β_2 -adrenergic receptor	69
3.11	Comparison of dimer interfaces of β_1 -adrenergic receptor and β_2 -adrenergic receptor	72
3.12	Quantitative estimation of dimer contact interfaces observed between the two β_2 -adrenergic receptors during an extended period of simulation.	73
4.1	Bilayer thickness profile around β_2 -adrenergic receptor	81
4.2	Spatial distribution of POPC around β_2 -adrenergic receptor	84
4.3	Maximum occupancy of POPC around β_2 -adrenergic receptor	85
4.4	β_2 -adrenergic receptor: POPC binding site	86
4.5	β_2 -adrenergic receptor system: Interaction energetics	87
5.1	Serotonin _{1A} receptor : Initial system setup for dimer simulation	93
5.2	Characterization of serotonin _{1A} receptor orientations of in the dimeric state . .	95
5.3	Serotonin _{1A} receptor dimerization	98
5.4	Relative orientations of serotonin _{1A} receptors in the dimer state	99
5.5	Favorable contact interfaces in serotonin _{1A} receptor dimer	101
5.6	Characterizing the unfavorable dimer interfaces during serotonin _{1A} receptor dimerization	103
5.7	Direct and indirect cholesterol effects during serotonin _{1A} receptor dimerization	105
5.8	Maximum cholesterol occupancy around serotonin _{1A} receptor in monomer regime	106
5.9	Maximum cholesterol occupancy around serotonin _{1A} receptor in dimer regime .	107
5.10	Cholesterol occupancy and its correlation to dimer interface: cholesterol as a molecular lubricant	108
5.11	Maximum POPC occupancy around serotonin _{1A} receptor in monomer regime .	109
6.1	Serotonin _{1A} receptor : Initial system setup for oligomer simulation	116
6.2	Serotonin _{1A} receptor oligomerization	119
6.3	Serotonin _{1A} receptor oligomer population	120
6.4	Contact interfaces between serotonin _{1A} receptors in oligomeric state	121
6.5	Contact interfaces between serotonin _{1A} receptors during transient association .	122
6.6	Correlation between cholesterol occupancy around transmembrane helix and its involvement at contact interface	123

6.7	Serotonin _{1A} receptor : Interaction energetics	125
6.8	Increased oligomerization of serotonin _{1A} receptors after removing cholesterol . .	127
7.1	Interaction of GM1 with the serotonin _{1A} receptor	137
7.2	Time course showing evolution of interaction between GM1 and serotonin _{1A} receptor	138
7.3	GM1 occupancy around the serotonin _{1A} receptor	139
7.4	Interaction sites of GM1 on the extracellular loop 1 of serotonin _{1A} receptor . .	141
7.5	Schematic representation of serotonin _{1A} receptor interaction with GM1	142
7.6	Interaction of W102 in extracellular loop 1 of serotonin _{1A} receptor with GM1 .	143
7.7	Radial distribution of lipids around serotonin _{1A} receptor	145
7.8	GM1 occupancy around each amino acid residue of the serotonin _{1A} receptor in the dimer conformation	149
8.1	Hypothesis for functional regulation by GPCR oligomerization	158

List of Tables

2.1	Chemical building blocks for coarse-grained particles	49
2.2	MARTINI coarse-grained interaction matrix	51
3.1	β_2 -adrenergic receptor dimerization: Initial system setup, composition and simulation details	57
3.2	Ballesteros Weinstein (B-W) numbering of transmembrane helices in β_2 -adrenergic receptor	69
4.1	Length of hydrophobic segment of transmembrane helices in β_2 -adrenergic receptor	82
5.1	Serotonin _{1A} receptor simulations: Initial system setup, composition and simulation details	94
5.2	Transient associations during serotonin _{1A} receptor dimerization	102
6.1	Serotonin _{1A} receptor oligomer simulations: Initial system setup, composition and simulation details	115
6.2	Relative population of cluster sizes of serotonin _{1A} receptor observed at different cholesterol concentrations	118
7.1	Serotonin _{1A} receptor - GM1 interaction : Initial system composition	133
7.2	Preferential partitioning of membrane components in POPC/Chol/GM1 bilayer	144
7.3	Cholesterol “flip-flop” rates	146

Introduction

“Begin at the beginning,” the King said, gravely, “and go on till you come to an end; then stop.”

– Lewis Carroll, *Alice in Wonderland*



G-protein coupled receptors (GPCRs) are a special class of transmembrane proteins involved in signal transduction¹. This superfamily consists of several members which respond to an equally diverse group of ligands that serve as primary signals for physiological functions²⁻⁴. Since its discovery in early 1970s, biophysical, pharmacological, biochemical, structural and computational studies have provided valuable information about structure, function and organization of GPCRs^{5,6}. These properties of GPCR appear to be regulated by membrane lipids surrounding the receptor⁷⁻¹². In order to characterize the nature of lipid-receptor interaction(s) involved in regulating GPCR properties, it is essential to have a comprehensive understanding of the receptor and its membrane environment. This chapter begins by providing a detailed physicochemical description of cell membrane and GPCRs, followed by a review of studies over the past three decades characterizing higher order organization of GPCRs.

1.1 Cell membrane: Structure and composition

Cell membrane forms the frontier between the cell and its environment. It is selectively permeable and regulates the transport of molecules in and out of the cell through active and passive processes. It also serves as a site for several metabolic and bioenergetic activities¹³.

In its simplest form, cell membrane is a lipid bilayer measuring $\sim 3.0\text{-}5.0$ nm in thickness¹³. Although the discovery of cell membrane was made in 1855 by Carl Nageli and C Cramer, it was not until the early 20th century that the first prediction of its structure was made. The plasma membrane was suggested to be a two-layered lipid sheet surrounding the cell¹⁴. A major breakthrough occurred with the proposal of “fluid mosaic” model based on thermodynamic organization of lipids and proteins, and evidence of asymmetry and lateral mobility within the membrane matrix¹⁵. This model stated that:

- biological membranes are composed of a mosaic structure of alternating globular proteins and phospholipid bilayer.
- phospholipids are “fluid or dynamic” in nature, although a small fraction of it may specifically interact with the membrane protein.
- proteins integral to the membrane have an amphipathic structure with the ionic and highly polar groups protruding into the aqueous phase and the nonpolar groups buried in the hydrophobic interior of the membrane. They usually span the length of the phospholipid bilayer and are randomly distributed.
- other proteins, called extrinsic or peripheral proteins are transiently associated with the membrane through weak non-covalent interactions.
- carbohydrates are linked to proteins or lipids to form glycoproteins or glycolipids.

Since its prediction, there have been significant improvements made to the “fluid mosaic” membrane model. Wealth of new information on membrane protein structure and function have redefined our understanding of membrane architecture (Fig. 1.1). The classical concept that cell membrane is a “sea of lipids” with integral proteins embedded and freely floating in it has been replaced by idea of ordered lipid patches surrounded by a generally disordered state of lipids^{16,17}. Lipid and/or protein composition of these membrane “microdomains” appear to be distinct than that of the bulk membrane (Fig. 1.1). The ordered “microdomains”, often also termed as “lipid rafts” are rich in saturated phospholipids, sphingolipids and cholesterol¹⁸. Formation of these “microdomains” and their properties (structure, size, composition etc) are suggested to be regulated by a combination of lipid-lipid and lipid-protein interactions^{19–22}.

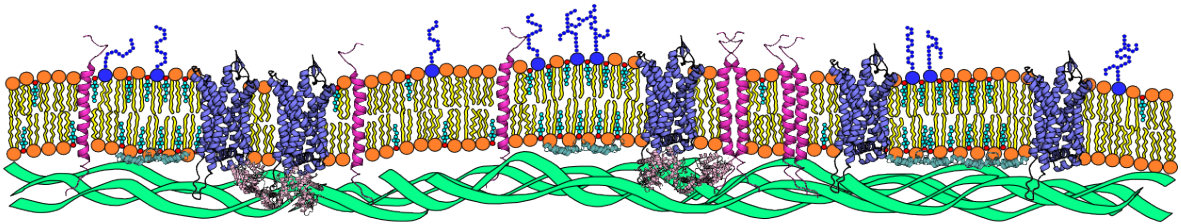


Figure 1.1: A schematic representation highlighting protein and lipid diversity in an eukaryotic cell membrane. Phospholipids are depicted with their head groups in orange and acyl chains in yellow. Glycolipids are shown in deep blue. Cholesterol is shown with its sterol ring, hydrocarbon tail in cyan and hydroxyl head group in red. Single-pass transmembrane proteins, as representative of ErbB family of receptors, are shown in magenta, Multi-pass GPCRs are shown in purple. Peripheral proteins, such as G-protein and caveolin are shown in pink and light blue respectively. Another complex peripheral protein, actin cytoskeleton, is shown as green lattice beneath the lipid bilayer.

Biophysical properties of these microdomains have been extensively investigated using model systems. Membranes with binary or ternary lipid composition show phase separation of lipids into ordered and disordered domains driven by the differences in miscibility arising from the chemical nature of the lipid species^{23,24}. The planar sterol ring of cholesterol stabilizes the elongated *trans*-conformation of the saturated acyl chain. This results in ordered packing of the lipids along with cholesterol²⁵. The packing order introduced by cholesterol in the ordered domain is intermediate between a solid ordered (gel, S_o) phase and liquid disordered (L_d) phase. Hence it is referred to as liquid ordered (L_o) domain¹⁹. Presence of a double bond stabilizes the *cis*-conformation in the unsaturated acyl chain resulting in a kink that prevents ordered packing of lipids in the L_d domain. The diffusion rates of lipids in the L_o domain is lower than that of bulk lipids constituting the L_d domain¹⁹. Higher order in L_o domain also corresponds to increased bilayer thickness. However the ordered microdomains are yet to be directly visualised *in vivo* and recent reports suggest an important role of cytoskeleton in modulating domain properties^{26–28}.

Cell membrane constitutes a wide range of chemically diverse lipid species. About 5% of the mammalian genome is dedicated towards lipid synthesis²⁹ which clearly highlights the importance of lipid specificity in biological processes. The lipid composition of membrane varies with cell types, physiological conditions and age^{30–33}. Phospholipids form the largest fraction ($\sim 65\%$) of these lipids, followed by cholesterol ($\sim 25\%$), and other lipids such as sphingolipids ($\sim 10\%$), glycolipids ($\sim 2\%$) and so on³⁴.

The general structure of a phospholipid consists of two fatty acyl chains ester-linked to the hydroxyl groups at the *sn-1* and *sn-2* position, and a phosphate group esterified to the remaining hydroxyl group on the glycerol backbone (Fig. 1.2). Variation in the acyl chains linked to the *sn-1* and *sn-2* position and the chemical species ester-linked to the phosphate, gives rise to a large variety of phospholipids³⁵. The major class of phospholipids in mammalian cell membrane include phosphocholine, phosphoethanolamine, phosphoserine, phosphoglycerol, phosphoinositol and phosphatidic acid³⁶. Cholesterol consists of a near planar tetracyclic fused steroid ring and a flexible isooctyl hydrocarbon tail (Fig. 1.2). The presence of 3 β -hydroxyl group at C3 position gives cholesterol an amphiphilic character. The sterol ring packs well with phospholipids and membrane proteins. The polar hydroxyl group lies in proximity to the ester bonds of phospholipids³⁷. Sphingolipids contain a long chain amino-alcohol, sphingosine which forms the lipid backbone (Fig. 1.2). A long chain fatty acid is usually attached to the amine through an amide bond. Phosphate group or carbohydrates are linked to the hydroxyl group through an ester linkage and forms the lipid head group. By varying the fatty acid and the head group substituent, a number of sphingolipids are synthesized in mammalian cells. Sphingomyelin form the largest fraction (\sim 80-85%) of sphingolipids in cell membrane while the remaining population consists mainly of a variety of glycosphingolipids³⁸.

Lipids show asymmetric distribution in the cell membrane. In mammalian cells, the outer monolayer of the membrane is enriched in neutral lipids, mainly phosphatidylcholine and sphingolipids. The inner monolayer, however, has a higher fraction of the neutral lipid phosphatidylethanolamine and negatively charged lipids such as phosphatidylserine and phosphatidylinositol^{29,39,40}. As a consequence, there is unequal charge distribution across the two leaflets, with the outer leaflet having a net neutral charge while the inner leaflet is more negatively charged. Phospholipid composition across the two leaflets are maintained by dedicated class of proteins called “flippases”^{29,41,42}. Several studies also show that cholesterol is unequally distributed between the two leaflets, but the leaflet that hosts the larger cholesterol population is still largely debated. Increased cholesterol concentration has been observed in the lower leaflet of mouse synaptic plasma membrane, fibroblasts, human erythrocytes and plasma membrane of Chinese hamster ovary cell line⁴³. Cholesterol concentration in the outer leaflet has been shown to vary from as little as 13% in mouse synaptic membranes⁴⁴ to as much as

67% in human erythrocytes⁴⁵. Cholesterol is known to have strong interactions with sphingolipids which are exclusively localized to the upper leaflet⁴⁶. This could possibly lead to an underestimation of its content in the upper leaflet. Recent studies using molecular dynamics simulation suggest preferential localization of cholesterol in the lower leaflet⁴⁷ or equal distribution between the two leaflets⁴⁸. Cholesterol asymmetry is dynamic and altered by several factors such as chronic ethanol consumption, statins, aging and apolipoprotein E⁴³.

1.2 Membrane proteins

Besides lipids, the cell membrane hosts a wide range of proteins. These are broadly classified as peripheral proteins and integral proteins based on membrane association (Fig. 1.1)¹³. Peripheral proteins are usually bound to surface of the membrane through weak electrostatic interactions and can be easily extracted using salt solutions⁴⁹. Most notable among these are the ones located on the cytosolic side of the membrane where they oligomerize to form the membrane “cytoskeleton”. They provide structural rigidity to the membrane and also serve as anchor for integral proteins⁴⁹. Other peripheral proteins such as enzymes, signal transduction factors *etc* exhibit functional roles⁴⁹. Integral membrane proteins are embedded into the lipid bilayer and have domains that protrude from the extracellular and/or intracellular side of the membrane³⁵. Genome-sequencing suggests that integral proteins account for $\sim 20\text{-}30\%$ of all encoded proteins⁵⁰.

Transmembrane proteins constitute a large fraction of integral proteins. A typical eukaryotic cell membrane mainly constitutes receptors such as receptor tyrosine kinases (RTKs), GPCRs, channels such as ion and water channels, integrins and a host of other proteins⁵¹. Like lipids, the composition of these proteins is dependent on cell type, age and physiological conditions⁵²⁻⁵⁴. Depending upon the number of instances the protein spans the bilayer, they can be classified as single-pass or multi-pass transmembrane proteins³⁵. The segment of transmembrane protein buried in the hydrophobic portion of the lipid bilayer show definite secondary and tertiary structural conformation while the terminal domains may or may not be structured^{13,55}. Membrane environment is highly crowded unlike that stated in “fluid mosaic” membrane model with lipid-to-protein ratio as high as 1⁵⁶. Proteins occupy around 15-35% of total membrane surface area with concentrations of ~ 25000 proteins/ μm^2 ^{57,58}

**Specific Effect :
Direct Contact**

**Non-Specific Effect :
Membrane Perturbations**

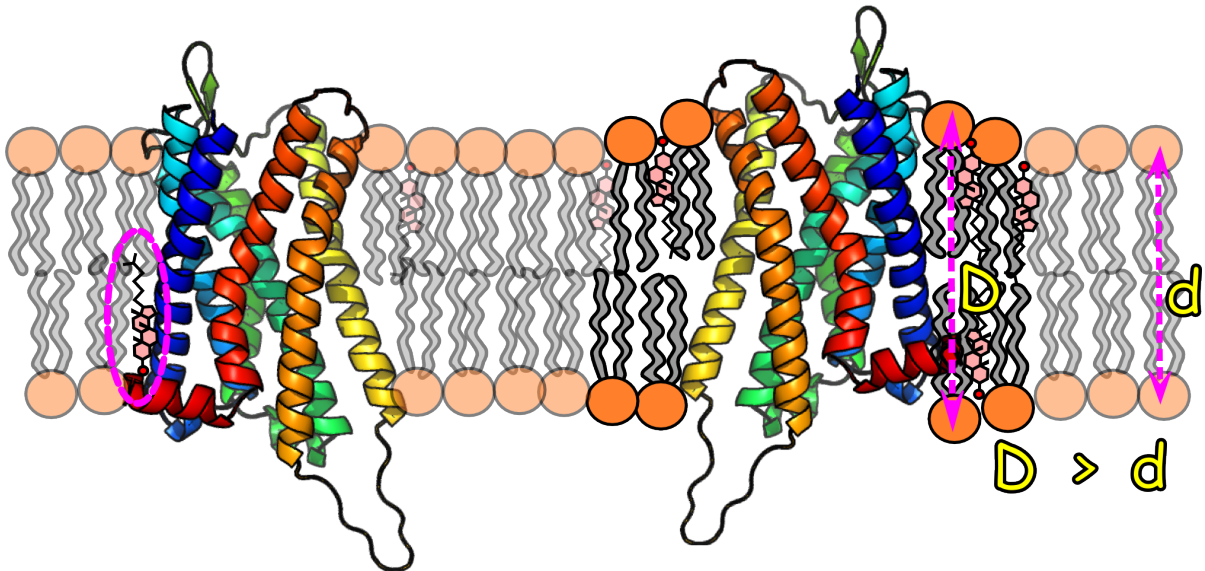


Figure 1.3: A schematic representation showing specific and non-specific interaction between lipids and membrane proteins.

1.3 Lipid protein interaction

Transmembrane proteins are surrounded by shells of lipid molecules. Composition of lipids in these shells are usually different from that of the bulk membrane^{59–63}. It is these lipids that play an important role in influencing structural and functional properties of the membrane protein by either specific and/or non-specific effects (Fig. 1.3)^{62,64–68}. The shell of lipid molecules in the immediate vicinity of the membrane proteins are termed “annular” lipids while those further away from the protein surface are termed “bulk” lipids. The rate of exchange of lipids between annular shell and bulk phase is an order of magnitude slower than the exchange observed in bulk phase arising from lateral translational motion of lipids⁶⁹. Certain sites on the receptor surface, usually deep clefts formed at intrahelical or interhelical sites, serve as specific lipid binding sites. Lipids occupying these sites are termed as “non-annular” lipids. These lipids are not easily accessible to annular or bulk lipids and therefore have lower exchange rate^{69,70}. Some transmembrane proteins also exhibit conserved amino acid sequence in their hydrophobic domain which act as binding sites for specific lipids^{71–74}.

When the length of the hydrophobic segment of the protein differs from the hydrophobic bilayer thickness, it is referred as “hydrophobic mismatch”. Several mechanisms are possible to relieve the energetic constraints resulting from the hydrophobic mismatch⁷⁵. When the hydrophobic segment of the protein is larger than that can be accommodated by the hydrocarbon chains of the lipid bilayer (positive mismatch), the proteins oligomerize to reduce the overall exposed hydrophobic surface area. Alternatively, the transmembrane helices might tilt or even lie embedded inside the bilayer to minimize hydrophobic exposure to water. In addition, the hydrocarbon chains of annular lipids would extend out to match with the hydrophobic segment of the protein, resulting in local membrane thickening. When the hydrophobic segment of the protein is smaller than that of the lipid bilayer, the proteins are suggested to oligomerize to minimize overall line tension or adopt surface localization. Hydrophobic chains of the annular lipids, in this case, would constrict by disordering, to minimize their exposure, resulting in local membrane thinning. Another possible mechanism involves lateral lipid reorganization to ensure lipids with the right hydrophobic thickness are matched with the hydrophobic segment of the transmembrane protein⁷⁵.

1.4 G-protein coupled receptors: Structure, classification and function

GPCRs are the largest and most diverse class of transmembrane proteins in eukaryotes. Around 800 GPCRs have been identified in the human genome¹. Several classification systems have been employed to categorize GPCRs. One of the popular systems categorizes GPCRs into 6 classes: class A (rhodopsin-like), class B (secretin receptor family), class C (metabotropic glutamate), class D (fungal mating pheromone receptors), class E (cyclic AMP receptors) and class F (frizzled/smoothened)^{76,77}. A more recent classification system called GRAFS uses phylogenetic analysis to cluster GPCRs into 5 families: Glutamate (15 members), Rhodopsin (701 members), Adhesion (24 members), Frizzled/taste (24 members) and Secretin (15 members)⁷⁸. A large number of GPCRs are yet to be classified as their physiological function remains unknown. All GPCRs have similar structural feature: a conserved domain consisting of 7 right-handed α helices embedded in the membrane and interconnected by alternating extracellular and intracellular loops (Fig. 1.4)¹. The size and structure of the loops show

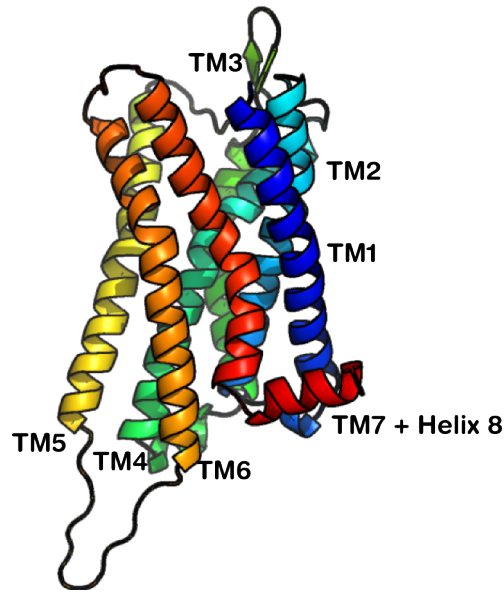


Figure 1.4: A cartoon representation of the crystal structure of GPCR. Each of the transmembrane helices are labelled and shown in different colours

considerable variation among different GPCR members⁷⁹. The N-terminal segment is directed extracellularly while the C-terminus lies intracellularly. GPCRs are primarily involved in signal transduction across the membrane and respond to a wide variety of ligands⁸⁰. They play a central role in regulating several physiological processes⁸¹.

Even in the absence of ligand, there exists an equilibrium between active and inactive conformations of the receptor. As a result, the receptor shows basal activity. Binding of the ligand stabilizes the active state. Based on the effect of ligand binding on the conformation of the receptor and its subsequent functional properties, ligands may be classified as agonists (complete receptor activation), partial agonists (reduced receptor activation), inverse agonists (inhibit basal activity) and antagonists (block binding of other ligands, basal activity unaffected). In its active state, the receptor brings about conformational changes in the G-protein coupled to it at its cytoplasmic domain. G-protein is heterotrimeric and composed of G_{α} , G_{β} and G_{γ} subunits. G_{α} subunit dissociates from the activated G-protein by exchanging its bound GDP for GTP and initiates downstream signaling (Fig. 1.5).

Depending on the type of G_{α} subunit involved, it can (a) activate adenylyl cyclase ($G_{\alpha s}$) and increase levels of cyclic AMP (cAMP) (b) inhibit adenylyl cyclase activity ($G_{\alpha i}$) and decrease cAMP levels (c) activate phospholipase C ($G_{\alpha q}$) which cleaves phosphatidylinositol to

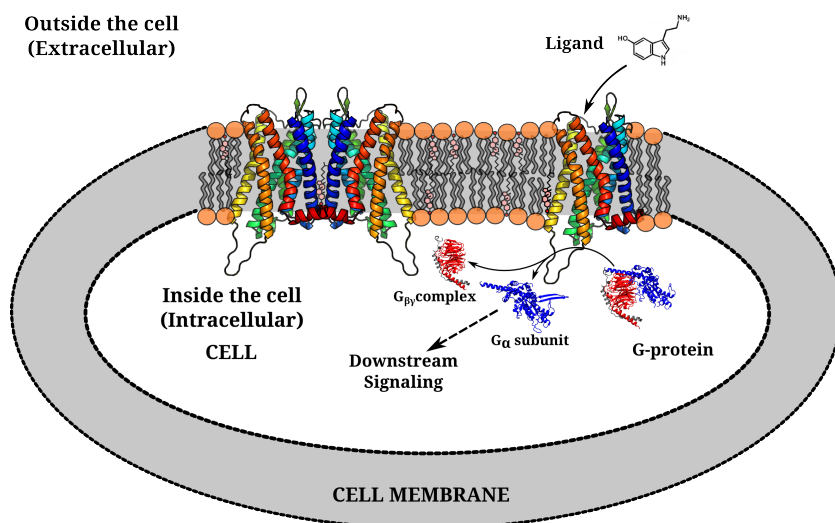


Figure 1.5: A schematic representation showing GPCR signaling mechanism. When GPCR is activated, following ligand binding, it undergoes conformational change which is relayed to the G-protein bound at the cytoplasmic end of the receptor. The heterotrimeric G-protein undergoes conformational change, exchanges GDP for GTP, and dissociates to give G_{α} and $G_{\beta\gamma}$ subunits. The G_{α} subunit initiates primary downstream signaling which culminates as physiological response.

diacylglycerol and inositol triphosphate (d) initiate other downstream signaling molecules along with $G_{\beta\gamma}$ subunit ($G_{\alpha12}$, $G_{\alpha13}$ etc)^{82,83}. GPCR internalization mediated by arrestin binding regulates signaling⁸⁴. The pivotal role of GPCRs in regulating several physiological processes makes them a central focus in drug research. In fact $\sim 50\%$ of all clinically marketed drugs invariably target GPCRs^{85,86}.

1.5 Rhodopsin-like GPCRs: β_2 -adrenergic and serotonin_{1A} receptors

Rhodopsin is the first GPCR whose three-dimensional structure was resolved^{87,88}. Remarkable advancements in our understanding of GPCR field, particularly structure, activation and organization have been achieved from studying rhodopsin with molecular insights provided from its crystal structure⁸⁹⁻⁹². It has often been used as structural template in molecular modeling and drug designing for diseases related to GPCR signaling pathways⁹³⁻⁹⁵. Rhodopsin represents a special case among GPCRs in that it has a covalently bound chromophore ligand, 11-*cis*-retinal which undergoes photoisomerization to an all-trans state, upon absorbing photons accompanied

by conformational change in the receptor from its inactive to its active conformation (Meta II). In this state, rhodopsin recruits and binds G-protein resulting in a downstream signaling cascade that ultimately culminates in an electrical impulse to the visual cortex of the brain. Soon after activation, chromophore reverts back to its cis-conformation to regenerate fresh rhodopsin⁹⁰. Another feature that sets apart this GPCR from other members of its family is its expression at very high density in the rod outer segment of retinal rod cells. A large fraction of the disk membrane area is occupied by rhodopsin, while the remaining space is occupied by phospholipids and cholesterol^{96,97}. These features discourage rhodopsin to be considered as an ideal candidate to study properties of the general GPCR species.

Several rhodopsin-like GPCRs play a central role in regulating essential physiological processes⁷⁹. Of these, two members are well known for their interaction with membrane lipids, particularly cholesterol, and its influence on receptor structure, function and organization.

1.5.1 β_2 -adrenergic receptor

In the last decade, with advancements in membrane receptor crystallization techniques, structures of several GPCRs have been resolved at high resolution⁷⁹. One such receptor that has gained particular interest in GPCR community is β_2 -adrenergic receptor. This receptor is mainly expressed in smooth muscle tissues and serve as important targets for diseases such as asthma, hypertension and cardiac failure^{98,99}. It was the first GPCR to be cloned for invitro expression¹⁰⁰ and, following rhodopsin, was the second GPCR whose structure had been elucidated¹⁰¹. Another interesting feature of the β_2 -adrenergic crystal structure is the resolution of bound cholesterol¹⁰². Binding sites for these cholesterol molecules around the receptor appears to be physiologically relevant and not experimental artifacts arising during crystallization⁷⁴. Furthermore, specific interaction between receptor and cholesterol finds significance in the context that cholesterol is reported to be essential for structural stability and regulates function of β_2 -adrenergic receptor^{74,103–105}. In vitro studies have shown that β_2 -adrenergic receptor preferentially sequesters to cholesterol-rich domains and partitions out upon stimulation^{106–108}. These domains are also enriched in G-proteins, the first downstream signaling molecule that makes direct contact with the receptor¹⁰⁹. Till date, it is the only GPCR for which a crystal structure of its agonist-occupied monomeric active state in complex with nucleotide-free G_s heterotrimer is available¹¹⁰. Structural insights from this complex has been instrumental in

identifying molecular signatures in GPCRs associated with receptor activation and G-protein coupling¹¹¹. Although the receptor is known to retain its function when reconstituted invitro in its monomeric form¹¹², it does not rule out the possibility of forming higher order clusters which could have regulatory influence on receptor function¹¹³. β_2 -adrenergic receptor is reported to exist as dimers and possibly higher order oligomers in cell membranes under normal physiological conditions¹¹⁴⁻¹¹⁶.

1.5.2 Serotonin_{1A} receptor

Serotonin_{1A} receptor is an important member of the serotonergic receptor family. It is expressed mainly in the central nervous system and has been well characterized due to the availability of a selective ligand 8-OH-DPAT (8-hydroxy-2-(di-N-propylamino)tetralin)¹¹⁷. It plays a central role in neuronal development and is involved in regulation and modulation of various cognitive and behavioural responses¹¹⁷. The plasma membrane of brain cells are highly enriched in cholesterol¹¹⁸. Cholesterol has been reported to be essential for structural stability and function of the receptor¹¹⁹⁻¹²¹. Serotonin_{1A} receptor is the first member of GPCR superfamily for which a definitive role of cholesterol in modulating higher order oligomerization has been well established^{122,123}. Although there are no high resolution structure available for serotonin_{1A} receptor yet, sequence alignment indicates $\sim 48\%$ homology with a related member of adrenergic family, β_2 adrenergic receptor¹²⁴. Homology model of serotonin_{1A} receptor built from the β_2 adrenergic receptor crystal structure as template has been instrumental in understanding membrane lipid-receptor interaction and its role in modulating higher order receptor organization¹²⁴⁻¹²⁶. Interaction of cholesterol with serotonin_{1A} receptor is suggested to be highly specific¹²⁷.

1.6 Higher order organization of GPCRs

Association of membrane proteins to confer functional role appears to be a common feature among transmembrane proteins¹²⁸. The idea that GPCRs function and exist only as monomers, however, has been prevalent for several decades although there are no concrete evidence to support this claim. This understanding possibly arose from the observation that GPCRs are expressed by a single gene and the polypeptide generated has the necessary pharmacology and

capacity to carry out function¹²⁹. The presence of higher order species is well known among class C GPCRs. Furthermore, heterodimerization between closely related members of class C GPCRs is shown to be necessary for receptor function (Fig. 1.6)^{130–133}.

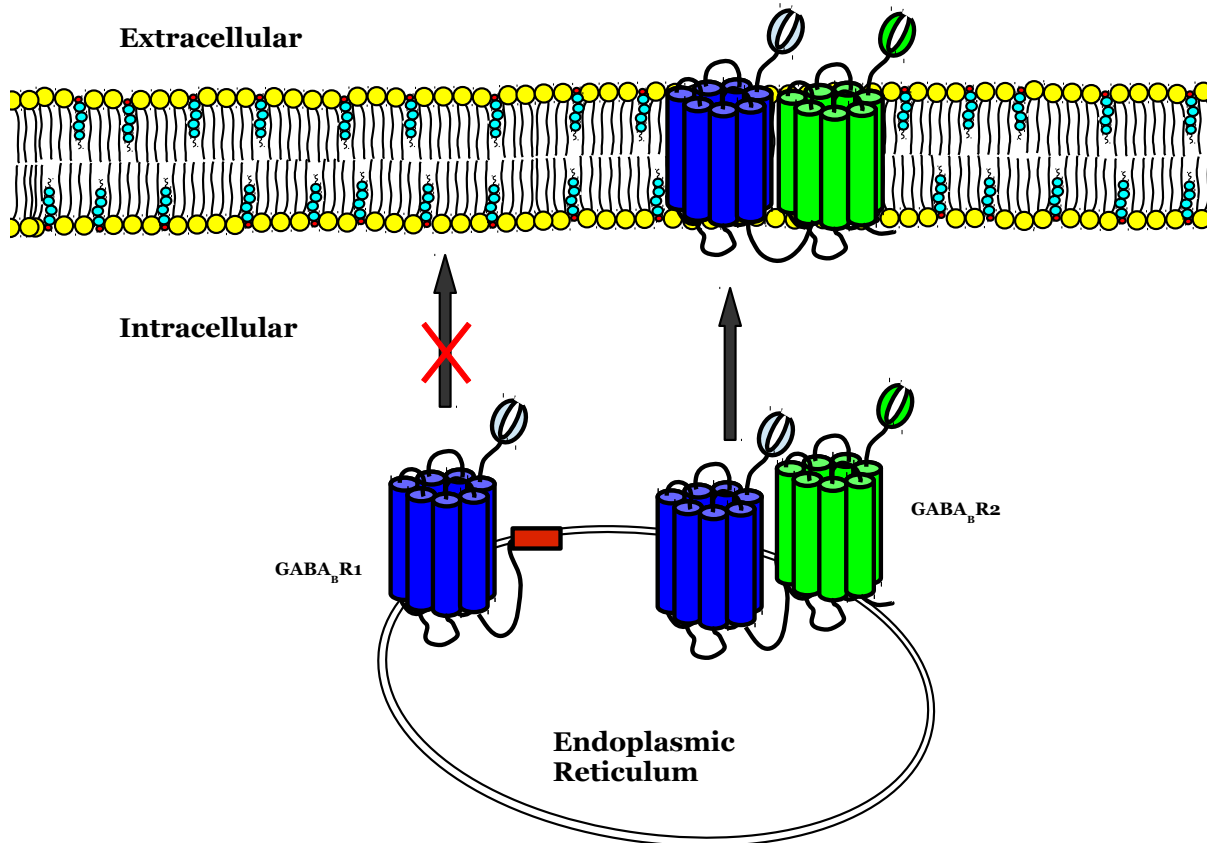


Figure 1.6: Heterodimeric association between $GABA_B$ receptors. Endoplasmic retention sequence in $GABA_B R1$ (shown as red bar) prevents its trafficking to cell surface. Binding of $GABA_B R2$ to $GABA_B R1$ masks the retention sequence resulting in translocation of the heteromeric complex to cell surface.

These findings further foster the notion that such oligomeric species could exist even among GPCR members of other class with possible functional significance¹³⁴. However, class A GPCRs reconstituted as monomers in membrane nanodiscs were reported to remain functional^{112,135,136}. This evidence does not refute the idea that they may exist as higher order oligomers. Indeed, over the last two decades, numerous evidences have provided evidence-beyond-doubt for the existence of higher order oligomers among class A GPCRs (Fig. 1.7)^{116,137–149}.

1.6.1 Evidences for GPCR oligomerization

Pharmacological methods

The first evidence for existence of GPCRs as dimers emerged from pharmacological methods. Binding of radiolabeled agonist to β -adrenergic receptors exhibited Hill plots with slope less than 1. In addition, the dissociation rate of bound radiolabeled agonist was significantly higher in presence of excess concentration of unlabeled agonist suggesting negative cooperativity among receptors¹⁵⁰.

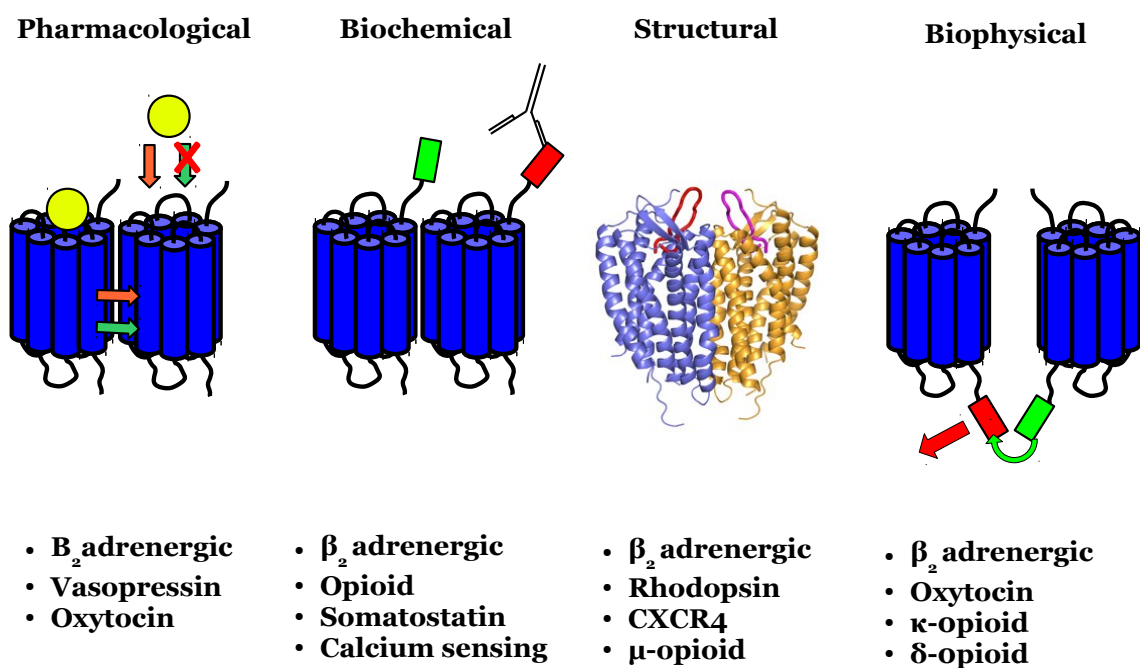


Figure 1.7: A schematic representation highlighting the various experimental techniques employed in studying GPCR oligomerization.

Radiolabeled studies also identified positive cooperativity in binding of ligand to GPCRs such as muscarinic receptors, vasopressin and oxytocin receptors^{151–154}. Such co-operative process can be easily explained on the basis of receptor oligomerization which can modulate

ligand-binding to receptors through cross-talk between the protomers, thereby suggesting that GPCRs probably exist as oligomers at cell surface.

Biochemical techniques

An interesting study involving antibody mediated indirect clustering of Gonadotropin-releasing hormone (GnRH) receptor also provided an indirect indication of GPCR dimerization and function. A peptide antagonist of GnRH when dimerized and bound by a divalent antibody raised against it, surprisingly demonstrated agonist-like activity. This cross-linking experiment suggested that the antibody-bound peptide dimer serves to bring the receptor molecules within physical interacting distance resulting in formation of receptor microaggregate which by itself is functional¹⁵⁵. Another indirect approach predicting higher association was provided by target size analysis of several GPCRs using radiation inactivation technique. This method predicted the molecular weight of β_2 -adrenergic receptor, α_1 adrenergic and gonadotropin-releasing hormone receptors to be much larger than that of a monomer suggesting that the receptors indeed exist and function as multimers^{156,157}.

Additional experimental support for the existence of GPCR dimers was provided by the observation that, even under denaturing conditions, dopamine D3 receptors isolated from brain tissues as well as transfected cells showed immunoreactive bands with molecular weight corresponding to that of dimers or tetramers¹⁵⁸. Co-immunoprecipitation of differential epitope-tagged β_2 -adrenergic receptors by Hebert *et al.*¹⁵⁹ further strengthened the notion of higher-order GPCRs. This approach was subsequently employed to provide evidence for dimers in other GPCRs^{160–163}.

Transcomplementation studies provided a direct function-based evidence for existence of GPCR dimers. Mutant/chimeric muscarinic, adrenergic, angiotensin and calcium sensing receptors, which by themselves were non-functional, exhibited restored activity following co-expression^{164–166}. Functional restoration of these inactive receptors can be explained based on direct interaction or by domain-swapping mechanism, both of which necessitates that the receptors remain associated with each other¹⁶⁷. Although this technique was employed to predict association among other GPCR subtypes, its implication for assessing receptor interaction in case of V2 Vasopressin receptor has been questioned¹⁶⁸. Further mutational studies for analyzing dimer formation was provided by engineering endoplasmic reticulum (ER) retention

sequences within receptors^{169–171}. These modified receptors were shown to form complex with the co-expressed wild type receptor and prevent their trafficking to cell membrane surface. The interaction between GPCR subtypes appears to be specific¹⁶⁹.

Biophysical approach

The ability to monitor receptor clustering in living cells has been possible by energy transfer approaches such as fluorescent resonance energy transfer (FRET) and bioluminescence resonance energy transfer (BRET)¹⁷². The principle underlying both these techniques involves energy transfer from a donor molecule (fluorescent molecule/luciferase enzyme) whose emission spectra overlaps with the excitation spectrum of the acceptor molecule (fluorescent molecule). The two molecules are required to be in very close proximity to each other as the efficiency of energy transfer is inversely proportional to the sixth power of distance between them¹⁷³.

FRET employs fluorescent proteins such as green fluorescent protein (GFP) and its variants such as yellow fluorescent protein (YFP), red fluorescent protein (RFP), cyan fluorescent protein (CFP) etc. which are tagged with GPCRs to produce fusion-proteins. The fluorescent protein combinations are carefully chosen to ensure overlap of emission spectrum¹⁷⁴. FRET was employed to predict GPCR oligomerization for the first time in yeast α -factor receptor. Coexpression of CFP or YFP tagged receptors exhibited energy transfer which was shown to be due to stable association rather than random collision¹⁷⁵. This method was also employed to predict homomeric interactions in gonadotropin releasing hormone receptor, C5a receptor^{176–178} and many other GPCR subtypes^{154,179}. Using fluorophore-conjugated ligands as an alternative to fluorescent protein tags, FRET revealed dimerization of oxytocin receptors in mammary glands of lactating rats¹⁸⁰. Variants of FRET technique such as photobleaching FRET^{181,182} and homogenous time-resolved FRET^{183,184} have also been used to study GPCR homodimerization.

BRET is similar to FRET except that it uses enzyme catalyzing bioluminescent light emission (luciferase enzyme from *Renilla reniformis* or aequorin enzyme from *Aequorea victoria*) as the energy donor and a fluorophore (small molecule or fluorescent protein) as the energy acceptor. This method has been used to investigate homodimerization of β_2 -adrenergic receptors¹¹⁴, melatonin receptors¹⁸⁵, δ and κ opioid receptors^{184,186}, adenosine A_{2A} receptors¹⁸⁷ and calcium-sensing receptors¹⁸⁸ in living cells.

Single molecule fluorescent imaging technique has emerged as a reliable method for direct estimation of GPCR dimerization and characterization of the monomer-dimer equilibrium¹⁴⁴. This method was first employed to study M1 muscarinic receptor¹⁸⁹ and later successfully applied to class A GPCRs. At physiologically expressed levels in transfected cells, N-formyl peptide receptor revealed dynamic equilibrium between monomers and dimers with rapid dissociation of dimers at a comparably fast rate than monomers associating to form dimer. Binding of ligand to the receptor did not appear to affect monomer-dimer equilibrium¹⁹⁰. The propensity to exist as monomers or dimers differs between different GPCRs. β_2 -adrenergic receptor shows greater tendency to form dimers compared to β_1 -adrenergic receptor¹¹⁶. GABA_B receptor appear to be organized as tetramers and higher order oligomers, are largely immobile and organized in rows owing to its interaction with actin cytoskeleton¹¹⁶.

Spatial intensity distribution analysis uses fluorescence intensity histogram obtained from scanning microscopy of cells expressing fluorescent-tagged proteins¹⁹¹. Using this biophysical method, presence of higher-order oligomers has been reported in serotonin_{2C} receptor. Treatment with antagonists/inverse agonists results in dissociation of oligomeric species into monomers predominantly¹⁹². Fluorescence correlation spectroscopy with post acquisition photon counting histogram analysis has also shown presence of preformed dimers in 5-hydroxytryptamine 2C receptor¹⁴⁸, homodimers and heterodimers of luteinizing hormone receptor (LHR) and the follicle stimulating hormone receptor¹⁹³. Super resolution microscopic techniques such as photoactivation localization microscopy (PALM), stimulated emission depletion (STED) and stochastic optical reconstruction microscopy (STORM) have been successful in providing spatial resolutions as small as 10 nm and could be useful in examining GPCR organization in cells^{194–196}.

Structural evidence

Crystal structure of GPCRs also provide substantial evidence suggesting GPCR association. Structural data from bovine rhodopsin shows the molecules to be arranged as dimer in each asymmetric unit^{197,198}. β_2 -adrenergic receptor crystals adopt type I packing with a multilayered arrangement. In each layer, protein molecules form parallel arrays of symmetry-related dimers¹⁰². A parallel, two-fold symmetric arrangement of receptors with significantly large buried surface area at the region of contact is observed in the crystal structures of CXCR4¹⁹⁹

and μ opioid receptor¹⁴⁶. Crystal structure of the dimer of β_1 -adrenergic receptor¹⁴⁷ and metabotropic glutamate receptor 1²⁰⁰ further provides strong evidence to support GPCR association. These structural results suggest that GPCRs exist as dimers.

Direct visual evidence for existence of higher order GPCR oligomers comes from the visual observation of rhodopsin clusters using atomic force microscopy in native retinal tissue^{201,202}. The rhodopsin molecules predominantly appear to be arranged in rows of dimers with a relatively large packing density. However projecting this evidence for suggesting higher order association in GPCRs is questionable since rhodopsin represents a special case where receptors are physiologically overexpressed in native tissue.

1.6.2 Interaction pattern observed in GPCR association

With the concept of dimer formation in GPCR gaining more acceptance, a parallel emphasis is laid on understanding the association pattern between the receptors. Several experimental techniques as well as computational methods have provided critical predictions on the molecular nature of interaction between receptors.

Experimental findings

Peptide inhibition technique

Hebert *et al.*¹⁵⁹ provided an indirect approach towards predicting helices involved in interaction between GPCRs. A peptide corresponding to transmembrane helix VI of β_2 -adrenergic receptor reduced the relative dimer population as determined by immunoprecipitation. Similar studies in Dopamine D2 receptor employing transmembrane helix VI and VII also inhibited dimer formation¹⁶². Interestingly in Dopamine D1 receptor, a synthetic peptide mimicking transmembrane helix VI had no effect on oligomerization but inhibited ligand binding and G-protein activation. This could possibly be mediated by disrupting certain critical intermolecular interactions within the receptor which are necessary to maintain the three-dimensional conformation required for agonist interaction and signal transduction²⁰³.

Another interface which has been shown to be essential for organization and function of several GPCRs is transmembrane helix IV. Homodimerization of CXCR4 receptors, reported both in normal as well as malignant blood lymphocytes, was significantly reduced by a synthetic peptide targeting helix IV²⁰⁴. Residues on the lipid-exposed surface of transmembrane helix

IV was shown to be essential for receptor association and G-protein activation in secretin and calcitonin receptors^{205,206}.

Apart from transmembrane helices, peptide mimicking the loop regions were also shown to disrupt dimer structural organization suggesting their involvement in mediating receptor association²⁰⁷.

Resonance energy transfer methods

Time resolved FRET in combination with co-immunoprecipitation studies using helix fragments in α_{1B} adrenoceptor demonstrated symmetric interaction between transmembrane helices I and IV suggesting that such interactions may support formation of large clusters²⁰⁸.

Förster resonance energy transfer, in combination with other experimental techniques, showed that transmembrane helix V peptide analogues of adenosine A_{2A} receptor have the ability to self-associate and form oligomeric structures in SDS micelles and lipid vesicles. Mutation at M193 position disrupted dimer formation²⁰⁹. Site-directed mutagenesis of residues in transmembrane helix IV of serotonin $_{1A}$ receptor decreased its ability to dimerize in vitro as assessed by photobleaching-Förster resonance energy transfer. These results were further validated by docking studies and molecular dynamic simulations²¹⁰.

Microscopy

Models based on observation of rhodopsin clusters by atomic force microscopy predicted involvement of transmembrane helices IV and V for dimerization. Transmembrane helices I, II and cytoplasmic loop connecting helix V with VI are suggested to be involved in formation of dimer rows.^{91,201,202}

Cysteine cross-linking method

Cross-linking studies, using either endogenous cysteine residues or cysteine mutants engineered into receptor, have been useful in studying the interaction pattern of several GPCR homomers. In Dopamine D2 receptor, mutation of an endogenous cysteine residue at the extracellular end of transmembrane helix IV completely prevented cross-linking suggesting that this residue is involved in forming symmetrical homodimer interface²¹¹. Cross linking studies also identified that transmembrane helix I and cytoplasmic helix VIII are involved in forming symmetric dimer contacts in rhodopsin in native membranes²¹². Cysteine substituted at extracellular ends of transmembrane helix IV and V in δ opioid receptor resulted in cross-linking

between the receptors when treated with oxidizing agents, confirming involvement of these helices in dimer formation²¹³. Single cysteine residue mutations engineered into α -factor receptor (Ste2p) showed that a portion of N-terminal that exhibits β -stranded structure also forms the dimer interface²¹⁴. Single cysteine mutation along with modeling studies characterized the dimer interfaces as transmembrane helix IV, V, intracellular loop 2 and transmembrane helix I - cytoplasmic helix VIII in M₃ muscarinic receptors²¹⁵

Crystal structure data interpretation

A direct structural visualization of possible dimer interfaces and conformational packing of GPCRs has been possible due to recent reports on crystallization of few GPCRs. Crystal structure of the oligomeric turkey β_1 -adrenergic receptor in a ligand-free state shows two dimer interfaces: one interface involves transmembrane helix I, II, C-terminal helix VIII and extracellular loop 1 while the other interface engages residues from transmembrane helices IV, V, intracellular loop 2 and extracellular loop 2¹⁴⁷. Transmembrane helix I - cytoplasmic helix VIII interaction interface between two symmetry-related molecules is observed in crystal structure of β_2 -adrenergic receptor¹⁰². Although these helices are not proposed to be involved in dimerization for this receptor from previous studies¹⁵⁹, interaction between these helices have been reported in rhodopsin²¹⁶. In CXCR4, the crystal structure reveals a parallel, symmetric receptor dimer with transmembrane helices V and VI at the interface when bound to small molecule antagonist IT1t and transmembrane helices III and IV on binding cyclic peptide CVX15¹⁹⁹. This correlates partially with experimental studies that suggest transmembrane helix IV to be essential for homodimerization and function²⁰⁴. The crystal structure of μ -opioid receptor reveals it to be associated in pairs along the crystallographic two-fold axis. The association reveals two different contact regions between receptors: a prominent transmembrane helix V, VI interface and a relatively limited parallel association between transmembrane helix I, II and cytoplasmic helix VIII. A significantly large buried surface area for a single protomer is observed for at the region of contact for both associations suggesting that μ -opioid receptors may exist as dimers or higher-order oligomers¹⁴⁶. Although class C GPCRs are known to form homo- or heterodimers mediated by a large N-terminal extracellular domain, crystal structure of metabotropic glutamate receptor 1 shows close packing of helix I at the dimer interface mediated by cholesterol²⁰⁰.

Computational modeling and simulations

Bioinformatic studies

Evolutionary trace method, a data mining approach to determine significant level of amino acid conservation, predicted functionally important residue clusters on transmembrane helices V and VI for over 700 GPCRs. Similar clusters were also reported on transmembrane helices II and III. These helices are predicted to be involved in dimerization, though it does not distinguish between contact based and domain-swapped dimer. Identification of two different interfaces with probable involvement in dimerization suggests possibility for heterodimerization or higher order oligomerization²¹⁷.

Involvement of transmembrane helices IV, V and VI, with helix IV playing a prominent role, in mediating inter-monomer interactions was deduced from docking model of lutropin homology model²¹⁸. Support vector machine-based method by Nemoto *et al.* predicts interaction pattern for GPCR oligomerization by integrating the structure and sequence information of GPCRs²¹⁹. This method has proved successful in predicting the dimer interface as observed in Glutamate receptor type 1²¹⁹

Molecular dynamics simulations

Analytical methods investigating GPCR structure, function and organization are largely limited by their ability to provide accurate information at lower spatial and temporal resolutions. For example, crystallography and related methods provide only static structural information about the receptors at atomic resolution, with very little insight into the underlying conformational dynamics²²⁰. On the other hand, spectroscopic techniques provide indirect and time-averaged information about the conformational changes sampled by the receptor. In this context, molecular modeling and simulations have emerged as a promising approach to provide a dynamic insight into the key molecular changes associated with the receptor function, especially when paralleled with experiments^{221–223}. With improvements in computational resources and sampling algorithms, it has been possible to examine biophysical processes at longer length and time-scales^{224–228}.

Atomistic simulations

Atomistic molecular dynamics simulation of a semi-empirical rhodopsin dimer model constrained to exhibit transmembrane helices IV and V at interface, were carried out in a dipalmitoyl phosphatidylcholine (DPPC) lipid bilayer for 0.1 μ s. This study showed that transmembrane helix IV remains in close contact with helix V as well as intracellular loop 2 and extracellular loop 2 suggesting that the interface is relatively stable. Although it was a biased simulation, it provided interesting details such as (i) structural changes encountered by the receptor during dimerization, (ii) hydrophobic interactions as main stabilization force in dimers and (iii) role of the second intracellular and extracellular loops in driving dimer formation and stabilization with subtle differences in side chain interactions between subunits resulting in tilts and kink angles²²⁹. Similar interface-biased simulation was also carried out for modeled vasopressin V2 receptor tetramer (1 active and 3 inactive receptors) in POPC lipid membrane for 5 ns. Stability of the active monomer and structural changes in the inactive receptor in close contact with active receptor at transmembrane helix IV/III - transmembrane helix VI/VII interface suggested a possibility of dimerization as a necessity for transactivation of ligand-free receptor in the dimer unit²³⁰.

Brownian dynamics simulation of TSH receptor in a membrane environment exhibited two potential dimer interfaces with two pairs of residues interacting between transmembrane helices II and V, and one pair of residues between transmembrane helices I and IV. Cysteine mutants of these residues showed cross-linking of the receptors indicating close proximity of the predicted helices²³¹. Truncation of helices harbouring the interacting residues but not their point mutation abolished receptor association. This indicates that formation of contact interfaces in TSH receptor is not controlled by single residue but involves cumulative effects of the interfacing residues²³¹.

Coarse-grained simulations

Coarse-grained molecular dynamics simulations offers an advantage over atomistic simulations in that relatively longer timescales can be sampled as it maps groups of atoms into beads thus reducing degrees of freedom²³². This allows sampling of several microseconds which is sufficient to study self assembly of GPCRs as has been recently demonstrated for rhodopsin²³³. Simulation of multiple rhodopsin monomers in a model lipid bilayer resulted in an organizational pattern primarily involving tail-to-tail conformation with interaction between transmembrane helices I, II at extracellular surface and cytoplasmic helix VIII²³⁴. An additional interaction

interface involving transmembrane helices IV, V and VI facilitated higher order organization which was relatively less stable since their association exhibited a free energy barrier for delipidation of helix surfaces²³⁴. Coarse-grained self assembly simulations of opioid receptors (μ -OR, δ -OR and κ -OR) showed a filiform arrangement for both homodimers and heterodimers²³⁵. The dimer conformations sampled by the associated species involved a symmetric interface involving transmembrane helices I, II, cytoplasmic helix VIII and asymmetric interfaces involving transmembrane helices I, II of one receptor and transmembrane helices IV, V/helices V, VI of the other receptor. Certain dimer interfaces showed kinetic preference over others during receptor oligomerization depending on the type of the receptor involved²³⁵.

Free energy simulations of β_1 and β_2 -adrenergic receptor homodimers were carried out in an explicit POPC/cholesterol bilayer to assess the relative stability of two putative contact interfaces (involving transmembrane helix I/cytoplasmic helix VIII and transmembrane helix IV/helix III) designed based on high-resolution inactive crystal structures²³⁶. The simulations were biased to allow sampling of only two interfaces out of the 49 different dimer conformations that can be possibly arise during interaction between the monomers. Enhanced sampling of the two dimer conformations was achieved by applying harmonic umbrella restraint applied to separation between center-of-mass of each protomer and history-dependent Gaussian bias applied to pre-defined rotational angle range. Results showed that transmembrane helix I/cytoplasmic helix VIII interface was more stable and long-lived (minutes) while transmembrane helix IV/helix III was significantly transient (hundreds of μ s to ms) in nature²³⁶.

Coarse-grained well-tempered metadynamics simulations of two different dimeric arrangements of δ opioid receptor (predicted from cysteine cross-linking experiments) involving transmembrane helix IV alone or with helix V confirmed the presence of two structurally and energetically similar configurations of transmembrane helix IV dimer. Umbrella sampling simulations of the transmembrane helix IV symmetric interface dimer revealed this arrangement to be more stable than transmembrane helix IV-helix V dimer.²¹³

Based on evidences from experimental and modeling data, there appears to be a complete absence of a “consensus” interaction interface among GPCR subtypes. Indeed, even for the same GPCR subtypes, different analytical approaches have predicted variation in interaction interface. This probably suggests that interaction between GPCRs is not strictly sequence based and that there is greater plasticity among the different accessible interfaces during higher order

organization.

1.7 Factors regulating GPCR organization

Diffusion of transmembrane proteins in the lipid bilayer brings them in close contact with each other. Most of these associations are relatively unstable and possibly have no functional relevance^{234,236}. Fewer interactions gives rise to conformations that could be physiologically significant. Although contacts between the membrane proteins appear to be stochastic in nature, several factors regulate their associations. In case of GPCRs, a large fraction of the receptor remains embedded within the membrane and therefore it is not surprising that membrane environment largely affects its organization. Lipid-protein interactions are known to play a significant role in modulating GPCR oligomerization²³⁷. These effects are mediated either (i) by direct interaction of lipids at specific sites on the receptor, (ii) by localized alteration of bilayer physical properties around the protein, or (iii) by a combination of both^{70,233,238–240}. However role of lipid-protein interactions in regulating GPCR association and the underlying molecular details have are not yet well established.

It is known that lipids and proteins are not homogenously distributed in the cell membrane²⁴¹. The “mosaic” nature of the cell membrane is not entirely dynamic owing to the lateral segregation. Cytoskeleton underlying the membrane appears to contribute towards maintaining spatial and temporal heterogeneity by aiding the formation of “microdomains”^{242–244}. Destabilizing cytoskeleton in serotonin_{1A} receptor expressing transfected cells allows receptor reorganization leading to formation of larger oligomers¹²². Intrinsic factors such as post-translational modification^{245–247} as well as extrinsic factors such as ligand²⁴⁸ have been show to affect GPCR organization.

1.8 Functional significance of GPCR oligomerization

Although there are several reports supporting functional significance of heterodimerization between different GPCR subtypes^{249–253}, there are relatively few evidences that focus on the relation between homodimerization and function (Fig. 1.8). An essential requirement of dimerization for function has been suggested in Leukotriene BLT1 receptor. Binding of heterotrimeric G-protein to Leukotriene BLT1 receptor occurred only in the presence of the agoinst LBT4 which

was also shown to increase the dimer population. Treatment with peptide mimicking helix VI resulted not only in dissociation of dimers but also detachment of the G-protein coupled to the receptor. Substituting one of the monomers in the dimer with helix VI peptide prevented association between the receptor and G-protein, although the monomer was capable of binding to the ligand and retained features associated with active state²⁵⁴.

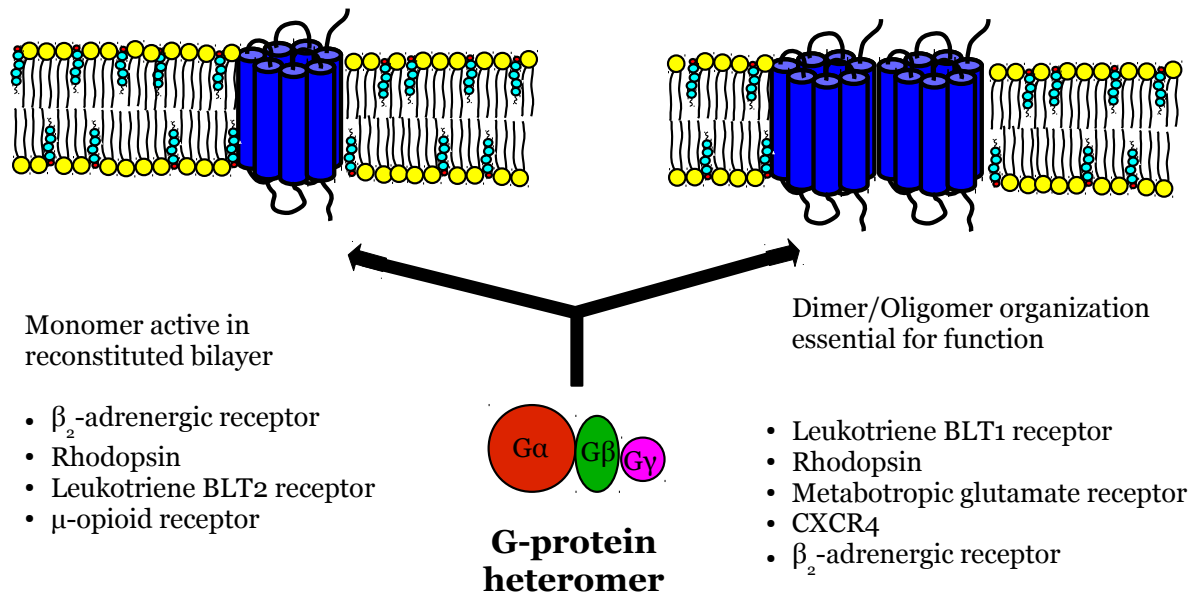


Figure 1.8: Functional role of higher order organization of GPCRs. There are contradicting evidences for functional form of GPCRs with G-protein coupling and downstream signaling being reported for both monomer and dimer/oligomers.

There are also reports for functional significance of receptor dimer-G-protein complex among other GPCRs. Based on data obtained from imaging native disk membrane using atomic force microscopy, rhodopsin appears to arrange as higher order clusters including dimers which complex with G-protein to form homodimer-G-protein heteropentamer complex⁹¹. Although there are evidences suggesting that monomeric rhodopsin serves as a minimal functional

unit^{112,136,255,256}, it has been demonstrated that rhodopsin activity increases with higher order oligomerization, thus suggesting that increased association of rhodopsin is essential for its function⁹².

Dimerization also appears to be essential for function in case of class C GPCRs. Monomeric metabotropic glutamate receptor, when purified and reconstituted into nanodiscs, effectively coupled with G-protein upon activation by positive allosteric modulator. However only a full-length reconstituted dimer was able to activate the coupled G-protein upon glutamate binding, suggesting that dimerization is required for ligand induced activation²⁵⁷.

Indirect evidence for functional role of dimerization has been provided by peptide inhibition studies. A peptide derived from transmembrane helix VI of β_2 -adrenergic receptor disrupted dimerization and agonist-induced cAMP production¹⁵⁹. Similarly, disruption of CXCR4 dimerization using synthetic peptide targeting transmembrane helix IV was shown to reduce cell migration in malignant as well as normal blood leukocytes²⁰⁴.

Recent studies in 5-HT₇ and 5-HT_{2A} serotonin receptors carried out both invitro and in-vivo strongly supports the functional role of homodimers. Binding of an pseudo-irreversible antagonist (“inactivator”) to the orthosteric site one protomer in a homodimer abolished activity completely although only 50% of the available binding-sites were occupied. Subsequent treatment with competitive antagonist followed by “wash-out” of the drugs released both the inactivator and competitive antagonist from their binding sites allowing the entire complex to return to an active state. This suggests allosteric crosstalk between the protomers, thereby providing crucial evidence that GPCRs can exist and function as homodimers¹³⁸.

Functional complementation following co-expression of two inactive mutant receptors also provides an indirect indication for homodimer function. Domain swapping and direct interaction between inactive mutant or chimeric receptors have been suggested as possible mechanism to explain the activity observed when these non-functional receptors are co-expressed¹⁶⁷. Evidences for association based functional restoration has been shown in dopamine, opioid, angiotensin II and somatostatin receptors^{165,182,258,259}. Such associations between mutant receptors could play physiologically significant roles^{260,261}.

1.9 “Molecular insights” into GPCR oligomerization : Revisiting concepts with new approach

A wealth of information about GPCR oligomerization and its regulation has been provided from a wide variety of experimental approaches²⁶². However, there are inconsistencies among the results reported from these methods. One of the major limitation faced by many experimental techniques is the inability to provide direct molecular spatio-temporal resolution of interaction between receptors and with membrane components. Computational approaches allow modeling and simulation of biophysical processes at sub-molecular resolution. With recent recent advancements in computational resources, sampling techniques and simulation algorithms, it has been possible to study larger systems and examine processes occurring at longer timescales, such as GPCR association^{63,233,234,263,264}. At the start of this thesis, there were very limited structural studies that focused on the role of lipids on GPCR oligomerization. Periole *et al.* characterized the effect of varying bilayer thickness on modulating oligomer conformations in rhodopsin. Results suggested local hydrophobic mismatch to play a central role in driving and modulating GPCR association. Although this study provided valuable information on the biophysical mechanisms regulating association between the receptors, biological relevance of the system used as representative model for understanding GPCR oligomerization is limited. This is due to the fact that (i) rhodopsin is not an ideal candidate for studying GPCR association, and (ii) the study considers single lipid type membranes, each with different bilayer thickness, which does not accurately reproduce the biophysical properties of cell membrane. In addition, contribution of specific lipid-protein interaction towards modulating oligomer conformation was not investigated. With technical advancements, crystal structures of several new GPCR species have been elucidated²⁶⁵. There has been significant improvements in MARTINI force field for lipids and is successful in reproducing several membrane biophysical properties^{215,232,266–277}.

In this thesis, we have investigated the role of membrane lipids, particularly cholesterol, in modulating higher order organization of well known GPCR members: β_2 -adrenergic receptor and serotonin_{1A} receptor. These receptors are involved in regulating essential physiological processes^{98,117}. Structural details such as specific lipid interaction and G-protein coupling have been well characterized for β_2 -adrenergic receptor^{74,102,110}. On the other hand, lipid-mediated

effects have been known to influence homo-oligomerization in serotonin_{1A} receptor^{122,123} although the order of the oligomers formed is not well established. Additionally there are no high resolution structural data available for this receptor. Since cholesterol is known to influence properties of both these receptors, they serve as ideal candidates for understanding lipid-mediated effects in GPCR oligomerization. The work carried out in this thesis is directed towards bridging the gap between static molecular structural information available for lipid-receptor interaction and the ensemble lipid-mediated effects which influence receptor association. Using coarse-grained molecular dynamics, we have been successful in providing sub-molecular resolution of oligomerization process in β_2 -adrenergic and serotonin_{1A} receptors and characterizing the contribution of different lipid-mediated effects in modulating receptor association. Our results suggest that lipids, through a combination of specific and non-specific effects regulate receptor organization in β_2 -adrenergic receptor and serotonin_{1A} receptor, though these findings, we believe, could be generalized across other GPCR members also.

This chapter (Chapter I) provides an overview of membrane and membrane proteins, particularly GPCRs, with comprehensive evidence for receptor oligomerization from previous studies and its possible functional significance.

Chapter II discusses the theory of molecular dynamics simulation approach with detailed description about practical aspects of simulation. It also provides a general outlook about a popular coarse-grained force-field, MARTINI which has been extensively used to carry out all simulations reported in this thesis.

In Chapter III, we examine the role of cholesterol in dimerization of a prototypical GPCR, β_2 -adrenergic receptor. Our work provides a molecular perspective on the dynamic and specific interaction of cholesterol at various sites on the receptor and its influence on modulating the dimer conformation.

Chapter IV investigates further into the non-specific interaction between lipids and β_2 -adrenergic receptor. It discusses the interplay between specific and non-specific protein-lipid interaction along with membrane-protein energetics in modulating dimerization of β_2 -adrenergic receptor.

In Chapter V, we extend our investigation of lipid-mediated effects on receptor dimerization to serotonin_{1A} receptor, another well studied member of GPCR family. We used a homology model built from the crystal structure of β_2 -adrenergic receptor to investigate the specific and

non-specific effects of membrane lipids on serotonin_{1A} receptor dimerization.

In Chapter VI, we scaled our system size to investigate higher order oligomerization in serotonin_{1A} receptor. As in our dimerization studies (Chapter III, IV and V), we investigated specific and non-specific interaction between membrane lipids and receptor and its effect on modulating cluster size and conformation.

Chapter VII investigates the interaction between serotonin_{1A} receptor and the sphingolipid, ganglioside. In this study we examine the specific binding sites for ganglioside on serotonin_{1A} receptor and the influence of cholesterol on regulating its spatial distribution and interaction around the receptor.

Finally, Chapter VIII provides a consolidated report on lipid-protein interactions examined in this thesis and its role in modulating GPCR association. It also discusses about the functional significance of having multiple dimer/oligomer conformations. Lipid-mediated modulation of these conformations could have considerable implications in drug research.

Methodology

“... a mind needs books as a sword needs a whetstone, if it is to keep its edge.”

– Tyrion Lannister, *George R.R. Martin’s “A Game of Thrones”*



Biological phenomenon that we encounter have a simple or a complex set of underlying physical/chemical processes involving large number of molecules. Although experiments allow us to study these biological activities, they sometimes fail to provide a detailed “molecular picture” of these processes due to technical limitations in capturing smaller length and time-scale resolutions. Investigation of such systems would be highly impossible using quantum mechanical methods which are currently restricted to solving exact energy function for limited number of particles. In some of these cases, it is possible to develop suitable models that mimic the behaviour of these molecules and molecular systems. The development of such accurate models to understand molecular details is known as “molecular modeling”. Molecular simulations allows us to examine the interaction between these chemical models by solving a set of underlying equations using classical Newtonian mechanics wherein the electronic motions are ignored. This assumption is based on Born-Oppenheimer approximation which states that the nuclear and electronic motions can be de-coupled. Since electron motion is much faster than the nuclear motion, the energy of a molecule in its ground electronic state can be solely considered as a function of its nuclear coordinates. Simulations serve as a link between microscopic interactions and macroscopic observations. The structure and interaction between these chemical models can be fine-tuned as precisely as deemed necessary to accurately match bulk properties obtained from experiments. The two main families of simulation technique

are molecular dynamics and Monte Carlo; additionally there is a whole range of techniques that combine features of both. Molecular dynamics has the obvious advantage of providing a time-dependent evolution of the interaction between chemical species in the system.

2.1 Force field

Force field refers to a set of functions and parameters that can be used to describe the energy of a system from the nuclear co-ordinates of its particles. The parameters are obtained from *ab initio*, semi-empirical quantum mechanical calculations or by fitting to experimental data such as neutron, X-ray and electron diffraction, NMR, infrared, Raman and neutron spectroscopy *etc.* The functional form of the force field is usually simple but closely reproduce the properties of the system in the area of interest (Fig. 2.1). One such typical functional form is given by:

$$\mathcal{V} = \sum_{bonds} \frac{1}{2} k_b (r_{ij} - r_{0(ij)})^2 + \sum_{angles} \frac{1}{2} k_a (\theta_{ijk} - \theta_{0(ijk)})^2 + \sum_{torsions} \frac{1}{2} V_n [1 + \cos(n\phi_{ijkl} - \gamma)]$$

$$+ \sum_{i=1}^N \sum_{j=i+1}^N 4\epsilon_{ij} \left[\left(\frac{\sigma_{ij}}{r_{ij}} \right)^{12} - \left(\frac{\sigma_{ij}}{r_{ij}} \right)^6 \right] + \sum_{i=1}^N \sum_{j=i+1}^N \frac{q_i q_j}{4\pi\epsilon_0 r_{ij}}$$
(2.1)

Here the first three terms correspond to intramolecular interactions involving particles $i - i+3$ while the last two term refers to non-bonded interactions: both intramolecular (interactions beyond $i - i+3$) and intermolecular.

- The first term of the function describes bond stretching between particles i and $j=i+1$. This functional form models bond vibration as a harmonic motion given by Hooke's law where energy (\mathcal{V}_{bond}) varies parabolically with the square of displacement from the reference bond length, r_0 with k_b corresponding to the stiffness of the bond.
- The second term of the function describes bond vibration between particles i and $i+2$. Angle bending is also modelled by a harmonic function where energy (\mathcal{V}_{angle}) shows parabolic variation with square of displacement from the reference bond angle, r_θ , and k_θ corresponding to the stiffness of the angle.
- Variation of energy during rotation about chemical bonds *i.e* torsional potential ($\mathcal{V}_{torsion}$), is expressed as a cosine series function, as shown by the third term in the above equation.

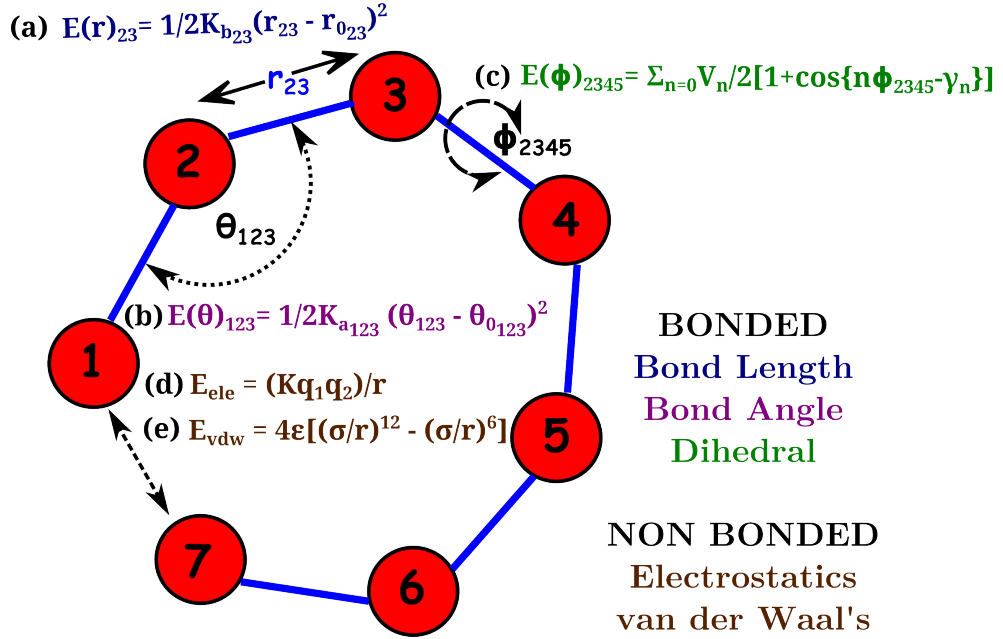


Figure 2.1: Schematic representation of a molecule depicting functional forms for bonded: (a) bond stretching (b) angle bending (c) Torsional; and non-bonded (d) electrostatic (e) van der Waal's potential

V_n represents the “barrier” height for rotation, ϕ is the torsion angle, n is the multiplicity and δ determines the phase factor.

- The fourth term of the function represents 12-6 form of Lennard-Jones potential which accounts for short-range van der Waals interactions. ϵ is the well depth corresponding to the energy minimum and σ is the diameter of the hard sphere representing the atom. The first component of the term (given within the square brackets) corresponds to the repulsion part that varies as r^{-12} while the second component corresponds to the attraction part that varies as r^{-6} .
- Long-range interactions are accounted for by the Coulombic interaction represented by the last term in the above equation. q_i and q_j represent pairwise charges while ϵ_0 corresponds to permittivity of the medium.

2.1.1 Properties of a force field

- **Unique representation:** A force field is a unique combination of functional form and parameters. Two different force fields may have same functional form but different parameters or vice versa. It is generally not advisable to mix individual functional terms and/or parameters between force fields, although in some cases few functional terms (bond and angle terms) make an exception to this rule.
- **Limited applicability:** A force field can be applied only to predict/reproduce those properties against which it has been characterized and parameterized. While it may serve to answer properties not included in parameterization, it should be considered with caution.
- **Transferability:** Often force fields are parameterized for small chemical groups which are then combined to generate force field for larger molecules. Also parameters developed and tested on relatively smaller number of cases can be extrapolated to wider range of problems *i.e.* parameters are transferable. This feature is essential to avoid reparameterization of each new molecule.
- **Empirical:** All force fields are empirical or semi-empirical in nature *i.e.* there is no “unique” or “standard” form for a force field. Functional form used in force fields are often a compromise between accuracy and computational efficiency. The choice of functional form to be employed in a force field depends upon the accuracy required of the simulation. Most accurate functional forms are often computationally expensive.

2.2 Statistical mechanics

Biological molecules are usually complex organic compounds made up of large number of atoms. It is possible to model these molecules as N-body interacting particles which can assume multiple conformations to generate an ensemble¹. The conformations or “states” assumed by these molecules, at or near thermodynamic equilibrium, can be represented by a unique combination of position and velocity for the N particles. All possible states *i.e.*, positions and velocities, that

¹An *ensemble* is a collection of all possible systems which have different microscopic states but an identical macroscopic or thermodynamic state

can be accessed by the N particles comprising the system is collectively called “phase space”. A N -particle system has a phase space of $6N$ dimensions. Statistical mechanics involves a set of rigorous mathematical expressions that can be used to express macroscopic properties of the system in terms of positions and velocities of the N -particles constituting the system.

The property of the system, such as pressure or temperature, can therefore be defined by the positions and momenta of the N -particles comprising the system. The value of property A , as measured experimentally, is an ensemble average given by

$$\langle A \rangle_{ensemble} = \int_N \int_N d\mathbf{p}^N d\mathbf{r}^N A(\mathbf{p}^N, \mathbf{r}^N) \rho(\mathbf{p}^N, \mathbf{r}^N) \quad (2.2)$$

where our property of interest A is expressed as a function of momenta \mathbf{p} , and positions, \mathbf{r} of the N particles. The integration is over all possible values of \mathbf{p} and \mathbf{r} accessible by the system. $\rho(\mathbf{p}^N, \mathbf{r}^N)$ is the probability density of the ensemble, *i.e.*, the probability of finding a configuration with momenta \mathbf{p}^N and positions \mathbf{r}^N . Under conditions of constant number of particles, volume and temperature,

$$\rho(\mathbf{p}^N, \mathbf{r}^N) = \frac{1}{Q} \exp(-E(\mathbf{p}^N, \mathbf{r}^N)/k_B T) \quad (2.3)$$

where $E(\mathbf{p}^N, \mathbf{r}^N)$ is the energy, k_B is Boltzmann’s constant T is the temperature and Q is the partition function

$$Q_{NVT} = \frac{1}{N!} \frac{1}{h^{3N}} \int_N \int_N d\mathbf{p}^N d\mathbf{r}^N \exp\left[-\frac{H(\mathbf{p}^N, \mathbf{r}^N)}{k_B T}\right] \quad (2.4)$$

The instantaneous value of the property A can be written as $A(\mathbf{p}^N(t), \mathbf{r}^N(t))$ where $\mathbf{p}^N(t)$ and $\mathbf{r}^N(t)$ represent the N momenta and positions respectively at time t . The value measured experimentally is an average of A over the time of measurement and is known as *time average*.

$$A_{avg} = \lim_{\tau \rightarrow \infty} \frac{1}{\tau} \int_{t=0}^{\tau} A(\mathbf{p}^N(t), \mathbf{r}^N(t)) dt \quad (2.5)$$

According to *ergodic hypothesis*, a fundamental axiom of statistical mechanics, ensemble average is equal to the time average. Therefore

$$\int_N \int_N d\mathbf{p}^N d\mathbf{r}^N A(\mathbf{p}^N, \mathbf{r}^N) \rho(\mathbf{p}^N, \mathbf{r}^N) = \lim_{\tau \rightarrow \infty} \frac{1}{\tau} \int_{t=0}^{\tau} A(\mathbf{p}^N(t), \mathbf{r}^N(t)) dt \quad (2.6)$$

2.3 Molecular dynamics

Molecular dynamics generates an ensemble of successive conformations for a system by integrating Newton's equations of motion. The phase space sampled is stored as a "trajectory" that describes evolution of position, velocities and acceleration of the particles with time. Molecular dynamics is a deterministic method, *i.e.*, it is possible to predict the state of the system at any time using the information about positions and velocities of the atoms in the system. At each time point, forces acting on the particles are derived and combined with their current positions and velocities to generate new coordinates and velocities for the particles at the next time point. Thermodynamic properties can be calculated from the sampled conformations using Eqn.2.5 (Fig. 2.2).

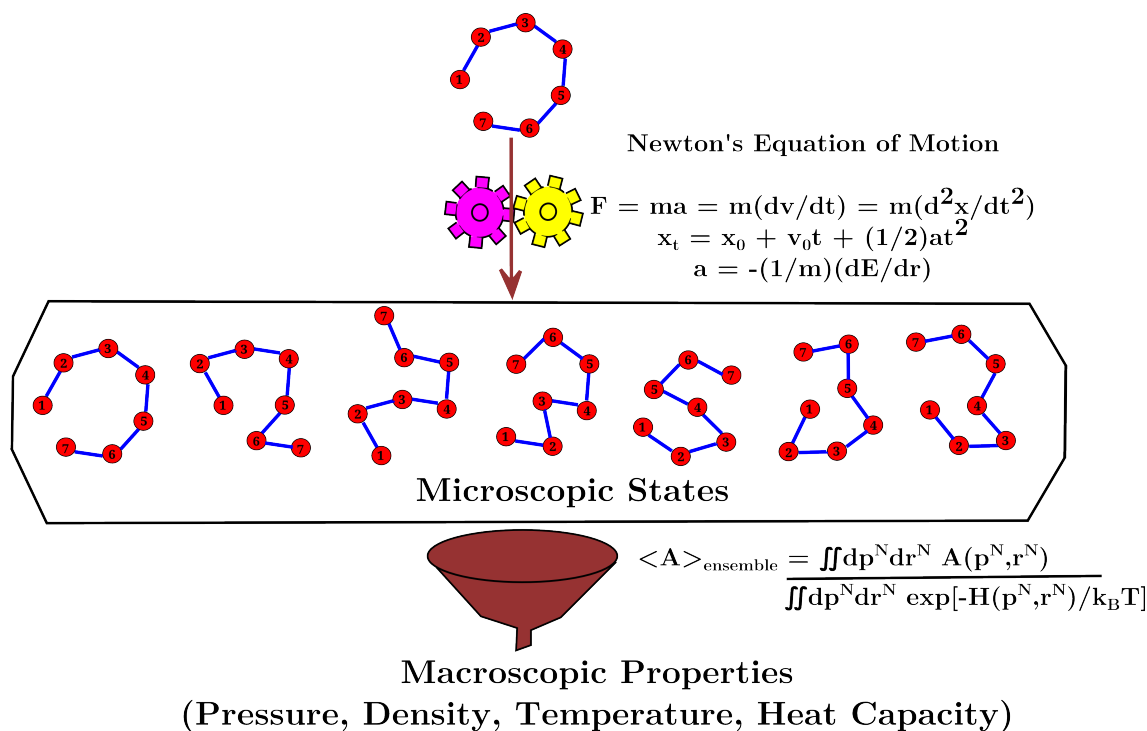


Figure 2.2: A general overview of molecular dynamics simulation. Newton's equation of motion are used to solve for evolution of co-ordinates and velocities as a function of time. This generates an ensemble from which thermodynamic properties can be extracted using statistical mechanics.

2.3.1 Practical aspects of simulation

This subsection discusses the different aspects commonly employed in molecular dynamics simulation. For a detailed description of these factors, please refer^{278,279}

Initial conditions

It is necessary to have a suitable configuration of the system before simulation can be performed. For simulating systems at equilibrium, it would be ideal to choose a configuration close to the local minima state at which simulation needs to be performed. This is achieved by performing energy minimisation on the initial configuration to ensure that the initial configuration is free of any high-energy interactions. To commence simulation, initial coordinates and velocities for all particles in the system are required. Velocities for the particles at time $t=0$ are assigned from Maxwell distribution centered about the desired temperature. Updated velocities are used thereafter at later time points.

Boundary condition

During simulation, a definite boundary must be considered for the system as it enables to calculate “macroscopic” properties using limited number of particles. Rigid boundary conditions are suitable for simulating condensed liquid/gas phases. However, for systems where “bulk” properties needs to be calculated, it is unfeasible to set rigid boundaries. This is because the fraction of atoms within the influence of the boundary wall is usually proportional to $N^{-1/3}$ (N denotes the number of particles in the system). It means that even for a system with 1000 particles, 10 would be at the boundary. This drawback is overcome by using periodic boundary conditions where the simulation box is surrounded by an infinite number of replicas so that the particles experience forces as if they were in bulk fluid. During simulation, only the N particles within the original simulation box are considered explicitly. If a particle leaves the box during simulation, it is replaced by the image of the particle from the replica which enters the system from the opposite side. The total number of particles in the original simulation box remains constant. Thus the original simulation box with its replicas resemble the “real” system. The main drawback of using periodic boundary condition is that it results in an artificial periodicity at intervals of box length. It is not possible to simulate fluctuations that have a wavelength

greater than the length of the cell. Therefore, the box should be sufficiently large to account for long-range correlations.

Speeding up simulations

- Minimum image convention:** The most time-consuming part of molecular dynamic simulations is calculation of non-bonded interactions since it increases as the square of the number of atoms (for pairwise interaction) with an order N^2 . A simple approach to overcome this limitation is by using minimum image convention. In this method, each atom interacts with only one image of every other atom in the system for which the energy and/or force is calculated. This is done by using a non-bonded cutoff such that all pairwise interactions beyond the cutoff value are set to zero, taking into account the closest image. The cutoff should be no more than half the length of the cell to prevent a particle from seeing its own image and also interacting with the same molecule twice. The use of non-bonded cutoff is justified by the observation that van der Waal's interaction modelled using Lennard-Jones potential is short ranged and falls off very rapidly with distance (r^{-6}).
- Ewald summation method:** Long-range electrostatic interactions diminish as r^{-1} and thus would result in interaction with its own image beyond the box dimension and also with multiple images of same molecules. Interaction between charges in the central box and images of all particles in the replicas is given by:

$$\psi = \frac{1}{2} \sum_{|n|=0}^{\prime} \sum_{i=1}^N \sum_{j=i+1}^N \frac{q_i q_j}{4\pi\epsilon|r_{ij} + n|} \quad (2.7)$$

where n ($L_n x L_n y L_n z$; L is the length of unit cell) represents a cubic lattice point at which the central box is positioned. A straight forward way to overcome this anomaly is to use the box dimensions that are sufficiently large to diminish these interactions, but this is usually impractical. However, long-range interactions are commonly dealt with using

specialized methods such as Ewald summation.

$$\begin{aligned} \mathcal{V} = \frac{1}{2} \sum_{i=1}^N \sum_{j=i+1}^N \left\{ \sum_{|n|=0}^{\infty} \frac{q_i q_j}{4\pi\epsilon_0} \frac{\frac{2}{\sqrt{\pi}} \int_r^{\infty} \exp(-t^2) dt (\alpha|r_{ij} + n|)}{|r_{ij} + n|} \right. \\ + \sum_{k \neq 0} \frac{1}{\pi L^3} \frac{q_i q_j}{4\pi\epsilon_0} \frac{4\pi^2}{k^2} \exp\left(-\frac{k^2}{4\alpha^2}\right) \cos(k \cdot r_{ij}) \\ \left. - \frac{\alpha}{\sqrt{\pi}} \sum_{k=1}^N \frac{q_k^2}{4\pi\epsilon_0} + \frac{2\pi}{3L^3} \left| \sum_{k=1}^N \frac{q_k}{4\pi\epsilon_0} r_k \right|^2 \right\} \end{aligned} \quad (2.8)$$

In Eqn. 2.8, the first term represents the modified form of Eqn 2.7 in which each charge is considered to be surrounded by a neutralising charge distribution of equal magnitude but opposite sign represented in a Gaussian functional form. This summation is performed in real space. The second term represents charge distribution which counteracts neutralising distribution in the first term. This summation is performed in reciprocal space. The third term removes all instances corresponding to interaction of Gaussian charge distribution with itself. The fourth term represents an energy correction term which is included if the medium surrounding the charge distribution is vacuum. Particle-mesh method of fast fourier transform (FFT) algorithm, where point charges with continuous coordinates are replaced by grid-based charge distributions, is commonly employed for solving computationally intensive Ewald summation. FFT algorithm scales as $N \ln N$ as compared to N^2 scaling for traditional Ewald summation.

- **Neighbour and cell list:** Although using a cutoff (R_c) reduces the number of pairwise interaction energy calculations, it is still required to calculate distance between an atom i with the remaining $N-1$ atoms to decide which ones lie within its sphere of radius R_c . This is averted using non-bonded neighbour list method where a list of all atoms within a distance of $R_c + \Delta_{\text{list}}$ is maintained, where $\Delta_{\text{list}} \ll R_c$. At each time step, search for atoms within R_c of a given atom i is done only for those included in its neighbour list. The list needs to be updated at suitable frequency (10-20 steps) to account for atoms leaving or entering the sphere. Cell list is used when for systems where $L \gg R_c$. In this method, the system is divided into M^3 subcells, such that average number of atoms in each subcell is N/M^3 . For a given atom i , it is sufficient to consider those in the

neighbouring subcells within R_c ($27N/M^3$ atoms).

- **Intramolecular constraints:** Computational efficiency is also limited by the time-step (Δt) used during the simulation. Ideally Δt should be much smaller than the fastest motion in the system. These motions usually correspond to bond vibrations where the relative displacement of atoms is usually negligible. By constraining these high frequency low amplitude motions, larger time-step can be used.
- **Coarse-graining:** Another commonly used strategy to improve sampling is to use coarse-grained models where a group of bonded atoms are combined into a single interaction site. Effective number of particles in the system are reduced which decreases the total number of degrees of freedom as well as permitting the use of larger time-steps. United atom representation is one such commonly used model where CH_2 and CH_3 are represented as single interaction sites.

Integration algorithm

There are many algorithms that can be used to integrate Newton's equation. The common requirements of a good integrator algorithm are:

- Should conserve energy and momentum.
- Should be computationally efficient *i.e.* minimal number of numerical calculations to evaluate force per time step.
- Should be stable when using longer time step for integration.
- Should be time reversible.
- Should be accurate.

In general, Taylor series expansion can be used to determine positions, velocities and accelerations.

$$r(t + \delta t) = r(t) + \frac{1}{1!} \frac{dr}{dt} \delta t + \frac{1}{2!} \frac{d^2r}{dt^2} \delta t^2 + \frac{1}{3!} \frac{d^3r}{dt^3} \delta t^3 + \frac{1}{4!} \frac{d^4r}{dt^4} \delta t^4 + \dots \quad (2.9)$$

Here the first term on the RHS of the equation corresponds to position, the second term corresponds to velocity (first derivative of position with respect to time), the third term corresponds to acceleration (second derivative of position with respect to time) and so on. Molecular

dynamics procedure can be given as follows:

1. System of N particles with initial positions ($r_{t=0}^{i,i+1,\dots,N}$), velocities ($v_{t=0}^{i,i+1,\dots,N}$, obtained from Maxwell distribution at given temperature) and a defined time step δt .
2. Calculate forces from bonded and non-bonded potential terms $F = -\frac{\delta}{\delta r}\mathcal{V}(r)$. Calculate acceleration from force $a = -\frac{1}{m}\frac{\delta}{\delta r}\mathcal{V}(r)$
3. Increment time: $t_1 = t_0 + \delta t$
4. Integrate positions: $r_{t=1}^{i,i+1,\dots,N} = r_{t=0}^{i,i+1,\dots,N} + v_{t=0}^{i,i+1,\dots,N}\delta t + \frac{1}{2}a^{i,i+1,\dots,N}\delta t^2$. Calculate velocities at $t + \delta t$.
5. Repeat steps 2 to 4.

The most commonly used integration algorithms are:

1. **Verlet algorithm:** This algorithm uses positions and accelerations at time t, and positions from previous time step to calculate new positions and velocities.

$$r(t + \delta t) = r(t) + v(t)\delta t + \frac{1}{2}a(t)\delta t^2 + \dots \quad (2.10)$$

$$r(t - \delta t) = r(t) - v(t)\delta t + \frac{1}{2}a(t)\delta t^2 - \dots \quad (2.11)$$

Adding these two equations, we get:

$$r(t + \delta t) = 2r(t) - r(t - \delta t) + a(t)\delta t^2 \quad (2.12)$$

Velocities do not explicitly appear in Verlet algorithm but can be calculated by:

$$v(t) = [r(t + \delta t) - r(t - \delta t)]/2\delta t \quad (2.13)$$

Features:

- * Minimal calculation steps and storage requirement.
- * Loss in precision due to addition of a small term ($a(t)\delta t^2$) to larger terms ($2r(t)$ and $r(t-\delta t)$).

- * Calculation of velocities at time t requires positions (r) at time $t+\delta t$.
- * At time $t=0$, $r(t-\delta t)$ is undetermined and must be obtained by other means such as Taylor series truncated after the first term *i.e.* $r(-\delta t) = r(0) - v(0)\delta t$

2. **Leap-frog algorithm:** In this algorithm, velocity calculation advances that of position by a time step of $\frac{1}{2}\delta t$.

$$v(t + \frac{1}{2}\delta t) = v(t - \frac{1}{2}\delta t) + a(t)\delta t \quad (2.14)$$

$$r(t + \delta t) = r(t) + v(t + \frac{1}{2}\delta t)\delta t \quad (2.15)$$

Velocities at time t can be calculated from:

$$v(t) = \frac{1}{2} \left[v(t + \frac{1}{2}\delta t) + v(t - \frac{1}{2}\delta t) \right] \quad (2.16)$$

Thus velocities ‘leap’ over positions to give values at $t+\frac{1}{2}\delta t$ and then positions ‘leap’ over velocities to give values at $t+\delta t$.

Features:

- * Velocities calculated explicitly. More precise since it does not involve calculation of differences of large numbers.
- * Calculations of positions and velocities not synchronised. Therefore it is not possible to calculate kinetic energy contribution to the total energy at the same time when positions are defined which are used to determine potential energy.

3. **Velocity-Verlet algorithm:**

$$r(t + \delta t) = r(t) + v(t)\delta t + \frac{1}{2}a(t)\delta t^2 \quad (2.17)$$

$$v(t + \frac{1}{2}\delta t) = v(t) + \frac{1}{2}a(t)\delta t \quad (2.18)$$

$$v(t + \delta t) = v(t) + \frac{1}{2}\delta t \left[a(t) + a(t + \delta t) \right] \quad (2.19)$$

Features:

- * Positions, velocities and accelerations are calculated at the same time

* No loss of precision.

4. Beeman's algorithm:

$$r(t + \delta t) = r(t) + v(t)\delta t + \frac{2}{3}a(t)\delta t^2 - \frac{1}{6}a(t - \delta t)\delta t^2 \quad (2.20)$$

$$v(t + \delta t) = v(t) + \frac{1}{3}a(t + \delta t)\delta t + \frac{5}{6}a(t)\delta t - \frac{1}{6}a(t - \delta t)\delta t \quad (2.21)$$

Features:

- * Accurate expression for velocity resulting in better energy conservation.
- * Computationally more expensive.

Thermodynamic ensembles

Integrating Newton's equation of motion for particles in the system maintains constant the number of particles (N), volume (V) and total energy (E) of the system. Thus simulations sample phase space in a microcanonical or NVE ensemble. Although total energy of the system remains constant, there would be fluctuations in kinetic and potential energy contributions. As a result, the temperature of the system would vary during simulation until equilibrium is attained. It is generally preferred to maintain constant temperature and pressure during the simulation in order to compare simulation results with experiment *i.e.* convert NVE ensemble to NVT or canonical ensemble. This is generally done by coupling the system to thermostats and barostats maintained at a given temperature and pressure respectively.

- **Constant temperature simulations:** Temperature is related to time average of kinetic energy and is given by

$$\langle \mathcal{K} \rangle_{\text{NVT}} = \frac{3}{2}Nk_B T \quad (2.22)$$

- * *Velocity rescaling:* Velocities at each time step are multiplied by a factor λ to control

system temperature

$$\Delta T = \frac{1}{2} \sum_{i=1}^N \frac{2}{3} \frac{m_i (\lambda v_i)^2}{N k_B} - \frac{1}{2} \sum_{i=1}^N \frac{2}{3} \frac{m_i v_i^2}{N k_B} \quad (2.23)$$

$$\Delta T = (\lambda^2 - 1) T(t) \quad (2.24)$$

$$\lambda = \sqrt{T_{\text{new}}/T(t)} \quad (2.25)$$

$$\lambda = \sqrt{T_{\text{req}}/T_{\text{curr}}} \quad (2.26)$$

- * *Berendsen thermostat*: System is coupled to an external heat bath maintained at desired temperature. Velocities are scaled at each step such that rate of change of temperature is proportional to difference in temperature between bath and system:

$$\frac{dT(t)}{dt} = \frac{1}{\tau} (T_{\text{bath}} - T(t)) \quad (2.27)$$

$$\Delta T = \frac{\delta t}{\tau} (T_{\text{bath}} - T(t)) \quad (2.28)$$

$$\lambda^2 = 1 + \frac{\delta t}{\tau} \left(\frac{T_{\text{bath}}}{T(t)} - 1 \right) \quad (2.29)$$

where τ is the coupling parameter between heat bath and system.

- * *Anderson thermostat*: Temperature is controlled using stochastic collision induced by reassigning velocity selected randomly from Maxwell-Boltzmann distribution at the desired temperature to a particle randomly chosen at definite intervals. The mean rate of stochastic collision is given by:

$$\nu = \nu_c / N^{2/3} \quad (2.30)$$

- * *Nosé Hoover thermostat*: Thermal reservoir is represented by an additional degree of freedom, s . Potential energy of the reservoir is given by $(f + 1)k_B T \ln(s)$, where f is the number of degrees of freedom. Kinetic energy of the reservoir is given by $Q/2(ds/dt)^2$, where Q represents the ‘‘fictitious’’ mass of the extra degree of freedom. The magnitude of Q determines coupling between reservoir and system which controls the temperature. The velocities of atoms in system is given by:

$$v_i = s \frac{dr_i}{dt} \quad (2.31)$$

where r_i is the position of the particle i and v_i is the real velocity of the particle.

- **Constant pressure simulations:** Constant pressure during the simulations is maintained by scaling the volume of the simulation box or by coupling the system to a pressure bath maintained at desired pressure. The rate of change of pressure is given by:

$$\frac{dP(t)}{dt} = \frac{1}{\tau_p}(P_{\text{bath}} - P(t)) \quad (2.32)$$

$$\lambda = 1 - \kappa \frac{\delta t}{\tau_p}(P - P_{\text{bath}}) \quad (2.33)$$

where κ is the isothermal compressibility of the substance and is given by:

$$\kappa = -\frac{1}{V} \left(\frac{\partial V}{\partial P} \right)_T = \frac{1}{k_B T} \frac{\langle V^2 \rangle - \langle V \rangle^2}{\langle V^2 \rangle} \quad (2.34)$$

The volume of the simulation box is scaled by a factor of λ , which is the same as scaling the particle coordinates by a factor of $\lambda^{1/3}$. The new coordinates are given by:

$$r'_i = \lambda^{1/3} r_i \quad (2.35)$$

2.3.2 Steps involved in molecular dynamics simulation

1. **System setup:** This step involves generating the initial conformation of the system using pre-existing models of the molecules constituting the system. The initial conformation of the constituent molecules could be completely random (as in self assembly simulation) or ordered (as in crystal lattice simulation). Appropriate force fields for the constituent molecules, cut-off values for non-bonded interactions and method to treat long-range interactions are defined.
2. **Equilibration:** The starting conformation is subjected to energy minimisation to relieve steric stress arising from atoms that are too close to each other than that permitted by the force field parameters. The starting conformation may be far from the thermodynamic conditions under which simulation needs to be carried out. A relatively short NPT simulation (at the desired temperature and pressure) is carried out by coupling the system to a thermostat and barostat, so that it achieves the equilibrium density corresponding to

the desired pressure and temperature. An adequate time-step, boundary conditions, cut-off values for non-bonded interactions, methods to treat long-range interaction, update frequency for neighbour list and intramolecular constraints if any are selected for the simulation. Sometimes restraints may be imposed on the solute to allow the solvent molecules to orient themselves around the solute molecule at the desired thermodynamic condition.

- 3. Production:** Once the system has been well equilibrated, it is subjected to production run. Basically, production run is similar to equilibration in the absence of restraints applied in the previous step. Occasionally, a more stringent thermostat and/or barostat than that used during equilibration may be employed during production run since the system is now equilibrated to the desired temperature and pressure and needs only be maintained at those conditions. The length of the simulation run depends upon the process under investigation. Ideally the simulation must be sufficiently long to ensure adequate sampling of the events of interest. A trajectory of the simulation (*i.e* positions, velocities and forces) is saved at a regular frequency which should be smaller than the fastest event in the simulation to be investigated.
- 4. Analysis:** The simulation provides us with the positions, velocities and forces sampled by the system as a function of time which can be used to determine thermodynamic properties using statistical mechanics. Structural changes such as root mean square deviation, radial and spatial distribution, and kinetic properties such as rates of diffusion, association-dissociation *etc* can also be extracted from the simulation.

2.4 Coarse-graining : The MARTINI model

Physiological processes occur on a wide range of length and timescales with structural changes ranging from pm to mm and dynamics occurring at ps to s. It would be beneficial to examine these processes at finer spatiotemporal resolutions to gain a “molecular-level” understanding. Experimental techniques are, however, limited in providing direct temporal resolution better than ms to μ s and in resolving structural changes at macromolecular level (μ m to nm). Computational approaches, such as molecular modeling, can be used to model biological structures

at “atomic” resolution based on experimental data. However, it is computationally expensive to examine biophysical processes that occur at μs to ms timescale due to numerical integration for the large number of atoms that constitute the system to be simulated.

A possible solution to enhance sampling and simulate longer and reach timescales comparable with those resolved using conventional experimental approaches is by coarse-graining. In a coarse-grained model, a group of atoms (preferably those belonging to similar chemical specificity) are substituted by a “pseudo” particle. The resultant model is parameterized by matching it to specific distribution from atomic simulation using various methods such as iterative Boltzmann distribution, force matching, relative entropy optimization *etc.* Due to the reduction in the degrees of freedom and absence of fine interaction details, simulations can be extended to longer length and timescales than that accessible using all-atom representation.

MARTINI is a popular coarse-grained model²⁸⁰ that has been extensively used to study a wide range of bio-molecular processes. Initially developed for phospholipids^{232,281,282}, this model has been extended to peptides and proteins²⁸³, sterols^{232,284}, polarizable water²⁸⁵, nucleic acids²⁸⁶, glycolipids²⁸⁷, bolalipids²⁸⁸ and other small molecules^{289–292}. Unlike conventional coarse-grained models that aim to reproduce the structural distribution pattern of the mapped atomic representation^{293,294}, the focus of MARTINI coarse-graining is to develop a simple, easy to use model with a force field that can be used for a broad range of applications without the need for frequent re-parameterization. This is achieved by calibrating non-bonded interactions of its chemical building blocks to match experimental data, especially thermodynamic data such as oil/water partitioning coefficients. The approach is particularly useful in studying membrane-based studies such as lipid self assembly, protein-lipid interaction, protein-protein association in membrane which depends critically on the degree to which the constituents partition between polar and non-polar environments.

This following subsections discuss the different aspects of MARTINI coarse-graining. For a detailed description, please refer^{232,280}.

2.4.1 Mapping scheme

A four-to-one mapping scheme is generally used to represent MARTINI coarse-grained particles *i.e.* on average, four non hydrogen atoms are represented by a single reaction center (Fig. 2.3, Table 2.1). Four main types of interaction centers are considered: polar (P), apolar (C), non

polar (N) and charged (Q). Each particle has a number of subtypes to accurately represent the chemical nature of the underlying atomic structure. These are distinguished by a letter denoting hydrogen-bonding capabilities (d = donor, a = acceptor, da = both, 0 = none) or by number indicating the degree of polarity (from 1, low polarity to 5, high polarity). In case of ring structures, such as those seen in benzene/cyclohexane-like molecules, a relatively fine mapping scheme (2-to-1 or 3-to-1) is used to preserve the local geometry and is represented by a particle S.

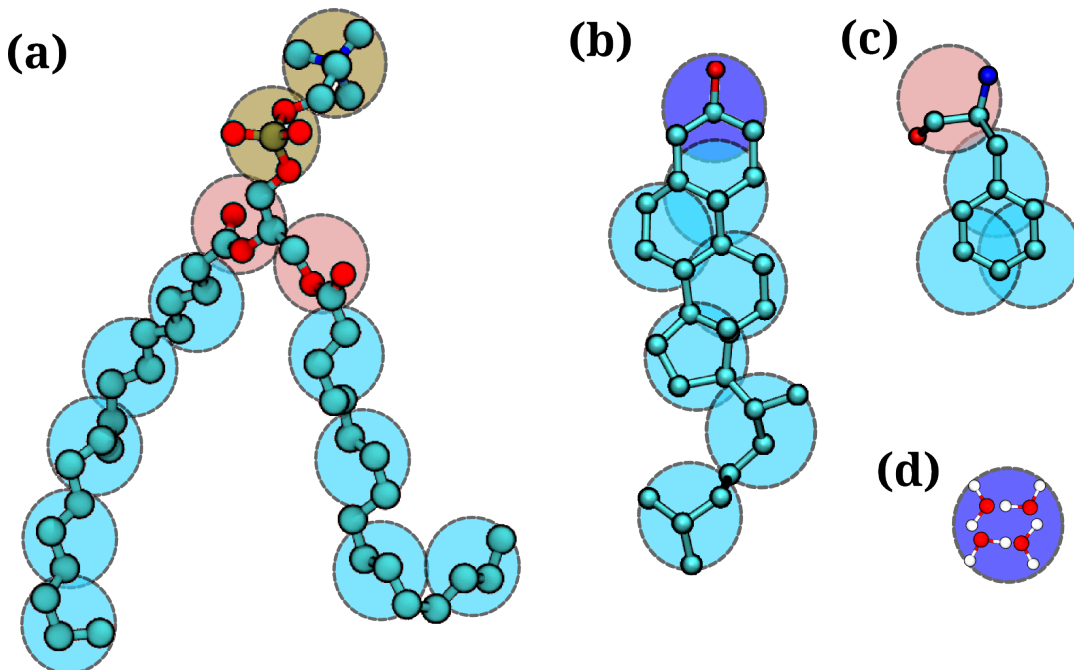


Figure 2.3: *MARTINI coarse-grained 4:1 mapping for (a) phospholipids (b) cholesterol (c) amino acid phenylalanine and (d) water. Chemical nature of the coarse-grained bead: tan = charged, pink = non polar, cyan = apolar, blue = polar. Adapted and modified from^{232,280}*

2.4.2 Non-bonded interactions

A 12-6 form of Lennard-Jones potential is used to model dispersion pairwise interactions between interaction sites i and j .

$$\mathcal{V}_{\text{LJ}}(r) = \sum_{i=1}^N \sum_{j=i+1}^N 4\epsilon_{ij} \left[\left(\frac{\sigma_{ij}}{r_{ij}} \right)^{12} - \left(\frac{\sigma_{ij}}{r_{ij}} \right)^6 \right] \quad (2.36)$$

σ_{ij} represents the closest distance of approach between the two hard-spheres. ϵ_{ij} , which

Table 2.1: *Chemical building blocks for coarse-grained particles*²³²

Type	Building Block	Examples
Q _{da}	H ₃ N ⁺ -C ₂ -OH	ethanolamine (protonated)
Q _d	H ₃ N ⁺ -C ₃	1-propylamine (protonated)
	NA ⁺ OH	sodium (hydrated)
Q _a	PO ₄ ⁻	phosphate
	Cl ⁻ HO	chlorine (hydrated)
Q ₀	C ₃ N ⁺	choline
P ₅	H ₂ N-C ₂ =O	acetamide
P ₄	HOH (x 4)	water
	HO-C ₂ -OH	ethanediol
P ₃	HO-C ₂ =O	acetic acid
	C-NH-C=O	methylformamide
P ₂	C ₂ -OH	ethanol
P ₁	C ₃ -OH	1-propanol 2-propanol
N _{da}	C ₄ -OH	1-butanol
N _d	H ₂ -N-C ₃	1-propylamine
N _a	C ₃ =O	2-propanone
	C-NO ₂	nitromethane
	C ₃ =N	propionitrile
	C-O-C=O	methylformate
	C ₂ HC=O	propanal
N ₀	C-O-C ₂	methoxyethane
C ₅	C ₃ -SH	1-propanethiol
	C-S-C ₂	methyl ethyl sulfide
C ₄	C ₂ =C ₂	2-butyne
	C=C-C=C	1,3-butadiene
	C-X ₄	chloroform
C ₃	C ₂ =C ₂	2-butene
	C ₃ -X	1-chloropropane 2-bromopropane
C ₂	C ₃	propane
C ₁	C ₄	butane isopropane

denotes the value of LJ well depth, indicates the strength of their interaction. The value of σ_{ij} is set to 0.47 nm for all interaction pairs. Exceptions are made for interaction between (i) particles in molecules with ring geometry where σ_{ij} is set to 0.43 nm and the corresponding ϵ_{ij} scaled to 75% of the original value; (ii) antifreeze particles where interaction, σ_{ij} , is scaled to 0.57 nm to prevent lattice packing of solvent molecules. The strength of the interaction, ϵ_{ij} remains the same; (iii) charged (Q-type) and most apolar type (C1 and C2) where σ_{ij} is set to 0.62nm to account for the range of repulsion between the two particles. There are 10 levels of interaction between the particle types which allows for fine-tuning the differences in solubilities (see Table 2.2). The interaction strength ϵ of each of the interaction levels is as follows: O, $\epsilon = 5.6$ kJ/mol; I, $\epsilon = 5.0$ kJ/mol; II, $\epsilon = 4.5$ kJ/mol; III, $\epsilon = 4.0$ kJ/mol; IV, $\epsilon = 3.5$ kJ/mol; V, $\epsilon = 3.1$ kJ/mol; VI, $\epsilon = 2.7$ kJ/mol; VII, $\epsilon = 2.3$ kJ/mol; VIII, $\epsilon = 2.0$ kJ/mol; and IX, $\epsilon = 2.0$ kJ/mol (with $\sigma = 0.62$ nm). Interaction levels between different coarse-grained interaction sites is summarized in Table 2.2. Level O, which represents the most polar interaction is used to model compounds that are solid at room temperature and for strong hydration shell around charged species. The level I interaction models strong polar interactions as in bulk water, levels II and III model more volatile liquids such as ethanol or acetone, level IV models the nonpolar interactions in aliphatic chains, and levels V to VIII are used to mimic various degrees of hydrophobic repulsion between polar and nonpolar phases. Level IX describes the interaction between charged particles and a very apolar medium.

Coulombic potential energy function is used to model interaction between charged groups which are assigned a full charge q

$$\mathcal{V}_{\text{elec.}}(r) = \frac{q_i q_j}{4\pi\epsilon_0\epsilon_r r} \quad (2.37)$$

Charge interactions are explicitly screened with a relative dielectric constant $\epsilon_r = 15$ to account for reduced set of partial charges and resulting dipoles observed in atomistic force field.

A shifted type of non-bonded interaction potential is employed during simulation to mimic distance dependent screening and is set to 0 at cut-off distance $r_{\text{cut}} = 1.2\text{nm}$. The electrostatic potential is shifted from $r_{\text{shift}} = 0.0$ nm to r_{cut} while LJ potential is shifted from $r_{\text{shift}} = 0.9$ nm to r_{cut} . In newer versions of MARTINI force field, polarizable water models have been introduced to account for orientational polarizability while retaining the dielectric screening of

Table 2.2: *MARTINI coarse-grained interaction matrix*²³²

		Q				P					N				C				
	sub	da	d	a	0	5	4	3	2	1	da	d	a	0	5	4	3	2	1
Q	da	O	O	O	II	O	O	O	I	I	I	I	I	IV	V	VI	VII	IX	IX
	d	O	I	O	II	O	O	O	I	I	I	III	I	IV	V	VI	VII	IX	IX
	a	O	O	I	II	O	O	O	I	I	I	I	III	IV	V	VI	VII	IX	IX
	0	II	II	II	IV	I	O	I	II	III	III	III	III	IV	V	VI	VII	IX	IX
	5	O	O	O	I	O	O	O	O	O	I	I	I	IV	V	VI	VI	VII	VIII
P	4	O	O	O	O	O	I	I	II	II	III	III	III	IV	V	VI	VI	VII	VIII
	3	O	O	O	I	O	I	I	II	II	II	II	II	IV	IV	V	V	VI	VII
	2	I	I	I	II	O	II	II	II	II	II	II	II	III	IV	IV	V	VI	VII
	1	I	I	I	III	O	II	II	II	II	II	II	II	III	IV	IV	IV	V	VI
	da	I	I	I	III	I	III	II	II	II	II	II	II	IV	IV	V	VI	VI	VI
N	d	I	III	I	III	I	III	II	II	II	II	III	II	IV	IV	V	VI	VI	VI
	a	I	I	III	III	I	III	II	II	II	II	II	III	IV	IV	V	VI	VI	VI
	0	IV	IV	IV	IV	IV	IV	IV	III	III	IV	IV	IV	IV	IV	IV	IV	V	VI
	5	V	V	V	V	V	V	IV	IV	IV	IV	IV	IV	IV	IV	IV	IV	V	V
	4	VI	VI	VI	VI	VI	VI	V	IV	IV	V	V	V	IV	IV	IV	IV	V	V
C	3	VII	VII	VII	VII	VI	VI	V	V	IV	VI	VI	VI	IV	IV	IV	IV	IV	IV
	2	IX	IX	IX	IX	VII	VII	VI	VI	V	VI	VI	VI	V	V	V	IV	IV	IV
	1	IX	IX	IX	IX	VIII	VIII	VII	VII	VI	VI	VI	VI	V	V	V	IV	IV	IV

bulk water. With these models, a much lower dielectric constant is used because of increased explicit screening.

2.4.3 Bonded interactions

Bonded interactions are modeled using a common form of potential energy function. Non-bonded interaction involving particles i to $i + 3$ are excluded.

$$\mathcal{V}_{\text{bond}}(r) = \frac{1}{2}K_{\text{b}}(r_{ij} - r_{0(ij)})^2 \quad (2.38)$$

$$\mathcal{V}_{\text{angle}}(\theta) = \frac{1}{2}K_{\text{a}}(\theta_{ijk} - \theta_{0(ijk)})^2 \quad (2.39)$$

$$\mathcal{V}_{\text{dihedral}}(\phi) = K_{\text{d}}[1 + \cos(n\phi_{ijkl} - \delta)] \quad (2.40)$$

$$\mathcal{V}_{\text{imp. dih.}}(\theta) = K_{\text{id}}(\theta_{ijkl} - \theta_{0(ijkl)})^2 \quad (2.41)$$

The structural distribution pattern for the mapped groups are determined from the atomistic simulation which are then compared to particle distribution in the coarse-grained simulation. The structural parameters for the coarse-grained particles are then fine-tuned in an iterative way until it matches satisfactorily with the pattern observed for the atomistic simulation distribution. In case of proteins and peptides, PDB database is used as reference

for optimizing molecular geometry. Bond lengths, bond angles and dihedral distributions are closely matched to the pattern observed among the structures reported in PDB databank. Restraints and elastic networks (in newer versions of MARTINI) are imposed on the secondary structure of proteins as the absence of directional hydrogen bonding prevents realistic folding in MARTINI model.

2.4.4 Scaling factor for kinetic processes

Coarse-graining removes several degrees of freedom, particularly those corresponding to fast motions such as C-H, C-C bond vibrations. The resultant potential energy surface is therefore much smoother and the dynamics much faster than that observed in atomistic models. In most cases the kinetic properties of most biophysical processes show good agreement with experimental measurements after scaling by a factor of 4. Since dynamic rates largely depend on the mass of the particle, a standard mass of 72 amu (corresponding to four water molecules) is assigned to all coarse-grained particles. Exceptions are observed for those involved in ring conformation for which a reduced mass is assigned. Ideally, realistic masses should be assigned to each particle to accurately model the kinetics. But this would result in the need for multiple particle subtypes thereby increasing the complexity of the model. In case of homogeneous systems, kinetic properties can be scaled based on mass differences after performing the simulations.

2.4.5 Validation for MARTINI coarse-grained model

MARTINI coarse-grained model has been carefully parameterized by validating it against thermodynamic values obtained from experimental procedures such as free energy of hydration, free energy of vapourization and partitioning free energy between water and several organic solvents. All parameterizations for coarse-grained particles have been carried out at 300K and at 1 atm pressure. These particles have been used to construct a wide variety of biomolecules including lipids, sterols, peptides and proteins, sugars, polymers, nanoparticles, dendrimers and many more. The assumption involved in developing these models is that molecules can be characterized by the properties of the coarse-grained particles used in its construction. Bilayer properties such as area per lipid head group, spontaneous curvature, condensation effect of cholesterol on area per lipid show good agreement with experimental estimates while free

energy profile for lipid “flip-flop” match closely to atomistic simulations²³². Similarly, for proteins, partitioning of amino acid side chain analogues as well as model peptides in lipid bilayer, side-chain-side-chain interaction and peptide orientation in bilayer show good agreement with the pattern observed in atomistic interactions and also match with experimental results²⁸³.

2.4.6 MARTINI based applications

The first applications of MARTINI was carried out just over a decade ago and involved modeling processes such as spontaneous aggregation of lipids into unilamellar vesicles²⁸¹ and fusion in small lipid vesicles²⁸². These studies were carried out using one of the earliest prototype MARTINI force field²⁹⁵. Since then, several improvements have been made to increase the chemical complexity of particle types for modeling many other biophysical processes while striving to maintain the simplicity of the coarse-grained model. A few of these notable achievements involve simulating formation of membrane tethers²⁷¹, membrane domains²⁶⁷, lipid organization in plasma membrane²⁶⁹, implicit-solvent version of MARTINI for studying lipid membrane properties²⁷² and effect of bilayer physical properties in on higher order organization of membrane proteins and model peptides^{233,266,296}.

2.4.7 Limitations of MARTINI coarse-grained model

The purpose of any model is to understand a complex process in terms of a set of parameters which are known to influence its properties and which can be qualitatively and quantitatively controlled in a simplistic design built using these parameters. Although a model system helps us to gain a detailed understanding of the underlying process, it is still only a representation and has its limitations. MARTINI, like any other multiscale model, also has its own set of limitations.

- Limited structural resolution due to standard 4:1 mapping: Lauryl (with 12 carbon atoms) and myristoyl (with 14 carbon atoms) acyl chains are both represented using 3 Martini beads²⁹⁵. All amino acids are represented by either 1 to 4 MARTINI beads²⁸³. In sugars, distinction between different ring conformations and anomers is lost²⁸⁹.
- Cannot be used for folding peptides/proteins since there is no directionality of backbone

interactions indicated by hydrogen bonding. Constraints are imposed to maintain extended and helical secondary structures. As a result local secondary structural changes cannot be modeled.

- Reducing degrees of freedom smoothens the underlying energy landscape and thereby speeds up the kinetics of the system. A common scaling factor of 4 compared to atomistic simulations is assumed for most kinetic processes based on lateral diffusion rates of lipid and transmembrane proteins. However, not all degrees of freedom have same kinetic rates²⁹⁷.
- Loss of entropy due to coarse-graining the degrees of freedom is compensated by reduced enthalpy term. Therefore temperature-dependance of Maritini coarse-grained model is not correct. For example, the estimated free-energy of hydration for alkanes is more over-estimated in coarse-grained compared to atomistic simulations at higher temperatures²⁹⁸.
- Unreliable outside temperature range used for parameterization (270K-330K).
- Interaction strength of polar species in nonpolar environments is underestimated owing to implicit screening. Therefore processes involving partition of charged/polar molecules in apolar environment such as formation of water pore through lipid bilayer cannot be accurately modeled²³².
- MARTINI water model shows tendency to “freeze” even at temperatures between 280-300K around ordered surfaces. This is primarily attributed to lack of explicit charges and absence of long-range electrostatic interactions. MARTINI water model shows poor representation for interfacial tension and isothermal compressibility²⁹⁹.

Cholesterol Modulates the Dimer Interface of the β_2 -Adrenergic Receptor via Cholesterol Occupancy Sites

“It’s much better to do good in a way that no one knows anything about it.”

– Leo Tolstoy, *Anna Karenina*

3.1 Introduction

Membrane lipids have been recently implicated in the modulation of GPCR oligomerization^{11,122,123}. Spatial organization of serotonin_{1A} receptor, including dimerization and higher-order oligomerization, has been reported to be influenced by membrane cholesterol^{122,123,300}. It has been speculated that cholesterol alters GPCR function and organization by either direct interactions with the receptor or indirect alterations of membrane biophysical properties^{9,301}. An interesting feature of a number of recently solved high-resolution crystal structures of GPCRs, such as the A_{2A} adenosine receptor³⁰², β_1 -adrenergic receptor³⁰³ and β_2 -adrenergic receptor^{74,102}, is the close association between cholesterol molecules and the receptor. Recent molecular-dynamics simulations revealed cholesterol-binding sites in GPCRs,

although relatively weak interactions were observed^{125,304,305}. However, despite the increasing number of reports regarding a GPCR-cholesterol interaction, the exact role of cholesterol at the molecular level in GPCR structure and function continues to be elusive.

The β_2 -adrenergic receptor is an important member of the GPCR superfamily and serves as an excellent prototype for monitoring GPCR organization and function. This receptor type is expressed mainly in muscle tissues. The β_2 -adrenergic receptor is involved in muscle relaxation after activation³⁰⁶ and dysfunction of this receptor is associated with cardiac diseases and asthma^{307,308}. It was reported that the β_2 -adrenergic receptor can exist as dimers *in vivo*¹¹⁴, and dimerization is functionally important¹⁵⁹, although a monomeric receptor was shown to be the minimal functional unit necessary for signaling²⁵⁵. A direct receptor-cholesterol interaction was revealed by the cocrystallization of cholesterol in the crystal structure of the β_2 -adrenergic receptor⁷⁴. In addition, receptor function was shown to be dependent on membrane cholesterol^{104,105}. Yet, the molecular relevance of cholesterol's association with the receptor is still not clear.

In this work, we carried out coarse-grained molecular dynamics simulations to analyze the molecular nature of the interaction between membrane cholesterol and the β_2 -adrenergic receptor, and explore the effect of cholesterol on the dimerization of the receptor. We simulated the β_2 -adrenergic receptor in a POPC membrane bilayer in the presence of increasing concentrations of cholesterol, which were chosen to mimic the biological environment of the receptor. We used the MARTINI force field in our study since it has been shown to be suitable for applications such as membrane protein association^{233,234,309–311} and partitioning of membrane proteins between membrane domains of varying compositions^{266,312}. Our results show that cholesterol binds to transmembrane helix IV and has an increased occupancy at that site, in both the monomeric and dimeric regimes. Interestingly, our results show that cholesterol occupancy modulates the dimerization process of the receptor, altering the dimer structure and the helices involved in the interface. These novel (to our knowledge) results constitute one of the first reports to explore the correlation between cholesterol's association with the receptor and its oligomerization and organization at a molecular level.

3.2 Materials and methods

3.2.1 System setup

Molecular-dynamics simulations of the β_2 -adrenergic receptor embedded in POPC membranes were carried out in the presence and absence of cholesterol. The systems were represented using the MARTINI coarse-grained force field (version 2.1)^{232,283}. A homology model of the β_2 -adrenergic receptor (amino acid residues 29–342) was generated from the crystal structure¹⁰² (PDB: 2RH1) using SWISS-MODEL software³¹³. The PDB structure 2RH1 is a chimera of the β_2 -adrenergic receptor with the protein T4 lysozyme fused for crystallization. The homology model was built by removing the T4 lysozyme part and replacing it with the intracellular loop 3 of β_2 -adrenergic receptor. The atomistic structure obtained was minimized and then mapped to its coarse-grained representation. Bilayers containing POPC with increasing cholesterol concentration (0%, 9%, 30%, and 50%) were generated from an initial conformation of randomly placed POPC, cholesterol, and water beads. The bilayer formed in the simulation was equilibrated for 5 μ s, leading to uniform distribution of cholesterol in the bilayer. Details regarding the number of lipids, cholesterol, and water used for each system are given in Table 3.1.

Table 3.1: *Summary of simulations performed*

System	Initial minimum distance (nm)	Simulation			Number of Molecules		
		Period (μ s)	POPC	cholesterol	water		
POPC	3.2	32	15	15	568	0	11280
POPC/ 9% cholesterol	3.0	33	10	10	520	24	10452
POPC/ 30% cholesterol	3.4	28	10	10	520	158	11776
POPC/ 50% cholesterol	3.4	24	16	12	520	260	11800

Two copies of the coarse-grained model of the β_2 -adrenergic receptor were inserted into each of the equilibrated bilayers such that the inter-receptor distance (center of mass) was at least 6 nm (minimum distance of at least 3 nm). A top view of the β_2 -adrenergic receptor, in which the transmembrane helices are labeled, and the starting structure of a representative simulation are shown in Fig. 3.1, a and b.

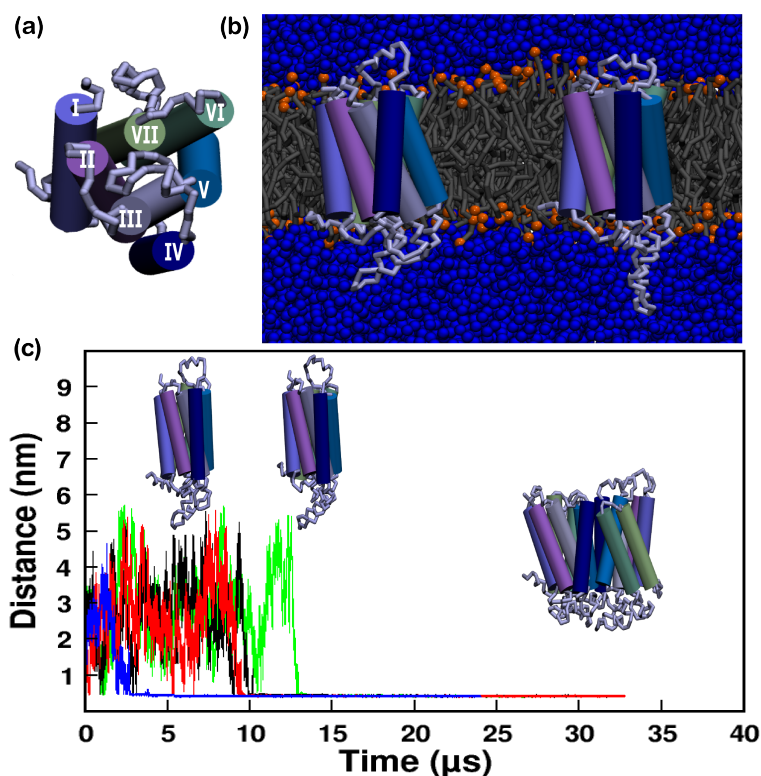


Figure 3.1: Schematic representation of the β_2 -adrenergic receptor. (a) Top view of the receptor with individual helices marked. (b) Starting structure of the two monomers of the β_2 -adrenergic receptor in the POPC bilayer. The two receptors are shown in shades of blue corresponding to panel a; lipid molecules are shown in gray, the phosphate bead of lipid is in orange, and the surrounding water molecules are in blue. (c) Time course of dimerization of the β_2 -adrenergic receptor in POPC bilayers with increasing cholesterol concentration. The minimum distance between two receptors (defined as the distance between the closest beads from two individual receptors, as shown in the figure) during the course of the simulation is plotted for receptor association in POPC bilayers alone (black); and in the presence of 9% (red), 30% (green) and 50% (blue) cholesterol concentration. A representative simulation from each of the four systems is plotted.

3.2.2 Simulation parameters

All simulations were performed using the GROMACS simulation package, version 4.5.4³¹⁴. The cutoff for nonbonded interactions was 1.2 nm, with electrostatic interactions shifted to zero in the range of 0–1.2 nm, and Lennard-Jones interactions shifted to zero in the range of 0.9–1.2 nm. A relative electrostatic screening of 15 was used. The temperature for each group was weakly coupled using the Berendsen thermostat algorithm³¹⁵ with a coupling constant of 0.1 ps to maintain a constant temperature of 300 K during simulation. Semi-isotropic pressure was maintained using the Berendsen barostat algorithm³¹⁵ with a pressure of 1 bar independently in the plane of the membrane and perpendicular to the membrane, a coupling constant of 0.5

ps, and a compressibility of $3 \times 10^{-5} \text{ bar}^{-1}$. The time step used in the simulations was 20 fs. Simulations were rendered using VMD software³¹⁶.

3.2.3 Analysis

A transmembrane helix of a receptor was considered to be at the dimer interface if it was within a cutoff of 0.5 nm of the other receptor. This value was chosen based on the minimum distance of approach between two beads in the MARTINI coarse-grained model^{232,283}. A lipid or cholesterol molecule was defined to be bound to a particular transmembrane helix or amino acid residue (site) if it was within 0.5 nm of that site. The maximum occupancy time was defined as the longest time a given cholesterol molecule was bound at a particular site. The values were normalized for all simulation lengths. A value of one implies that the same cholesterol molecule was present at the site during the entire simulation, and zero implies that cholesterol was never present at that site. The binding region for POPC/cholesterol on a given helix was determined by calculating the distance map. The distance cutoff was 0.5 nm as described above. The results showed no qualitative changes when a larger cutoff of 0.6 nm was used.

3.3 Results

3.3.1 The β_2 -adrenergic receptor dimerizes in the membrane bilayer

To analyze the effect of cholesterol on dimerization of the β_2 -adrenergic receptor, we carried out coarse-grained molecular-dynamics simulations of the receptor in POPC bilayers and POPC/cholesterol bilayers with increasing cholesterol concentrations (9%, 30%, and 50%). Multiple μs -timescale simulations were performed, for a total simulation time of 200 μs corresponding to $\sim 800 \mu\text{s}$ of effective time (atomistic simulation time)^{232,283}. Two copies of the receptor were initially placed in a POPC bilayer (with and without cholesterol) such that the interreceptor distance (center of mass) was at least 6 nm. Previous umbrella sampling calculations²⁶⁶ showed that the free energy of association between two receptors is close to zero at a 1.5 nm distance separation (minimum distance between receptors). In our study, the receptors were initially placed at two times this distance, i.e., with a minimum distance of 3 nm. The initial setup of the system and the top view of the receptor are shown in Fig. 3.1. During the course of the simulation, the receptors diffused freely in the membrane and associated with each

other on a μs timescale. The minimum distance between the two receptors during the course of representative simulations in each case is shown in Fig. 3.1 c. Several close associations were observed between the two receptors before the final dimerized structure was obtained. We calculated the phase space sampled by the receptors in the monomer regime in one of the representative systems (Fig. 3.2).

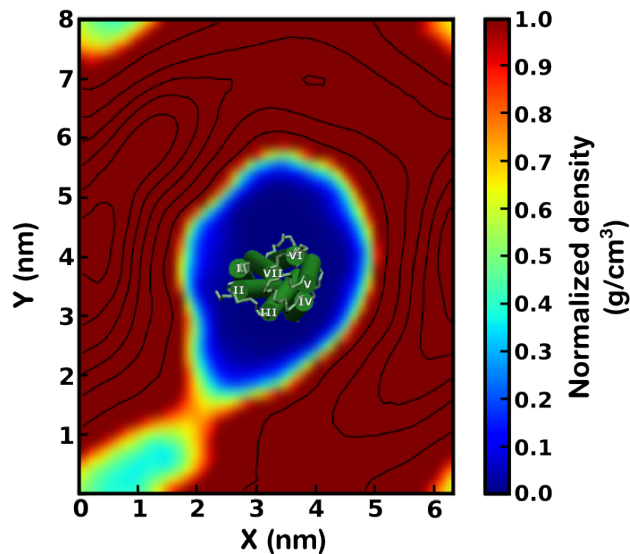


Figure 3.2: Contour plot showing the average density of a receptor around the second receptor (centered). Only the monomer regime has been used to calculate the density. The central receptor has been overlaid on the plot and its transmembrane helices labeled for comparison.

It is evident from the figure that all orientations around the central receptor were sampled, except for a narrow pathway leading to the central receptor. The sampling of the receptors in the monomer regime demonstrates that the dimer conformations were not biased according to the starting configurations, and adequate orientational and translational sampling was achieved. The time taken to form a stable dimer was variable and ranged from 2 to 15 μs . In most cases, the initial contact between two receptors that led to a stable contact was made by intracellular loops II and III. Several occurrences of the N-terminal region and the C-terminal helix VIII were also observed at the contact interface. Once the dimer was formed, it was stable during the course of the simulation, although small rearrangements of the two receptors relative to each other were observed. The final inter-receptor distance (i.e., the distance between the center of mass of the two receptors in the final dimer) was calculated to be ~ 3.2 nm.

3.3.2 Dimer interface of the β_2 -adrenergic receptor in the POPC bilayer

To further characterize the dimer structures, we analyzed the transmembrane helices involved at the dimer interface. A representation of the dimer interface (top and side views of the transmembrane helices) is shown in Fig. 3.3, a and e.

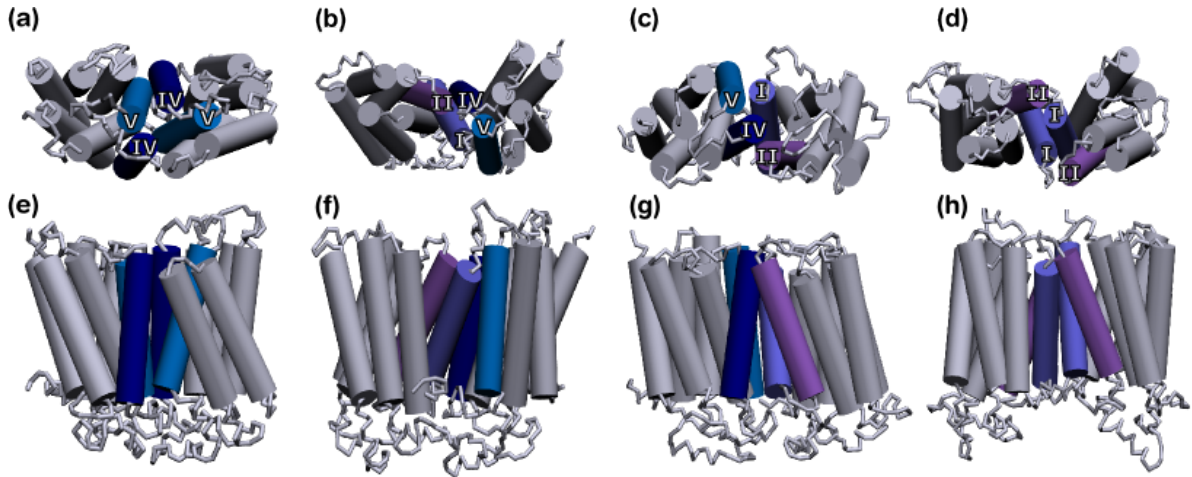


Figure 3.3: Schematic representation depicting the modulation of transmembrane helices of the β_2 -adrenergic receptor involved at the dimer interface with increasing cholesterol concentration. (a and e) POPC bilayer. (b-d and f-h) POPC bilayers containing 9% (b and f), 30% (c and g), and 50% (d and h) cholesterol. Representative top and side views of the transmembrane helices are shown for clarity. The transmembrane helices that comprise the dimer interface are colored and labeled. The remaining helices are colored gray.

Transmembrane helices IV and V from both receptors were present at the dimer interface in POPC bilayers. The simulations were repeated three times with different starting velocities, and each time transmembrane helices IV and V were observed to be present at the interface. A contact map of all helix-helix contacts, normalized over the time of occurrence, is shown in Fig. 3.4.

Since the most frequently observed dimer interface involved symmetric interhelical contacts, we termed such an interface a homo-interface (i.e., the same transmembrane helices from both receptors are involved at the dimer interface). In this conformation, an increased accessibility to membrane lipids was observed for transmembrane helices I and VII relative to transmembrane helices IV and V.

A visual inspection of the final dimer structures that formed in POPC bilayers revealed the presence of a phospholipid (POPC) molecule at the dimer interface (Fig. 3.5).

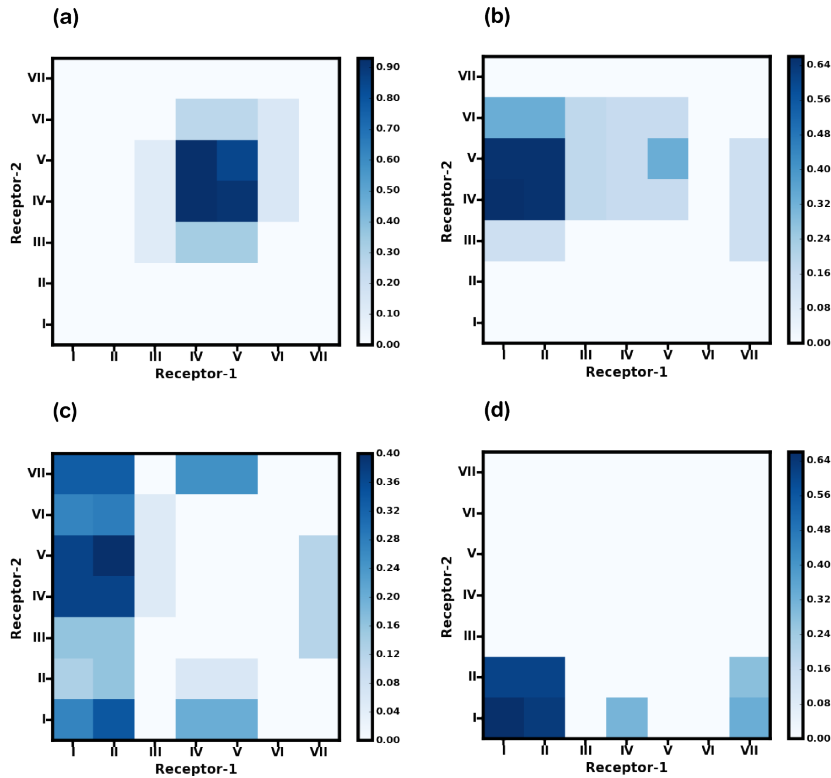


Figure 3.4: Contact maps depicting the helix-helix interactions between the two receptors. (a) POPC bilayer. (b–d) POPC bilayers containing 9% (b), 30% (c), and 50% (d) cholesterol. The values were calculated as an average over all simulations and normalized by the time of occurrence and simulation length. A cutoff distance of 0.5 nm was used to determine the contact residues.

The POPC molecule was present at the interface in all three simulations. The binding of the POPC molecule to the groove region formed by transmembrane helices IV and V of the interacting monomers occurred simultaneously with the dimerization process. The POPC molecule remained at the contact interface during the remaining simulation time. Energetically favorable interactions with several aromatic amino acid residues on transmembrane helices IV and V were seen to stabilize the POPC molecule.

3.3.3 Cholesterol modulates helices involved at the dimer interface

Interestingly, the dimer interfaces observed in our simulations with POPC bilayers were altered in the presence of cholesterol. Fig. 3.3, b–d, f–h, show the progressive change in the dimer interface with increasing concentrations of cholesterol in the membrane. A contact map of the dimer interfaces with varying concentrations of cholesterol is shown in Fig. 3.4, b–d. In

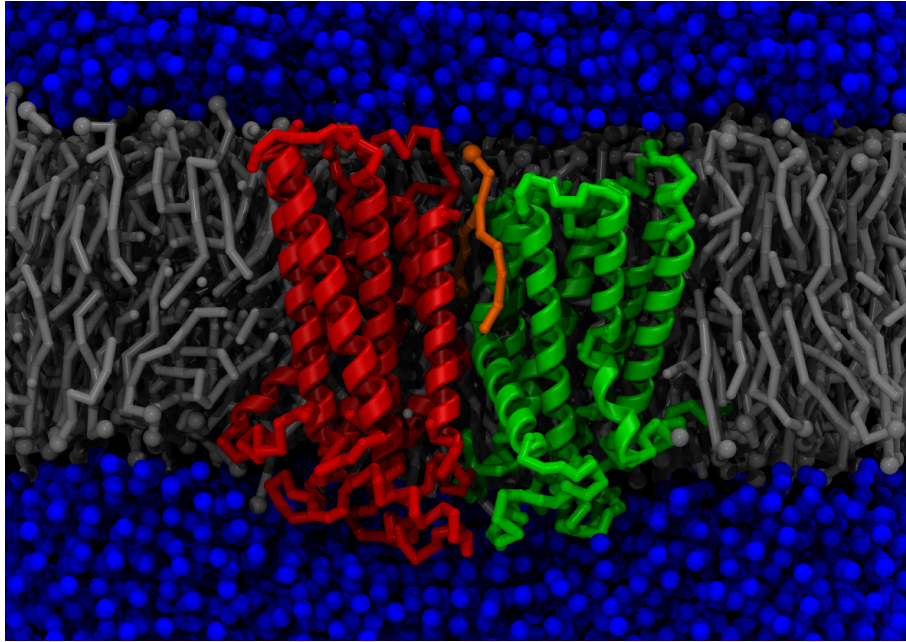


Figure 3.5: *The dimer structure of β_2 -adrenergic receptor in POPC bilayer. Two receptor molecules are shown in red and green; lipid molecules are shown in gray, and the surrounding water molecules in blue. A POPC molecule that was found to be present at the dimer interface is highlighted in orange.*

general, an increased presence of transmembrane helices I and II was observed with increasing cholesterol concentrations. We refer to an interface containing different transmembrane helices from the two receptors as a hetero-interface. The dimer interface in membranes containing 9% and 30% cholesterol was most often a hetero-interface, formed by transmembrane helices I and II of one receptor and transmembrane helices IV and V of the other. An example of a homo-interface was also observed in membranes containing 9% cholesterol involving transmembrane helices IV and V. At 30% membrane cholesterol, the rotation of the receptors around the contact point led to the occasional involvement of the adjacent transmembrane helices III and VII. At 50% membrane cholesterol, the dimer interface was formed mainly by transmembrane helices I and II from both receptors (see Fig. 3.3, d and h). A snapshot of the final dimer structure is shown in Fig. 3.6.

The adjacent transmembrane helix VII was also observed to be occasionally involved at the dimer interface due to rotation of the receptors around the contact point (see Fig. 3.4d). In this conformation, the C-terminal helix VIII was also occasionally found to be present at the dimer interface. The results obtained were consistent for the three replicate simulations performed.

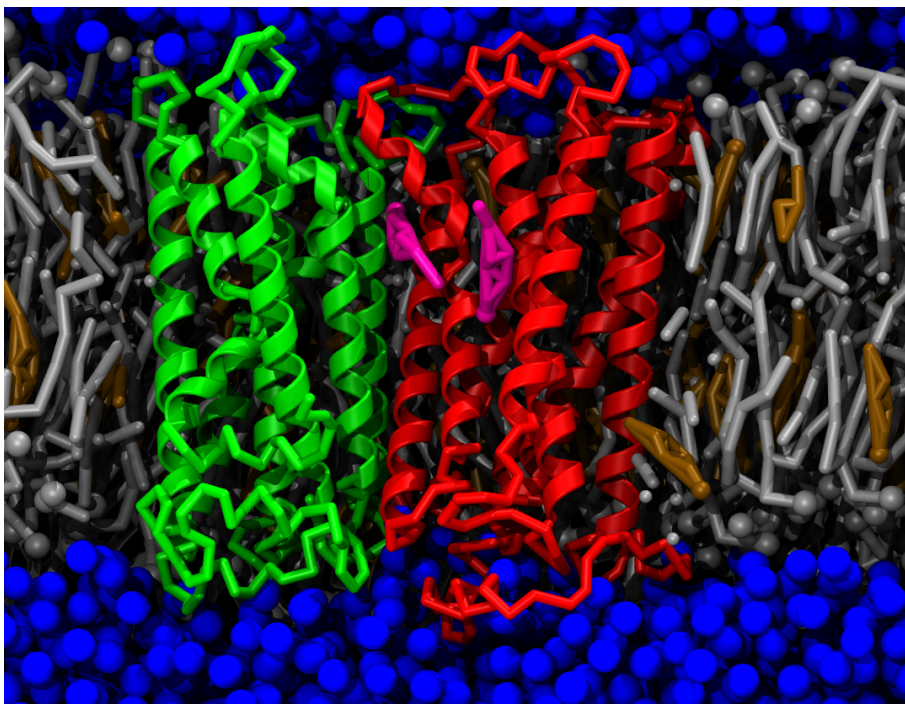


Figure 3.6: *The dimer structure of β_2 -adrenergic receptor in POPC bilayer containing 50% cholesterol. Two receptor molecules are shown in red and green; lipid molecules are shown in gray, cholesterol molecules in brown, and the surrounding water molecules in blue. Cholesterol molecules bound at the dimer interface and on transmembrane helix IV are highlighted in magenta.*

Taken together, these results show that the presence of cholesterol in the membrane increases the involvement of transmembrane helices I and II, and restricts the presence of transmembrane helix IV at the dimer interface of the β_2 -adrenergic receptor. This observation could have potential implications for designing drugs for GPCR targets (see below).

3.3.4 Cholesterol occupancy at transmembrane helix IV restricts its involvement in the dimer interface

To understand whether a direct receptor-cholesterol interaction or indirect effects (such as the alteration of membrane properties) are responsible for the modulation of the dimer interface with increasing membrane cholesterol content, we analyzed cholesterol density around the transmembrane helices. A density map of the cholesterol population around the receptor, analyzed over several z slices, is shown in Fig. 3.7.

We identified three sites of high cholesterol density in the outer leaflet and four sites in the lower leaflet. Importantly, we identified a site on transmembrane helix IV with the highest

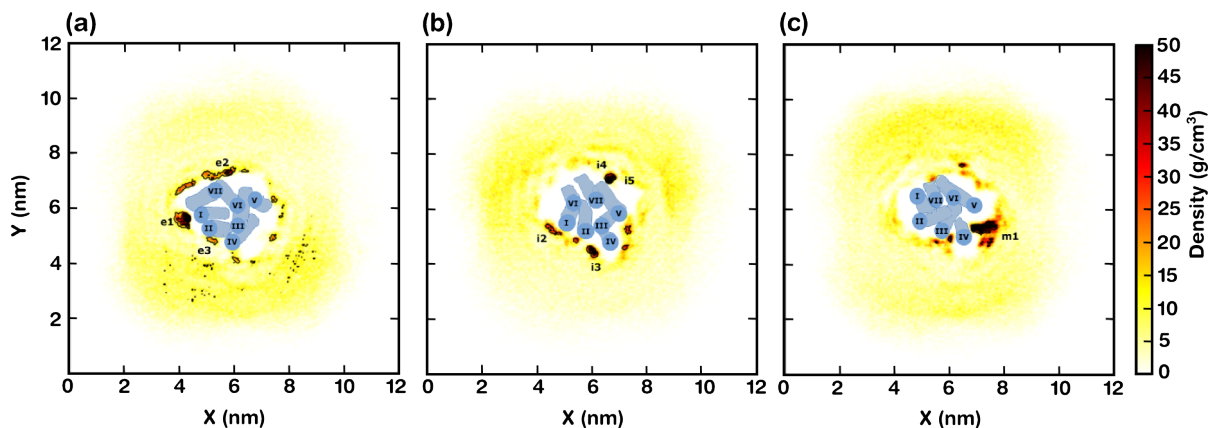


Figure 3.7: The 2-D projections of the spatial density function (SDF) of cholesterol around a monomer of the β_2 -adrenergic receptor. The SDFs were calculated for Z-slices along (a) the extracellular leaflet, (b) the intracellular leaflet and (c) the center of the membrane, respectively. The cartoon representation of the helix backbone atoms (2-D projection) of the receptor is shown in blue for comparison. The regions of highest cholesterol density are marked with e (extracellular leaflet), i (intracellular leaflet) and m (membrane) as defined in Cang et al. (³⁰⁵).

density in the middle of the bilayer. Although a few hot spots of interactions could be identified, very few unbinding events at the highest density sites were observed since the cholesterol occupancy at these spots was of the order of μ s. In the absence of sampling (i.e., in the absence of adequate binding/unbinding events at all interaction sites), measures based on population densities will necessarily be biased. To exclusively account for specific binding events, we calculated the maximum occupancy time of cholesterol around each of the transmembrane helices during the simulation. We defined the maximum occupancy time as the maximum time a given cholesterol molecule was continuously bound to a given site, normalized to the simulation length. A value of one implies that the cholesterol molecule was present at the given site throughout the entire simulation time, and zero implies it was never present at that site. The simulations were divided into two regimes: the first corresponding to monomeric receptors and the second corresponding to the receptor dimers. The maximum occupancy time of cholesterol around the transmembrane helices averaged over the three replicates performed for each cholesterol concentration is shown in Fig. 3.8.

In general, we observed the longest occupancy of cholesterol at transmembrane helix IV. In the monomeric regime (Fig. 3.8, a, c, and e), the maximum occupancy at transmembrane helix IV increased with increasing cholesterol concentration. At the highest cholesterol concentration (50%), the maximum occupancy of cholesterol at transmembrane helix IV was considerably

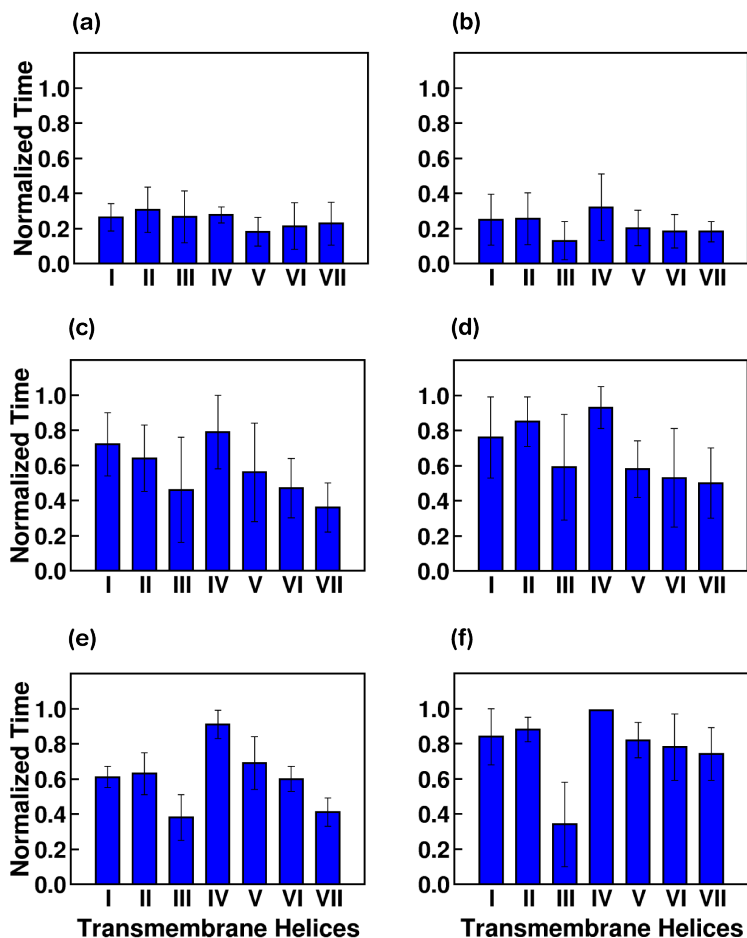


Figure 3.8: Cholesterol occupancy at the β_2 -adrenergic receptor (maximum occupancy time of cholesterol, *i.e.*, the maximum time a given cholesterol molecule was continuously bound to each of the transmembrane helices). (a–f) The values shown are normalized and averaged for three simulations at increasing cholesterol concentrations: 9% (a and b), 30% (c and d), and 50% (e and f). The simulations were divided into two regimes: the monomer regime (a, c, and e) and the dimer regime (b, d, and f). A maximum occupancy time of one implies that a given cholesterol molecule was present at the given site throughout the entire simulation time, and a value of zero implies it was always absent from that site. The error bars represent the Standard Deviation (SD) between the simulations.

higher than in other transmembrane helices (Fig. 3.8, e and f). Taken together, these results point to a cholesterol-binding site on transmembrane helix IV whose occupancy is stochastic and dependent on the membrane cholesterol concentration. In the absence of several binding/unbinding events, the highest-occupancy sites observed in our simulations compare well with the highest-density sites, but need not correspond to binding sites with large favorable free energy.

Interestingly, the increased presence of a cholesterol molecule at transmembrane helix IV in

the monomeric regime correlated well with the decreased presence of this helix at the final dimer interface. At 50% membrane cholesterol concentration, the maximum occupancy of cholesterol at transmembrane helix IV was much higher than at 9% cholesterol, and a lower involvement of transmembrane helix IV was observed at the dimer interface. At 9% and 30% membrane cholesterol concentrations, the occupancy of cholesterol at transmembrane helix IV was usually higher in one of the receptors compared with the other, and in general a hetero-interface involving transmembrane helices I and II from one receptor and transmembrane helices IV and V from the other was observed (see Fig. 3.4, b and c). At 9% cholesterol concentration, a single instance of homointerface involving only transmembrane helices IV and V was observed. Analysis of that individual trajectory showed that the cholesterol occupancy around transmembrane helix IV in the monomeric regime was very low in both receptors under that condition. We therefore hypothesize that a high occupancy of cholesterol at transmembrane helix IV, i.e., a stable occupancy of cholesterol at that site, interferes with its subsequent participation in dimer interface formation.

3.3.5 Cholesterol occupancy site at transmembrane helix IV

To explore the molecular details of the cholesterol occupancy site at transmembrane helix IV, we calculated a residue-based distance map between the bound cholesterol and the amino acid residues on transmembrane helix IV. A high dynamics was observed at the site and a few representative snapshots are depicted in Fig. 3.9.

One of these sites (Fig. 3.9, a and b) corresponds to the CCM site reported in the crystal structure⁷⁴. This site is at amino acid residues R151, I154, and W158 (the corresponding Ballesteros-Weinstein numbers are given in Table 3.2).

The cholesterol molecule diffuses on a μ s timescale (Fig. 3.9, c-f) to sample site m1 (as defined in Fig. 3.7) at amino acid residues W158 and I159. In the first site, the polar bead of the cholesterol molecule (modeling the terminal hydroxyl group), interacts with the charged residue R151. At site m1, the polar bead interacts mainly with the aromatic residue W158. The nonpolar beads of the cholesterol molecule interact mainly with nonpolar amino acid residues, such as I153, I154, V157, and I159. Although the most favorable interaction between the cholesterol molecule and the receptor occurs on transmembrane helix IV, several contacts are also observed with the adjacent transmembrane helices II and III.

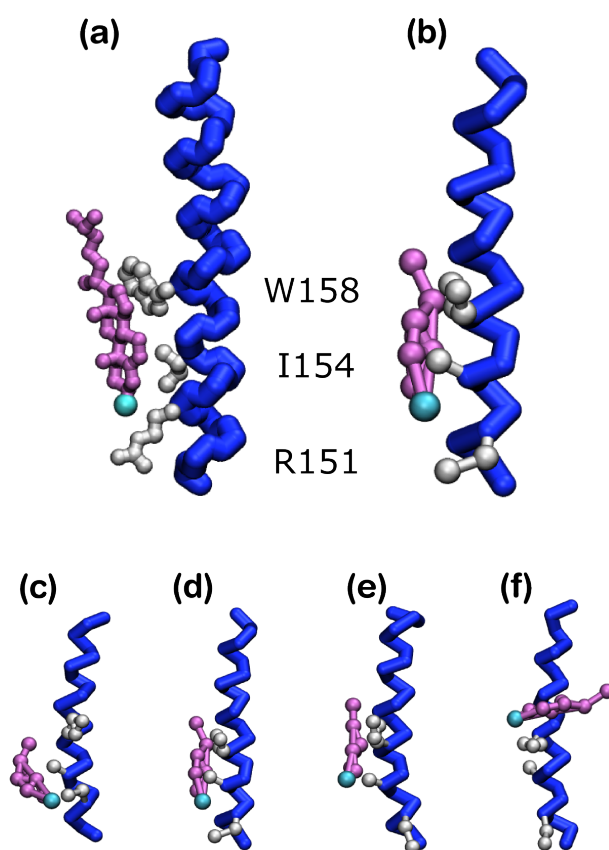


Figure 3.9: Cholesterol-binding sites on transmembrane helix IV of the β_2 -adrenergic receptor. (a) The CCM site observed in the crystal structure (⁷⁴). (b) The cholesterol-binding site identified in the coarse-grained simulations that directly corresponds to the CCM site. (c-f) A high dynamics was observed for the cholesterol and additional conformations of the cholesterol near the site. The backbone of transmembrane helix IV is shown in blue, and the side chains of the amino acid residues R151, I154, and W158 are shown in gray. The bound cholesterol molecule is shown in magenta and the polar bead representing the -OH group is depicted in blue. For clarity, the surrounding receptors, lipid, cholesterol, and water molecules are not shown.

3.3.6 POPC binding site at the dimer interface

As discussed above, the final dimer structures formed in POPC bilayers revealed the presence of a phospholipid molecule at the dimer interface (see Fig. 3.5). The binding of the POPC molecule at the dimer interface was also observed at 30% and 50% membrane cholesterol. Due to the variation in the transmembrane helices present at the interface in the absence and presence of cholesterol, we could not discern any consensus sequence. Two such POPC-binding sites are shown in Fig. 3.10 and correspond to the bilayers of POPC and POPC/30% cholesterol.

The zwitterionic head group of the POPC interacts with either a charged residue such

Table 3.2: Ballesteros Weinstein (B-W) numbering of transmembrane helices in β_2 -adrenergic receptor

Transmembrane helix	Sequence	B-W numbering	Most conserved residue
I	G35-I58	1.34 - 1.57	N51
II	I72-L95	2.43 - 2.66	D79
III	E107-D130	3.26 - 3.49	R131
IV	R151-Y174	4.43 - 4.66	W158
V	Q197-S220	5.36 - 5.59	P211
VI	L275-I298	6.37 - 6.60	P288
VII	E306-S329	7.33 - 7.56	P323

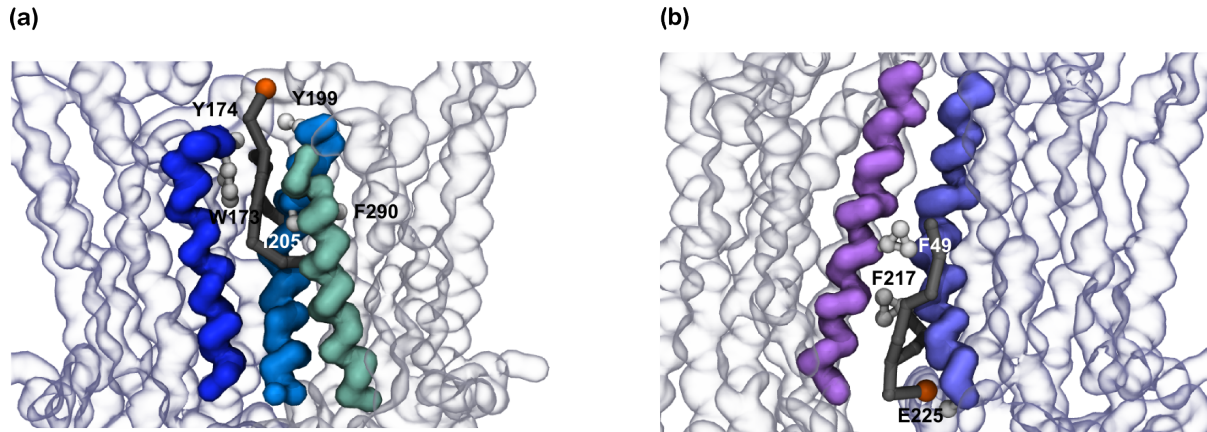


Figure 3.10: Two representative snapshots of the POPC binding sites at the dimer interface of the β_2 -adrenergic receptor. The helices that directly interact with the lipid are colored in the color scheme used previously (see Fig. 3.1); the remaining helices are shown as translucent. The amino acid residues interacting with the lipid are labeled. The bound POPC molecule is shown in dark gray with the head group bead represented in orange. Surrounding lipid, cholesterol and water molecules are not shown for clarity.

as E225 or polar aromatic residues such as Y199. The fatty acyl chain of the phospholipid molecule interacts mainly with nonpolar residues such as I205 or aromatic residues such as F217.

3.4 Discussion

GPCR organization represents a crucial determinant in cellular signaling³¹⁷. The heterogeneous distribution of GPCRs in membrane domains characterized by different lipid compositions has given rise to new challenges and complexities in receptor signaling. Therefore, cellular signaling

has to be considered in the context of organization of various signaling components, including receptors, lipids, and G-proteins. In this context, several questions remain unexplored regarding the molecular details of receptor association and oligomerization. In this work, we analyzed the effect of membrane cholesterol on the dimerization of the β_2 -adrenergic receptor. The novel (to our knowledge) aspect of our work stems from the fact that we correlated the molecular-level receptor-cholesterol interaction with modulation of the receptor dimerization process. We performed multiple μ s-timescale, coarse-grained simulations that allowed us to explore the interface for receptor dimers in lipid bilayers at several cholesterol concentrations. We showed that cholesterol modulates the dimer interface of the β_2 -adrenergic receptor by binding to a cholesterol occupancy site on transmembrane helix IV.

3.4.1 Exploring the energy landscape by unbiased simulations

It is difficult to explore the complex energetics of GPCR organization due to the limited methodologies available to probe these processes. Unbiased atomistic molecular dynamics simulations have been used extensively to probe protein and membrane dynamics that occur on the nanosecond timescale^{304,305,318–325}. With increasing computational power, unbiased atomistic simulations have been used to study phenomena on the μ s timescale^{225,326,327}. Unbiased coarse-grained simulations are increasingly being used to explore μ s-timescale dynamics and organization^{268,328–333}. In particular, coarse-grained simulations using unbiased sampling have improved our understanding of GPCR association^{233,334}. Although unbiased molecular-dynamics simulations can better represent the equilibrium evolution of the system without any external bias (potential/force) or reaction coordinate, they are limited by the phase space they sample^{225,335}. Biased simulations such as umbrella sampling and force pulling are often performed to improve sampling, and with careful analysis can be used to estimate the underlying unbiased true energy landscape. In two previous studies, these methods were employed to calculate a potential of mean force (PMF) of GPCR association along a given reaction coordinate (interhelical distance)^{234,236}. In both studies, a 1D PMF was calculated for only limited dimer interfaces (e.g., a 1/7 interface) and the sampling of the other dimer interfaces was absent. Importantly, recent work suggested that even for the association of single transmembrane helices, 1D PMFs result in limited sampling and overestimate the energetics^{336–338}. The limited sampling arises from slow membrane dynamics, and biased simulations of membrane

partitioning were recently shown to over- or underestimate the underlying (unbiased) energy landscape^{339–341}. Consequently, it still remains difficult to achieve a complete thermodynamic understanding of GPCR association in different membrane compositions. In this work, we carried out multiple unbiased coarse-grained simulations totaling ~ 1 ms to analyze the association between two GPCRs and probe the role of the membrane lipid environment. The membrane’s effects in driving and modulating receptor association within membranes have been usually neglected and the focus of our work is to understand these effects.

3.4.2 The dimer interface and comparison with experimental data

Most studies of the dimer interface of the β_2 -adrenergic receptor have employed indirect methods, and several dimer interfaces have been proposed^{159,342}. Interfaces involving transmembrane helix VI¹⁵⁹ or helix VIII³⁴² have been proposed based on results obtained by different techniques. The most direct evidence for dimer interfaces comes from the related β_1 -adrenergic receptor¹⁴⁷. The crystal structure of the ligand-free basal structure of the β_1 -adrenergic receptor shows two distinct dimer structures: one involving transmembrane helices I and II and helix VIII, and the other involving transmembrane helices IV and V. The two dimer interfaces observed in the crystal structure correspond to the two homo-interfaces observed in our simulations (see Fig. 3.11), and no crystal contacts were observed that correspond to the hetero-interface.

However, we propose that although both dimer interfaces are energetically favorable, the membrane environment (cholesterol) tunes the energetics to modulate the relative populations.

3.4.3 Structural plasticity of the dimeric interface

The various dimer interfaces of the β_2 -adrenergic receptor revealed by various experimental methods^{147,159,342} suggest that the energetics of association via the different dimer interfaces are comparable and perhaps dependent on the experimental conditions. In a recent biased molecular dynamics simulation of the β_2 -adrenergic receptor, Johnston et al.²³⁶ calculated the energetics of two interfaces and reported comparable stabilities for these two dimer interfaces. Although the dimer interfaces they considered were distinct from those observed in this report, their results confirmed a structural plasticity in the dimer structure. Similarly, relatively weak binding energetics was recently reported for different rhodopsin dimer interfaces and suggested

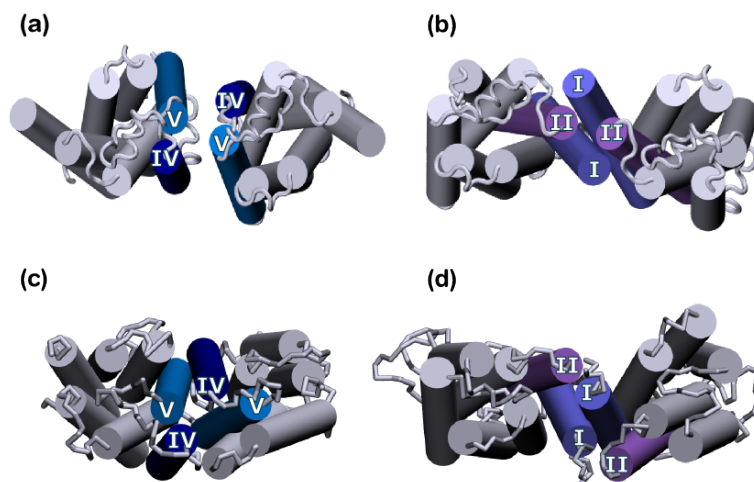


Figure 3.11: Comparison of the dimer interfaces of the β_1 -adrenergic receptor and the β_2 -adrenergic receptor. (a and b) Crystal structure of the β_1 -adrenergic receptor (83). (c and d) Dimer structures of the β_2 -adrenergic receptor obtained from coarse-grained simulations at 0% and 50% cholesterol concentration, respectively. The transmembrane helices that comprise the dimer interface are colored and labeled.

to be relevant in the context of the supramolecular organization of GPCRs²³⁴. Our data suggest a similar plasticity of the dimer interface for the β_2 -adrenergic receptor, further modulated by the membrane cholesterol. A total of 49 orientations are possible, considering a simple interaction matrix between the seven transmembrane helices. In our set of 12 simulations, several of these interfaces were sampled. To test the plasticity and relative stabilities of the dimer interfaces, we performed 10 additional shorter simulations at each cholesterol concentration. A comprehensive contact map with the increased sampling is shown in Fig. 3.12.

The highest-population interfaces correspond to the most stable interfaces observed in the first set of simulations, i.e., a homo-interface involving transmembrane helices IV and V, a hetero-interface with transmembrane helices IV and V, and I and II, and another homo-interface involving transmembrane helices I and II. The plasticity in the dimer interfaces can be easily appreciated in terms of the relative populations of interfaces observed in the contact maps. Since the plasticity emerges from the comparable energetics of the interfaces, the modulation of the energetics by the environment results in changes in the relative populations of these interfaces.

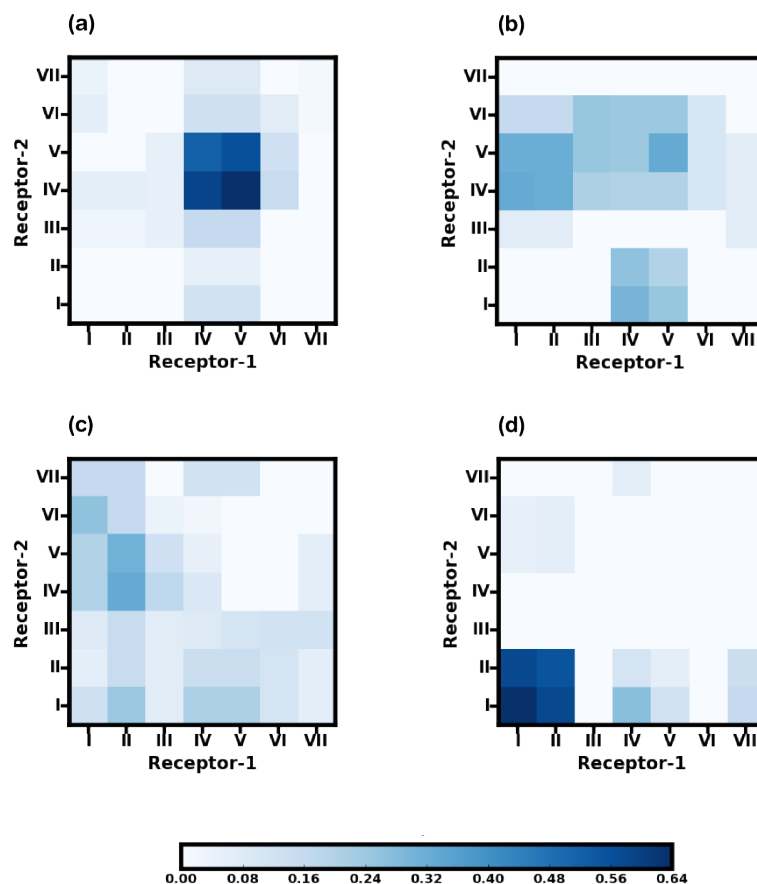


Figure 3.12: Contact maps depicting the helix-helix interactions between the two receptors. The contact maps were calculated for a total of 52 simulations (original set and additional 10 X 4 simulations). Panel (a) corresponds to POPC bilayer; panels (b), (c) and (d) correspond to POPC bilayers containing 9, 30, and 50% cholesterol, respectively. The values were calculated as an average over all simulations and normalized by the time of occurrence and simulation length. A cut-off distance of 0.5 nm was used to determine the contact residues.

3.4.4 Cholesterol occupancy sites

Lipid-receptor interactions are especially significant for GPCRs because they undergo conformational changes to carry out their function, giving rise to structural plasticity^{343,344}. These cooperative conformational changes involve the participation of surrounding lipid molecules, and various conformations are stabilized by the binding of different lipids. One of the first reports of a cholesterol-binding site in GPCRs was based on the crystal structure of the β_2 -adrenergic receptor^{74,102}, in which a stably bound cholesterol was reported. It should be noted that GPCRs are known to behave differently in cubic and lamellar lipidic mesophases³⁴⁵, and the cholesterol-binding site, termed the cholesterol consensus motif (CCM), could be specific to

the membrane lipid environment. Interestingly, one of the binding modes of cholesterol at helix IV we observed in our coarse-grained simulation correlates well with the CCM site reported in the crystal structure⁷⁴, indicating that cholesterol occupancy at this site is independent of the lipid packing arrangement (see Fig. 3.9). Cholesterol occupancy on helices V and VII, which contain another putative cholesterol-binding site (the CRAC motif³⁴⁶), is also relatively high, but much lower than on helix IV. These results are consistent with the dynamic nature of cholesterol binding to GPCRs predicted from previous molecular-dynamics studies^{125,304,305}. High occupancy of cholesterol at this site on helix IV was observed in both monomer and dimer states. More importantly, our results show that cholesterol occupancy at this site leads to modulation of the final dimer structures obtained. As stated above, this implies that the underlying energy landscape of receptor dimerization, i.e., the relative stabilities of these dimer interfaces, can be modulated by interaction with membrane cholesterol.

3.4.5 Functional significance of cholesterol-mediated dimer interfaces

The β_2 -adrenergic receptor was recently cocrystallized with the stimulatory G-protein (Gs), and the receptor-Gs protein interface was shown to be formed by transmembrane helices V and VI¹¹⁰. Although monomers of the β_2 -adrenergic receptor were reported to be sufficient for signaling¹¹², the receptor was demonstrated to be present as a dimer *in vivo*¹¹⁴, and receptor organization was shown to be important for its function¹⁵⁹. If the receptor-Gs protein interaction includes a receptor dimer, the dimer interface observed in our simulations in POPC bilayers could lead to potential steric hindrance with the Gs protein since it involves transmembrane helix V. In the presence of increasing membrane cholesterol, transmembrane helix V from either one receptor or both receptors becomes progressively available for association with the G α s subunit. We speculate that in the altered dimer conformation in the presence of cholesterol, the β_2 -adrenergic receptor dimer can interact more favorably with the G α s subunit. Due to the comparable energies of the different dimer interfaces of β_2 -adrenergic receptor^{234,236}, the dimer interfaces observed in our simulations in the presence and absence of cholesterol only represent the most populated dimer interfaces and it is possible that other dimer conformations could be sampled under different conditions. To the best of our knowledge, our results constitute the first report of the modulation of the dimeric structure of a GPCR by the membrane cholesterol.

Knowledge about GPCR dimer models would allow the development of dimeric or bivalent

drugs that could interact with both monomers in a dimer, and open up new possibilities in drug discovery³⁴⁷. The modulation of GPCR dimer structure by membrane cholesterol could have interesting and far-reaching applications in cellular physiology and drug discovery. Cellular cholesterol is known to be developmentally regulated and its content increases with aging^{348,349}. This could imply that the organization of GPCR oligomers is age dependent. The efficacy of a specific drug designed to target a GPCR dimeric interface could therefore change with the process of aging. Interestingly, the membrane lipid environment of GPCRs has been implicated in disease progression during aging³⁵⁰. In addition, there is a strong asymmetry in the manner in which cholesterol is distributed among various organs and tissues in the human body. In other words, the distribution of cholesterol among various tissues is not uniform. The central nervous system, which accounts for only $\sim 2\%$ of the body mass, contains $\sim 25\%$ of the free cholesterol present in the whole body³⁵¹. This means that GPCR oligomerization could be tissue specific. With the development of new technologies to detect GPCR oligomers in native tissues¹⁵⁴, this could represent an exciting possibility. Importantly, the fact that the same GPCR could be present in multiple tissues may pose a considerable challenge in designing drugs suitable for the dimer interface.


In conclusion, using multiple coarse-grained simulations of the β_2 -adrenergic receptor in membranes with varying lipid composition, we have shown that the dimerization process of the β_2 -adrenergic receptor is modulated by membrane cholesterol. More specifically, we showed that cholesterol occupancy at transmembrane helix IV restricts its involvement at the dimer interface and stabilizes a dimer interface with transmembrane helices I and II instead of transmembrane helices IV and V. However it is unclear if conformational modulation of dimer interface in β_2 -adrenergic receptor is solely mediated through specific interaction between the receptor and cholesterol. Based on our results, it appears that dimer plasticity is relevant not just as an organizational principle but also as a regulatory principle for GPCR function. Understanding the cross talk between GPCRs and cholesterol represents an important step in our overall understanding of GPCR function in health and disease.

Role of Lipid-Mediated Effects in β_2 -Adrenergic Receptor Dimerization

“It sounds plausible enough tonight, but wait until tomorrow. Wait for the common sense of the morning.”

– H.G. Wells, *The Time Machine*

4.1 Introduction

The molecular details of receptor-lipid interactions are being increasingly probed at the atomistic resolution by computational methods, such as molecular dynamics simulations. With increase in computational power, longer timescale atomistic simulations of GPCR monomers have been performed^{352–355}. The simulations have probed detailed GPCR dynamics and identified several important protein-lipid interactions. Specific cholesterol binding sites have also been proposed based on μ s timescale simulations^{125,304,305}. To understand the more complex higher-order organization of GPCRs, coarse-grained methods have been used^{233,334} that suggest hydrophobic mismatch as an important driving force. Additionally, we have shown that membrane composition can directly modulate the dimer interface of the β_2 -adrenergic receptor²³⁸. Dimerization profiles have also been calculated by biased molecular dynamics for a few interfaces, but focused mainly on the protein energetics^{234,236}. It is becoming increasingly clear that GPCR association is modulated by the membrane environment, although a more

detailed investigation of the receptor-lipid interactions is still missing. Importantly, the significance of cholesterol in modulating receptor organization has been established, but the role of the phospholipids in modulating organization remains largely unexplored.

In this work, we study the interaction of the β_2 -adrenergic receptor with the membrane lipids and explore the direct and indirect membrane effects that could be important in receptor dimerization. In a previous study, we have carried out coarse-grained molecular dynamics simulations of the β_2 -adrenergic receptor in membranes of varying cholesterol composition²³⁸. We have shown that cholesterol “hot-spots” present on the receptor surface could modulate the receptor dimerization. Here, we examine the role of the membrane lipids in driving and modulating receptor dimerization. We first calculate the hydrophobic mismatch in the monomeric and dimeric regimes, and compare its role in driving association. We also explore direct lipid binding sites in the receptor monomers and dimers. We have identified a putative lipid-binding site between transmembrane helices I and VII that shows a high occupancy by a lipid molecule. Our results show that both direct and indirect membrane effects contribute toward the dimerization of the receptor.

4.2 Methods

4.2.1 System setup

Molecular dynamics simulations of the membrane embedded β_2 -adrenergic receptor were carried out in POP bilayers in the absence and presence of 50 % cholesterol. The systems were represented using the MARTINI coarse-grained force-field (version 2.1)^{232,283}. We have used the MARTINI forcefield in our study since it has been shown to be suitable for applications such as membrane protein association^{234,309–311} and partitioning of membrane proteins between membrane domains of varying compositions^{266,312}. A homology model of β_2 -adrenergic receptor (amino acid residues 29–342) was generated from crystal structure (PDB: 2RH1) using the software SWISSMODEL³¹³. Bilayers containing POPC and with 50% cholesterol concentration were generated from an initial conformation of randomly placed POPC, cholesterol and water molecules. For the simulations of the monomeric receptor, a single copy of the receptor in its coarse-grained representation was embedded at the middle of an equilibrated bilayer and simulated for 5 μ s. For the dimer simulations, two copies of the receptor, in its coarse-grained

representation, were embedded into the equilibrated membrane, such that the inter-receptor distance (centre of mass) was at least 6 nm (minimum distance at least 3 nm). After the receptors associated, the dimer regime was simulated for a further 20 μ s. Further details of the simulations are described in our previous study²³⁸.

4.2.2 Simulation parameters

All simulations were performed using the GROMACS simulation package, version 4.5.4³¹⁴. The cut-off for nonbonded interactions was 1.2 nm with electrostatic interactions shifted to 0 in the range 0-1.2 nm and Lennard-Jones interactions shifted to 0 in the range 0.9-1.2 nm. A relative electrostatic screening of 15 was used. The temperature for each group was weakly coupled using Berendsen thermostat algorithm with a coupling constant of 0.1 ps to maintain a constant temperature of 300 K during simulation³¹⁵. Semi-isotropic pressure was maintained using Berendsen barostat algorithm with a pressure of 1 bar independently in the plane of the membrane and perpendicular to the membrane with a coupling constant of 0.5 ps and a compressibility of $3 \times 10^{-5} \text{bar}^{-1}$. The time step used in the simulations was 20 fs. Simulations were rendered using VMD software³¹⁶.

4.2.3 Analysis

Local membrane thickness:

The local membrane thickness was calculated from the difference in the z -position of the PO_4 bead of the POPC molecule. The values were calculated by binning the bilayer into 0.5 nm bins and averaging over the trajectory. To compare between different membrane compositions, a normalized membrane thickness has been defined: $X_{norm} = X/X_{av}$, where X is the local bilayer thickness and X_{av} the average bilayer thickness in the bulk membrane. Correspondingly, the bilayer thickness far from the receptor is 1, and local thickening or thinning will be denoted by a value greater than or less than 1, respectively. A snapshot of the receptor has been superimposed on the 2D local thickness profile.

Spatial density function (SDF):

The spatial distribution of the phospholipid molecules around the β_2 -adrenergic receptor was calculated as the 3D spatial distribution function of the lipid beads. The SDF was calculated from the last 5 μ s trajectory by using the g-spatial program in the Gromacs package. The voxel element was set to 0.1 nm in each direction. In general, the SDF reflects the average 3D density distribution of the lipids and therefore points toward the locations where lipid molecules reside with higher probability. The calculated 3D SDFs were averaged over the extracellular and intracellular leaflets by projecting onto the upper and lower membrane planes, respectively. A snapshot of the receptor has been superimposed on the projected SDFs.

Energetics:

The protein-protein, protein-lipid, and lipid-lipid interaction energies were calculated by summing the Lennard-Jones and Coulomb terms. For POPC-cholesterol bilayers, the contributions from POPC and cholesterol were summed. The values were binned at a bin size of 0.1 nm inter-receptor distance.

4.3 Results

Coarse-grained molecular dynamics simulations of β_2 -adrenergic receptors were performed in POPC bilayers in the absence and presence (50 %) of cholesterol. We have previously shown that cholesterol modulates the dimer interfaces of the β_2 -adrenergic receptor via cholesterol “hot-spots”²³⁸. Here, we extend our previous work to analyze the effects mediated by the lipids, both the direct and indirect effects, and probe their relation to receptor association.

4.3.1 Indirect effects: Hydrophobic mismatch around the receptor

We analyzed the local membrane thickness around a β_2 -adrenergic receptor, embedded in POPC bilayers containing 0 and 50% cholesterol (see Fig. 4.1). Since the thickness of the POPC-cholesterol bilayer is larger than the POPC bilayer³⁵⁶, we compare a normalized thickness between the two bilayers. The normalized thickness is defined as $X_{norm} = X/X_{av}$, where X is the local bilayer thickness and X_{av} the average bilayer thickness in the bulk membrane. This measure allows us to directly compare the local variations in the thickness compared to the

bulk membrane. In POPC bilayers, the thickness profile shows two distinct areas of increased thickness (Fig. 4.1a).

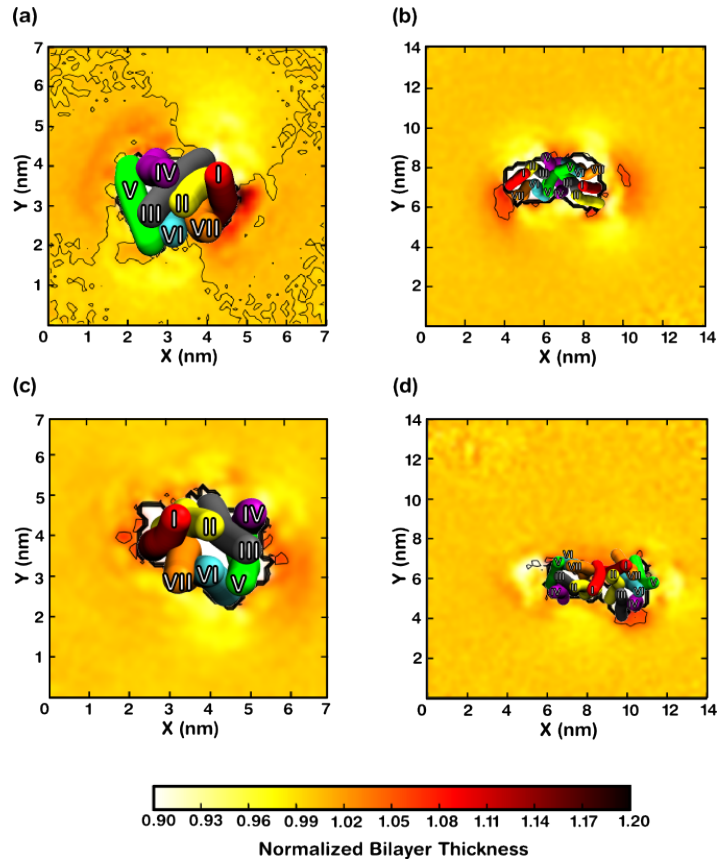


Figure 4.1: Bilayer thickness profile around the β_2 -adrenergic receptor in POPC bilayers with 0% (a and b) and 50% (c and d) cholesterol concentration. The profiles correspond to the monomer (left) and dimer (right) regimes of the receptor. To compare the local variations in the bilayer thickness, a normalized bilayer thickness is plotted. The top views of the receptor monomer and dimers are superimposed on the plots and transmembrane helices labeled. The transmembrane helices have been color coded as follows: I (red), II (yellow), III (gray), IV (purple), V (green), VI (cyan), VII (orange). Thickness profiles were generated with previously developed tools³⁵⁷.

The first site is localized around helix I and VII and the second site is located at helices IV and V. At the other faces of the receptor, membrane thinning was observed around the grooves formed by helices I, II and helices VI, VII. The same two sites show a positive mismatch in POPC-cholesterol bilayers (Fig. 4.1c), but the magnitude of the mismatch is less. The decrease in the magnitude of the mismatch is due to the increased membrane thickness in the presence of cholesterol. It is difficult to correlate residue-based hydrophobic length of the helices to the bilayer perturbations due to helix tilting, apolar flanking residues and asymmetric distribution

of apolar residues on different helix faces (Table 4.1).

Table 4.1: Length of the hydrophobic segment of the transmembrane helices in β_2 -adrenergic receptor

Transmembrane Helix	Helix Length (nm)	Helix length along the bilayer normal (nm)
I	3.7	2.6
II	3.6	2.9
III	3.8	3.4
IV	3.1	3.1
V	3.5	3.3
VI	3.7	3.5
VII	3.8	3.7

^a The hydrophobic segment of each transmembrane helix was calculated by measuring the average distance between the terminal backbone beads. To account for helix tilting, a second measure of the length component of transmembrane helix parallel to the bilayer normal was also calculated. The hydrophobic region of the bilayer, calculated as the average distance between the beads representing Sn2 glycerol ester carbon of POPC, is 3.25 nm.

To analyze the membrane profile around the receptor in the dimer regime, two dimer states corresponding to the most sampled states in our simulations were considered (see¹⁰¹). The dimer structure most populated in POPC bilayers with 0% cholesterol is defined by helices IV and V at the interface. At 50% cholesterol concentration, the most populated dimer structure comprised of helices I and II at the interface. A distinct relationship is seen between the helices that define the dimer interface and those that show a positive hydrophobic mismatch with the bilayer. The differences in the membrane thickness were less pronounced in the dimer regime, for both dimer structures. Interestingly, in the dimers observed in POPC bilayers, the thickness changes around helix I were reduced (Fig. 4.1b), although the helix was not in the dimer interface. In the dimer states in POPC bilayers with 50% cholesterol, an asymmetric thickening around helix I persisted, though it was involved at the dimer interface (Fig. 4.1d). Although there appears to be a distinct connection between hydrophobic mismatch and dimer interfaces, the relationship between the two is not straightforward. The decreased populations of helix I in the dimer interface in POPC bilayers, despite a high hydrophobic mismatch in the monomer regime, coupled with a complex mismatch pattern in the dimer states, points toward more complex dimerization behavior of the receptor.

4.3.2 Direct effects: Specific protein-lipid interactions

The spatial distribution function (SDF) of lipid molecules around the monomer was calculated for a representative simulation set and is plotted in Fig. 4.2. The density profiles of the POPC molecules was calculated over several z-slices and averaged over the extracellular and the intracellular leaflets separately. The regions of high density correspond to sites with the highest probability of finding a POPC molecule.

The SDF profile shows one distinct site between helices I and VII in the extracellular leaflet (Fig. 4.2a). In the inner leaflet, a more spread-out density was observed (Fig. 4.2b). The first site was centered around helix IV, and was close to the putative cholesterol binding site (CCM). The remaining sites were spread out over helices V, VI and VII. In the presence of cholesterol, a competition was observed between POPC and cholesterol molecules and at most sites POPC binding persisted. On the extracellular site, the SDF is high in the same groove, i.e. between I and VII, although the location appears to be shifted (Fig. 4.2c). The magnitude of the SDF in this groove is similar to that in POPC bilayers. In the intracellular site, the main region of high lipid distribution is located around helix IV, although the magnitude is reduced (Fig. 4.2d). The remaining regions of high density observed in POPC bilayers are further reduced in magnitude. Upon dimerization, the sites of high lipid density persist (Fig. 4.2e-h). Taken together, these results suggest a competition between cholesterol and POPC molecules at the putative cholesterol binding site at helix IV. In contrast, the high SDF site at helix VII appears to be stable and we propose it to be a putative lipid binding site.

To test the robustness of the density data and to exclusively account for the specific binding events, we calculated the maximum occupancy time of POPC around each of the transmembrane helices during the simulation (Fig. 4.3).

We defined the maximum occupancy time as the maximum time a given PO_4 bead of the POPC molecule was continuously bound to a given site, normalized to the simulation length. A value of 1 implies that the lipid molecule was present at the given site throughout the entire simulation time and 0 implies it was never present at that site. The values were averaged over ten simulations and the error bars denote the standard deviation between the simulations. A similar trend to the density profiles is observed in maximum occupancies. The maximum occupancy of POPC was the highest at helix VII at the extracellular leaflet and the highest at helix IV on the intracellular leaflet. In presence of cholesterol, the occupancy at both the sites

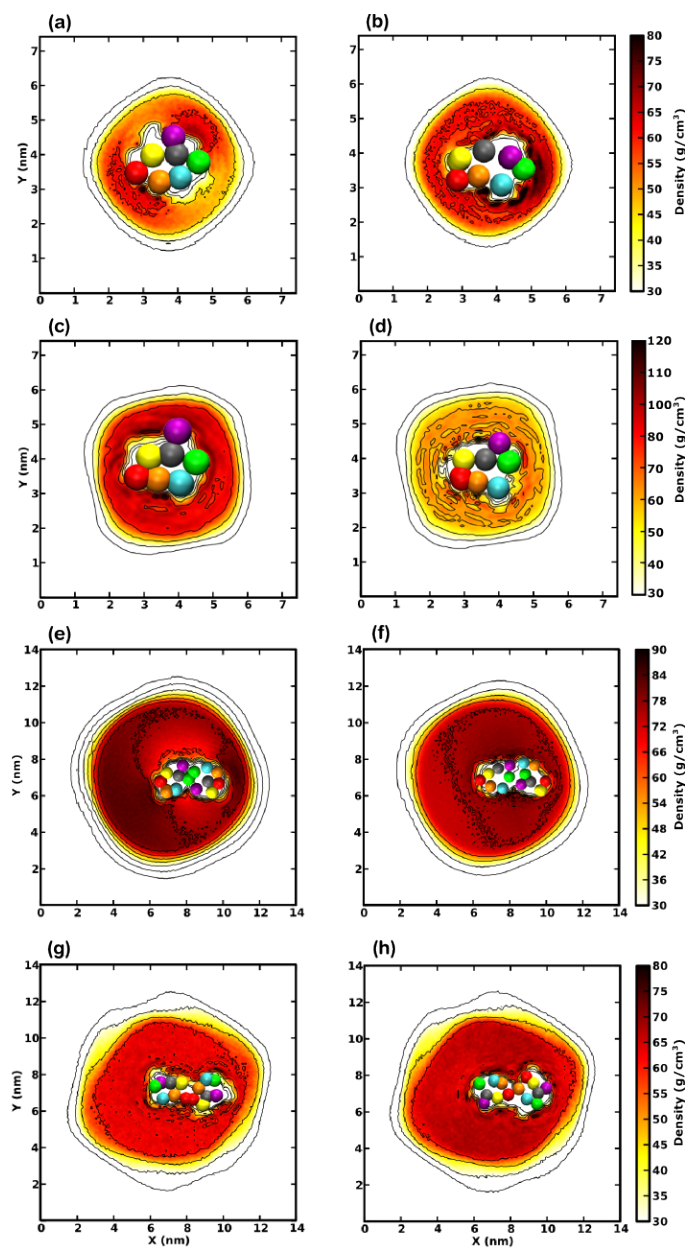


Figure 4.2: The spatial distribution function (SDF) of POPC around the β_2 -adrenergic receptor monomer in POPC bilayers with 0% (a,b) and 50% (c,d) cholesterol. The SDF is represented for the extracellular (a,c) and intracellular (b,d) leaflets separately. The SDF around the receptor dimer is shown for the extracellular (e,g) and intracellular (f,h) leaflets in POPC bilayers with 0% (e,f) and 50% (g,h) cholesterol concentration. The top views of the receptor monomer and dimers are superimposed on the plots.

decreases although the trend persists. Combining our data on the SDFs and occupancies, it is clear that POPC binding to some of these sites is specific.

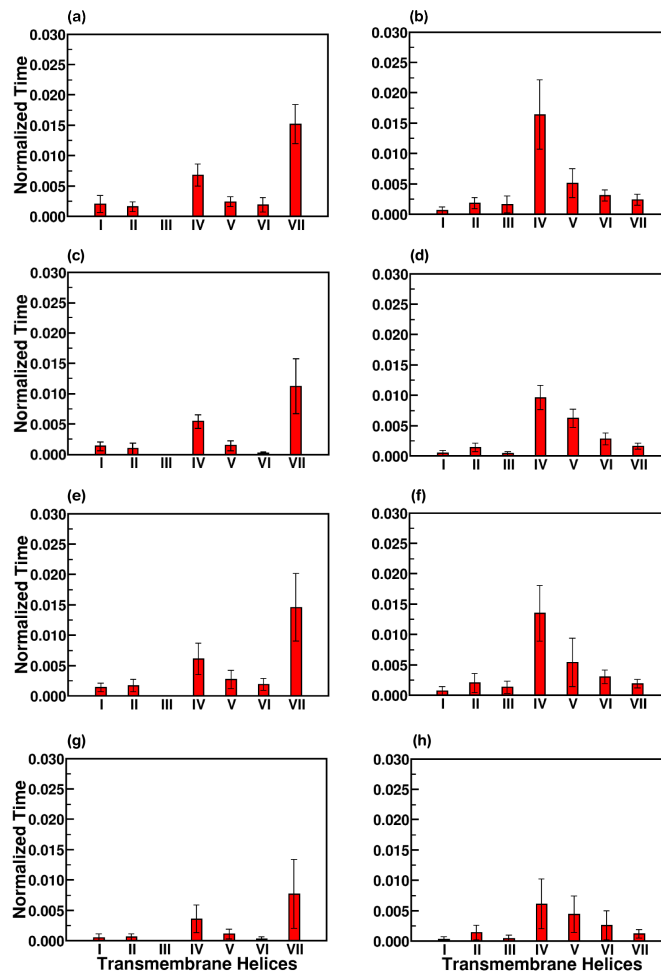


Figure 4.3: Maximum occupancy of POPC molecules around the β_2 -adrenergic receptor monomer in POPC bilayers with 0% (a,b) and 50% (c,d) cholesterol. The occupancy is shown for the extracellular (a,c) and intracellular (b,d) leaflets separately. The occupancy around the receptor dimer is shown for the extracellular (e,g) and intracellular (f,h) leaflets in POPC bilayers with 0% (e,f) and 50% (g,h) cholesterol concentration.

4.3.3 Characterization of the lipid site at helix I

To explore the molecular details of the POPC occupancy site at transmembrane helix VII, we calculated a residue-based distance map between the bound POPC molecule and the amino acid residues on transmembrane helix I and VII. A representative snapshot is shown in Fig. 4.4.

The head group beads are observed to interact with a charged residue, Glu306. Several aromatic and apolar residues line the lipid occupancy groove. Interestingly, the same site

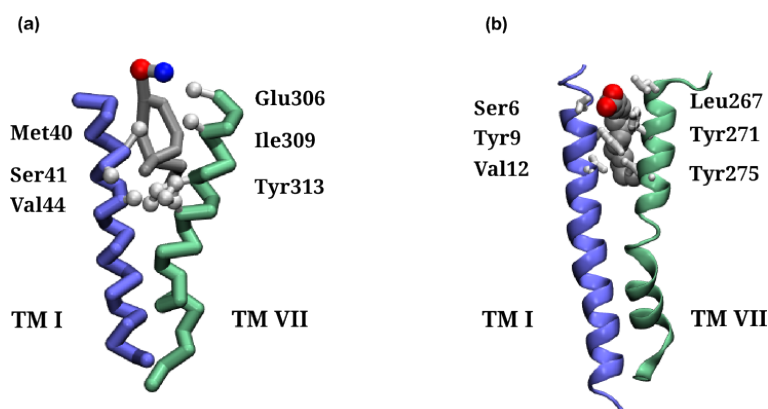


Figure 4.4: A schematic representation of (a) the high lipid occupancy site in seen in coarse-grained simulations and (b) the putative lipid binding site in the crystal structure of A_{2A} -adenosine receptor. Only transmembrane helices I and VII are shown for clarity. The side chains that are involved at the site are shown in light grey. The POPC molecule is represented in dark grey and the head-group PO_4 and $NC3$ beads are depicted as spheres.

has been identified as a putative lipid binding site in a recent high resolution A_{2A} -adenosine receptor structure³⁰². The lipid binding groove between helices I and VII from the crystal structure of the A_{2A} -adenosine receptor is also depicted in Fig. 4.4.

4.3.4 Exploring the energetics of association

The membrane effects described above are a consequence of the interplay between the energetics of the protein and the lipid. We have calculated the interaction energies as a function of inter-receptor separation (shown in Fig. 4.5).

The values shown are averaged over ten simulations, totaling about 130 μ s of total simulation time and are distinct from the free energy of dimerization. In POPC and POPC-cholesterol bilayers, the protein-protein interaction energy decreases expectedly as the receptors approach each other (Fig. 4.5a, b). A minimum could not be discerned at low inter-receptor distances, possibly due to the lack of sampling of unfavorable close contacts. Multiple smaller minima could be discerned along the pathway that could correspond to meta-stable states along the dimerization pathway. The protein-lipid interaction energy increased as the receptors approach each other due to the de-lipidation of the protein (Fig. 4.5c, d). The lipid-lipid interaction energy decreases correspondingly as the receptors associate and interact with each other (Fig. 4.5e, f). To fully understand the energetics of receptor association, free-energy calculations sampling over all possible receptor interfaces is required, that still remains a challenge within

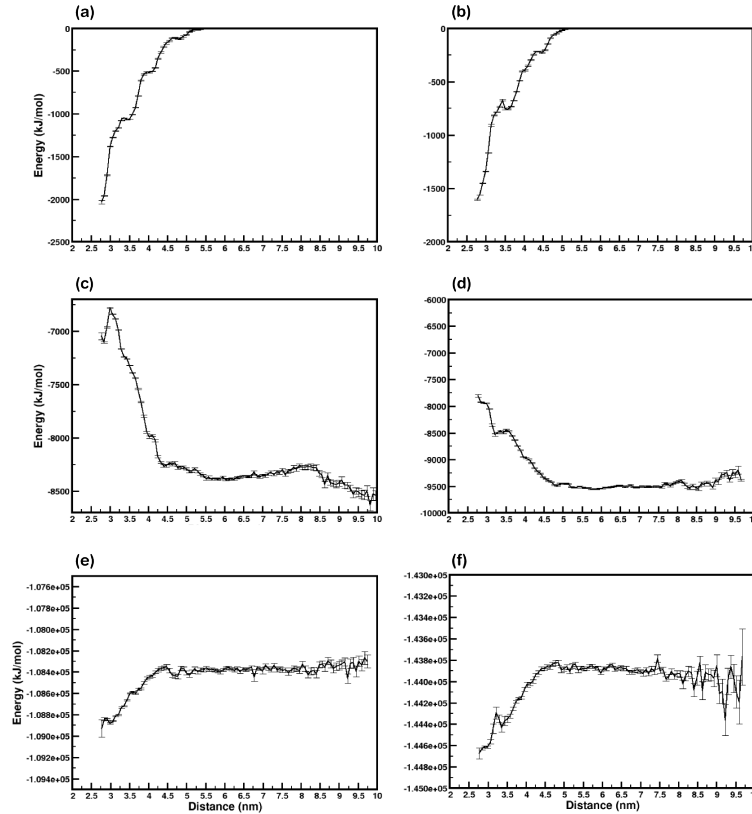


Figure 4.5: *The interaction energies as a function of inter-helical distance calculated for the protein-protein contacts in (a) POPC and (b) POPC-cholesterol bilayers; the protein-membrane interaction energies in (c) POPC and (d) POPC-cholesterol bilayers and the membrane-membrane interactions in (e) POPC and (f) POPC-cholesterol bilayers. The values for each membrane were calculated from ten simulations totaling about 130 μ s of simulation time.*

current computational methods.

4.4 Discussion

GPCR organization is a critical factor in cellular signaling³¹⁷ and understanding these processes within heterogeneous membrane compositions gives rise to new challenges and complexities. It is becoming clear that cellular signaling in general and GPCR function in particular has to be considered in the context of membrane organization and composition. In specific, the interplay between the receptor and the constituent membrane molecules needs to be probed. In this work, we have analyzed the membrane effects around the β_2 -adrenergic receptor. Both direct and indirect effects have been probed, together with the estimation of the membrane-protein

energetics. We have analyzed multiple μ s time scale coarse-grained simulations that allows us to explore the membrane effects in the presence and absence of cholesterol.

Hydrophobic mismatch as a driving force for GPCR association has been proposed previously for β_2 -adrenergic receptor³³⁴, rhodopsin^{233,358} and the opioid receptor³⁵⁹. Although there appears to be a distinct connection between the helices with the maximum hydrophobic mismatch and those present subsequently at the dimer interfaces, the relationship between the two is not straightforward. The decreased populations of helix I in the dimer interface is observed in POPC bilayers, despite a high hydrophobic mismatch in the monomer regime. This, coupled with a complex mismatch pattern in the dimer states, points toward more complex driving forces for receptor association. A more direct effect of the membrane environment on GPCR stability and organization is suggested based on the lipid and cholesterol binding sites that have been resolved in several GPCR crystal structures^{102,302}. Although cholesterol binding sites have been probed in detail^{125,304,305}, the lipid binding sites remain less explored. Here, using multiple μ s time scale coarse-grained simulations we propose a high occupancy site of POPC at helix VII of the β_2 -adrenergic receptor. A similar site has been observed in previous atomistic simulations of the β_2 -adrenergic receptor, but was not further characterized³⁰⁵. Interestingly, the same site is also proposed to be a lipid binding site based on the recent high-resolution crystal structure of the A_{2A}-adenosine receptor³⁰². We suggest that this site could play a role in the subsequent organization of the receptor and modulate the population of the dimer structures with helices I/VII at the interface.

Our results highlight the regulation of receptor dimerization in β_2 -adrenergic receptor through specific and non-specific interaction of cholesterol and phospholipid with the receptor. Cholesterol is shown to influence receptor organization in serotonin_{1A} receptor, a closely related member of serotonergic family^{122,123}. Specific sites for cholesterol binding have also been identified in serotonin_{1A} receptor^{125,346}. Given the role of specific cholesterol interaction in modulating dimerization in β_2 -adrenergic receptor²³⁸, such lipid-mediated effects could also be possibly involved in influencing receptor association in other GPCRs.

In conclusion, using multiple coarse-grained simulations of the β_2 -adrenergic receptor in POPC bilayers in the absence and presence (50%) of cholesterol, we have characterized lipid-protein interactions that could play an important role in the stabilization and organization of the receptor. We show the presence of hydrophobic mismatch at helices I/VII and IV/V,


that is reduced in the presence of cholesterol. Although there is a relation between the helices with maximum hydrophobic mismatch and its subsequent presence in the dimer interface, the relationship is not straightforward. We have further suggested a putative lipid binding site at helix VII that could play an important role in modulating the dimer interfaces. Based on our results, it appears that lipid-protein interactions play an important role in receptor dimerization. Understanding the underlying membrane-protein interactions will help us appreciate the complex nature of GPCR organization and its link to GPCR function in health and disease.

Cholesterol- dependent Conformational Plasticity in GPCR Dimers

“I cannot fix on the hour, or the spot, or the look or the words, which laid the foundation. It is too long ago. I was in the middle before I knew that I had begun.”

– Jane Austen, *Pride and Prejudice*

5.1 Introduction

olecular details on GPCR conformational states have begun to emerge as a result of recent success in structure determination of several GPCRs^{101,102,360}. In addition, recent advances in computational and NMR approaches have helped uncover molecular mechanisms of receptor activation^{361–366}. On the other hand, the molecular organization of GPCRs, especially in the context of their physiological role, is less explored^{367,368}. Recent studies have shown that the oligomerization of certain GPCRs is dynamic^{190,317} and constitutive^{122,369}. Membrane lipids (particularly cholesterol)^{122,123,238,370} and the cytoskeletal network^{122,370} have been implicated in the modulation of GPCR function and oligomerization. Receptor oligomerization has been suggested to increase the cross-talk between receptors³⁷¹ and potential downstream signaling capabilities of GPCRs, thereby providing a framework for

efficient and controlled signal transduction³⁶⁷. Receptor oligomerization assumes greater significance for better therapeutic strategies and recent exploratory studies have confirmed the increased specificity of multivalent drugs³⁷², as well as ligand sensitivity of the various dimer interfaces³⁷³. In this overall context, GPCR oligomerization is an emerging paradigm, and needs to be explored in detail to improve our understanding of GPCR function in health and disease.

In our previous studies, we characterized the molecular mechanisms of lipid mediated effects on receptor dimerization in β_2 -adrenergic receptor^{238,239}. In order to examine whether such mechanisms also modulate association among other GPCR members, we extended our investigation to serotonin_{1A} receptor, a member of the serotonergic family which shares $\sim 48\%$ sequence similarity with β_2 -adrenergic receptor¹²⁴. The serotonin_{1A} receptor is an important neurotransmitter receptor that is implicated in various cognitive, behavioral, and developmental functions^{117,374}. The agonists and antagonists of the serotonin_{1A} receptor represent major classes of molecules with potential therapeutic applications in anxiety- or stress-related disorders³⁷⁵. As a result, the serotonin_{1A} receptor serves as an important drug target for neuropsychiatric disorders such as anxiety and depression as well as in neuronal developmental defects³⁷⁶. It is one of the first receptors for which cholesterol dependence of ligand binding and signaling function was demonstrated^{7,9,121}. Highly dynamic cholesterol interactions have been identified on the receptor surface using coarse-grained simulations^{125,377}. The serotonin_{1A} receptor has been shown to oligomerize in a constitutive manner¹²² which is dependent on membrane cholesterol content^{122,123}. However, the molecular interplay between membrane cholesterol and receptor oligomerization is still lacking.

In this work, we have used coarse-grained molecular dynamics simulations to analyze the dimerization of the serotonin_{1A} receptor in membranes of varying cholesterol content. A major finding from our results is the high conformational plasticity of the dimer with increasing cholesterol concentration. We postulate that increased cholesterol concentration at the interface between the two receptors, reminiscent of “nonannular” sites⁷⁰, is responsible for the increased dimer rotational flexibility and plasticity. These results help explain the molecular mechanism governing cholesterol-dependent receptor oligomerization. We believe these results provide an important first step toward the design of therapeutic strategies that could be exploited for tissue-specific and age-dependent interventions.

5.2 Methods

5.2.1 System setup

Multiple coarse-grained molecular dynamics simulations of two membrane embedded serotonin_{1A} receptors were performed using the MARTINI force-field^{232,283}. Twenty simulations of 45 μ s each were carried out in POPC/cholesterol bilayers with varying cholesterol concentration, corresponding to a total of 900 μ s at each cholesterol concentration. The total simulation time equals 3.6 ms of coarse-grained simulation time, corresponding to 14.4 ms of effective simulation time^{232,283}. The coarse-grained representation of the homology model of serotonin_{1A} receptor and POPC bilayers with varying cholesterol concentration (0, 9, 30 and 50%) were obtained from earlier studies^{124,125}. Four orientations of the receptors, rotated about 90 degrees from each other were considered, with a minimum distance of 3.0 nm between the receptors. The schematic representations of the receptor and a representative initial system are shown in Fig. 5.1 (also see Table 1). Simulations of the monomeric receptor in POPC bilayers with varying cholesterol concentrations were performed under identical conditions (see Table 1).

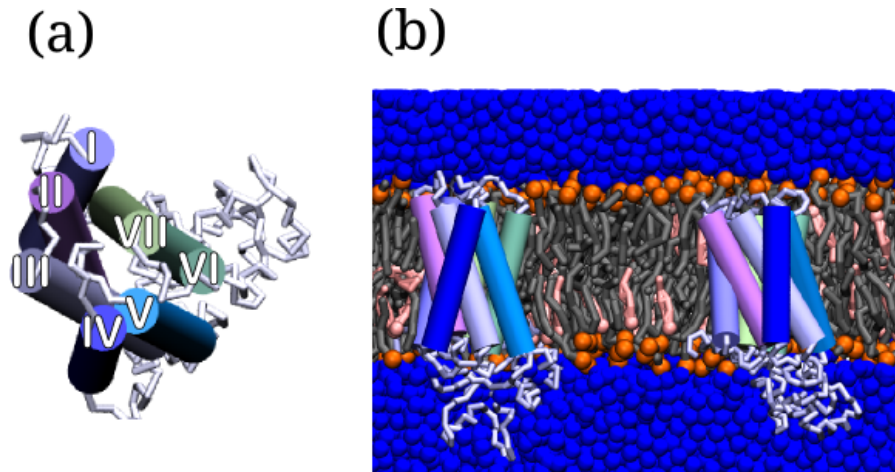


Figure 5.1: A schematic representation of the serotonin_{1A} receptor: (a) Top view of the receptor with individual helices numbered; (b) starting structure of the two monomers in POPC bilayers with 30% cholesterol. The receptors are shown in same colors as that in panel (a). Phospholipid molecules are shown in gray, the phosphate beads of the phospholipids are shown in orange, cholesterol is shown in pink and surrounding water molecules are shown in blue.

Table 5.1: *Summary of simulations performed*

System	Initial minimum distance (nm)	Simulation		Number of Molecules		
		Number	Length (μ s)	Receptor	POPC	Chol.
<i>Dimer simulations</i>						
POPC	3.2	20	45	2	568	0
POPC/ 9% cholesterol	3.5	20	45	2	520	48
POPC/ 30% cholesterol	3.6	20	45	2	520	158
POPC/ 50% cholesterol	3.1	20	45	2	520	260
<i>Monomer simulations</i>						
POPC	-	1	25	1	284	0
POPC/ 9% cholesterol	-	1	25	1	260	24
POPC/ 30% cholesterol	-	1	25	1	260	78
POPC/ 50% cholesterol	-	1	25	1	260	130

5.2.2 Simulation parameters

All simulations and analysis were performed using GROMACS version 4.5.5³¹⁴. The systems were represented by the MARTINI coarse-grained force-field version 2.1 for the protein and version 2.0 for the lipid parameters. Non-bonded interactions were used in their shifted form with electrostatic interactions shifted to zero in the range of 0-1.2 nm and Lennard-Jones interaction shifted to zero in the range of 0.9-1.2 nm. The temperature of each molecular group in the system was weakly coupled to a thermostat at 300 K using the Berendsen thermostat algorithm with a coupling constant of 0.1 ps³¹⁵. Pressure was maintained semi-isotropically at 1 bar independently in the plane of the bilayer and perpendicular to the bilayer using Berendsen's barostat algorithm with a coupling constant of 0.5 ps and a compressibility of $3 \times 10^{-5} \text{ bar}^{-1}$. Initial velocities for system were chosen randomly from a Maxwell distribution at 300 K. The LINCS algorithm was used to constrain bond length. A time step of 20 fs was used for the simulations with neighbor list updated every 10 steps. Periodic boundary conditions were maintained along x, y and z direction. Simulations were rendered using the VMD software³¹⁶ along with MARTINI secondary structure rendering scripts.

5.2.3 Analysis

Characterization of the rotational angles sampled by the receptors

The relative orientation of the receptors was calculated from the angle between the planes defined by residues from transmembrane helices I and IV (see Fig. 5.2).

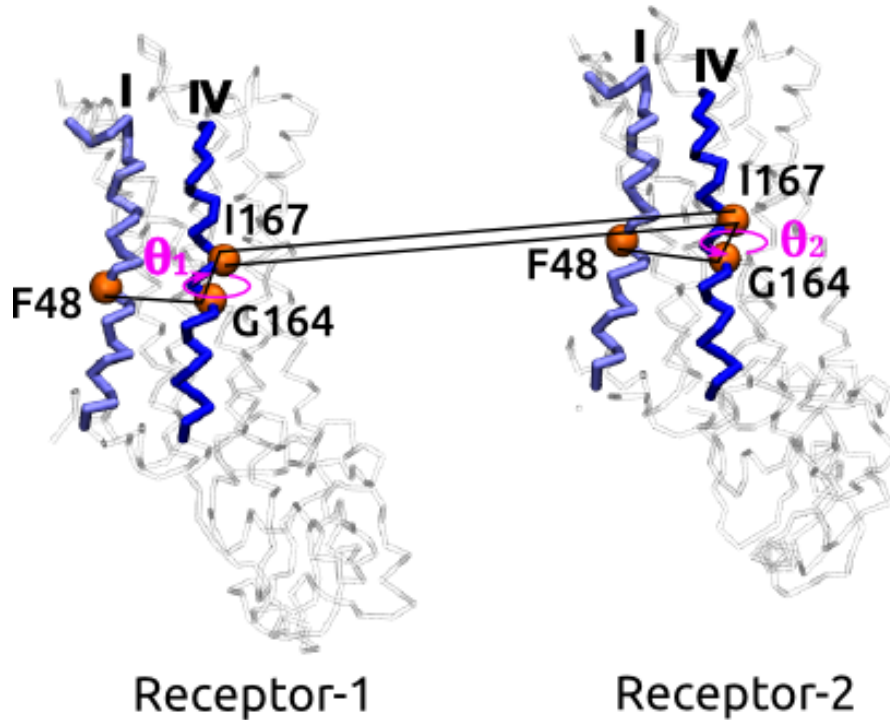


Figure 5.2: A schematic representation of the relative orientations of the two receptors. θ_1 refers to the relative orientation of receptor 1 relative to receptor 2 and θ_2 is the relative orientation of receptor 2 relative to receptor 1. The relative orientation is defined as the angle between the planes formed by the backbone beads of residues 48, 164, 167 of receptor 1 and residue 167 of receptor 2, as shown in the figure. The helices containing these residues, i.e., transmembrane helices I and IV, are shown.

θ_1 refers to the rotational angle of receptor 1 relative to receptor 2 characterized by the angle between the planes formed by the backbone beads of residues 48, 164 and 167 of receptor 1 and residue 167 of receptor 2 (residues numbered according to UNIPROT ID: P08908). Similarly, θ_2 refers to the rotational angle of receptor 2 relative to receptor 1 characterized by the same residues. To account for reduced dimer interactions in POPC/cholesterol bilayers with 50% cholesterol concentration, an equal number of random simulations were considered for the remaining membranes.

Quantitative estimation of involvement of transmembrane helices at dimer interface

The transmembrane helices at the dimer interface were determined from the dimer regime by using a cut-off of 0.5 nm, using the same methodology as in our earlier work¹²⁵. Long-lived dimer species were identified as those where no subsequent dissociation (larger than cut-off) was observed. Transient dimers were characterized as those in which a dissociation event (minimum distance of 1.5 nm) was observed subsequently in the trajectory.

Maximum cholesterol occupancy around each residue of receptor

Maximum cholesterol occupancy is defined as the maximum (normalized) time for which a cholesterol molecule remains associated with a particular site. The definition was based on our earlier work^{125,238,239}. Hydrophobic mismatch around transmembrane helices. The normalized bilayer thickness profile around the monomer was calculated from the phosphate bead distances of the bilayer based on previous work²³⁹. A value >1 indicates local thickening (positive hydrophobic mismatch) and a value <1 indicates local thinning (negative hydrophobic mismatch).

Cholesterol occupancy at dimer interfaces

To quantify the cholesterol occupancy at the dimer interface, we calculated normalized lipid occupancy for each dimer interface which we term as ‘interface occupancy score’. The ‘interface occupancy score’ is defined for each helix in a given dimer conformation as the product of the normalized cholesterol occupancy and the probability of that dimer conformation. In the interface occupancy matrix, the diagonal elements correspond to high cholesterol occupancy at the helices at the dimer interface and the off-diagonal elements correspond to high cholesterol occupancy at transmembrane helices not occurring at the dimer interface. To reduce noise in the calculations, only the helices with at least 70% probability of occurrence at the interface were considered. Similarly, only helices with a maximum cholesterol occupancy of 0.7 were considered.

5.3 Results

The dimerization of membrane-embedded serotonin_{1A} receptors was analyzed from a series of coarse-grained molecular dynamics simulations, totaling to 3.6 ms of simulation time. To investigate the dependence of receptor dimerization on membrane lipid composition, simulations were performed in POPC bilayers and POPC/cholesterol bilayers with increasing cholesterol concentration. A schematic representation of the receptor and a representative initial system are shown in Fig. 5.1. Twenty independent simulations of 45 μ s were performed for each membrane composition for the receptor dimer (Table 5.1).

5.3.1 Receptor association is dependent on cholesterol concentration

During the course of simulation, the receptors diffused freely, with a μ s time scale encounter frequency. A time-distance plot showing the minimum distance between the two receptors for each simulation is shown in Fig. 5.3.

The monomeric regime when the two receptors diffuse independently is characterized by distances larger than 1 nm. The dimer regime corresponds to smaller distances (<0.5 nm closest approach), depicted by the dark blue stretches in Fig. 5.3. Receptor dimerization was observed in all membrane compositions. In most cases, several close associations between the two receptors were observed prior to dimer formation. The time taken to form a dimer was variable and ranged from 1 to 45 μ s. The most favorable long-lived dimer species were stable in the time scale of the simulations, although transient dimer species were observed as well. Interestingly, the number of dimers observed in the simulations exhibited a dependence on cholesterol concentration. At higher cholesterol concentrations (30 and 50%), the number of dimer species observed was lower relative to what was observed in POPC bilayers and POPC/cholesterol bilayers with 9% cholesterol. For example, only 14 long-lived stable dimers (in a total of 20 simulations) were observed in POPC/cholesterol bilayers with 50% cholesterol. In addition, dimerization was less frequent at higher cholesterol concentrations, as evident from the length of the dark blue stretches in Fig. 5.3.

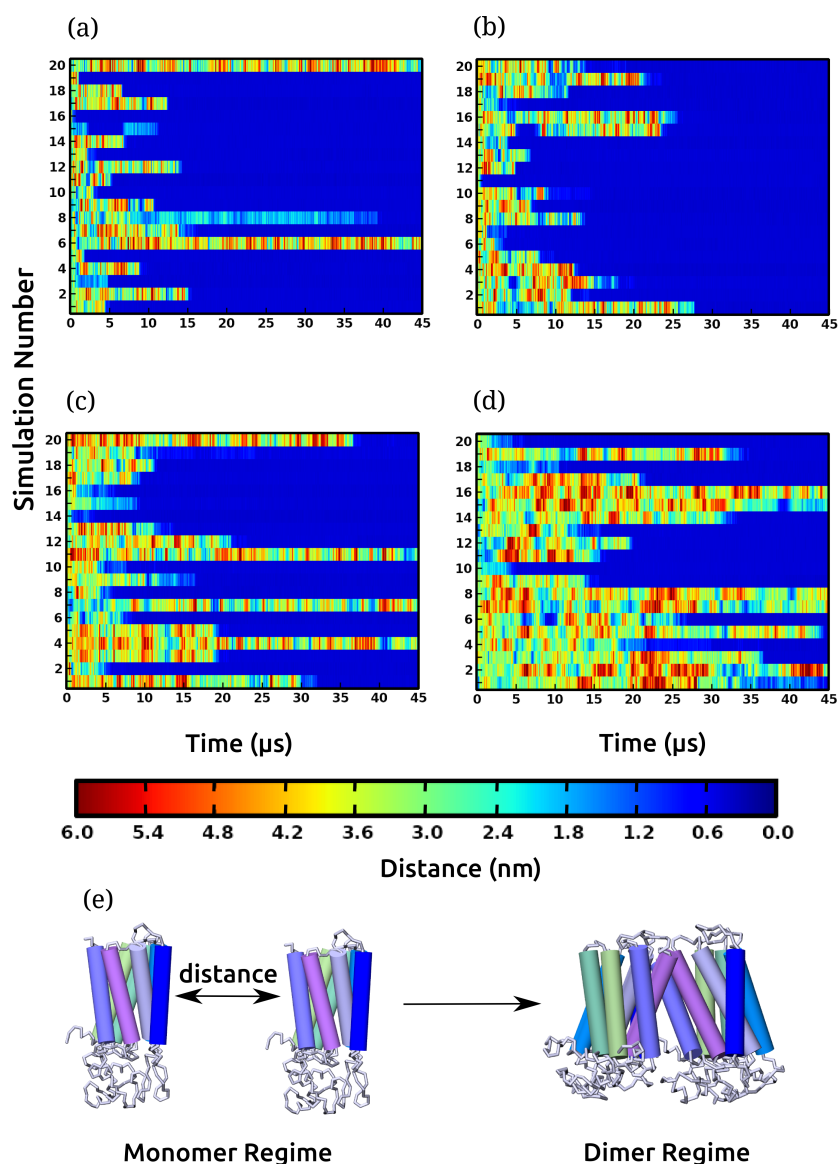


Figure 5.3: Schematic representations of the minimum distance between the transmembrane segments of the two receptors during the course of the simulation in (a) POPC bilayers and POPC/cholesterol bilayers with (b) 9 (c) 30 and (d) 50% cholesterol concentrations. The range of distances between the monomers is color coded and shown as a scale bar. The dimer regime is characterized by distances less than 0.5 nm, corresponding to the dark blue stretches in the plot. The monomer regime corresponds to the red, yellow, green and light blue regions in the plot. Each row in every panel represents an independent simulation (numbered along the ordinate), thereby corresponding to a total of 80 simulations of 45 μs each. (e) A schematic representation of the two receptors in the monomer and dimer regime. See Methods for other details.

5.3.2 Cholesterol increases plasticity of dimer conformers

To analyze the dimer conformations observed in the simulations, we calculated the relative orientations of the receptors in the dimer regime. The conformations were characterized by

measuring the rotational angle of the two receptors relative to each other, defined by two arbitrary angles θ_1 and θ_2 for the two receptors (See Methods and Fig. 5.2 for further details). Two-dimensional plots of the population densities of the relative orientations at each membrane composition are shown in Fig. 5.4.

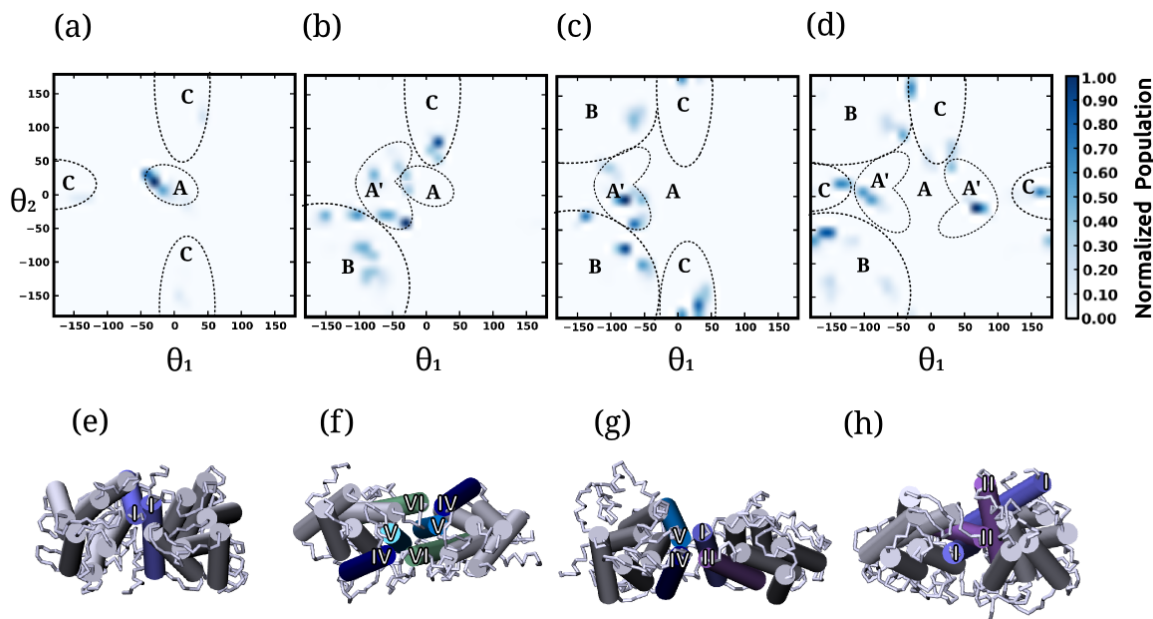


Figure 5.4: Normalized population of the relative orientations of the two receptors in the dimer regime defined by the angles θ_1 and θ_2 (see Methods for details). The populations were averaged over the dimer regime for simulations in (a) POPC bilayers and POPC/cholesterol bilayers with (b) 9 (c) 30 and (d) 50% cholesterol concentrations. The relative orientations can be broadly mapped to four conformations (A, B, C and A') that are marked in panels (a-d). The four conformations correspond to two sites at the receptor: site 1 comprising of transmembrane helices I and II and site 2 comprising of transmembrane helices IV, V and VI. (e) Conformation A corresponds to a non-flexible homo-interface with only a single helix from site 1 (transmembrane helix I). (f) Conformation B corresponds to homo-interfaces at site 2. (g) Conformation C corresponds to hetero-interfaces comprising of transmembrane helices from sites 1 and 2. (h) Conformation A' corresponds to a flexible interface at site 1.

The most striking feature of the rotational orientations sampled is that only a few of the conformations were sampled in POPC bilayers and the conformational diversity appeared to increase with increase in cholesterol concentration. We broadly mapped the relative orientations to four conformations (A, B, C and A'). A visual inspection of these four conformations revealed that they correspond to mainly two sites at the receptor: site 1 comprising of transmembrane helices I and II (and occasionally VII) and site 2 comprising of transmembrane helices IV, V and VI. Schematic representations of the conformers (i.e., A, B, C and A') are shown in Fig.

5.4(e-h).

In POPC bilayers, the most favorable conformer was A (see Fig. 5.4a,e) which corresponds to a symmetric homodimer (values of θ_1 and θ_2 are close to zero). The interface was observed to have low rotational flexibility and consists of only transmembrane helix I from site 1 of the receptor. Additional conformations (B and C) were sampled, but with reduced population. In POPC/cholesterol bilayers with 9% cholesterol (Fig. 5.4b), several dimer conformations were sampled. Conformer B (Fig. 5.4f) was observed to have a high population. A visual inspection revealed that conformer B correspond to several related conformers at site 2 (transmembrane helices IV, V and VI). These interfaces were observed to be very flexible and small rotations around each monomer resulted in variable transmembrane helices at the dimer interface. In addition, the population of conformer A decreased, but a related conformer A' (Fig. 5.4h) was found. Conformer A' corresponds to a more flexible interface than conformer A, but at the same site 1 of the receptor. At increased cholesterol concentrations (30 and 50%), several instances of conformer C (Fig. 5.4g) were sampled. Conformer C corresponds to heterointerfaces of helices from sites 1 and 2. Interestingly, at these higher concentrations, conformer A (prominently observed in POPC bilayers) was not observed at all. In these cases, the more flexible conformer A' was observed.

Taken together, the results suggest that cholesterol modulates dimer conformations in a way so as to populate the conformer space with more plastic and flexible dimers. This is particularly evident in case of the less flexible conformer A that was not observed at higher cholesterol concentrations (Fig. 5.4c,d). A related flexible conformer A' was observed at higher cholesterol concentrations, but not in the absence of cholesterol (Fig. 5.4a). In addition, more conformers were sampled at increased cholesterol concentration, highlighting the role of cholesterol in the increased flexibility and plasticity of the dimer conformations.

5.3.3 Cholesterol modulates the receptor dimer interface

We further analyzed the dimer conformations and estimated the relative contributions of the individual transmembrane helices at the dimer interface. Only the long-lived stable dimer conformations that did not exhibit any subsequent dissociation were considered. Contact maps representing the transmembrane helix pairs at the dimer interfaces at different cholesterol concentrations are shown in Fig. 5.5.

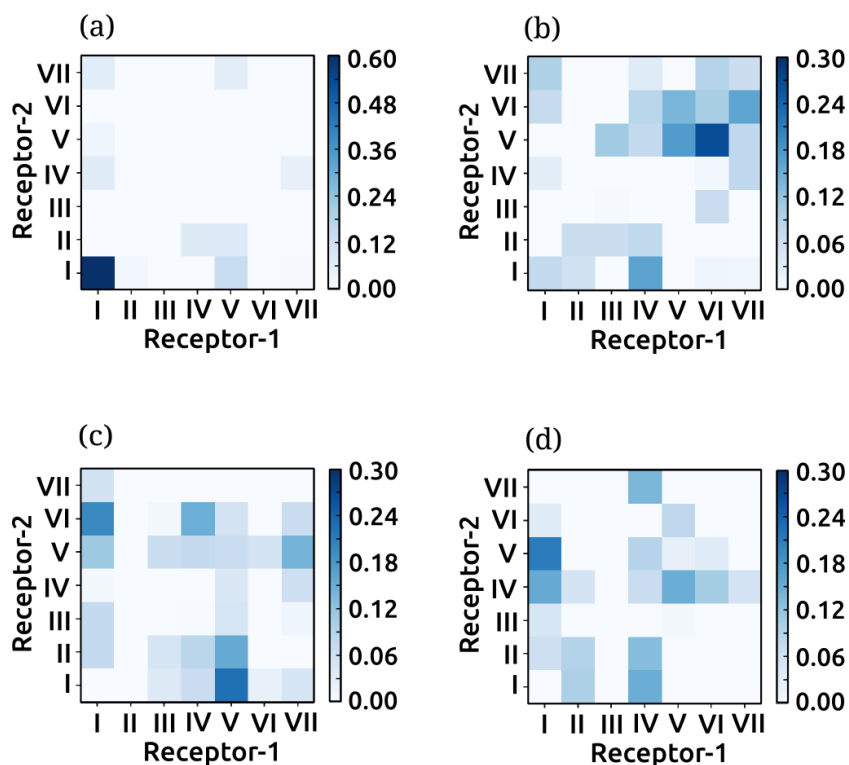


Figure 5.5: Contact maps depicting the helix-helix interactions at the dimer interface in (a) POPC bilayers and POPC bilayers containing (b) 9% (c) 30% and (d) 50% cholesterol. The dimer interfaces were calculated from the long-lived stable dimers not exhibiting any subsequent dissociation in the time scale of the simulation. The values were calculated as an average over all simulations and normalized by the time of occurrence and simulation length. A cut-off distance of 0.5 nm was used to determine the contact residues. The color scale bar indicates the normalized population. For better clarity, the color scale bar for the dimer interfaces sampled in POPC bilayers is different from the POPC/cholesterol bilayers. See Methods for further details.

A distinct difference was observed in the contact maps with increasing cholesterol concentration in the membrane. The most striking feature that emerges is the predominant occurrence of the transmembrane helix I-I homodimer in POPC bilayers (see Fig. 5.5a). This interface was sampled less in POPC/cholesterol bilayers with 9% cholesterol (Fig. 5.5b) and was completely absent at higher cholesterol concentrations (Fig. 5.5c,d). Another prominent feature of the contact maps is the increased plasticity, i.e., presence of multiple favorable helix-helix contacts, in presence of cholesterol. The main features of the contact maps are in agreement with the rotational orientations sampled (Fig. 5.4), and additionally allow us to characterize the dimer interfaces at a molecular level.

5.3.4 Unfavorable dimer interfaces dissociate at ns to μ s time scale

A detailed analysis of the minimum distance between the receptors over the simulation period pointed to several dissociation events (Fig. 5.3). Several of the unfavorable dimers that dissociate had been stably bound at μ s time scale, and are distinct from the multiple close-contacts formed prior to the formation of a long-lived dimer. One such example was observed in set 15 in POPC/cholesterol bilayers with 9% cholesterol (Fig. 5.3b). A dimer was observed for almost 3 μ s between 4.8 and 7.8 μ s, after which it dissociated. The two receptors freely diffused away, moving apart by as much as 6 nm (shown as red), and consequently dimerize again at 23 μ s and remain associated until 45 μ s. Another example of such a dissociation event was observed in set 6 in POPC/cholesterol bilayers with 50% cholesterol (see Fig. 5.3d). Four dimer association/dissociation events were observed, in which the dimer species was observed for at least 1 μ s, followed by subsequent dissociation. The receptors were observed to diffuse away and finally re-associate after several μ s. Taken together, ~ 124 dissociation events were observed, ranging from ns to μ s time scale. The unstable dimer species was observed in all membrane compositions (see Fig. 5.3), but the number of dissociation events considerably increased with increasing cholesterol concentration (see Table 5.2). In POPC/cholesterol bilayers with 50% cholesterol concentration, the number of dissociation events was the largest, despite a slower initial association (see Fig. 5.3d).

Table 5.2: *Quantitative estimation of number of transient associations during serotonin_{1A} receptor dimerization*

System	Number of transient associations
POPC	8
POPC/9% cholesterol	28
POPC/30% cholesterol	40
POPC/50% cholesterol	48

We characterized the nature of these transient interactions by analyzing the dimer conformers sampled during these short-lived unstable associations. Contact maps of the dimer conformers sampled during the unstable short-lived associations are shown in Fig. 5.6.

In POPC bilayers, the dissociation events are low (Fig. 5.6a), and the transient dimer conformers consisted of transmembrane helices IV/I and V/IV. In POPC/cholesterol bilayers with 9% cholesterol concentration (see Fig. 5.6b), the transient dimer conformers consisted of

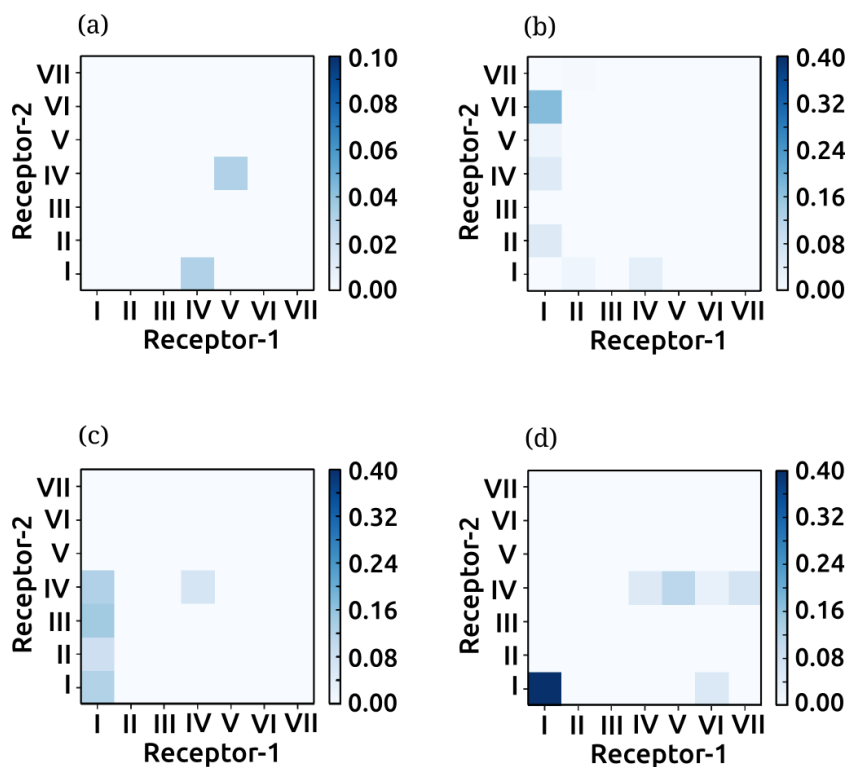


Figure 5.6: Contact maps depicting the helix-helix interactions at the dimer interface for transiently associated dimers in (a) POPC bilayers and POPC bilayers containing (b) 9% (c) 30% and (d) 50% cholesterol. The dimer interfaces were calculated from the short-lived unstable dimers that subsequently dissociate during the simulation. The values were normalized to the transient association period and the maximum total number of transient association instances (see Table 5.2). The color scale bar indicates the normalized population. For better clarity, the color scale bar for the dimer interfaces sampled in POPC bilayers is different from the POPC/cholesterol bilayers. See Methods for further details.

transmembrane helix I in most cases, in combination with transmembrane helix II, IV and VI. In POPC/cholesterol bilayers with 30% cholesterol (Fig. 5.6c), the transient dimer conformers mostly included transmembrane helix I. In particular, the I-I homodimer was found to dissociate in several instances. In POPC/cholesterol bilayers with 50% cholesterol (Fig. 5.6d), the least favorable dimer conformer was the I-I homodimer.

Interestingly, the I-I homodimer, predominantly sampled in POPC bilayers (Fig. 5.5a), never dissociated within the μs time scales of the current simulations (Fig. 5.6a). In sharp contrast to this, in POPC/cholesterol bilayers with increased cholesterol concentrations (Fig. 5.5c,d), the I-I homodimer was not observed in the stable dimer regime and dissociated in case the initial contacts were formed (Fig. 5.6c,d). These results therefore indicate that the

presence of cholesterol modulates both the initial approach between receptors and the relative stability of the favorable dimer conformers by fine-tuning the conformational energetics.

5.3.5 Cholesterol modulates receptor dimerization through direct and indirect effects

To examine the molecular basis of the modulation of the dimer conformations by cholesterol, we analyzed the possible direct and indirect effects of cholesterol³⁰¹. The direct effects arise from an interaction between the receptor and cholesterol and have been characterized by the occupancy of cholesterol around each residue of the receptor. Indirect effects arise from changes in the bilayer properties such as changes in bilayer thickness due to the presence of cholesterol.

Residue-wise cholesterol occupancy

The direct interaction of cholesterol with the receptor was analyzed by calculating the maximum occupancy of cholesterol at each residue of the receptor during the monomer regime of the simulations (see Methods for further details). Figure 5.7a shows cholesterol occupancy calculated around each residue, averaged over all simulations in POPC/cholesterol bilayers and normalized to the maximum value.

The highest cholesterol occupancy was observed at transmembrane helix VI. In addition, high cholesterol occupancy was observed at transmembrane helices I and V (>0.8). Interestingly we observed comparably higher cholesterol occupancy at the third intracellular loop of the receptor (between transmembrane helices V and VI), indicating interaction of the loop with the membrane. The values calculated considering each transmembrane helix is consistent (Fig. 5.8).

These results suggest that the presence of cholesterol at transmembrane helix I in the monomeric regime could be related to its subsequent absence at the dimer interface (see Fig. 5.5), although a direct correlation is difficult.

Hydrophobic mismatch around transmembrane helices

Membrane cholesterol is known to regulate lipid-protein interactions by increasing the thickness of the membrane bilayer. It has been previously reported that the bilayer thickness of POPC vesicles increases from ~ 26 Å to ~ 30 Å in presence of 30% cholesterol³⁵⁶. This could give rise to ‘hydrophobic mismatch’, i.e., a difference in the hydrophobic lengths of transmembrane proteins and the surrounding lipid annulus, that can lead to changes in membrane protein

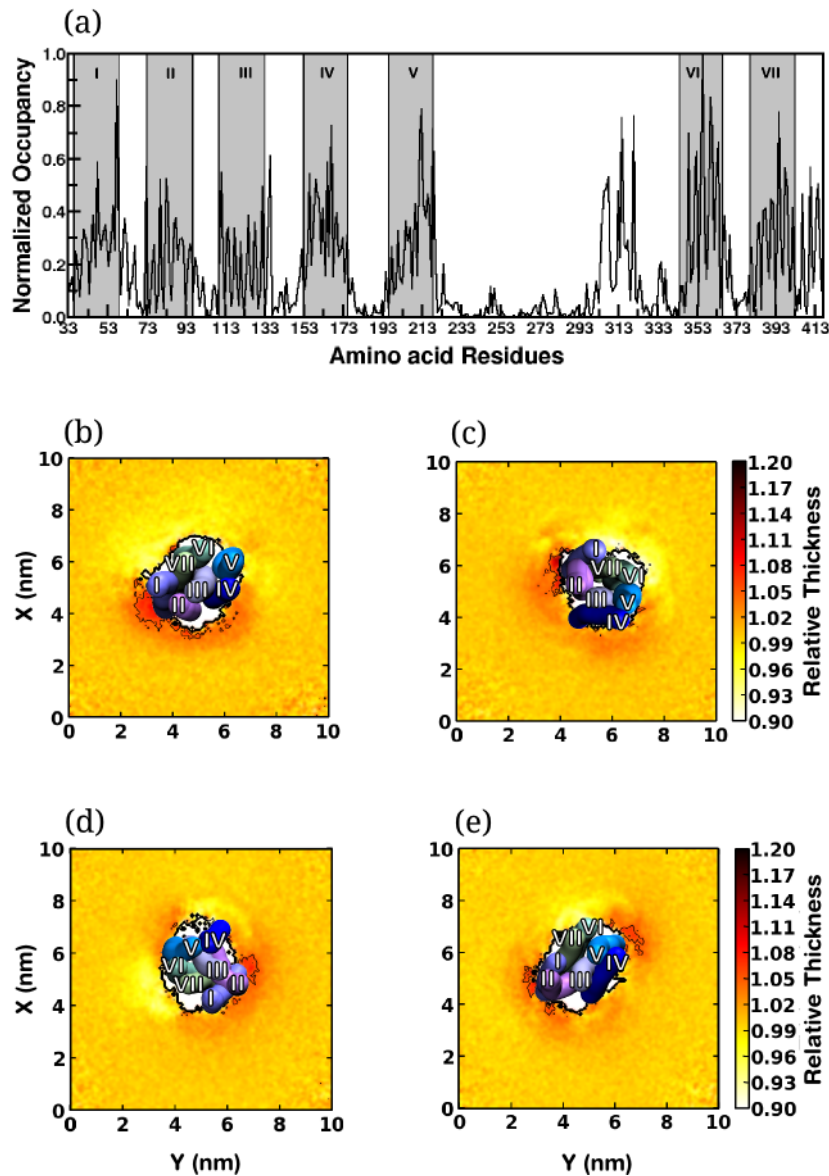


Figure 5.7: (a) Maximum cholesterol occupancy around each residue of the receptor in the monomer regime. The values were normalized to the simulation length of the monomer regime and averaged over two monomers from all simulations in POPC/cholesterol bilayers. The gray bands depict the segments corresponding to the transmembrane helices. (b-e) Bilayer thickness profiles around the receptor in (b) POPC bilayers and POPC/cholesterol bilayers with (c) 9 (d) 30 and (e) 50% cholesterol concentration. A top view representation of the transmembrane helices of the receptors is superimposed on the plots.

oligomerization^{233,239,334,378}. We analyzed the variation in the normalized bilayer thickness around the receptor monomer to directly compare the local bilayer thickness at all membrane

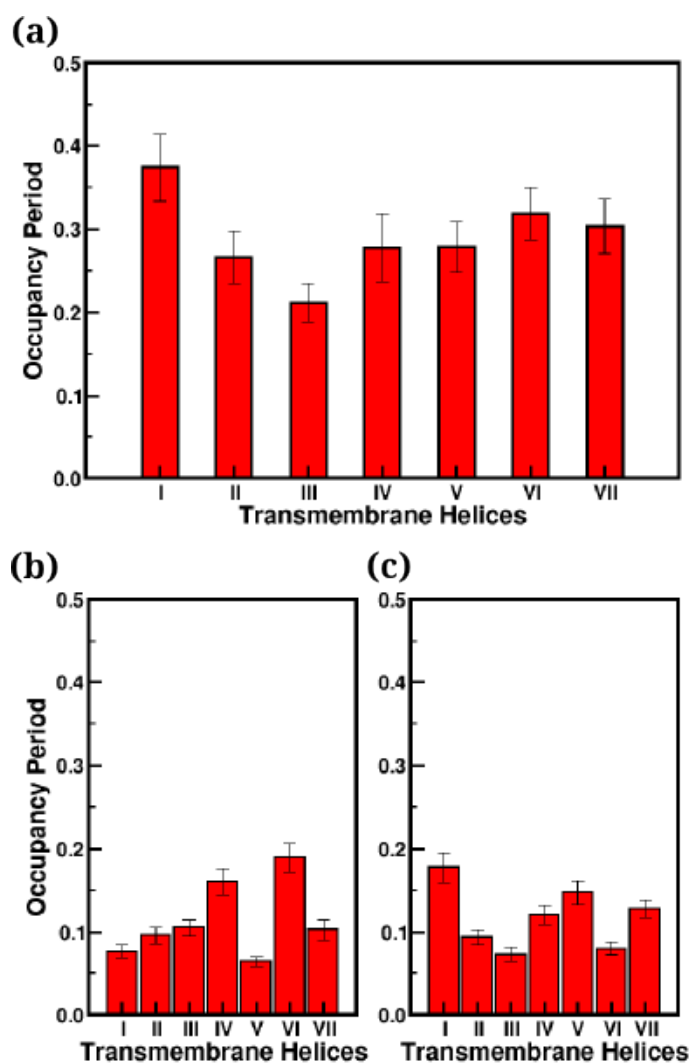


Figure 5.8: Maximum cholesterol occupancy around each transmembrane helix in the monomer regime. The values are reported for (a) the transmembrane helix as a whole and (b) upper and (c) lower leaflets separately. The values have been normalized to the simulation length of the monomer regime and averaged over the two receptors from all simulations in POPC/cholesterol bilayers.

compositions and quantitate the mismatch around the receptor. The normalized bilayer thickness profiles are shown in Fig. 5.7(b-e). In POPC bilayers, an increased bilayer thickness was observed at site 1 of the receptor, corresponding to transmembrane helices I and II (Fig. 5.7b). An increase in bilayer thickness was also observed around site 2 comprising of transmembrane helix IV, but was lower in magnitude. In POPC/cholesterol bilayers with 9% cholesterol (Fig. 5.7c), both sites 1 and 2 exhibit increased bilayer thickness. In POPC/cholesterol bilayers with 30 and 50% cholesterol (Fig. 5.7d,e), the positive hydrophobic mismatch at site 1 was reduced,

and the mismatch at site 2 was increased. Interestingly, the main dimer conformations observed in our simulations (Fig. 5.4) correspond to the sites of the receptor in which the membrane perturbations are high. However, a direct correlation is difficult. For example, the perturbations at site 1 persist even at high cholesterol concentrations, although a homodimer at this site, comprising of transmembrane helix I was observed to be unfavorable. Cholesterol-dependent receptor dimerization therefore appears to be a complex interplay between direct and indirect effects.

5.3.6 Nonannular cholesterol contributes to dimer flexibility and plasticity

Cholesterol occupancy in the dimer regime was found to be different from that in the monomer regime (see Fig. 5.7 and Fig. 5.9).

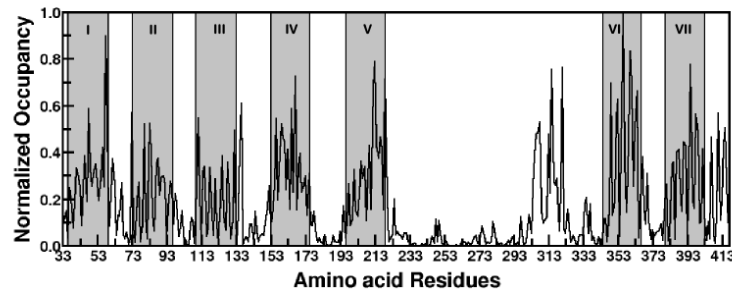


Figure 5.9: *Maximum cholesterol occupancy around each residue of the receptor in the dimer regime: The values have been normalized to the simulation length of the dimer regime and averaged over the two receptors from all simulations in POPC/cholesterol bilayers. The gray bands depict the segments corresponding to the transmembrane helices.*

High cholesterol occupancy was observed in the dimer regime around transmembrane helices IV, V and VI, similar to the monomer regime. However, cholesterol occupancy at transmembrane helix I decreased considerably in the dimer regime. To examine if the varying cholesterol occupancies were correlated to the dimer interface, we calculated an interface occupancy score (see Methods for details). The interface occupancy for cholesterol calculated for POPC/cholesterol membrane bilayers is shown in Fig. 5.10(a-c).

The diagonal elements in the plots correspond to high cholesterol occupancy at the transmembrane helices at the homodimer interface, and the off-diagonal elements correspond to the

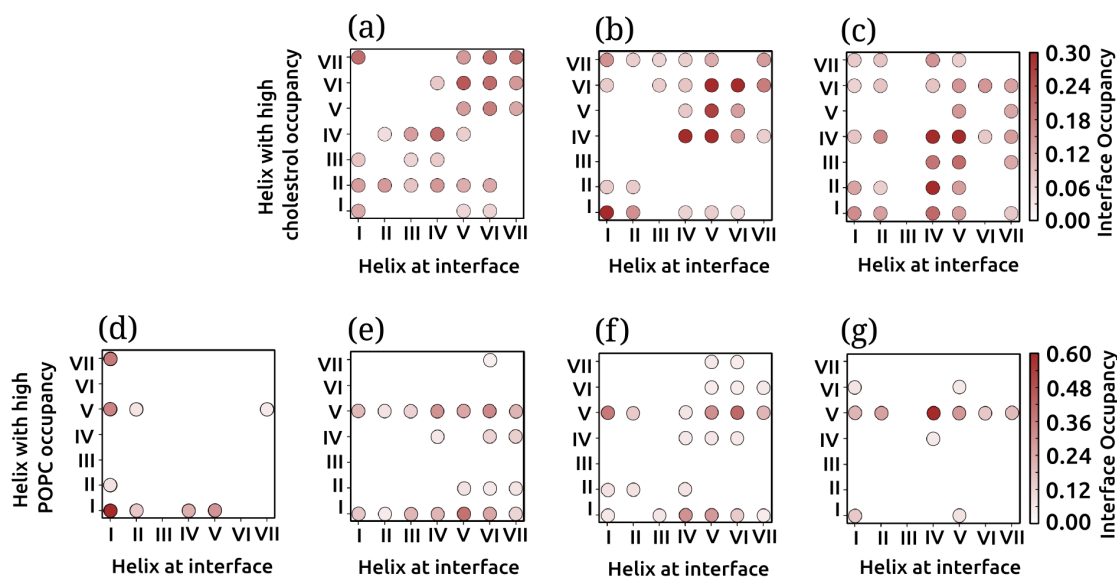


Figure 5.10: The normalized occupancy of cholesterol (panels a-c) and POPC (d-g) at each helix in the receptor dimer plotted as a function of the helices at the dimer interface. The interface occupancy scores (see Methods) of cholesterol are shown for POPC/cholesterol bilayers with (a) 9% (b) 30% and (c) 50% cholesterol concentrations. The interface occupancy scores of POPC are shown for (d) POPC bilayers and POPC/cholesterol bilayers with (e) 9% (f) 30% and (g) 50% cholesterol concentrations. The interface occupancy scores were normalized to the relative probability of occurrence of the transmembrane helix at the dimer interface (obtained from Fig. 5.5) and highest maximum cholesterol occupancy for each receptor (from Fig. 5.7). The diagonal elements correspond to high occupancy of cholesterol (or POPC) at helices that constitute the dimer interface. The off-diagonal elements correspond to occupancy of cholesterol (or POPC) at the helices not at the dimer interface. The presence of cholesterol at the dimer interface is reminiscent of nonannular lipids⁷⁰ and is believed to act as a ‘molecular lubricant’ by modulating the energetics of helix-helix interaction (see text). See Methods for further details.

cholesterol occupancy away from the interface. In POPC/cholesterol bilayers with 9% cholesterol (Fig. 5.10a), the diagonal elements show high scores, suggesting that the cholesterol occupancy at the transmembrane helices at the dimer interface is high. The score for the off-diagonal elements, corresponding to cholesterol occupancy at receptor sites not at the dimer interface was relatively low, suggesting lower cholesterol at sites away from the dimer interface. Similarly, in POPC/cholesterol bilayers with 30% cholesterol (Fig. 5.10b), the scores of the diagonal elements were high, confirming the presence of cholesterol at the dimer interface. In POPC/cholesterol bilayers with 50% cholesterol (Fig. 5.10c), the effect was less pronounced and high cholesterol occupancy was observed at all transmembrane helices, both at the dimer interface and away from it. In sharp contrast, the occupancy of POPC was not related to

the dimer interface (Fig. 5.10d-g). POPC occupancy was high at transmembrane helix I and shifted to transmembrane helix V with increasing cholesterol concentration, consistent with the monomer regime (Fig. 5.11).

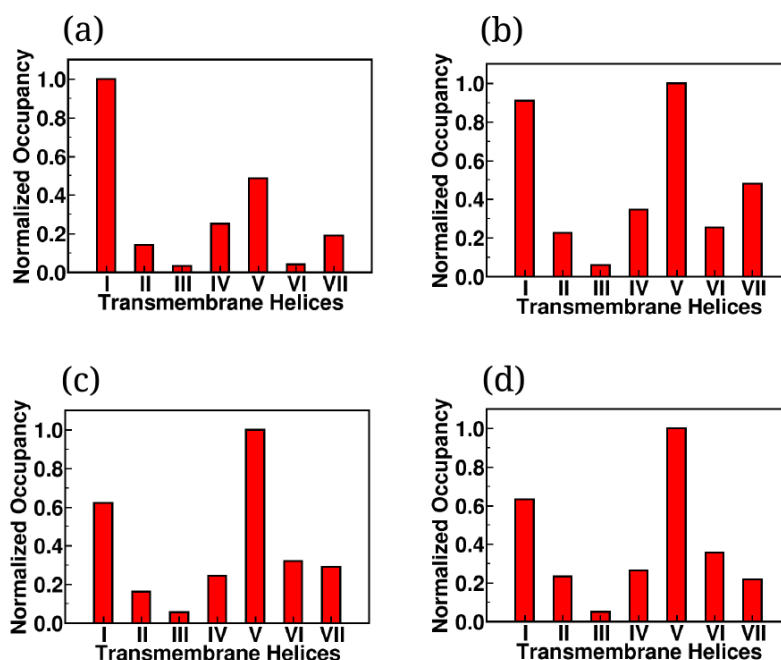


Figure 5.11: The maximum occupancy was calculated from the phosphate bead of the phospholipid molecule for simulations in (a) POPC bilayers and POPC/cholesterol bilayers with (b) 9 (c) 30 and (d) 50% cholesterol concentrations. The values have been normalized to the simulation length and averaged over the two receptors in the monomer regime.

Interestingly, the site of POPC association at transmembrane helix I is identical to that predicted by recent atomistic simulations³⁷⁹. The presence of high cholesterol occupancy at the dimer interface and the lack of correlation of POPC occupancy with the dimer interface, strongly point out the involvement of membrane cholesterol in receptor dimerization.

The high cholesterol occupancy at the dimer interface is reminiscent of nonannular sites that have been suggested to be present at inter-receptor sites as well as intra-receptor (inter-helical) sites⁷⁰. We propose that in case of the serotonin_{1A} receptor, the nonannular sites are related to both dimer plasticity as well as the rotational flexibility of the dimer interface. From this perspective, cholesterol could be thought of acting as a ‘molecular lubricant’, and could modulate the conformational energetics of helix-helix interaction in the membrane.

5.4 Discussion

GPCRs are important mediators of signaling networks that have been shown to be dependent on membrane cholesterol. Cholesterol appears to function in a receptor-dependent manner by modulating the structure and organization, but the molecular details of these mechanisms have been difficult to probe due to this inherent complexity. In addition, GPCR organization is important not just as an organizational principle but also as a regulatory paradigm influencing receptor cross-talk and drug efficacy. In this work, we have analyzed the dimerization of the serotonin_{1A} receptor, an important GPCR, by comprehensive coarse-grained simulations, totaling to an effective time of ~ 15 ms (see Methods). By analyzing the dimerization behavior of the receptor in POPC bilayers with increasing concentration of cholesterol, we are able to delineate the subtle, yet functionally relevant, effect of cholesterol on receptor association. The dimer states display four distinct conformers with sharply defined boundaries that are dependent on membrane lipid composition (Fig. 5.4). We propose that the dynamics of association of cholesterol molecules at receptor dimer interfaces, promotes receptor rotational flexibility and conformational plasticity, much needed for their biological activity.

An interesting aspect of the current work is that although multiple dimer interfaces are observed, they can be mapped to mainly two sites: site 1 involving transmembrane helices I and II, and site 2 comprising of transmembrane helices IV, V and VI. A continuous interplay of each of these helices and rotation of the receptor gives rise to several dimer interfaces, fine-tuned by cholesterol concentration. These effects are mediated, possibly through specific interaction. Indeed, cholesterol has been shown to bind at specific sites on GPCRs by atomistic^{304,305,380,381} and coarse-grained simulations^{125,238,377,382}. In addition, cholesterol association kinetics at the ns and μ s time scales has been reported by NMR studies³⁸³. An interesting feature of our results is the observation that conformational plasticity in terms of populations of the various dimer species and rotational flexibility in terms of helices at the dimer interface are increased in presence of cholesterol (see Figs 5.4 and 5.5). Previous studies on oligomerization of related GPCRs, rhodopsin and the opioid receptor have identified similar sites on the receptor as important protein-protein contacts^{234,235}. Molecular dynamics simulations have suggested that GPCR oligomerization is dynamic with comparable energetics of helix-helix interactions^{234,236}. Similarly, two different dimer interfaces were observed in

the oligomeric crystal structure of β_1 -adrenergic receptor¹⁴⁷ and μ -opioid receptor¹⁴⁶. Mutational studies combined with protein-protein docking suggested the presence of transmembrane helices IV and V in the dimer interface of the serotonin_{1A} receptor²¹⁰. Importantly, such a dynamic association can explain the effect of cholesterol on the organization in serotonin_{1A}^{122,123} and the neurotensin³⁸⁴ receptors. Modulation of conformational plasticity by cholesterol could contribute toward modulation of the oligomer populations. On the other hand, serotonin_{2C} receptor exhibits a high population of receptor dimers on the plasma membrane^{385,386}, similar to the endoplasmic reticulum and Golgi, although the lipid composition differs³⁸⁵. Our work validates the dynamic nature of the receptor-receptor interface, and establishes the importance of cholesterol in regulating and modulating receptor organization.

An important feature of the current work is the identification of short-lived dimer species with unfavorable dimer interfaces. The large number of dissociations observed, especially at high cholesterol concentrations (Fig. 5.6c,d) points toward a comprehensive sampling of the dimerization process at the sub-ms time scale regime. Previous studies of GPCR association have focussed on oligomeric species and due to limitations in the time scales sampled, were unable to identify these unfavorable dimer interfaces^{233,235,238,334}. The presence of the short-lived dimer species supports the importance of cholesterol in modulating the energetics of receptor-receptor interaction, thereby increasing the flexibility and plasticity of serotonin_{1A} receptor dimers.

These results from our current work provide a “molecular insight” to the lipid-mediated modulation of dimer conformation in serotonin_{1A} receptor. Our findings match well with the experimental evidence which suggests that membrane cholesterol induces higher order oligomerization in serotonin_{1A} receptor¹²². However, owing to limitation in spatial resolution, the study fails to clearly characterize the different oligomeric species. Also, results from our dimerization studies only postulates the formation of larger aggregates based on the multiple contact interfaces sampled between the two monomers. It would therefore be more informative to re-investigate the effect of cholesterol on “higher order” oligomerization using multiple ($n > 2$; where n denotes the number of receptors) serotonin_{1A} receptors in the system.

The increased conformational plasticity of the serotonin_{1A} receptor dimer by membrane cholesterol could be relevant in cellular physiology and drug discovery. Cellular cholesterol is known to be developmentally regulated and in a cell type dependent manner^{348,387}. This could

imply that the organization of the dimers is age and cell type dependent. Given the central role of the serotonin_{1A} receptor in anxiety and depression, this would suggest an age-dependent implication in disease progression. Further, the tissue-dependent organization of GPCRs could be important in the context of drug efficacy and specificity.


In conclusion, using multiple coarse-grained simulations we have been able to identify important cholesterol-dependent organizational principles in GPCRs. The conformational plasticity of the serotonin_{1A} receptor dimer has been demonstrated to be dependent on cholesterol. By occupying nonannular sites at the dimer interface, cholesterol is suggested to modulate helix-helix interaction and directly influence the protein contacts. Our work is an important step toward understanding GPCR function in healthy and diseased conditions.

Cholesterol Regulates Cluster Size and Conformation of Serotonin_{1A} Receptor Oligomers

*“If you want to know what a man’s like, take a good look at how he treats his inferiors,
not his equals.”*

– Sirius Black, *J.K. Rowling’s “Harry Potter and the Goblet of Fire”*

6.1 Introduction

 Recent advancements in single molecule analysis has made it possible to directly track fluorophore-labelled GPCRs in living cells and monitor their interaction with each other^{116,144}. However, owing to limitations in optical resolution and data fitting, oligomeric population larger than dimers cannot be accurately estimated. Quantitative estimation of oligomeric species is further complicated by the observation that fluorphores might be located

farther than their Förster distance (minimum distance between the fluorophores required for energy transfer) even though the receptors are in contact^{144,367}. Homo-oligomerization among GPCR members also appears to be largely influenced by membrane lipids, particularly cholesterol^{122,123}. Studies suggest that formation of homo-oligomers could play an essential role in receptor trafficking¹¹³ and signaling¹⁵⁹. Homo-oligomerization between the receptors generates oligomeric species with specific conformations that regulates ligand sensitivity^{373,388} and consequently specificity and efficacy of downstream signaling³⁸⁹. Therefore, GPCR oligomerization and factors influencing this process needs to be critically examined to understand its role in GPCR function in healthy and disease conditions.

Computational approaches such as coarse-grained molecular dynamics has been instrumental in investigating the molecular mechanism of GPCR oligomerization and provide valuable insight into the role of lipid-protein interactions in regulating receptor association^{233,235,334}. Different lipid-mediated effects have been identified to modulate oligomer conformation. While local hydrophobic mismatch around transmembrane helices appears to play a driving force for receptor-receptor interaction in rhodopsin²³³ and β_2 -adrenergic receptor³³⁴, lipid kinetics around the receptor surface influences the sites of contact between the GPCRs²³⁵. In a previous study, we examined dimerization in serotonin_{1A} receptor which showed that cholesterol increases conformational plasticity in dimer conformations¹²⁶. These effects were mediated by a combination of specific and non-specific interaction between cholesterol and receptor. Serotonin_{1A} receptor has been suggested to exist as oligomers under physiological conditions¹²³. However molecular details such as cluster size, oligomer conformation is not well characterized.

In order to examine the role of cholesterol in modulating the size and conformation of oligomeric species in serotonin_{1A} receptor, we scaled up our system size to include 9 randomly oriented receptors in POPC bilayer and POPC/cholesterol bilayers. The cholesterol concentrations chosen were identical to those used in our dimerization studies¹²⁶. During simulation the receptors freely diffused in the bilayer and associated with each other to form clusters of varying sizes. Relative population of the different cluster sizes showed a strong dependence on cholesterol concentration. Higher order oligomers (cluster size >5) were observed at lower cholesterol concentrations which reduced to smaller clusters at higher cholesterol concentrations. Hydrophobic mismatch appears to play an important role in driving receptor oligomerization.

However, a combination of direct and indirect lipid-mediated effects as well as interplay between receptor-lipid energetics appears to modulate the size and conformation of the resultant clusters.

6.2 Methods

6.2.1 System setup

Coarse-grained molecular dynamics simulation of serotonin_{1A} receptors embedded in bilayers with different lipid composition were carried out. The initial system consisted of 9 randomly oriented receptors arranged in a 3x3 fashion in bilayers with 0%, 9%, 30% and 50% cholesterol concentration. Details regarding the system compositions is given in Table 6.1.

Table 6.1: *Summary of simulations performed*

System	Initial minimum distance (nm) ^a	Simulation		Number of Molecules		
		Number	Length (μ s)	Receptor	POPC	Chol.
POPC	5.87 (10.41)	5	70	9	2556	0
POPC/ 9% cholesterol	7.81 (14.78)	5	70	9	2340	216
POPC/ 30% cholesterol	5.20 (10.36)	5	70	9	2340	702
POPC/ 50% cholesterol	7.87 (14.89)	5	70	9	2340	1170

^a The value in paranthesis indicates minimum distance between opposite receptors while that outside the paranthesis indicates distance between adjacent receptors.

Five simulations of atleast 70 μ s each were performed at each bilayer composition, giving a total simulation period of 1.4 ms which corresponds to 5.6 ms of effective simulation time. The coarse-grained representation of the homology model of serotonin_{1A} receptor and the POPC bilayers with different cholesterol concentrations were obtained from previous studies^{123,125}. A schematic top-view representation of the initial system is shown in Fig. 6.1. Data for monomer simulations of serotonin_{1A} receptor in bilayers with different cholesterol concentrations were obtained from our previous studies¹²⁶.

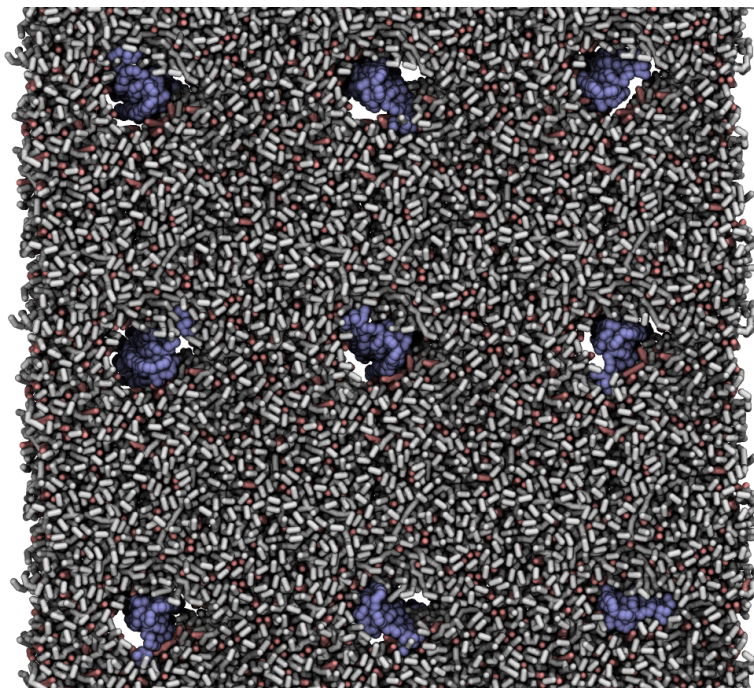


Figure 6.1: A schematic top-view representation of the initial configuration of the receptors in POPC bilayer with 50% cholesterol. The receptors are shown in blue, phospholipids in gray and cholesterol in pink. Water is not shown for clarity

6.2.2 Simulation parameters

All simulations and analysis were performed using GROMACS version 4.5.5³¹⁴. Systems were represented using MARTINI coarse-grained force-field 2.1 for the protein and version 2.0 for lipid parameters^{232,283}. Steepest-descent algorithm was used for energy minimization of the systems. Non-bonded interactions were used in their shifted form with electrostatic interactions shifted to zero in the range of 0-1.2 nm and Lennard-Jones interaction shifted to zero in the range of 0.9-1.2 nm. Berendsen thermostat algorithm³¹⁵ was used to maintain system temperature at 300K by weakly coupling the temperature of each molecular group to the thermostat with a coupling constant of 0.1 ps. Semi-isotropic pressure was maintained at 1 bar independently in the plane of the bilayer and perpendicular to it using Berendsen's barostat algorithm with a coupling constant of 0.5 ps and a compressibility of $3 \times 10^{-5} \text{ bar}^{-1}$. Initial velocities were chosen randomly from a Maxwell distribution at 300K. Bond lengths were kept constant using LINCS algorithm. A time step of 20 fs was used with neighbour list updated every 10 steps. Periodic boundary conditions were maintained along x, y and z direction. Simulations

were rendered using VMD software³¹⁶ and MARTINI secondary structure rendering scripts. Plots were generated using Grace.

6.2.3 Analysis

Quantitative estimation of transmembrane helices at contact interface

The transmembrane helices at the contact interface between two receptors were determined following their association using the same methodology as in our earlier work²³⁸. The cut-off considered for interaction between the receptors was set to 0.5 nm. The values were averaged over all stable contact instances between the receptors and all simulations for each system.

Cholesterol occupancy at contact interface

We quantitated the correlation between transmembrane helices showing increased lipid occupancy and their involvement at contact interface by calculating ‘interface occupancy score’ as discussed in our earlier work¹²⁶. The ‘interface occupancy score’ is defined for each helix in a given association between two receptors as the product of the normalized cholesterol occupancy and the probability of that conformation. The diagonal elements in the matrix correspond to helices at the contact interface with high cholesterol occupancy around it while the off-diagonal elements correspond to increased cholesterol occupancy around helices not involved at the contact interface. A similar interface occupancy matrix for quantitating POPC involvement was also calculated.

Non-bonded energetics

The protein-protein and protein-lipid non-bonded interaction energetics for all receptors were calculated as mentioned in our earlier work²³⁹. The values were binned at a bin size of 0.2 nm inter-receptor distance.

6.3 Results

We carried out multiple μ s simulations of serotonin_{1A} receptors in POPC bilayer and POPC/cholesterol bilayer with varying cholesterol concentrations to examine the concentration-dependant role of cholesterol in influencing higher order oligomerization. The receptors were

well separated from each other before initiating simulation to ensure bias-free self association. Multiple copies of the receptor were chosen to allow formation of dimers and other higher order oligomers during the simulation.

6.3.1 Cholesterol inhibits higher order oligomerization in serotonin_{1A} receptor

During the course of the simulation, the receptors freely diffused in the bilayer before interacting with each other at μ s timescale. A time-distance plot showing minimum distance between the receptors for a representative simulation from each cholesterol concentration is shown in Fig. 6.2.

Transient association between the receptors were observed at all bilayer compositions as shown by short stretches of dark blue patches in Fig. 6.2. Relative population of the different cluster sizes observed during the simulation is given in Table 6.2.

Table 6.2: *Relative population of cluster sizes of serotonin_{1A} receptor observed at different cholesterol concentrations*

Cluster size	POPC	POPC/ 9% cholesterol	POPC/ 30% cholesterol	POPC/ 50% cholesterol
Monomer	0.35	0.14	0.45	0.74
Dimer	0.07	0.50	0.33	0.12
Trimer	0.21	0.07	0.08	0.06
Tetramer	0.07	0.07	0.12	0.06
Pentamer	0.07	0.00	0.00	0.00
Hexamer	0.14	0.00	0.00	0.00
Heptamer	0.00	0.14	0.00	0.00
Octamer	0.07	0.07	0.00	0.00
Nonamer	0.00	0.00	0.00	0.00

In POPC bilayer, receptors associated to form higher order aggregates, ranging from dimers to octamers (Fig. 6.3).

The oligomer conformations showed a linear arrangement of receptors. Presence of cholesterol in the bilayer decreased the propensity of the receptors to form larger clusters. At higher cholesterol concentrations (30% and 50%), monomers were predominantly observed followed by dimers and occasionally trimers and tetramers (Fig. 6.3). Clusters larger than tetramers, seen in POPC bilayer and POPC/cholesterol bilayer with 9% cholesterol, were not observed in

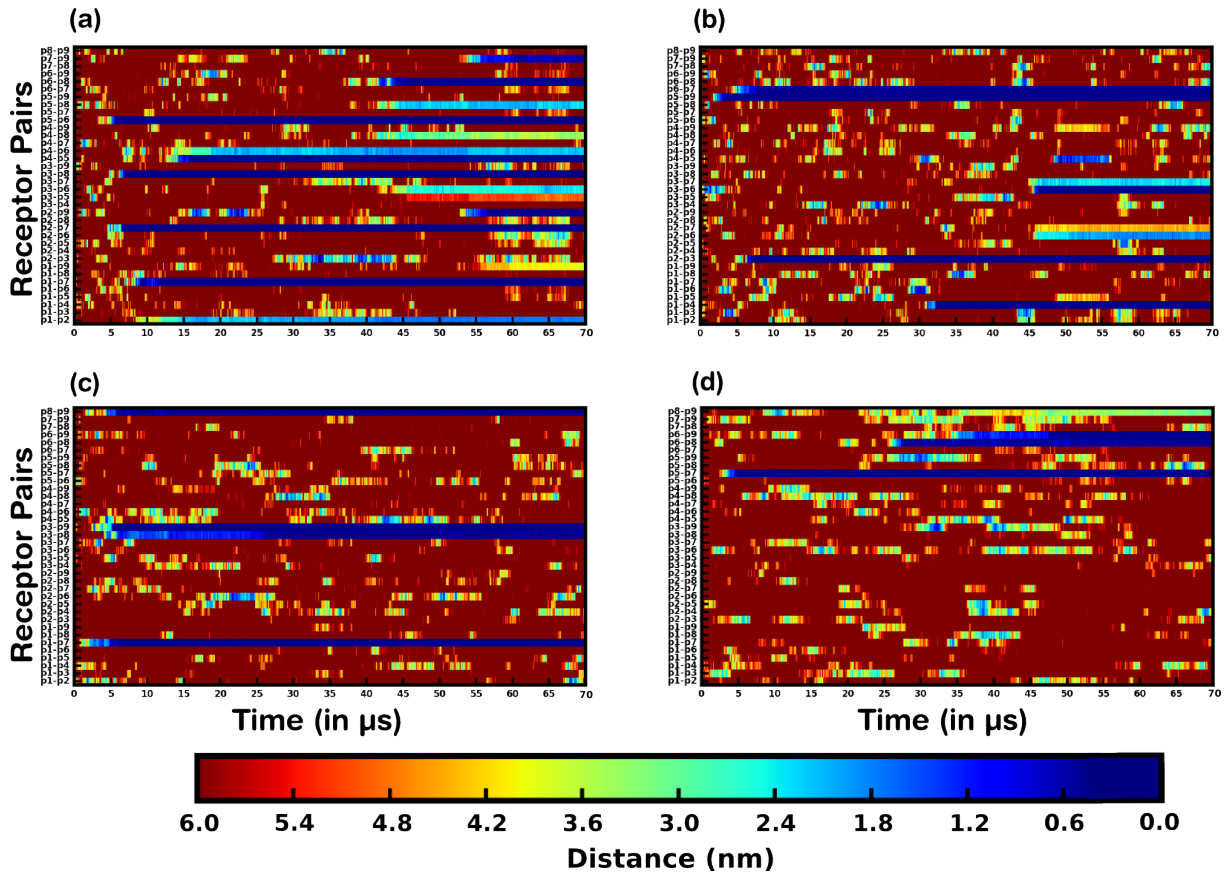


Figure 6.2: A representative time-distance plot showing minimum distance between the receptors during the course of the entire simulation period in (a) POPC bilayer and POPC bilayers with (b) 9% (c) 30% and (d) 50% cholesterol concentration. Distances between the receptors is color coded and shown as a scale bar. Association between the receptors is characterized by distances less than 0.5 nm shown by dark blue stretches in the plot. Each row in the panel corresponds to pair-wise distance between receptors. Distances between the receptors greater than 6 nm have been ignored for clarity and to ensure clear distinction between associated and non-associated states between the receptors.

bilayers with 30% and 50% cholesterol.

6.3.2 Cholesterol modulates contact interface between receptors

We characterized the conformation of the oligomer species observed at each cholesterol concentration in our simulations. Relative populations of different contact interfaces were quantitated and are represented by contact maps as shown in Fig. 6.4.

We observed multiple distinct contact interfaces in POPC bilayer and POPC/cholesterol

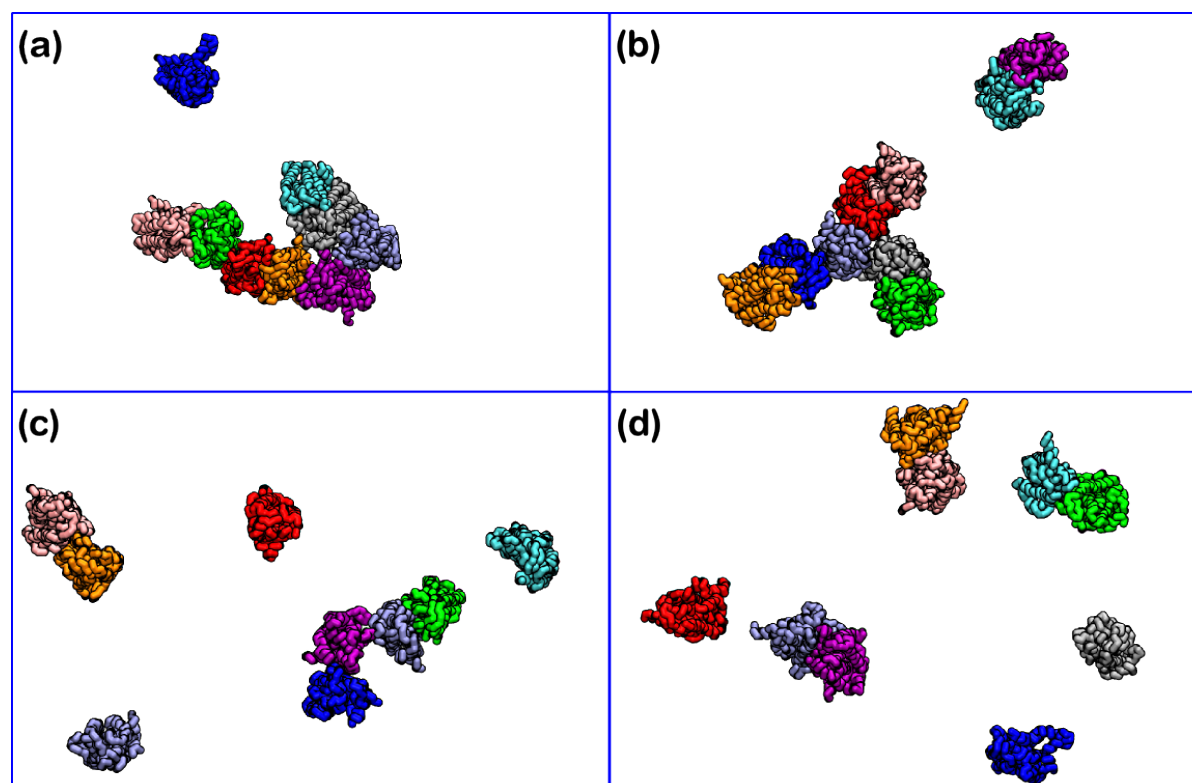


Figure 6.3: A schematic representation of the oligomer arrangement observed during simulation in (a) POPC bilayer and POPC bilayers with (b) 9% (c) 30% and (d) 50% cholesterol concentration. Each receptor in the simulation is represented by a different color.

bilayer with 9% cholesterol. Heteromeric contact involving transmembrane helix I of one receptor and helix V of the other was predominantly observed among the oligomeric species formed in the absence of cholesterol (Fig. 6.4a). This conformation appears to be relatively flexible as alternate contacts involving transmembrane helix I with helix IV and VI were also observed, though less frequently. Additionally, a homomeric contact between the receptors involving transmembrane helix I was also prominent among the interfaces observed in oligomers. This contact interface was sampled less frequently in POPC/cholesterol bilayer with 9% cholesterol (Fig. 6.4b) and completely absent in POPC/cholesterol bilayers with 30% and 50% cholesterol (Fig. 6.4c,d). Multiple contact interfaces between the receptors were also observed in POPC/cholesterol bilayers which decreased at higher cholesterol concentrations (Fig 6.4c,d). The predominance of heteromeric contacts involving transmembrane helix I of one receptor and helices IV, VI of the other persisted even at higher cholesterol concentrations (Fig. 6.4c,d). A different homomeric interface involving transmembrane helices V and VI was also prominently

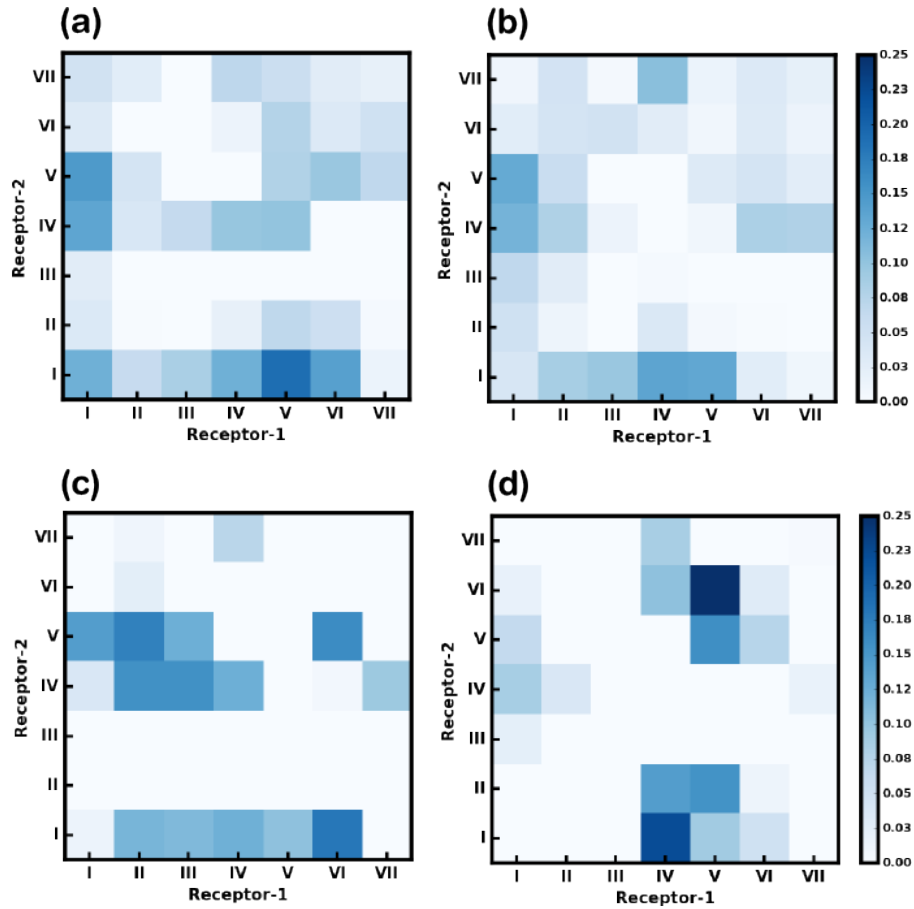


Figure 6.4: Contact maps showing the relative population of different contact interfaces in (a) POPC bilayer and POPC bilayers with (b) 9% (c) 30% and (d) 50% cholesterol concentration. The values were averaged over all instances, simulations and normalized by the time of occurrence and simulation length. The color scale bar indicates normalized population.

sampled at these cholesterol concentrations.

6.3.3 Different contact interfaces are sampled during transient association between receptors

The receptors showed transient associations with each other during the simulations ranging from several ns to μ s (Fig. 6.2). The contact interfaces sampled by the receptors during these transient interactions were quantitated and are represented by the contact maps as shown in Fig. 6.5.

In POPC bilayer, the transient association between the receptors primarily involved a homomeric contact between transmembrane helix I. In addition, a heteromeric contact between

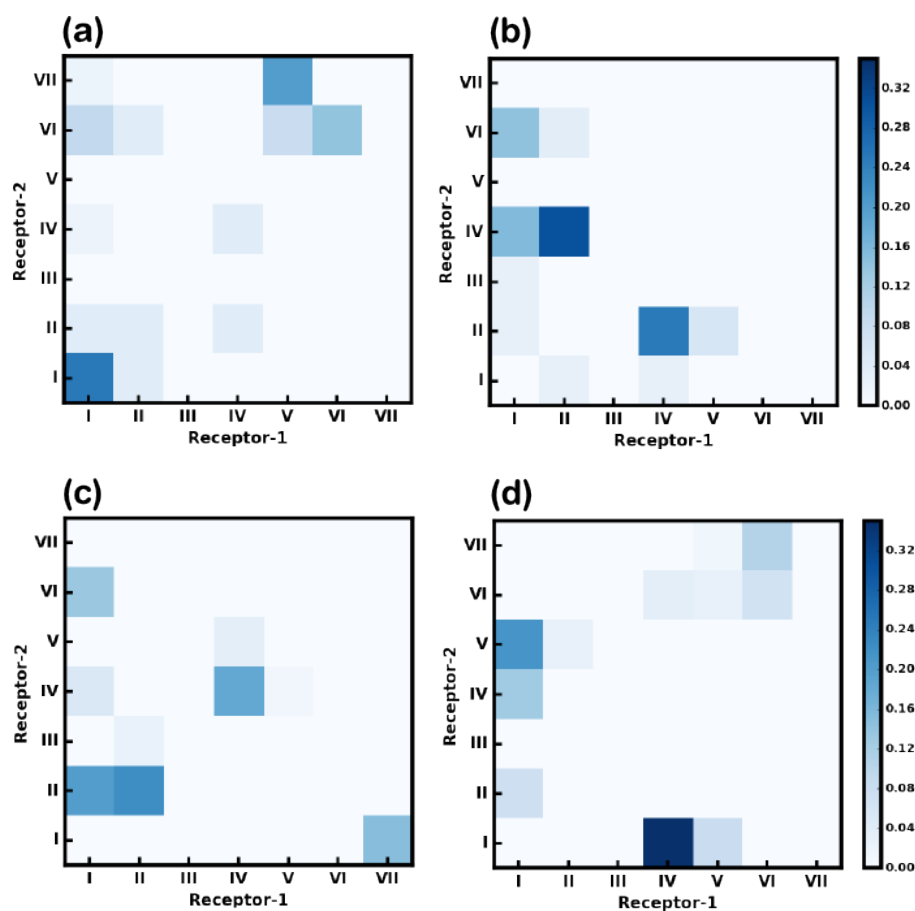


Figure 6.5: Contact maps showing the relative population of different contact interfaces sampled during the period of transient association between the receptors in (a) POPC bilayer and POPC bilayers with (b) 9% (c) 30% and (d) 50% cholesterol concentration. The values were averaged over all instances, simulations and normalized by the time of occurrence and simulation length. The color scale bar indicates normalized population.

transmembrane helices V and VII was also prominently observed, along with few other interfaces (Fig. 6.5a). In bilayers with cholesterol, multiple contact interfaces were sampled during transient associations between the receptors (Fig. 6.5b,c,d). Interestingly, the homomeric interface involving transmembrane helix I which was largely sampled in POPC bilayer, was not observed in bilayers with cholesterol.

6.3.4 Cholesterol occupancy around transmembrane helices correlates with its involvement at contact interface

To investigate if cholesterol association with transmembrane helices influences its involvement at contact interface, we quantitated the correlation between these processes using interface occupancy score (see Methods for details). Correlation plots for interface occupancy of cholesterol in POPC bilayers with different cholesterol concentrations is shown in Fig. 6.6(a-c).

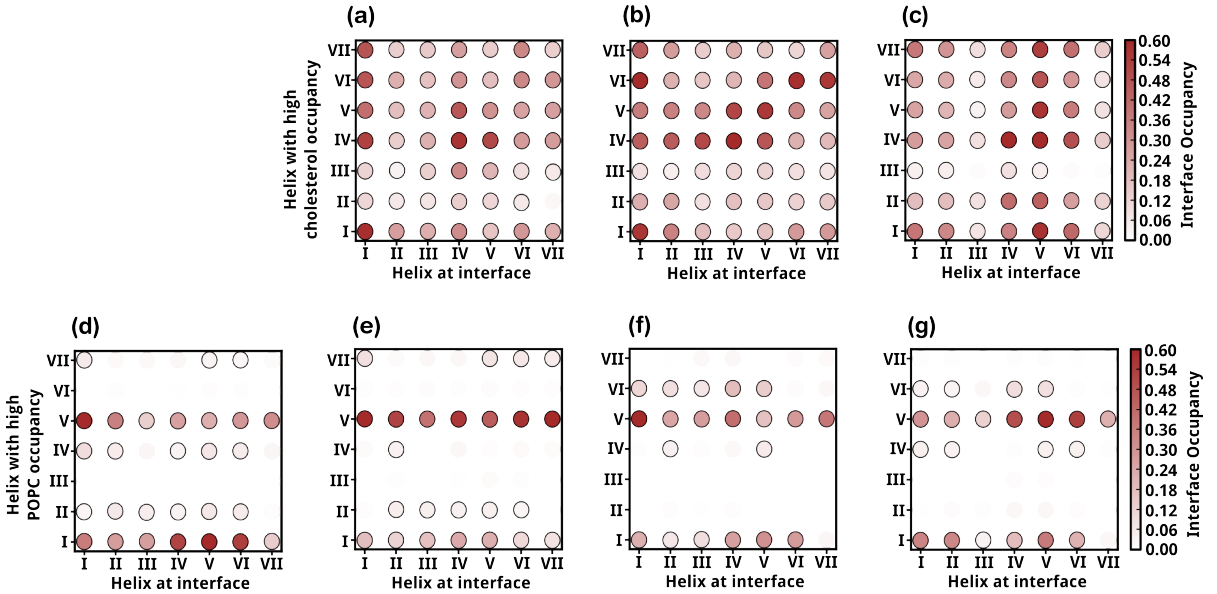


Figure 6.6: Normalized occupancy of cholesterol (a-c) and POPC (d-g) at each helix in the associated state between two receptors plotted as a function of the helices at the contact interface. The interface occupancy scores of cholesterol are shown for POPC bilayers with (a) 9 (b) 30 and (c) 50% cholesterol concentrations. The interface occupancy scores of POPC are shown for (d) POPC bilayers and POPC bilayers with (e) 9 (f) 30 and (g) 50% cholesterol concentrations. The interface occupancy scores were normalized to the relative probability of occurrence of the transmembrane helix at the contact interface and highest maximum cholesterol occupancy for each receptor. The diagonal elements correspond to high occupancy of cholesterol (or POPC) at helices that constitute the contact interface. The off-diagonal elements correspond to occupancy of cholesterol (or POPC) at the helices not at the contact interface.

Diagonal elements correspond to transmembrane helices with increased cholesterol occupancy and involvement at contact interface while off-diagonal elements correspond to cholesterol occupancy at helices away from the contact site. In POPC/cholesterol bilayer with 9% cholesterol, some diagonal elements showed high scores suggesting increased cholesterol occupancy around these helices at the contact interface (Fig. 6.6a). However, the correlation is not very prominent as few of the helices not at the interface also showed increased cholesterol

occupancy. In POPC/cholesterol bilayers with 30% and 50% cholesterol, very high interface occupancy scores were observed for diagonal elements suggesting increased correlation between cholesterol occupancy at transmembrane helices and their involvement at contact interface (Fig. 6.6b,c). At 50% cholesterol, correlation was less pronounced as high cholesterol occupancy was also observed around helices away from the contact interface (Fig. 6.6c). In contrast, POPC occupancy around transmembrane helices showed limited correlation with the involvement of these helices at contact interface (Fig 6.6d-g). As in our dimer studies¹²⁶, we observed increased cholesterol occupancy at contact interface and absence of a similar correlation for POPC, strongly suggesting the involvement of cholesterol in modulating oligomer conformation.

6.3.5 Protein-lipid interaction energetics regulates serotonin_{1A} receptor oligomerization

The contribution of the interaction energetics between lipid and membrane protein towards driving higher order cluster formation in serotonin_{1A} receptor was investigated as described in an earlier study²³⁹. Interaction energies were calculated as a function of inter-receptor separation (Fig. 6.7).

In POPC bilayer, the most favourable minima for protein-protein interaction was seen at a separation of 2.5 nm (Fig. 6.7a). With increasing cholesterol concentration, this minima occurred at larger separation between the receptors: 2.6 nm at 9%, 2.8 nm at 30% and 3.2 nm at 50% cholesterol concentration (Fig. 6.7c,e,g). Also the protein-protein interaction energy at the favourable minima increased at higher cholesterol concentrations. Multiple other minima were observed at larger distances between the receptors suggesting formation of meta-stable states during receptor association. Interestingly, protein-lipid interaction energy showed a trend opposite to that for protein-protein interaction, with relative increase in energetics at smaller receptor-receptor separation which increased at higher cholesterol concentrations (Fig. 6.7b,d,f,h).

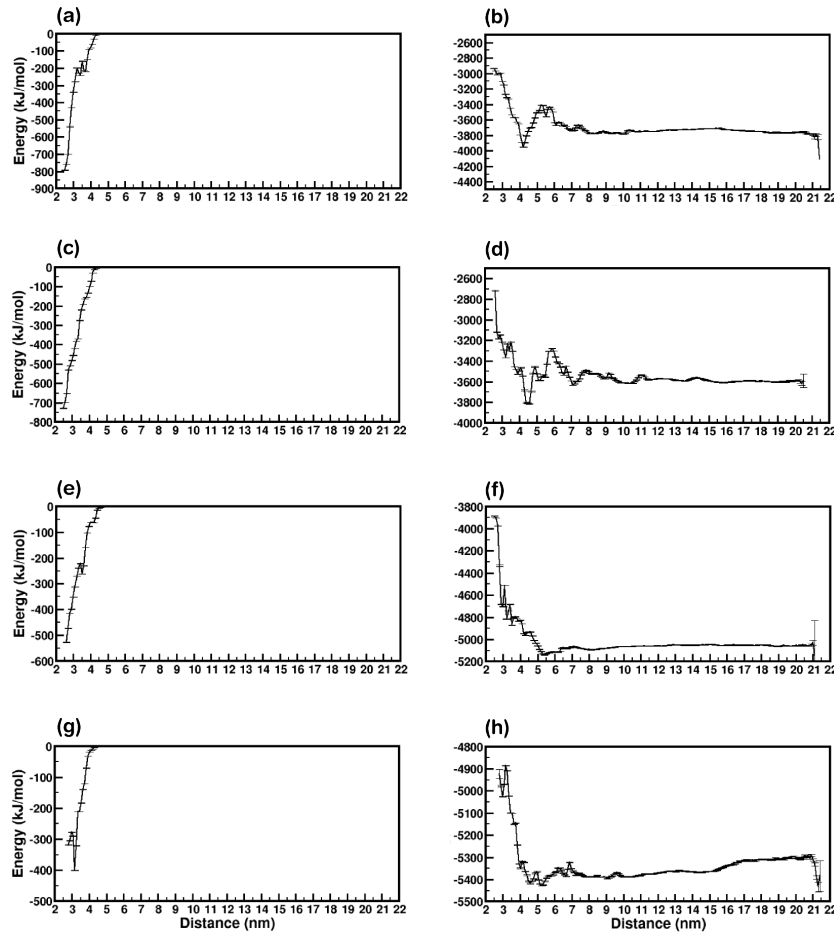


Figure 6.7: Interaction energy as a function of inter-receptor distance calculated for protein-protein contacts in POPC bilayers with (a) 0% (b) 9% (c) 30% and (d) 50% cholesterol concentration. Protein-lipid interaction energies in POPC bilayer and POPC bilayers with (e) 0% (f) 9% (g) 30% and (h) 50% cholesterol concentration. The values have been averaged over the total simulation period and across all simulations.

6.4 Discussion

Cholesterol an essential component of eukaryotic cell membrane, has been known to influence structure and function of membrane proteins, including GPCRs^{103,119,121}. Experimental studies have also revealed that cholesterol modulates higher order organization of GPCRs^{122,123} though the molecular details of the underlying mechanism has not been well examined. The aim of the current study was to provide a “dynamic and molecular insight” into oligomerization of serotonin_{1A} receptor using coarse-grained molecular dynamics simulation and investigate the role of cholesterol in the oligomerization process.

Cholesterol appeared to prevent higher order association of serotonin_{1A} receptor in a concentration-dependant manner. Hydrophobic mismatch between the transmembrane segment of membrane protein and the bilayer thickness is known to influence membrane protein association⁷⁵. In our simulations, we observed formation of larger clusters in POPC bilayer which was reduced drastically at higher cholesterol concentrations. Monomer simulations of serotonin_{1A} receptor in POPC bilayer reveal the presence of increased positive hydrophobic mismatch around the receptor¹²⁶. We believe that this mismatch serves as a driving force for the receptors to form clusters. The presence of cholesterol, however, alleviates the overall hydrophobic mismatch, thus allowing the receptors to exist as monomers and/or lower order oligomers at higher cholesterol concentrations.

Conformation of the clusters appears to be largely modulated by cholesterol occupancy around transmembrane helices and local membrane perturbation¹²⁶. The positive hydrophobic mismatch around serotonin_{1A} receptor in POPC bilayer was localized around transmembrane helices I and II¹²⁶. A relatively lower mismatch was also observed around transmembrane helix IV. Results from dimerization studies of serotonin_{1A} receptor in POPC bilayer showed increased population of dimers with a homomeric interface involving transmembrane helix I, suggesting that the increased perturbation around transmembrane helix I plays a key role in stabilizing the homomeric conformer¹²⁶. However in our current study, we observed formation of larger clusters with an increased occurrence of heteromeric association between transmembrane helices I and II of one receptor and helices IV and V of the other in addition to the homomeric transmembrane helix I interface. Interestingly, this homomeric interface was predominantly sampled during the transient association between the receptors (Fig 6.5). These results suggest that, although transmembrane helix I is involved in mediating association between the receptors, they occasionally dissociate to allow reorganization of the cluster, possibly to optimize protein-protein, protein-lipid and lipid-lipid interactions (Fig. 6.7). In POPC bilayers with 9% cholesterol, hydrophobic mismatch persists around transmembrane helices I and II but is reduced in magnitude. However, mismatch around transmembrane helices IV and V is relatively increased. This is reflected in the increased occurrence of a heteromeric interface involving transmembrane helix I of one receptor and helices IV and V of the other.

At higher cholesterol concentrations (i.e POPC bilayers with 30% and 50% cholesterol), hydrophobic mismatch persists around transmembrane helices IV and V resulting in their

increased involvement at the contact interface, while it is reduced in magnitude around helices I and II¹²⁶. Increased occupancy of cholesterol at transmembrane helix I further prevents its involvement at the contact interface despite the presence of residual local mismatch around it. Cholesterol exhibits multiple binding sites around the receptor¹²⁶. Association of cholesterol with the receptors possibly reduces their interaction with each other. The presence of cholesterol in the lipid bilayer appears to favour protein-lipid interaction over protein-protein interaction. This is shown by larger separation between the receptors at their energy minima with increasing cholesterol concentration (Fig. 6.7).

In a previous experimental study investigating the role of cholesterol on higher order organization of serotonin_{1A} receptor, it was reported that receptors reorganize into larger clusters upon acute cholesterol depletion¹²³. In order to verify this finding from our simulation, we depleted cholesterol from one of the receptor simulations carried out in POPC bilayer with 50% cholesterol. The receptors which existed predominantly as monomers and dimers at 50% cholesterol concentration soon formed larger clusters within a few μ s of simulation after cholesterol depletion (Fig. 6.8).

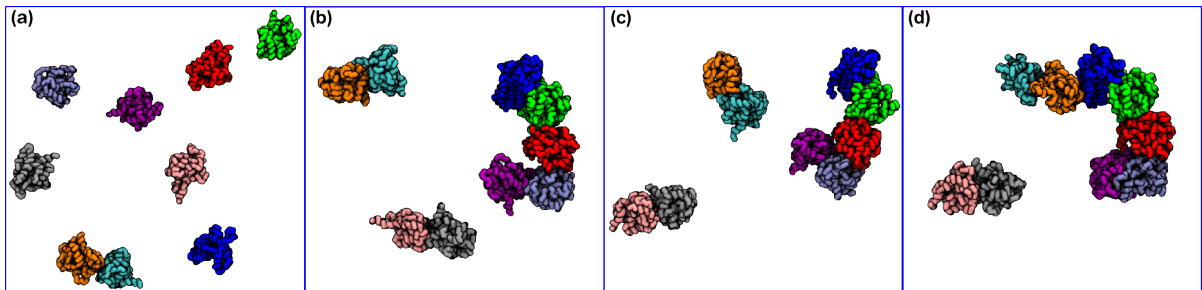


Figure 6.8: *Formation of higher order oligomers from 50% POPC/cholesterol bilayer after removing cholesterol. (a) Conformation of the receptors in 50% POPC/cholesterol bilayer at the end of 70 μ s. This is the starting conformation ($t=0 \mu$ s) after cholesterol removal. Time course evolution of oligomers shown at time $t=$ (b) 10 (c) 20 and (d) 30 μ s of simulation. Each receptor in the simulation is represented by a different color.*

Interestingly, a related study by the same group suggests the presence of higher-order oligomers of serotonin_{1A} receptors under physiological conditions and that, following acute cholesterol depletion, results in their reorganization into predominantly dimeric state¹²². Our results also match well with earlier computational studies investigating GPCR oligomerization in lipid bilayers with varying thickness²³³. Localized regions of positive hydrophobic mismatch

around rhodopsin formed sites for receptor-receptor association. Rhodopsin formed “string-like” clusters in lipid bilayers with shorter acyl chains and isolated aggregates in bilayers with longer acyl chains. Cholesterol increases lipid order and thereby the overall bilayer thickness^{390,391}. The presence of cholesterol at varying concentrations in POPC bilayer appeared to generate similar effects as observed for rhodopsin in bilayers with varying acyl chain lengths²³³. However, our findings suggest that membrane perturbation alone does not dictate conformation of the cluster as interaction of cholesterol with transmembrane helices also influences its involvement at the contact interface. Therefore, we suggest that a combination of direct and indirect lipid-mediated effects modulate oligomer conformation in serotonin_{1A} receptor.

Our results highlight the role of cholesterol in modulating the process of oligomerization and conformation of resultant oligomers through a complex combination of direct and indirect effects. Serotonin_{1A} receptors are expressed in brain cells which are known to have very high membrane cholesterol concentration¹¹⁸. Based on our findings, it appears that, under normal physiological brain cholesterol concentration, specific conformations of lower order serotonin_{1A} receptor oligomers are possibly more favoured which could have functional significance. Changes in metabolic homeostasis of brain cholesterol due to age and other factors could largely affect the equilibrium between the oligomeric species which could be implicative in neurodegenerative, cognitive and behaviour disorders due to functional dysregulation³⁹². A comprehensive understanding of the molecular modulation of receptor conformation by cholesterol would be essential for optimizing drug specificity and efficacy.

Besides cholesterol, brain cells are also highly enriched in sphingolipids³⁹³. Sphingolipids, in association with cholesterol, generate lateral asymmetry in lipid distribution and result in formation of membrane microdomains¹⁸. Sphingolipids have also been shown to be essential for serotonin_{1A} receptor function^{394,395}. Although reports suggest that sphingolipids do not alter serotonin_{1A} receptor organization¹²³, it could indirectly modulate conformation of associated states by altering cholesterol distribution around the receptor.

In conclusion, we have provided a molecular understanding of cholesterol-mediated effects in regulating oligomerization by carrying out several μ s timescale coarse-grained molecular dynamics simulation of multiple copies of serotonin_{1A} receptors under different bilayer compositions. Cholesterol prevents formation of higher order oligomers. We believe that cholesterol, through a complex combination of direct and indirect lipid-mediated effects, regulate both the


process of oligomerization and conformation of oligomers in a concentration-dependant manner. These findings could have valuable significance in target-specific drug development.

The Ganglioside GM1 Interacts with the Serotonin_{1A} Receptor via the Sphingolipid Bind- ing Domain

“It’s the possibility of having a dream come true that makes life interesting.”

– Paulo Coelho, *The Alchemist*

7.1 Introduction

ukaryotic cell membrane exhibits diversity in its lipid composition¹³. Phospholipids form the largest fraction of these lipids, followed by cholesterol and sphingolipids³⁴. In our previous studies, we have examined the specific and non-specific interaction of phospholipids (POPC) and cholesterol with serotonin_{1A} receptor¹²⁶. These lipid-mediated effects were shown to regulate higher order organization of the receptors. In this study, we investigate the binding sites for GM1 ganglioside, a glycosphingolipid, around serotonin_{1A} receptor and the effect of cholesterol on influencing sphingolipid distribution around the receptor.

Sphingolipids constitute ~ 10-20% of total membrane lipids and have been implicated in cell signaling, growth, differentiation and neoplastic transformation^{38,396}. The distribution of

sphingolipids in the bilayer has been extensively studied and it is postulated that they coalesce with cholesterol to form ordered lipid domains that laterally segregate from the bulk membrane^{46,60,397}. However, this view has been recently questioned^{26–28}. The function of several membrane proteins, including GPCRs, has been reported to be dependent on sphingolipids^{395,398}. One of the best studied GPCRs in the context of sphingolipid-dependent effects, is the serotonin_{1A} receptor³⁹⁵, a representative GPCR involved in behavior, development and cognition¹¹⁷.

Previous work by Chattopadhyay *et al.* and others has demonstrated that metabolic depletion of glycosphingolipids affects receptor function^{394,395,399}. Similar to phospholipids and cholesterol, the regulatory effect of glycosphingolipids on GPCR function could be a result of direct or indirect interaction, or a combination of both. Direct interactions are implicated by the fact that several sphingolipid-dependent membrane proteins appear to have a consensus ‘sphingolipid binding domain’ (SBD). SBD was initially identified and characterized in HIV-1 surface envelope glycoprotein gp120 and amyloid proteins that were known to exhibit sphingolipid-dependent conformational transitions, and was later identified in a wide range of proteins including receptors, toxins, and viral proteins^{400–402}. The SBD motif consists of a characteristic combination of aromatic, basic and turn-inducing residues. The aromatic residues in this domain have been predicted to be crucial in interaction with the sugar moiety of glycosphingolipids, with charged residues forming electrostatic bonds with sphingomyelin^{401,402}. We have previously shown that this motif is present in serotonin receptors and appears to be evolutionarily conserved in case of the serotonin_{1A} receptor⁴⁰³. Interestingly, the motif is present at the extracellular loop, and not at the transmembrane domain of the receptor. It has been recently reported that the SBD motif of the serotonin_{1A} receptor binds preferentially to gangliosides relative to other sphingolipids³⁹³. However, the nature of the interaction between GPCRs and sphingolipids in general, and glycosphingolipids in particular, remains poorly explored. To the best of our knowledge, no reports exist delineating direct or indirect interaction of glycosphingolipids with GPCRs.

In this work, we have explored the interaction of the ganglioside GM1, the most common glycosphingolipid type (typically ~ 2 –5% of total membrane lipids), with the serotonin_{1A} receptor. Toward this goal, we performed a series of coarse-grained molecular dynamics simulations, totaling 400 μ s, of the serotonin_{1A} receptor embedded in membrane bilayers containing

GM1. Our results show that GM1 binds to the serotonin_{1A} receptor predominantly at the extracellular loop 1 and specifically at the SBD site. The interaction of the receptor with GM1 appears to stabilize a ‘flip-out’ conformation in which W102 of the extracellular loop 1 flips out from the central lumen of the receptor toward the membrane. These results demonstrate that GM1 directly modulates conformational dynamics of the extracellular loop 1 of the serotonin_{1A} receptor, and could have important consequence in ligand binding and function of the receptor.

7.2 Methods

7.2.1 System setup

Molecular dynamics simulations of the serotonin_{1A} receptor were performed in the presence of GM1 to investigate GPCR-glycosphingolipid interaction. Simulations were performed in bilayers with different lipid compositions: POPC, POPC/cholesterol (POPC/chol), POPC/GM1 and POPC/GM1/cholesterol (POPC/GM1/chol) (Table 7.1).

Table 7.1: *Initial System composition*

System	Number of simulations	Simulation time (μ s)	Number of molecules			
			POPC	Chol.	GM1	Water
With Receptor:						
POPC	10	10	280	0	0	4828
POPC/chol	10	10	168	112	0	4094
POPC/GM1	10	10	274	0	6	5652
POPC/GM1/chol	10	10	232	160	8	5937
Without Receptor:						
POPC	1	10	280	0	0	4828
POPC/chol	1	10	168	112	0	4094
POPC/GM1	1	10	274	0	6	5652
POPC/GM1/chol	1	10	232	160	8	5937

The composition of the POPC/GM1/chol bilayer was chosen to so as to realistically represent the physiological cell membrane. POPC/GM1, POPC/chol and POPC bilayers were simulated as controls. All bilayer compositions including those with GM1 were self assembled from a random starting conformation and equilibrated for 50 ns. The bilayer was aligned such

that the GM1 cluster was on the upper leaflet, corresponding to the outer leaflet of the cell membrane. A coarse-grained representation of the homology model of serotonin_{1A} receptor¹²⁴, obtained from our earlier work^{125,379}, was inserted into the equilibrated bilayer such that the initial minimum distance between the receptor and any GM1 lipid was at least 2 nm. Ten independent simulations, each of 10 μ s, were performed with different starting receptor orientation and initial velocity. Lipid bilayers without the receptor were simulated as control for same time.

7.2.2 Simulation parameters

All simulations were carried out using GROMACS version 4.5.5³¹⁴, with MARTINI force-field version 2.2^{232,268,283,287,295}. Energy minimization was carried out using steepest descent algorithm. Shift potential were used for non-bonded interactions with electrostatic interactions shifted to zero in the range of 0.0-1.2 nm and van der Waals interaction shifted to zero in the range of 0.9-1.2 nm. Temperature of each molecular group in the system was weakly coupled to a thermostat at 300 K using the v-rescale algorithm⁴⁰⁴ with a coupling constant of 0.1 ps. Semi-isotropic pressure coupling was maintained at 1 bar independently in the plane of the bilayer and perpendicular to the bilayer using Berendsen's barostat algorithm³¹⁵ with a coupling constant of 0.5 ps and a compressibility of 3×10^{-5} bar⁻¹. Initial velocities for the simulations were chosen randomly from a Maxwell distribution at 300 K. Bond lengths were kept constant using the LINCS algorithm⁴⁰⁵. A time step of 5 fs was used for the simulations with neighbor list updated every 10 steps. Periodic boundary conditions were maintained along x, y and z direction. Simulations were rendered using VMD software³¹⁶ and MARTINI secondary structure rendering scripts. Plots were generated using Grace.

7.2.3 Analysis

Residue-wise maximum occupancy of GM1

The maximum occupancy of GM1 was calculated at each amino acid residue of the serotonin_{1A} receptor. We define maximum occupancy as the maximum time of the simulation for which GM1 remains associated with the residue, based on a cut-off distance of 0.55 nm¹²⁵. The value was averaged over all simulations for each bilayer composition and normalized. A value of 1 indicates that GM1 remains associated with the given residue for the longest time during the

simulation while a value of zero indicates that GM1 never interacted with the residue. In the plots corresponding to the occupancy of the individual GM1 beads, the MARTINI bead names (GM1-17) were replaced by the head group bead number (HG1-17), to avoid confusion. The mapping remains the same.

Spatial distribution of GM1 around the serotonin_{1A} receptor

Spatial density distribution of GM1 around the serotonin_{1A} receptor was calculated using the g-spatial routine in GROMACS package. The receptor was centered in the bilayer with its translational and rotational motion removed. The voxel element was set to 0.07 nm in each direction. The calculated 3D spatial distribution function was averaged over the extracellular leaflet.

Tryptophan orientation

The orientation of W102 residue in the extracellular loop 1 of the serotonin_{1A} receptor was calculated by measuring the angle made by the vector connecting coarse-grained beads SC1 and SC4 of W102 with the bilayer normal. The values were calculated for the entire simulation time in POPC and POPC/chol bilayers and subsequent to GM1 association in POPC/GM1 and POPC/GM1/chol bilayers.

Preferential partitioning of lipid species

Preferential partitioning of the membrane lipids (or receptor) is calculated as the relative number of contacts of a particular component with each of the other components, normalized for the total number of lipids (and receptor) in the system^{268,406}:

$$p_A = \frac{(c_A/n_A)}{\sum_x (c_x/n_x)} \quad (7.1)$$

where, p_A is the preferential partitioning with membrane component A, c_A the number of contacts with component A, n_A the number of molecules of component A. Contacts were defined with respect to GL1 and GL2 beads for POPC, AM1 and AM2 beads for GM1 and ROH bead for cholesterol. In case of the receptor, we chose CG beads of the receptor at the height of phosphate head group region of POPC as reference. Two molecules were considered

to be in ‘contact’ if they were within 0.55 nm. The preferential partitioning was calculated for the last 1 μ s of the simulation time from each of the sets and averaged across the sets.

Cholesterol ‘flip-flop’ rate

To calculate the rate of transbilayer diffusion (‘flip-flop’) of cholesterol, we calculated the number of transitions for each cholesterol molecule between the extracellular and intracellular leaflets during the entire simulation time. The value was averaged over the number of cholesterol molecules and the total simulation time.

7.3 Results

7.3.1 GM1 clusters interact with the serotonin_{1A} receptor

In order to probe the interaction of GM1 and the serotonin_{1A} receptor, coarse-grained simulations were performed with the receptor embedded in lipid bilayers of varying composition. In total, ten simulations of 10 μ s each were carried out in POPC/GM1/chol, POPC/GM1, POPC/chol and POPC bilayers. The total simulation time was 400 μ s, corresponding to 1.6 ms of effective simulation time. During the initial equilibration of the bilayer, GM1 molecules rapidly clustered in the outer leaflet, both in the presence and absence of cholesterol. A representative snapshot of the initial system in POPC/GM1/chol bilayers is shown in Fig. 7.1a.

In the initial state, the receptor was placed at a distance of at least 2 nm from the GM1 cluster. The time evolution of minimum distance between the receptor and GM1 during the simulations is shown in Fig. 7.1(b,c). The dark blue stretches in the plot correspond to stable GM1-receptor interactions and the multiple colored bands indicate binding and unbinding events. As evident from the figure, GM1 clusters diffused in the bilayer and subsequently interacted with the receptor at a sub-microsecond timescale. Representative time courses of the simulations containing GM1 are shown in Fig. 7.2.

It was observed that the initial contact sites did not always result in a continued stable association at that site. In most cases, after the initial contact with the receptor, GM1 clusters did not dissociate completely, but diffused around the receptor interacting with it at several non-overlapping sites. In a few cases, GM1 dissociated completely from the receptor and subsequently interacted at the same or different site. After the initial binding/unbinding events,

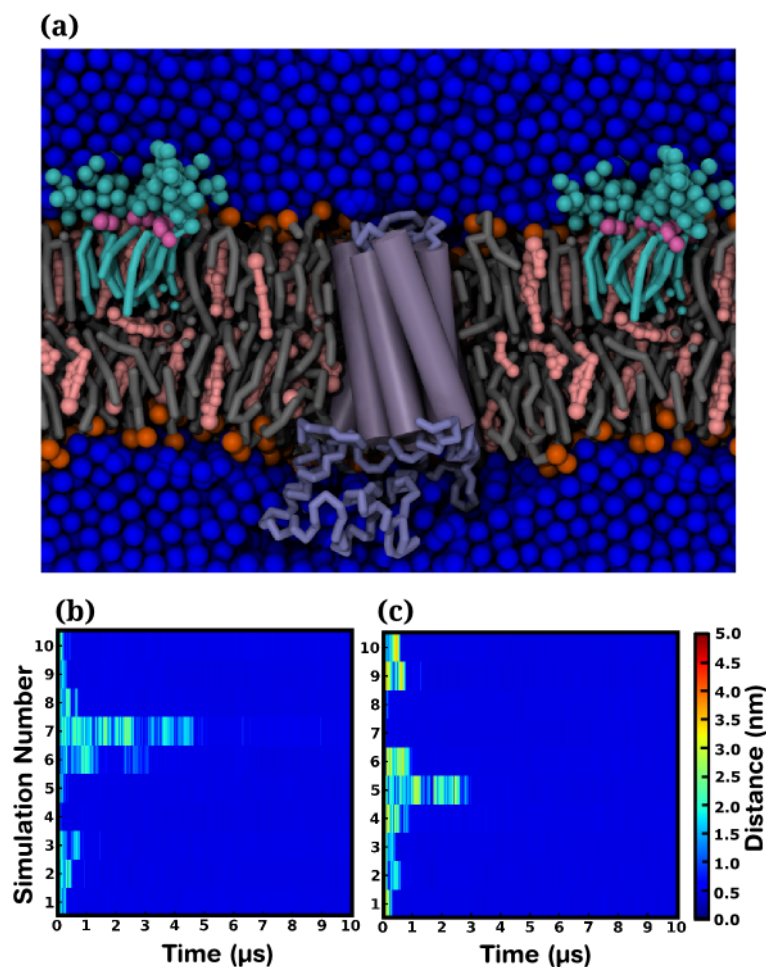


Figure 7.1: (a) A representative snapshot of the serotonin_{1A} receptor in POPC/GM1/chol bilayer at the start of the simulations. The receptor is shown as gray cylinders, with the loops in licorice representation. GM1 is shown in cyan, the phospholipids in gray (choline head group bead in orange), cholesterol in salmon and the water beads in blue. The minimum distance between the receptor and GM1 during the course of the simulation in (b) POPC/GM1/chol and (c) POPC/GM1 bilayers is shown. The color-coded scale bar shows the range of distance between the receptor and GM1. The interacting state, in which GM1 and the receptor interacts, is characterized by distances less than 0.55 nm, corresponding to the dark blue stretches in the plot. The non-interacting state is characterized by distances greater than 0.55 nm represented by yellow, green and light blue regions in the plot. Each row in the panels represents an independent simulation (numbered along the ordinate) while time is shown along the abscissa

the stable interaction sites were sampled and these did not alter significantly during the simulation. Interactions of the receptor with cholesterol and POPC were observed in all bilayers, as previously reported¹²⁵.

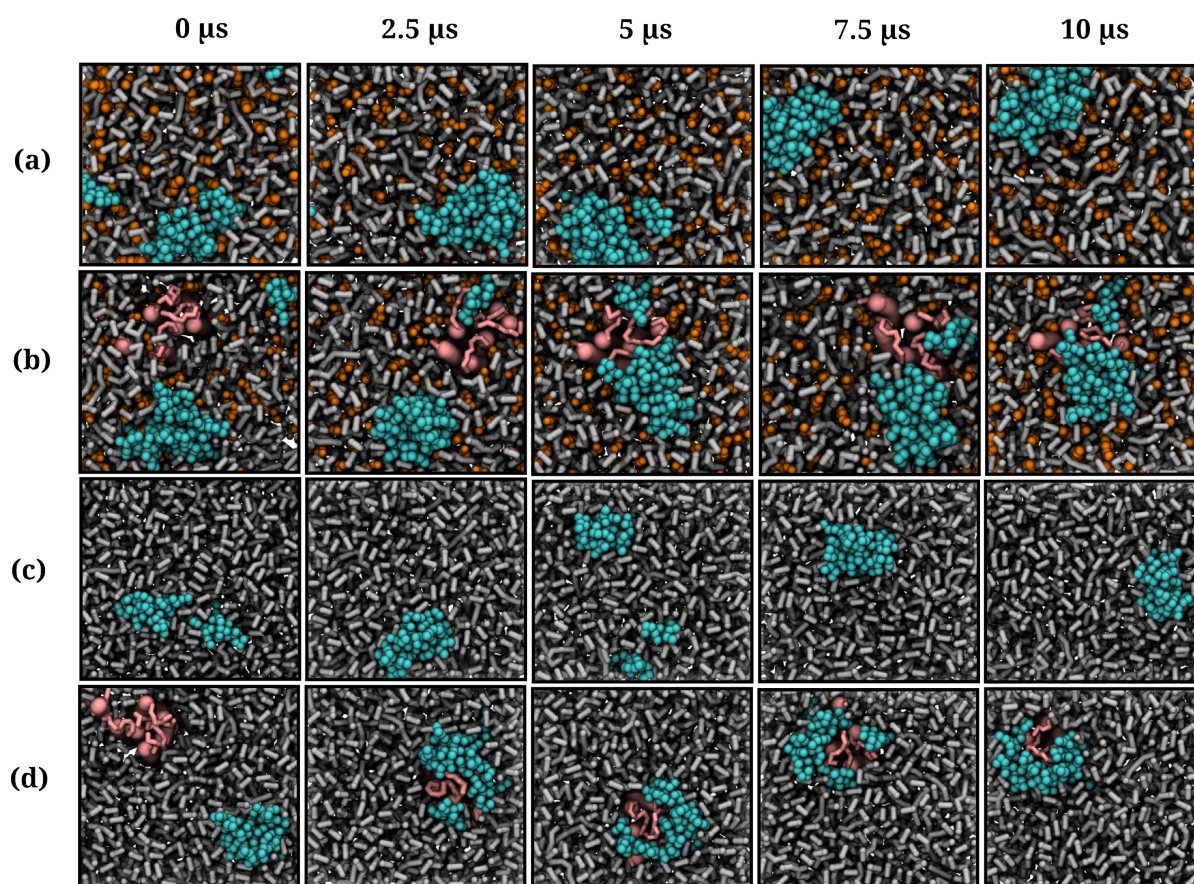


Figure 7.2: Time course of simulations of POPC/GM1/chol and POPC/GM1 bilayers with and without the serotonin_{1A} receptor. POPC is shown in light gray, cholesterol in orange, GM1 in cyan and the serotonin_{1A} receptor in pink. Representative snapshots were taken at regular time intervals of 2.5 μ s from the start of the simulation

7.3.2 GM1 interacts with the extracellular loop 1 of the serotonin_{1A} receptor

To analyze the interacting sites of GM1, we characterized its spatial distribution with respect to the receptor averaged over ten sets of simulations (Fig. 7.3a,b).

The receptor is superimposed on the density plots for clarity. In POPC/GM1/chol bilayers, high GM1 density was observed around the cleft formed by transmembrane helices II and III, followed by relatively low density at helices I, V and VI (Fig. 7.3a). In contrast, in POPC/GM1 bilayer, GM1 density was highest at transmembrane helices VI and VII (Fig. 7.3b). The GM1 density at the site of the cleft formed by transmembrane helices II and III reduced drastically and was close to zero.

To characterize the molecular determinants of this interaction, we calculated the maximum

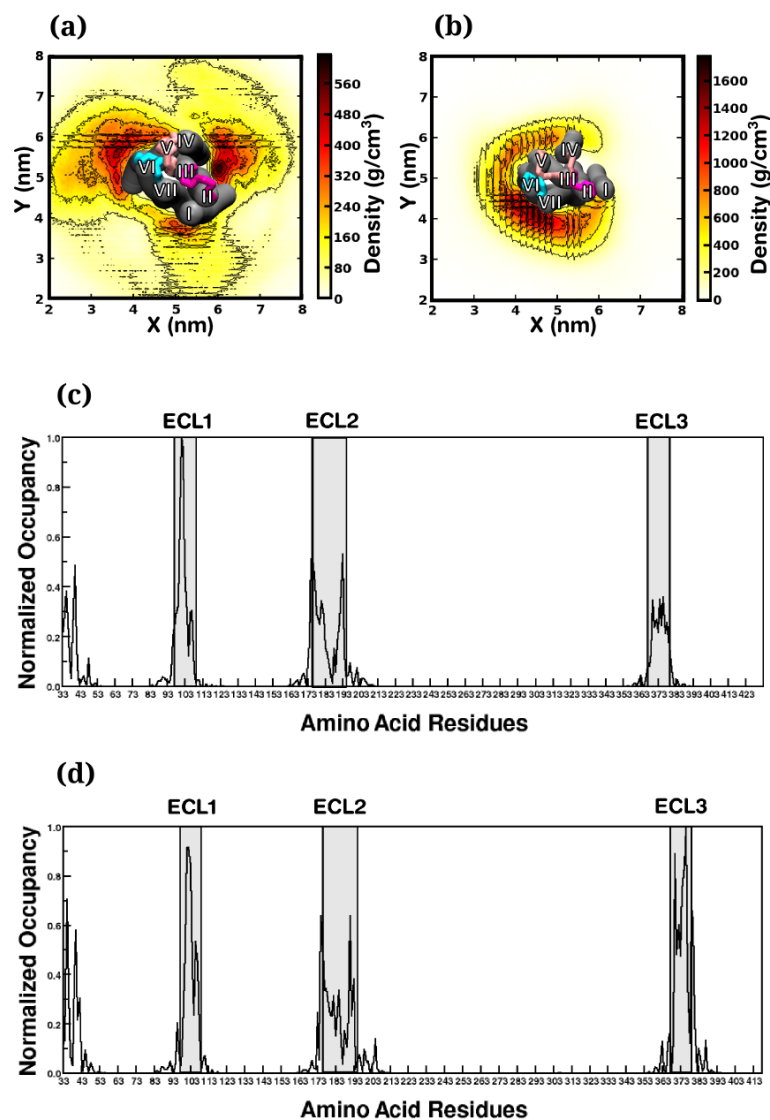


Figure 7.3: Spatial density distribution of GM1 around the serotonin_{1A} receptor in (a) POPC/GM1/chol and (b) POPC/GM1 bilayers. The spatial distribution corresponds to the xy membrane plane and is averaged over the z -axis along the extracellular leaflet. A top view of the receptor is superimposed on the density plot. Transmembrane helices are shown in gray and numbered accordingly. The extracellular loop 1 is shown in magenta, loop 2 in pink and loop 3 in cyan. The normalized maximum occupancy times of GM1 around each amino acid residue of the serotonin_{1A} receptor in (c) POPC/GM1/chol and (d) POPC/GM1 bilayers are shown. The shaded regions correspond to the extracellular loops and are labeled. Data shown are averages over 10 sets of simulations and normalized for each system.

occupancy time of GM1, that is the maximum time it interacts with each amino acid residue (Fig. 7.3c,d). Surprisingly, high GM1 occupancy was observed mainly at the extracellular loops and the N-terminal region of transmembrane helix I. A low or negligible occupancy of GM1

was observed around the transmembrane helices (as opposed to cholesterol or POPC¹²⁵). A visual observation confirmed that the bulky head group of GM1 made stable contact with the extracellular loops while the acyl chains were dynamic and did not appear to interact directly with the transmembrane helices. In both POPC/GM1/chol and POPC/GM1 bilayers, the highest occupancy of GM1 was observed around the extracellular loop 1 that connects transmembrane helices II and III (Fig. 7.3). In addition, in POPC/GM1 bilayers, an increased GM1 occupancy was observed at the extracellular loop 3. The high occupancy of GM1 at extracellular loop 1 is consistent with high density at the adjacent transmembrane helices II and III in POPC/GM1/chol bilayers (Fig. 7.3a). Surprisingly, GM1 density around transmembrane helices II and III was reduced in POPC/GM1 bilayers, despite its high occupancy at extracellular loop 1. This implies that the bulky head group of GM1 interacts with the extracellular loop 1 from sites further away over the top of the receptor. Taken together, these results suggest that GM1 interacts with multiple sites on the receptor, with the highest occupancy at the extracellular loop 1.

7.3.3 Characterizing the sphingolipid binding domain at the extracellular loop 1

To identify the specific sites of GM1 interaction, we calculated the maximum occupancy of each head group bead of GM1 at the residues (residues 97-109) comprising the extracellular loop 1 (Fig. 7.4).

The highest occupancy of the GM1 head group beads was at the residues in the central segment of the extracellular loop 1, in particular residues 100-104. In POPC/GM1/chol bilayers, the highest occupancy was at residues W102 and K101 with GM1 head group beads HG4 and HG7 (representing sugar moieties 2 and 3²⁸⁷), respectively (Fig. 7.4a). In addition, other flanking residues, particularly N100 and T103 displayed a high occupancy. Representative snapshots of the GM1 distribution around the receptor confirmed direct interaction of W102 and the flanking residues with GM1 (Fig. 7.5).

The same pattern was observed in POPC/GM1 bilayers. The highest occupancy was at the residue W102, followed by T103 (Fig. 7.4b). The corresponding interaction sites on GM1 head group were at HG2 and HG7 (representing sugar moieties 1 and 3^{268,287} respectively). Interestingly, high GM1 interaction sites on the extracellular loop 1 comprises the putative

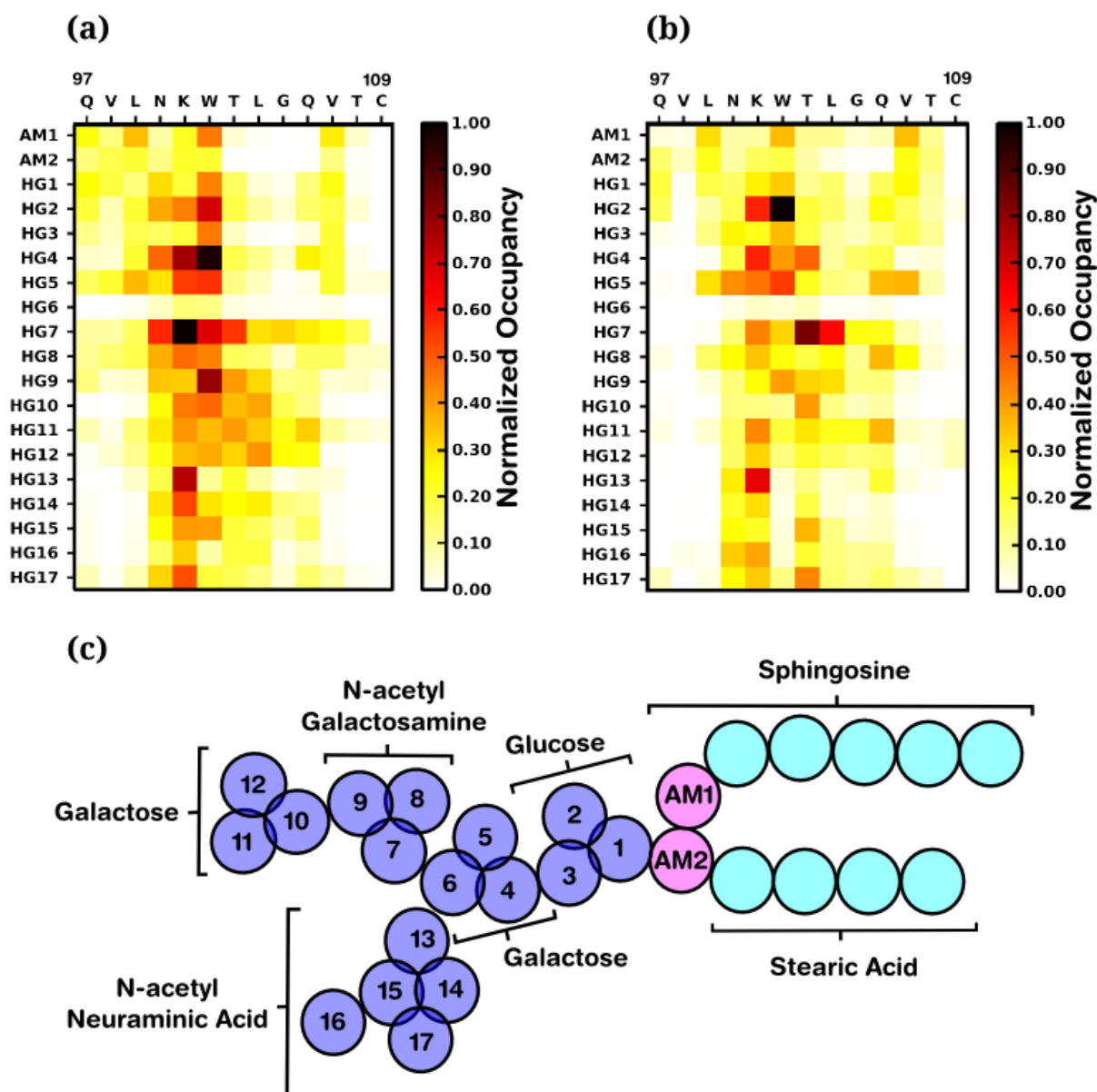


Figure 7.4: The maximum occupancy of GM1 head group beads at amino acid residues 97-109 of the extracellular loop 1 in (a) POPC/GM1/chol and (b) POPC/GM1 bilayers. The maximum occupancy was calculated for the head group beads (HG1-HG17) and the sphingosine backbone beads (AM1 and AM2). (c) A schematic representation of coarse-grain model of GM1. The sugar moiety is shown in purple, the backbone in magenta and the acyl chains in cyan. The head group beads (HG1-HG17) have been numbered from 1-17.

sphingolipid binding domain (SBD) identified earlier⁴⁰².

An important difference between GM1 binding mode in the presence and absence of cholesterol was in the head group beads of GM1 that interacted with the receptor. In

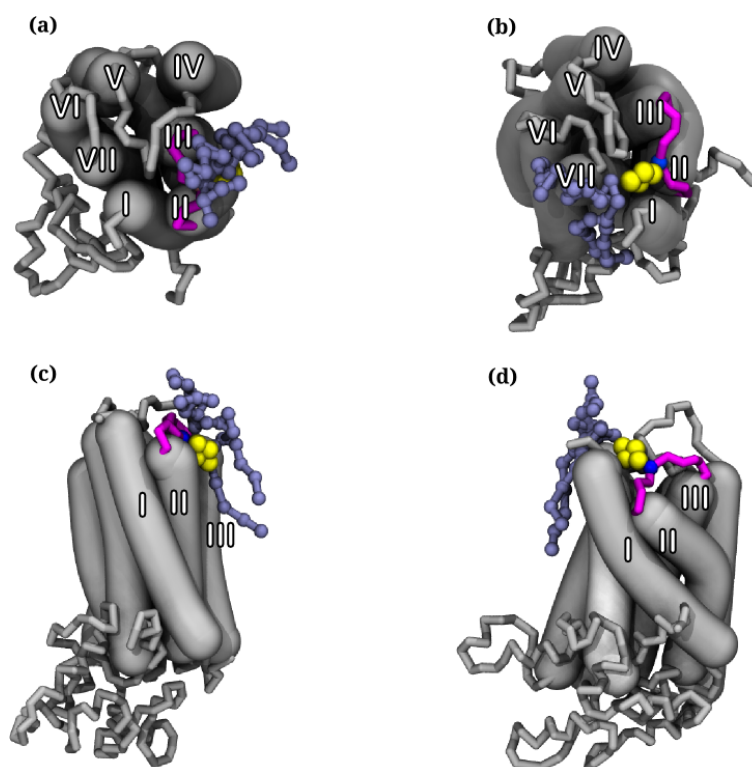


Figure 7.5: Schematic representation showing the top-view (a,b) and side-view of the serotonin_{1A} receptor, highlighting its interaction with GM1 in (a,c) POPC/GM1/chol and (b,d) POPC/GM1 bilayers. The extracellular loop 1 of the receptor is represented in magenta. Transmembrane helices and the remaining loops are shown in gray. GM1 is represented in blue and residue W102 in the extracellular loop 1 is shown in van der Waals representation with its backbone bead in blue and side chain in yellow.

POPC/GM1/chol bilayers, several head group beads, even those further away from the bilayer interacted with residues in the extracellular loop 1. Since the GM1 molecules clustered around transmembrane helices II and III (Fig. 7.3a), i.e., close to the extracellular loop 1, it allows an interaction with both the proximal and the distal head group beads (see Fig. 7.5a,c). However, in POPC/GM1, GM1 density was highest around transmembrane helices VI and VII (Fig. 7.3b) and the GM1 was further away from the extracellular loop 1. In this arrangement, the extracellular loop 1 would bend over the top of the receptor to interact with GM1 (Fig. 7.5b,d). As a result, the extracellular loop 1 could interact mainly with the GM1 head group beads close to the bilayer surface. Head group beads further away from the bilayer surface displayed a reduced interaction with residues in extracellular loop 1, relative to POPC/GM1/chol bilayers. These interaction sites identified were averaged over ten simulations and appeared to be consistent. Taken together, these results suggest that there exists a ‘specific binding site’

for GM1 on the serotonin_{1A} receptor, but sites on GM1 itself do not show any specificity in their association with the receptor.

7.3.4 GM1 stabilizes a ‘flip-out’ conformation of extracellular loop 1

A distinctive feature of GM1-receptor interaction was its association with the residue W102. To examine its role in GM1 interaction, we analyzed the orientational dynamics of W102 in the presence and absence of GM1. The orientation was calculated as the angle of the indole side chain to the membrane normal (Fig. 7.6a; see Methods for details).

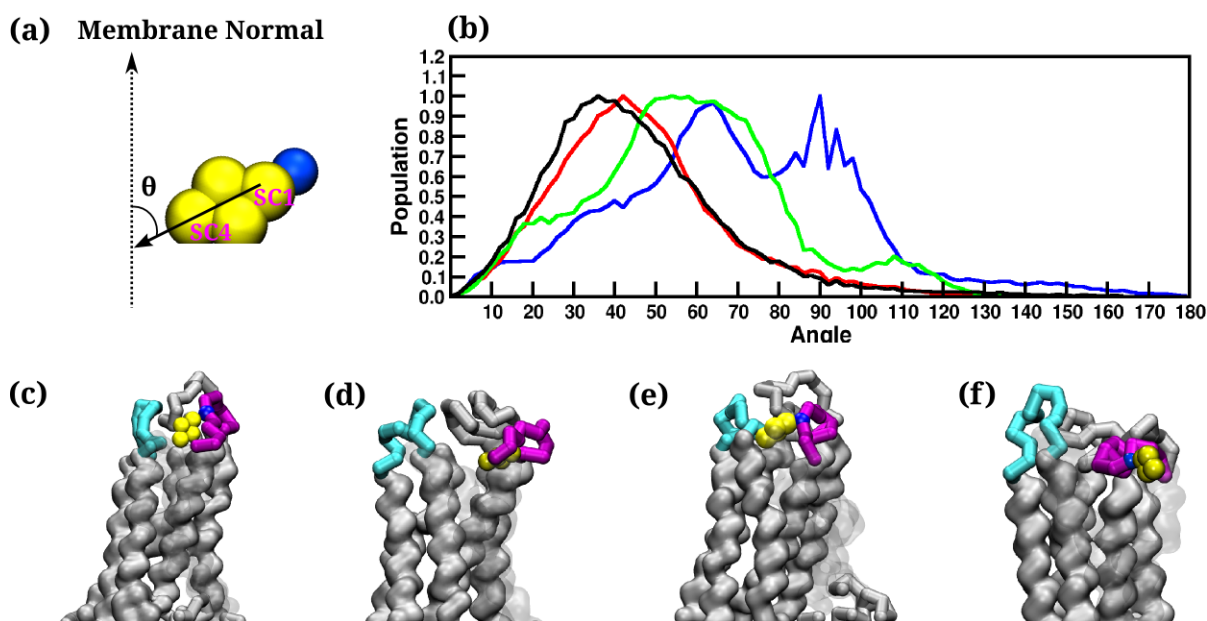


Figure 7.6: (a) A schematic representation of the orientation of W102 with respect to the bilayer normal. (b) The population distribution of W102 orientation in POPC (black), POPC/chol (red), POPC/GM1 (green) and POPC/GM1/chol (blue) bilayers. The schematic representation of the orientations of W102 in (c) POPC (d) POPC/chol (e) POPC/GM1 and (f) POPC/GM1/chol bilayers. Residue W102 is shown in van der Waals representation with its backbone in blue and side chain in yellow. The receptor is shown in gray. Extracellular loop 1 is highlighted in magenta and extracellular loop 3 is shown in cyan

In the absence of GM1, i.e., in POPC and POPC/chol bilayers, the side chain of W102 was oriented $\sim 45^\circ$ to the membrane normal (Fig. 7.6b). A visual inspection of these conformations showed that the residue was oriented toward the central lumen of the serotonin_{1A} receptor (Fig. 7.6c,d). In POPC/GM1 bilayers, W102 adopts an angle of $\sim 60^\circ$ with the membrane normal (Fig. 7.6b). In this conformation, the side chain was directed upward largely over the central lumen (Fig. 7.6e). Interestingly, a bimodal distribution was observed in the orientation of

W102 in POPC/GM1/chol bilayers, with peaks at $\sim 60^\circ$ and 90° (Fig. 4b), possibly indicating conformational plasticity in this complex mixture. In the first conformation (corresponding to the peak at $\sim 60^\circ$), the residue projects upward from the central lumen, similar to POPC/GM1 bilayers. Interestingly, in the second orientation (corresponding to the peak at $\sim 90^\circ$), W102 orients itself parallel to the plane of lipid head group (Fig. 7.6f) and points away from the receptor. As a consequence, the extracellular loop 1 itself points outward from the receptor lumen. The ‘flip-out’ conformation results from the interaction of W102 with GM1, leading to an outward orientation of the tryptophan side chain, in a cholesterol-dependent manner.

7.3.5 Identifying the effect of serotonin_{1A} receptor on GM1 clusters

Sphingolipids (including GM1) and cholesterol have been implicated to form lipid ‘microdomains’, in which they demonstrate a preferential partitioning of certain lipid components^{46,60,397}. To identify the effect of the receptor on the mixing of different lipid components, we calculated the ‘preferential partitioning’ of membrane components. Preferential partitioning has been previously used to characterize clustering of lipid species in multi-component bilayers^{268,406}. We calculated the preferential partitioning for each molecule in POPC/GM1/chol bilayers in the presence and absence of the receptor (Table 7.2; see Methods for details).

Table 7.2: *Preferential partitioning of membrane components, p_A in POPC/Chol/GM1 bilayers in the presence and absence of serotonin_{1A} receptor*

	Cholesterol	POPC	GM1	Protein
<i>With receptor:</i>				
Cholesterol	0.194	0.348	0.345	0.113
POPC	0.375	0.420	0.131	0.074
GM1	0.047	0.011	0.911	0.032
Protein	0.294	0.149	0.557	-
<i>Without receptor:</i>				
Cholesterol	0.116	0.404	0.480	
POPC	0.342	0.545	0.113	
GM1	0.038	0.010	0.952	

The values were calculated over the last microsecond of the simulation and averaged. As expected, GM1 exhibited the highest preference for interaction with itself ($p_A = 0.952$) resulting

in the formation of large clusters. The preferential partitioning of GM1 with cholesterol was much lower ($p_A = 0.038$) and it exhibited the lowest preference for POPC. Interestingly, the self association of POPC appears to be more favorable ($p_A = 0.545$) than its association with other lipids. Cholesterol shows least preference for self association among the lipids ($p_A = 0.116$), suggesting that it seldom forms ‘clusters’ at these concentrations. In the presence of the receptor, the ‘preferential partitioning’ of the membrane components remained qualitatively similar. The preferential partition of the receptor (protein) was the highest with GM1 ($p_A = 0.557$), followed by cholesterol ($p_A = 0.294$), and relatively low preference for POPC ($p_A = 0.149$). The reduced interaction of POPC and cholesterol with the receptor, compared to GM1 is consistent with the radial distribution function of lipid species (Fig. 7.7).

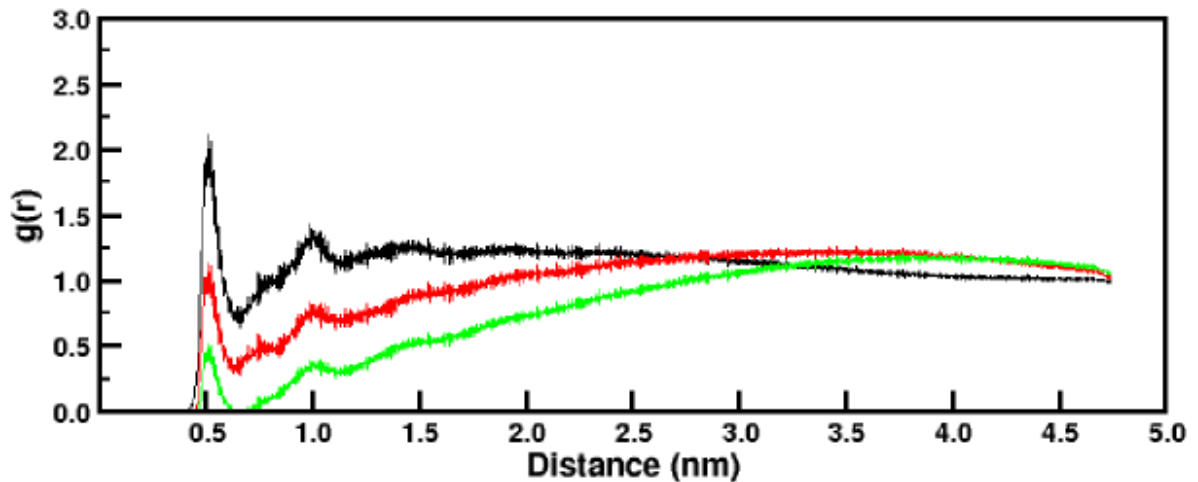


Figure 7.7: Radial distribution function ($g(r)$) of GM1 (black), cholesterol (red) and POPC (green) around the serotonin_{1A} receptor in POPC/GM1/chol bilayer.

The first peaks for cholesterol and POPC are at the same distance (~ 0.5 nm) from the receptor surface as in GM1, but are much smaller in magnitude. Increased partitioning of the receptor with GM1 suggests that serotonin_{1A} receptor preferentially localizes in GM1-rich regions. This effect could arise mainly from specific interaction between the receptor and GM1, since model peptides do not co-localize in sphingolipid-rich regions²⁶⁸. At the time scales of the simulations, cholesterol molecules exhibit both lateral as well as transbilayer diffusion in the membrane. Since GM1 and serotonin_{1A} receptor demonstrated an increased association with cholesterol compared to POPC, we quantitated the effect of these interactions on the rate of transbilayer diffusion (‘flip-flop’) of cholesterol (Table 7.3).

Table 7.3: Cholesterol “flip-flop” rates

System	“flip-flop” rate (no. of flips/ μ s)
Without Receptor	
POPC/chol	0.06 ± 0.01
POPC/GM1/chol	0.11 ± 0.01
With Receptor	
POPC/chol	0.09 ± 0.01
POPC/GM1/chol	0.10 ± 0.01

In POPC/chol bilayers, the average flip-flop rate of cholesterol was 0.06 flips/ μ s which increased to 0.09 flips/ μ s in the presence of receptor. In POPC/GM1/chol bilayers, cholesterol molecules showed more frequent transitions across the two leaflets. The average flip-flop rate increased to 0.11 flips/ μ s in absence of the receptor. In the presence of the serotonin_{1A} receptor, cholesterol flip-flop rate did not exhibit appreciable variation (0.10 flips/ μ s).

7.4 Discussion

The interaction of GPCRs with membrane components assumes relevance in the context of GPCR biology. Membrane cholesterol has been shown to be crucial for the organization and function of a variety of GPCRs^{7,9,10,121}. In this context, a number of structural features of membrane proteins have been suggested to be involved in preferential association with cholesterol^{407,408}. One of the most studied motifs in membrane proteins, that exhibit sensitivity to cholesterol content, is the CRAC motif^{407,409}. The CRAC motif was initially identified in peripheral-type benzodiazepine receptors⁴⁰⁹, and was later identified in GPCRs such as rhodopsin, the β_2 -adrenergic receptor, the serotonin_{1A} receptor³⁴⁶ and the human type I cannabinoid receptor⁴¹⁰. Similarly, proteins that interact with (glyco)sphingolipids often appear to have a characteristic amino acid sequence, termed the ‘sphingolipid-binding domain’ (SBD)^{400–403}. SBD has been identified in a number of proteins such as HIV-1 gp120, Alzheimer’s beta amyloid peptide and the prion protein⁴⁰⁰. We have previously identified the SBD motif (LNKWTLGQVTC) in the serotonin_{1A} receptor corresponding to amino acids 99 to

109. This specific sequence contains the characteristic combination of basic (K101), aromatic (W102) and turn-inducing residues (G105), usually found in SBDs^{401,411}. Interestingly, the SBD motif in the serotonin_{1A} receptor overlaps with the CRAC motif in transmembrane helix II.

Sphingolipids constitute a small but essential constituent of the eukaryotic cell membrane that regulate several physiological processes^{38,396}. They are reported to be required for endocytosis, protein sorting, ion conductance and GPCR function^{395,398}. Several membrane proteins involved in these physiological processes have been reported to interact directly with sphingolipids⁴¹¹. For example, the nerve growth factor receptor tyrosine kinase has been shown to interact directly with gangliosides⁴¹². Structural motifs for sphingolipid interactions, such as the SBD⁴⁰³ and the VXXTLXXIY signature sequence⁴¹³ have been identified. In this work, we have examined the interaction of GM1 with the serotonin_{1A} receptor using coarse-grained molecular dynamics simulations. Our results demonstrate that GM1 binds to the predicted SBD motif in the extracellular loop 1 of the serotonin_{1A} receptor. The sugar moiety of GM1 interacts with the aromatic residue W102, and flanking residues, K101 and T103. These results are in overall agreement with previous work which reported copatching of a fraction ($\sim 30\%$) of the serotonin_{1A} receptor with GM1⁴¹⁴.

We have previously shown that the serotonin_{1A} receptor possesses a characteristic SBD motif that is conserved over natural evolution across various phyla among serotonin receptors⁴⁰³. However, experiments with SBD peptide derived from the receptor did not exhibit significant binding in model membranes, thereby pointing to the importance of the overall context of the receptor architecture. Since the extracellular loop 1 interacts with the sugar moieties of GM1, located above the membrane, it is possible that such an interaction mode is not feasible with the truncated peptide alone. An interesting aspect of the interaction site is that though it is independent of cholesterol, the presence of cholesterol allows a closer and more extended interaction of GM1 with the receptor (Figs. 7.3 and 7.4). Previous studies suggested that cholesterol increases interaction affinity between HIV-1 gp120 glycoprotein and the glycosphingolipid, globotriaosylceramide (Gb3)⁴¹⁵.

Our work suggests that interaction of the receptor with GM1 stabilizes a ‘flip-out’ conformation, in which the aromatic residue (W102) in SBD points away from the central lumen of

the receptor and is exposed to the solvent. This conformation is dependent on the cholesterol-modulated GM1 distribution around the receptor (Fig. 7.6b). A similar outward-facing orientation of tryptophan residue has been reported in the crystal structure of Shiga-like toxin bound to an analogue of the Gb3 trisaccharide⁴¹⁶. In a previous study, it was shown that the Trp residue is directed toward the central pore of the Shiga-like toxin pentamer, but on interaction with the carbohydrate domain, a conformational change occurs leading to increased solvent exposure⁴¹⁷. It may be noted here that the Trp residue is structurally analogous to serotonin (5-hydroxytryptamine)⁴¹⁸, the natural ligand of serotonin_{1A} receptor. It would be interesting to speculate whether the ‘flip-out’ conformation of the tryptophan could facilitate the entry of the endogenous ligand (serotonin). This is based on our earlier observation that metabolic depletion of sphingolipids or removal of sphingomyelin head group modulates ligand binding and downstream signaling of the serotonin_{1A} receptor^{419–421}.

Cholesterol is known to associate with sphingolipids to form ordered lipid domains in cell membrane^{46,60,397}. Membrane lipids, particularly cholesterol and sphingolipids, are essential for serotonin_{1A} receptor function^{7,395}. Cholesterol has been shown to modulate higher order organization in serotonin_{1A} receptor¹²⁶. It would, therefore, be interesting to also investigate the effect of sphingolipids on serotonin_{1A} receptor organization. Previous studies have shown that sphingolipids have no significant effect on the oligomerization of the serotonin_{1A} receptor¹²³ and it is not clear a priori if the dimer formation will be affected by GM1 interactions or vice versa.

In case of the serotonin_{1A} receptor, several cholesterol interactions sites have been identified that display an ns- μ s timescale dynamics¹²⁵. Our current study shows that sampling of GM1 around the receptor surface occurs at μ s timescale before the interaction is stabilized. In light of the reduced diffusion of the GM1 clusters, and the large residence times, we would require simulations of several hundreds of μ s-ms to account for the effect of GM1-receptor interaction on the serotonin_{1A} receptor dimerization. This is further complicated by the limitation that the complex conformation of the GM1 glycosphingolipid carbohydrate head group in combination with the use of tight force constants currently restricts the simulation time step to 5 fs²⁸⁷. A statistically relevant sampling of the self assembly of serotonin_{1A} receptors in mixed bilayers containing GM1 therefore remains difficult to achieve.

The natural question that arises is what is the role of GM1 in dimerization? In chapter

5, we examined the role of varying cholesterol concentration on serotonin_{1A} receptor dimerization¹²⁶ and identified several dimer conformations. Two prominent dimer conformations observed in POPC/cholesterol bilayer are represented by: (i) transmembrane helices I and II, and (ii) transmembrane helices IV and V at the dimer interface. We simulated these dimer conformations in bilayers containing GM1 and cholesterol to identify possible GM1 interaction pattern around the dimer. The residue-dependent GM1 occupancy is shown in Fig. 7.8.

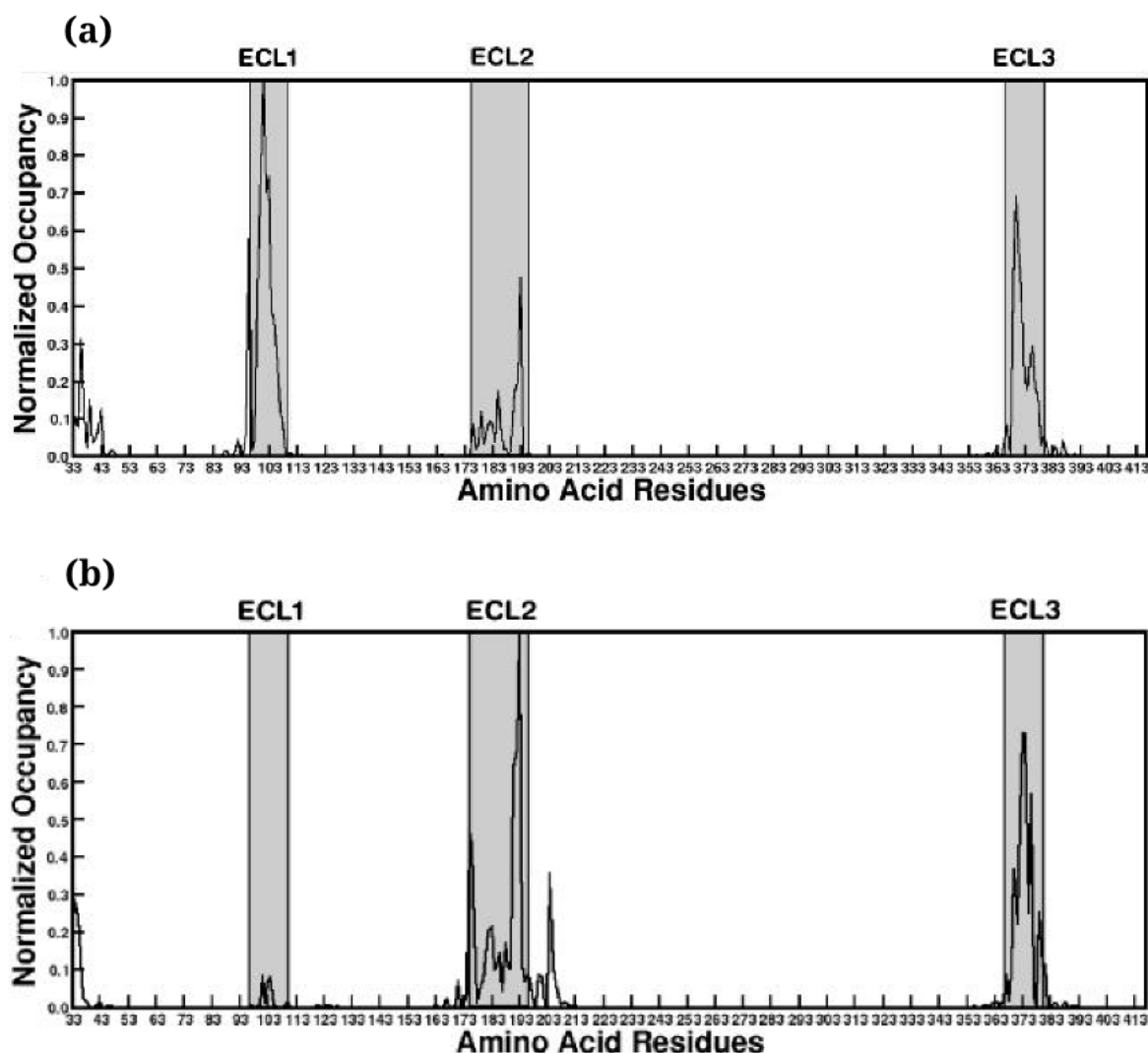


Figure 7.8: The normalized maximum occupancy of GM1 around each amino acid residue of the serotonin_{1A} receptor in the dimer conformation with (a) transmembrane helices IV and V, and (b) transmembrane helices I and II, at the dimer interface in POPC/GM1/Chol bilayers. The total simulation time was $\sim 6 \mu\text{s}$.

Increased occupancy of GM1 is observed at the SBD motif in extracellular loop 1 of the

serotonin_{1A} receptor for a IV/V dimer interface. However, the GM1 occupancy at extracellular loop 1 is drastically reduced when transmembrane helix II was at the dimer interface. Not surprisingly, when transmembrane helix II is present at the dimer interface, the accessibility of extracellular loop 1 is reduced, and reduces the interactions of GM1 at the SBD motif in the serotonin_{1A} receptor. These results suggest that sphingolipid distribution around the serotonin_{1A} receptor is also influenced by the conformational status of the receptor.

It is important to note here that the regulation of neuronal GM1 levels have been shown to be crucial, with any change in GM1 levels resulting in severe neurodegenerative disorders. For example, accumulation of GM1 due to the deficiency or malfunctioning of GM1- β -galactosidase (that catalyzes the hydrolysis of GM1) results in a neurodegenerative disorder called GM1-gangliosidosis, a class of sphingolipidoses (i.e., lysosomal sphingolipid storage diseases). GM1-gangliosidosis is an autosomal recessive disorder and to date, no successful treatment is available for this disease⁴²². On the other hand, deficiency of GM1 has been shown to be implicated in Parkinson's disease^{423,424}, a neurodegenerative disorder primarily characterized by defective motor symptoms. However, it is often accompanied by depression, anxiety and dementia, which have been shown to be tightly correlated with modulation of neuronal serotonergic system⁵². In particular, the role of serotonin_{1A} receptors in pharmacotherapy of Parkinson's disease has been reported⁴²⁵. In this context, our results showing specific interaction of GM1 with the serotonin_{1A} receptor, an important neurotransmitter receptor, assume relevance and could contribute to our overall understanding of the molecular mechanism of such diseases.

Our results highlight the significance of the extracellular loop 1 in receptor function. Although the effect of membrane lipids on the transmembrane domain is beginning to be established, the interaction of loop regions with membrane lipids and its effect on regulating GPCR function is less understood. The importance of extracellular loops in regulating GPCR function, especially ligand access has been previously reported⁴²⁶. In adenosine A_{2B} receptor, specific amino acid residues in the extracellular loop 1 were found to be crucial for ligand binding⁴²⁷. Similarly, presence of specific residues at critical positions in the extracellular regions have been reported for other GPCRs and shown to be crucial for ligand binding and receptor activation⁴²⁸⁻⁴³². In addition, lipid-mediated regulation of membrane protein function has been observed in dopamine transporter, where the N-terminus is involved in regulating substrate efflux^{433,434}. These findings further strengthen the idea that extracellular regions


regulate membrane protein function that could possibly be influenced by their interaction with membrane lipids.

In conclusion, we show here that GM1 binds to the serotonin_{1A} receptor, specifically at the proposed SBD site, by performing multiple coarse-grained molecular dynamics simulations of the receptor in membrane bilayers with varying compositions of GM1 and cholesterol. Interaction of GM1 with the receptor at the SBD results in a conformational change of the tryptophan (W102) residue away from the central lumen of the receptor, in a cholesterol-dependent manner. Our results suggest a direct role of GM1-GPCR interaction in modulating ligand binding and receptor function, and could provide novel insight in malfunctioning of neuronal GPCRs in neurodegenerative disorders involving GM1.

Conclusion

“Never forget what you are, for surely the world will not. Make it your strength. Then it can never be your weakness. Armour yourself in it, and it will never be used to hurt you.”

– Tyrion Lannister, *George R.R. Martin’s “A Game of Thrones”*

PCR oligomerization has received considerable interest in the past two decades. Several studies strongly suggest that GPCRs do exist as dimers and, possibly, higher order oligomers in cell membrane¹³⁷. Although this puts an end to the long debated question “Do GPCRs form higher order clusters?”, it has paved way for many more enquiries which have yet to be well addressed. The influence of lipids on the structure and function of GPCRs has gained interest in the past few years. Cholesterol, a crucial component of eukaryotic cell membrane, has been reported to be essential for the stability of several GPCRs^{103,119,383,435}. This is further supported by the evidence that crystallization of GPCRs requires cholesterol in the lipid matrix⁴³⁶, some of which reveal cholesterol bound to their transmembrane surface⁴³⁷. In addition, biophysical studies have shown that higher order structural organization of GPCRs is also cholesterol dependant. However finer details of protein-lipid interaction mediating these effects largely remains unresolved. The work carried out in this thesis provides molecular evidences for lipid-mediated effects involved in modulating GPCR association.

8.1 Cholesterol regulates GPCR association

Mismatch between equilibrium bilayer thickness and the hydrophobic stretch of the transmembrane segment plays a crucial role in driving membrane protein aggregation. This property has been well established for several transmembrane proteins including GPCRs^{233,334,358,438,439}. Cholesterol regulates membrane biophysical properties, such as order parameter and membrane thickness, in a concentration dependant manner^{440–442}. In order to investigate the consequences of these effects on GPCR association, we carried out self assembly of GPCRs in bilayers with different cholesterol concentrations.

Association between receptors was observed at all bilayer compositions. However, the presence of cholesterol appeared to reduce interaction between receptors. The time taken for receptor dimerization was relatively longer at higher cholesterol concentrations. Also, cluster size of receptor aggregates were smaller at these concentrations. Our results therefore suggest that, possibly, an overall increase in bilayer thickness mediated by cholesterol helps prevent higher order oligomerization in GPCRs. Evidence from experimental studies show that cholesterol modulates GPCR oligomerization. Cholesterol depletion from cells expressing serotonin_{1A} receptor resulted in possible re-organization of the receptor into ordered domains and increase in oligomeric status^{123,300}.

8.2 Membrane lipids show multiple binding sites around GPCR surface

The layer of lipids immediately surrounding the integral transmembrane proteins are referred to as “annular” lipids. It is observed that the rate of exchange of these lipids with the bulk is of an order of magnitude slower than that for bulk lipids resulting from translational diffusion. In addition, some membrane proteins have specific sites on their surface, called “nonannular” sites, which are limited in their accessibility to annular and bulk lipids⁴⁴³. Results from bioinformatics and structural studies have identified few of these lipid binding sites on GPCR transmembrane helices^{102,302,346}. We have examined the possible sites for lipid binding on GPCR by carrying out simulations of these receptors in bilayers with different lipid compositions. Although the cholesterol and phospholipid interactions sites are probed only from

coarse-grained studies in the thesis, we performed atomistic studies to confirm the presence of these sites³⁷⁹.

Based on our findings, it appears that there are multiple lipid binding sites around GPCR surface. These binding sites are not only restricted to the transmembrane helices but also present in the loop regions connecting these helices. For instance, certain regions on the large intracellular loop 3 region in serotonin $1A$ receptor show significant interaction with lipids, suggesting dynamic association of the loop with the bilayer. These interactions assume considerable significance since the association of intracellular loop 3 with the bilayer influences the accessibility of G-protein to its binding site located in the cytoplasmic domain between transmembrane helices V and VI¹¹⁰. Lipids show varied occupancy at each of these binding sites. Some of these binding regions showed relatively higher occupancy than others and matched well with those predicted in previous studies^{74,125,305,346}. Occupancy site for POPC predicted from atomistic simulations³⁷⁹ showed high similarity with those mapped in coarse-grained simulations^{126,239}. Our findings suggest that lipids bound to different binding sites may have different exchange rates with bulk lipids. Indeed, two different classes of cholesterol binding sites have been identified in β_2 adrenergic receptor by thermal unfolding and NMR³⁸³.

Different lipids exhibit distinct binding pattern around the receptors. Phospholipids and cholesterol showed increased occupancy around the transmembrane helices compared to the loop regions. However, in case of sphingolipids, interaction was largely restricted to N-terminus and extracellular loop regions with limited or absence of occupancy at the transmembrane helices. Lipids also show variation in binding pattern depending upon the GPCR and its organizational status (monomer or oligomer). Involvement of transmembrane helices at the contact interface between the receptors decreases its accessibility to annular lipids resulting in reduced binding probability of lipids at these regions. Binding sites for lipids also overlap with each other and they compete for occupying these sites on GPCR surface. Therefore the interaction pattern for lipids around a given receptor shows dynamic variation depending upon the presence of other membrane components.

8.3 Cholesterol modulates contact interface during GPCR association

Simulations have been useful in providing a “dynamic molecular insight” into GPCR oligomerization^{233–235,334}. These studies suggest that local membrane deformation due to hydrophobic mismatch between transmembrane helices and lipid bilayer determine the extent and orientational preference of receptor association. However, the role of other lipid-mediated effects in influencing receptor-receptor interaction is not well established. Indeed, crystal structure of β_2 -adrenergic receptor shows the presence of cholesterol at the crystal packing interface suggesting its involvement in receptor dimerization⁷⁴. A coarse-grained molecular dynamics simulation study to examine formation of homomeric and heteromeric complexes between opioid receptors, showed an inverse correlation between persistence of lipid molecules (POPC and cholesterol) around transmembrane helices and probability of their involvement at dimer interface²³⁵.

We carried out self assembly simulations of GPCRs in bilayers with different lipid compositions to examine the contributions of specific and non-specific lipid-protein interactions in driving GPCR association and influencing oligomer conformation. GPCRs show multiple contact interfaces between the receptors which occur with variable probabilities at different cholesterol concentrations. Thus cholesterol appears to modulate the interface pattern in a concentration-dependant manner. Contact interfaces sampled by the receptors also differ among GPCRs. There appears to be a correlation between positive hydrophobic mismatch around transmembrane helices and their involvement at contact interface, although, the relationship is not always straightforward. Increased occupancy of cholesterol around transmembrane helix reduces the propensity of its involvement at contact interface, despite persistence of local membrane thickening around it. Our results suggest that cholesterol mediates GPCR association by a combination of specific and non-specific effects.

8.4 Implications for GPCR oligomerization

8.4.1 Functional regulation

Although there are evidences to prove that GPCRs retain functionality even in their monomeric state, it is suggested that formation of higher order aggregates may play a significant role in

regulating receptor function^{138,444,445}. Formation of GPCR dimers can modulate ligand binding, signaling and trafficking properties of one or both the protomers⁴⁴⁶. Our results highlight the importance of understanding the molecular details of receptor association in influencing GPCR function. Dimer/oligomer conformation could have direct influence on activity. Plasticity observed in the interaction interface among GPCRs suggests that multiple sites on receptor are favourable for contacts between receptors although their stability would largely depend upon the most favourable protein-protein and protein-environment interaction. We speculate that this would permit formation of large clusters which are more compactly organized. Fewer permissible association interfaces between GPCRs would suggest formation of small clusters or more specifically organized clusters. Formation of such clusters may regulate the relative proportion of G-protein coupling with the oligomeric complex and thereby modulate function.

Ligand binding to GPCR has been shown to have contradicting effects on function, with agonists promoting association between receptors in some GPCRs while destabilizing higher order complexes in others^{447–449}. Binding of ligand to GPCR stabilizes active conformation. In cases where GPCRs are proposed to exist as dimers or higher order clusters under native condition and which destabilize on agonist treatment⁴⁴⁷, it could be postulated that ligand induces conformational change which destabilizes interaction with associated neighbours resulting in dissociation of cluster into monomers or smaller complexes (Fig 8.1).

Under these organizational state, coupling of larger population of G-proteins may be permitted which was earlier prevented due to receptor clustering resulting in enhanced activity. Contrastingly, if GPCR exist as monomers/smaller clusters and evidence suggest that oligomers are formed following agonist treatment^{448,449}, it could be hypothesized that the active conformation of the receptor following ligand binding may favour specific interaction or reorganize interaction pattern with neighbouring receptors resulting in formation of specifically organized cluster that maximizes G-protein interaction with the receptors and subsequent stabilization. Indeed the GPCR associated with the receptor directly interacting with G_{α} subunit, may possibly serve to stabilize the overall complex by providing binding site for $G_{\beta\gamma}$ subunit.

Our results emphasize the role of lipid-protein interactions in mediating GPCR oligomerization. Lipids modulate oligomer conformation in a concentration-dependant manner. These findings find prominence in the light that, under normal physiological conditions, the cell membrane exhibits lateral asymmetry in lipid distribution. GPCRs along with relevant signaling

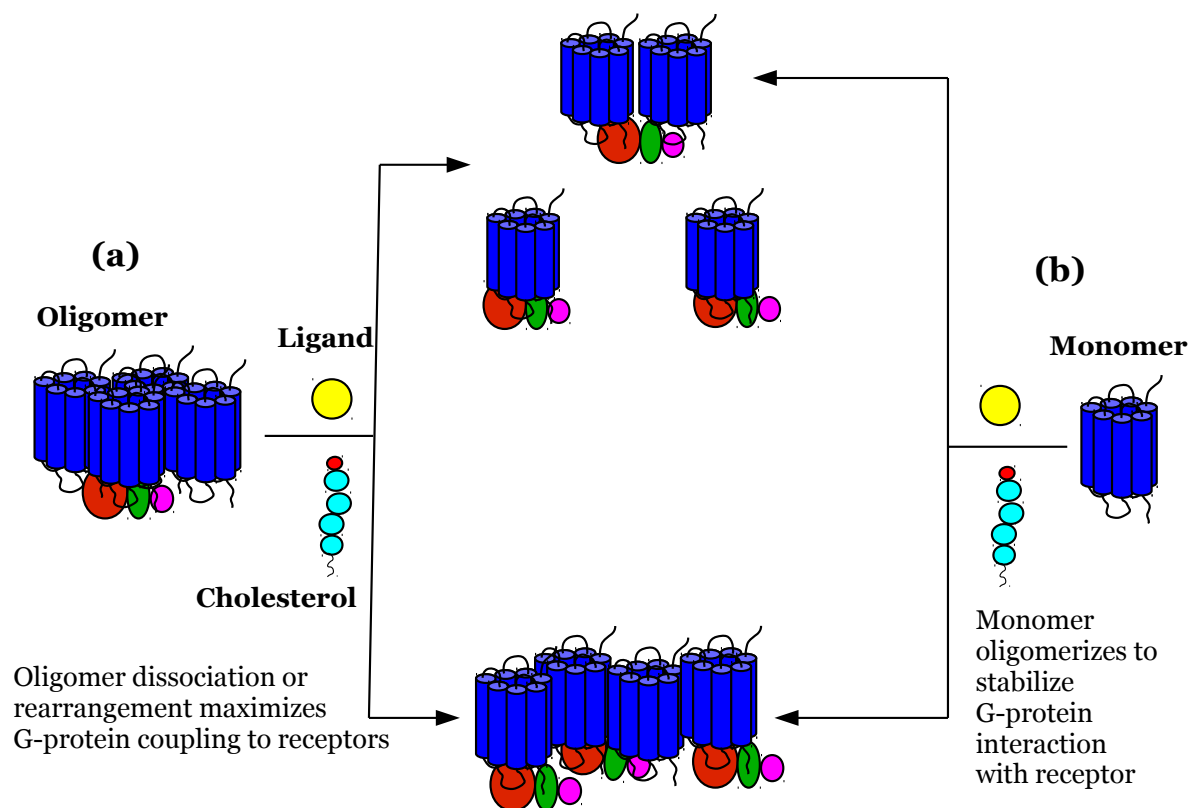


Figure 8.1: Hypothesis for functional modulation of GPCR by regulating interaction pattern between receptors mediated by ligand binding or lipid interaction. (a) Conformational change in receptor induces receptor disorganization or rearrangement allowing efficient coupling of G-proteins to the receptors. (b) Monomer forms dimer or larger clusters which stabilizes G-protein interaction with receptor

molecules preferentially partition into the ordered domains^{450,451}. The conformation of the oligomer in these domains would, in turn, influence its interaction with G-proteins and other downstream signaling molecules.

8.4.2 Drug research

Drug development is a complicated, long and expensive process, which can take more than a decade and cost billions of dollars per drug^{452,453}. Most therapeutic drugs are designed to target directly the protein of interest or its downstream signaling pathway⁴⁵². A large part of drug research is involved in screening potential therapeutics (small molecules or antibiotics)

to identify those with maximum desired response and minimal side effects. Drugs targeting GPCRs and/or their signaling pathway(s) have been largely focused on by pharmaceutical companies⁴⁵⁴, yet only few of them are approved⁴⁵⁵ as they generate the desired pharmacological response. The complication arises primarily due to limited available information on the active conformation that needs to be targeted and due to the ability of GPCRs to form homo- and hetero-oligomers under physiological conditions with functional consequences. Allosteric cross-talk between protomers in GPCR homodimers has been reported for serotonergic receptors¹³⁹. Oligomerization between GPCR members could also allosterically modulate receptor activities by influencing ligand binding affinity and/or downstream signaling mechanisms^{456,457}. This could result in generation of multiple unintended responses thereby reducing drug specificity and efficacy. It is therefore vital to identify possible GPCR oligomeric partners (in case of hetero-oligomers) and characterize molecular level structural details such as conformational changes in the monomers, contact interface between the monomers, distances between ligand binding pockets and potential downstream signaling partners for developing target specific drug molecules. Our results suggest that lipids play an important role in modulating dimer/oligomer conformations^{126,238,239}. Variations in lipid environment around the oligomers could dynamically alter equilibrium between these conformations. Therefore, a comprehensive molecular level understanding of these factors influencing GPCR association would be essential for designing effective therapeutics. Lipid composition of cell membrane is also known to vary with age, stress and state-of-health^{30,348,349,458}. These factors affect the function and expression of GPCRs and other related signaling proteins³⁵⁰. Understanding lipid-mediated effects on receptor structure, function and organization could therefore also be useful to modulate GPCR signaling at membrane level by pharmacologically regulating membrane lipid composition and structure for treatment of diseases⁴⁵⁹.

In conclusion, using coarse-grained molecular dynamics simulation approach, we have been able to investigate molecular details of higher order oligomerization in two well known, representative GPCR species. The results discussed in this thesis highlights the role of membrane lipids in higher order organization of β_2 -adrenergic receptor and serotonin_{1A} receptor, though we believe that these findings could possibly be generalized for other GPCR members too. Our studies further emphasize the role of membrane lipids in GPCR oligomerization. Cholesterol appears to modulate oligomerization and conformation of the oligomers by a combination

of direct and indirect lipid-mediated effects and protein-lipid energetics in a concentration-dependant manner. A dynamic equilibrium might exist between the conformations of different oligomer species in cell membrane under physiological conditions. Conformational modulation of these species by membrane lipids could have possible functional significance. These results find considerable importance in designing drugs that target specific oligomer conformations and allow pharmacological regulation of receptor function.

Bibliography

- [1] Kobilka, B. K. *Biochim. Biophys. Acta* **2007**, *1768*, 794–807.
- [2] Kroeze, W. K.; Sheffler, D. J.; Roth, B. L. *J. Cell Sci.* **2003**, *116*, 4867–4869.
- [3] Rosenbaum, D. M.; Rasmussen, S. G. F.; Kobilka, B. K. *Nature* **2009**, *459*, 356–363.
- [4] Granier, S.; Kobilka, B. *Nat. Chem. Biol.* **2012**, *8*, 670–673.
- [5] Hill, S. J. *Br. J. Pharmacol.* **2006**, *147*, S27–S37.
- [6] McNeely, P. M.; Naranjo, A. N.; Robinson, A. S. *Biotechnol. J.* **2012**, *7*, 1451–1461.
- [7] Pucadyil, T. J.; Chattopadhyay, A. *Prog. Lipid Res.* **2006**, *45*, 295–333.
- [8] Escribá, P. V.; Wedegaertner, P. B.; Goñi, F. M.; Vögler, O. *Biochim. Biophys. Acta* **2007**, *1768*, 836–852.
- [9] Paila, Y. D.; Chattopadhyay, A. In *Membrane Cholesterol in the Function and Organization of G-Protein Coupled Receptors*; Harris, R. J., Ed.; Springer Netherlands, 2010; pp 439–466.
- [10] Oates, J.; Watts, A. *Curr. Opin. Struct. Biol.* **2011**, *21*, 802–807.
- [11] Soubias, O.; Gawrisch, K. *Biochim. Biophys. Acta* **2012**, *1818*, 234–240.
- [12] Mahmood, M. I.; Liu, X.; Neya, S.; Hoshino, T. *Chem. Pharm. Bull.* **2013**, *61*, 426–437.
- [13] Alberts, B.; Bray, D.; Hopkin, K.; Johnson, A.; Lewis, J.; Raff, M.; Roberts, K.; Walter, P. *Essential Cell Biology, Fourth Edition*; Taylor & Francis Group, 2013.
- [14] Gorter, E.; Grendel, F. *J. Exp. Med.* **1925**, *41*, 439–443.

- [15] Singer, S. J.; Nicolson, G. L. *Science* **1972**, *175*, 720–731.
- [16] Engelman, D. M. *Nature* **2005**, *438*, 578–580.
- [17] Sonnino, S.; Prinetti, A. *Curr. Med. Chem.* **2013**, *20*, 4–21.
- [18] Simons, K.; Ikonen, E. *Nature* **1997**, *387*, 569–572.
- [19] Simons, K.; Vaz, W. L. *Annu. Rev. Biophys. Biomol. Str.* **2004**, *33*, 269–295.
- [20] Simons, K.; Sampaio, J. L. *Cold Spring Harb. Perspect. Biol.* **2011**, *3*,.
- [21] Diaz-Rohrer, B. B.; Levental, K. R.; Simons, K.; Levental, I. *Proc. Natl. Acad. Sci.* **2014**, *111*, 8500–8505.
- [22] Owen, D. M.; Williamson, D. J.; Magenau, A.; Gaus, K. *Nat. Commun.* **2012**, *3*,.
- [23] McConnell, H. M.; Vrljic, M. *Annu. Rev. Biophys. Biomol. Str.* **2003**, *32*, 469–492.
- [24] Elson, E. L.; Fried, E.; Dolbow, J. E.; Genin, G. M. *Annu. Rev. Biophys.* **2010**, *39*, 207–226.
- [25] Lingwood, D.; Simons, K. *Science* **2009**, *327*, 46–50.
- [26] Frisz, J. F.; Klitzing, H. A.; Lou, K.; Hutcheon, I. D.; Weber, P. K.; Zimmerberg, J.; Kraft, M. L. *J. Biol. Chem.* **2013**, *288*, 16855–16861.
- [27] Frisz, J. F.; Lou, K.; Klitzing, H. A.; Hanafin, W. P.; Lizunov, V.; Wilson, R. L.; Carpenter, K. J.; Kim, R.; Hutcheon, I. D.; Zimmerberg, J.; Weber, P. K.; Kraft, M. L. *Proc. Natl. Acad. Sci.* **2013**, *110*, E613–E622.
- [28] Kraft, M. L. *Mol. Biol. Cell* **2013**, *24*, 2765–2768.
- [29] van Meer, G.; Voelker, D. R.; Feigenson, G. W. *Nat. Rev. Mol. Cell Biol.* **2008**, *9*, 112–124.
- [30] Kalén, A.; Appelkvist, E.-L.; Dallner, G. *Lipids* **1989**, *24*, 579–584.
- [31] Borchman, D.; Tang, D.; Yappert, M. C. *Biospectroscopy* **1999**, *5*, 151–167.
- [32] Hazel, J. R.; Williams, E. E. *Prog. Lipid Res.* **1990**, *29*, 167–227.

Bibliography

- [33] Cuzner, M. L.; Davison, A. N. *Biochem. J.* **1968**, *106*, 29–34.
- [34] Parpart, A. K.; Dziemian, A. J. *Cold Spring Harb. Symp. Quant. Biol.* **1940**, *8*, 17–24.
- [35] Lodish, H.; Berk, A.; Baltimore, D.; Matsudaira, P.; Zipursky, S.; Darnell, J. *Molecular Cell Biology*; Macmillan Higher Education, 1995.
- [36] van Meer, G.; de Kroon, A. I. P. M. *J. Cell Sci.* **2010**, *124*, 5–8.
- [37] Villalaín, J. *Eur. J. Biochem.* **1996**, *241*, 586–593.
- [38] Bartke, N.; Hannun, Y. A. *J. Lipid Res.* **2009**, *50*, S91–S96.
- [39] Coskun, U.; Simons, K. *Structure* **2011**, *19*, 1543–1548.
- [40] Marquardt, D.; Geier, B.; Pabst, G. *Membranes* **2015**, *5*, 180–196.
- [41] Devaux, P. F.; Herrmann, A.; Ohlwein, N.; Kozlov, M. M. *Biochim. Biophys. Acta* **2008**, *1778*, 1591–1600.
- [42] Daleke, D. L. *J. Lipid Res.* **2003**, *44*, 233–242.
- [43] Gibson Wood, W.; Igbavboa, U.; Müller, W. E.; Eckert, G. P. *J. Neurochem.* **2011**, *116*, 684–689.
- [44] Hayashi, H.; Igbavboa, U.; Hamanaka, H.; Kobayashi, M.; Fujita, S. C.; Gibson Wood, W.; Yanagisawa, K. *Neuroreport*. **2002**, *13*, 383–386.
- [45] Fisher, K. A. *Proc. Natl. Acad. Sci. USA* **1976**, *73*, 173–177.
- [46] Ramstedt, B.; Slotte, J. P. *Biochim. Biophys. Acta* **2006**, *1758*, 1945–1956.
- [47] Yesylevskyy, S. O.; Demchenko, A. P. In *Cholesterol Behavior in Asymmetric Lipid Bilayers: Insights from Molecular Dynamics Simulations*; Owen, M. D., Ed.; Springer New York, 2015; pp 291–306.
- [48] Sharma, S.; Kim, B. N.; Stansfeld, P. J.; Sansom, M. S. P.; Lindau, M. *PLoS ONE* **2015**, *10*, 1–21.
- [49] Karp, G. *Cell and Molecular Biology: Concepts and Experiments*; John Wiley & Sons, 2009.

- [50] Wallin, E.; Heijne, G. V. *Protein Sci.* **1998**, *7*, 1029–1038.
- [51] Almén, M. S.; Nordström, K. J.; Fredriksson, R.; Schiöth, H. B. *BMC Biol.* **2009**, *7*, 1–14.
- [52] Tan, M. G.; Chua, W.-T.; Esiri, M. M.; Smith, A. D.; Vinters, H. V.; Lai, M. K. *J. Neurosci. Res.* **2010**, *88*, 1157–1169.
- [53] Herndler-Brandstetter, D. *How aging affects T lymphocyte-mediated immunity*; Frontiers Research Topics; Frontiers Media SA, 2015.
- [54] Vassilatis, D. K.; Hohmann, J. G.; Zeng, H.; Li, F.; Ranchalis, J. E.; Mortrud, M. T.; Brown, A.; Rodriguez, S. S.; Weller, J. R.; Wright, A. C.; Bergmann, J. E.; Gaitanaris, G. A. *Proc. Natl. Acad. Sci.* **2003**, *100*, 4903–4908.
- [55] Tusnády, G. E.; Dobson, L.; Tompa, P. *Biochim. Biophys. Acta* **2015**, *1848*, 2839–2848.
- [56] Zinser, E.; Sperka-Gottlieb, C. D.; Fasch, E. V.; Kohlwein, S. D.; Paltauf, F.; Daum, G. *J. Bacteriol.* **1991**, *173*, 2026–2034.
- [57] Dupuy, A. D.; Engelman, D. M. *Proc. Natl. Acad. Sci.* **2008**, *105*, 2848–2852.
- [58] Ramadurai, S.; Holt, A.; Krasnikov, V.; van den Bogaart, G.; Killian, J. A.; Poolman, B. *J. Am. Chem. Soc.* **2009**, *131*, 12650–12656.
- [59] Hayer-Hartl, M.; Schägger, H.; von Jagow, G.; Beyer, K. *Eur. J. Biochem.* **1992**, *209*, 423–430.
- [60] Brown, D. A.; London, E. *Annu. Rev. Cell Dev. Biol.* **1998**, *14*, 111–136.
- [61] Fyfe, P. K.; McAuley, K. E.; Roszak, A. W.; Isaacs, N. W.; Cogdell, R. J.; Jones, M. R. *Trends Biochem. Sci.* **2001**, *26*, 106–112.
- [62] Palsdottir, H.; Hunte, C. *Biochim. Biophys. Acta* **2004**, *1666*, 2–18.
- [63] Guixà-González, R.; Javanainen, M.; Gómez-Soler, M.; Cordobilla, B. n.; Domingo, J. C.; Sanz, F.; Pastor, M.; Ciruela, F.; Martinez-Seara, H.; Selent, J. *Sci. Rep.* **1991**, *173*, 2026–2034.

Bibliography

- [64] Marius, P.; de Planque, M. R.; Williamson, P. T. *Biochim. Biophys. Acta* **2012**, *1818*, 90–96.
- [65] Lee, A. G. *Biochim. Biophys. Acta* **2004**, *1666*, 62–87.
- [66] Hunte, C.; Richers, S. *Curr. Opin. Struct. Biol.* **2008**, *18*, 406–411.
- [67] Lee, A. G. *Trends Biochem. Sci.* **2011**, *36*, 493–500.
- [68] Hedger, G.; Sansom, M. S. *Biochim. Biophys. Acta* **2016**.
- [69] Contreras, F.-X.; Ernst, A. M.; Wieland, F.; Brügger, B. *Cold Spring Harb. Perspect. Biol.* **2011**, *3*.
- [70] Paila, Y. D.; Tiwari, S.; Chattopadhyay, A. *Biochim. Biophys. Acta* **2009**, *1788*, 295–302.
- [71] Lensink, M. F.; Govaerts, C.; Ruyschaert, J.-M. *J. Biol. Chem.* **2010**, *285*, 10519–10526.
- [72] Laganowsky, A.; Reading, E.; Allison, T. M.; Ulmschneider, M. B.; Degiacomi, M. T.; Baldwin, A. J.; Robinson, C. V. *Nature* **2014**, *510*, 172–175.
- [73] Qin, L.; Hiser, C.; Mulichak, A.; Garavito, R. M.; Ferguson-Miller, S. *Proc. Natl. Acad. Sci.* **2006**, *103*, 16117–16122.
- [74] Hanson, M. A.; Cherezov, V.; Griffith, M. T.; Roth, C. B.; Jaakola, V.-P.; Chien, E. Y.; Velasquez, J.; Kuhn, P.; Stevens, R. C. *Structure* **2008**, *16*, 897–905.
- [75] Killian, J. A. *Biochim. Biophys. Acta* **1998**, *1376*, 401–416.
- [76] Attwood, T. K.; Findlay, J. B. C. *Protein Eng.* **1994**, *7*, 195–203.
- [77] Kolakowski Jr., L. *Receptors Channels* **1994**, *2*, 1–7.
- [78] Fredriksson, R.; Lagerström, M. C.; Lundin, L.-G.; Schiöth, H. B. *Mol. Pharmacol.* **2003**, *63*, 1256–1272.
- [79] Shonberg, J.; Kling, R. C.; Gmeiner, P.; Löber, S. *Bioorg. Med. Chem.* **2015**, *23*, 3880–3906.
- [80] Ji, T. H.; Grossmann, M.; Ji, I. *J. Biol. Chem.* **1998**, *273*, 17299–17302.

- [81] Wettschureck, N.; Offermanns, S. *Physiol. Rev.* **2005**, *85*, 1159–1204.
- [82] McCudden, C. R.; Hains, M. D.; Kimple, R. J.; Siderovski, D. P.; Willard, F. S. *Cell. Mol. Life Sci.* **2005**, *62*, 551–577.
- [83] Dorsam, R. T.; Gutkind, J. S. *Nat. Rev. Cancer* **2007**, *7*, 79–94.
- [84] Bockaert, J.; Fagni, L.; Dumuis, A.; Marin, P. *Pharmacol. Ther.* **2004**, *103*, 203–221.
- [85] Overington, J. P.; Al-Lazikani, B.; Hopkins, A. L. *Nat. Rev. Drug Discov.* **2006**, *5*, 993–996.
- [86] Jarvis, L. *Chem. Eng. News* **2013**, *91*, 15–17.
- [87] Unger, V. M.; Hargrave, P. A.; Baldwin, J. M.; Schertler, G. F. X. *Nature* **1997**, *389*, 203–206.
- [88] Palczewski, K.; Kumasaka, T.; Hori, T.; Behnke, C. A.; Motoshima, H.; Fox, B. A.; Trong, I. L.; Teller, D. C.; Okada, T.; Stenkamp, R. E.; Yamamoto, M.; Miyano, M. *Science* **2000**, *289*, 739–745.
- [89] Okada, T.; Palczewski, K. *Curr. Opin. Struct. Biol.* **2001**, *11*, 420–426.
- [90] Zhou, X. E.; Melcher, K.; Xu, H. E. *Acta Pharmacol. Sin.* **2012**, *33*, 291–299.
- [91] Fotiadis, D.; Jastrzebska, B.; Philippsen, A.; Müller, D. J.; Palczewski, K.; Engel, A. *Curr. Opin. Struct. Biol.* **2006**, *16*, 252–259.
- [92] Jastrzebska, B.; Fotiadis, D.; Jang, G.-F.; Stenkamp, R. E.; Engel, A.; Palczewski, K. *J. Biol. Chem.* **2006**, *281*, 11917–11922.
- [93] Ballesteros, J.; Palczewski, K. *Curr. Opin. Drug Discov. Devel.* **2001**, *4*, 561–574.
- [94] Klabunde, T.; Hessler, G. *ChemBioChem* **2002**, *3*, 928–944.
- [95] Bosch, L.; Iarriccio, L.; Garriga, P. *Curr. Pharm. Des.* **2005**, *11*, 2243–2256.
- [96] Palczewski, K. *Annu. Rev. Biochem.* **2006**, *75*, 743–767.
- [97] Buzhynskyy, N.; Salesse, C.; Scheuring, S. *J. Mol. Recognit.* **2011**, *24*, 483–489.

Bibliography

- [98] Barnes, P. *Life Sci.* **1993**, *52*, 2101–2109.
- [99] Taylor, M. R. G. *Pharmacogenomics J.* **2006**, *7*, 29–37.
- [100] Dixon, R. A. F. et al. *Nature* **1986**, *321*, 75–79.
- [101] Rasmussen, S. G. F.; Choi, H.-J.; Rosenbaum, D. M.; Kobilka, T. S.; Thian, F. S.; Edwards, P. C.; Burghammer, M.; Ratnala, V. R. P.; Sanishvili, R.; Fischetti, R. F.; Schertler, G. F. X.; Weis, W. I.; Kobilka, B. K. *Nature* **2007**, *450*, 383–387.
- [102] Cherezov, V.; Rosenbaum, D. M.; Hanson, M. A.; Rasmussen, S. G. F.; Thian, F. S.; Kobilka, T. S.; Choi, H.-J.; Kuhn, P.; Weis, W. I.; Kobilka, B. K.; Stevens, R. C. *Science* **2007**, *318*, 1258–1265.
- [103] Zocher, M.; Zhang, C.; Rasmussen, S. G. F.; Kobilka, B. K.; Müller, D. J. *Proc. Natl. Acad. Sci.* **2012**, *109*, E3463–E3472.
- [104] Pontier, S. M.; Percherancier, Y.; Galandrin, S.; Breit, A.; Galés, C.; Bouvier, M. *J. Biol. Chem.* **2008**, *283*, 24659–24672.
- [105] Paila, Y. D.; Jindal, E.; Goswami, S. K.; Chattopadhyay, A. *Biochim. Biophys. Acta* **2011**, *1808*, 461–465.
- [106] Ostrom, R. S.; Gregorian, C.; Drenan, R. M.; Xiang, Y.; Regan, J. W.; Insel, P. A. *J. Biol. Chem.* **2001**, *276*, 42063–42069.
- [107] Rybin, V. O.; Xu, X.; Lisanti, M. P.; Steinberg, S. F. *J. Biol. Chem.* **2000**, *275*, 41447–41457.
- [108] Steinberg, S. F. *J. Mol. Cell. Cardiol.* **2004**, *37*, 407–415.
- [109] Simons, K.; Toomre, D. *Nat. Rev. Mol. Cell Biol.* **2000**, *1*, 31–39.
- [110] Rasmussen, S. G. F. et al. *Nature* **2011**, *477*, 549–555.
- [111] Venkatakrisnan, A. J.; Deupi, X.; Lebon, G.; Tate, C. G.; Schertler, G. F.; Babu, M. M. *Nature* **2013**, *494*, 185–194.
- [112] Whorton, M. R.; Bokoch, M. P.; Rasmussen, S. G. F.; Huang, B.; Zare, R. N.; Kobilka, B.; Sunahara, R. K. *Proc. Natl. Acad. Sci.* **2007**, *104*, 7682–7687.

- [113] Cao, T. T.; Brelot, A.; von Zastrow, M. *Mol. Pharmacol.* **2005**, *67*, 288–297.
- [114] Angers, S.; Salahpour, A.; Joly, E.; Hilairret, S.; Chelsky, D.; Dennis, M.; Bouvier, M. *Proc. Natl. Acad. Sci.* **2000**, *97*, 3684–3689.
- [115] Salahpour, A.; Bonin, H.; Bhalla, S.; Petäjä-Repo, U.; M., B. *Biol. Chem.* **2003**, *384*, 117–123.
- [116] Calebiro, D.; Rieken, F.; Wagner, J.; Sungkaworn, T.; Zabel, U.; Borzi, A.; Cocucci, E.; Zürn, A.; Lohse, M. J. *Proc. Natl. Acad. Sci.* **2013**, *110*, 743–748.
- [117] Pucadyil, T. J.; Kalipatnapu, S.; Chattopadhyay, A. *Cell. Mol. Neurobiol.* **2005**, *25*, 553–580.
- [118] Björkhem, I.; Meaney, S. *Arterioscler. Thromb. Vasc. Biol.* **2004**, *24*, 806–815.
- [119] Saxena, R.; Chattopadhyay, A. *Biochim. Biophys. Acta* **2012**, *1818*, 2936–2942.
- [120] Pucadyil, T. J.; Chattopadhyay, A. *Biochim. Biophys. Acta* **2004**, *1663*, 188–200.
- [121] Jafurulla, M.; Chattopadhyay, A. *Curr. Med. Chem.* **2013**, *20*, 47–55.
- [122] Ganguly, S.; Clayton, A. H.; Chattopadhyay, A. *Biophys. J.* **2011**, *100*, 361–368.
- [123] Paila, Y. D.; Kombrabail, M.; Krishnamoorthy, G.; Chattopadhyay, A. *J. Phys. Chem. B* **2011**, *115*, 11439–11447.
- [124] Paila, Y. D.; Tiwari, S.; Sengupta, D.; Chattopadhyay, A. *Mol. BioSyst.* **2011**, *7*, 224–234.
- [125] Sengupta, D.; Chattopadhyay, A. *J. Phys. Chem. B* **2012**, *116*, 12991–12996.
- [126] Prasanna, X.; Sengupta, D.; Chattopadhyay, A. *Sci. Rep.* **2016**, *6*, 31858.
- [127] Jafurulla, M.; Rao, B. D.; Sreedevi, S.; Ruysschaert, J.-M.; Covey, D. F.; Chattopadhyay, A. *Biochim. Biophys. Acta* **2014**, *1838*, 158–163.
- [128] Woolf, P. J.; Linderman, J. J. *Biophys. Chem.* **2003**, *104*, 217–227.
- [129] Lefkowitz, R. J. *Trends Pharmacol. Sci.* **2004**, *25*, 413–422.

Bibliography

- [130] Kniazeff, J.; Prézeau, L.; Rondard, P.; Pin, J.-P.; Goudet, C. *Pharmacol. Ther.* **2011**, *130*, 9–25.
- [131] Zhang, X. C.; Liu, J.; Jiang, D. *Protein Cell* **2014**, *5*, 492–495.
- [132] White, J. H.; Wise, A.; Main, M. J.; Green, A.; Fraser, N. J.; Disney, G. H.; Barnes, A. A.; Emson, P.; Foord, S. M.; Marshall, F. H. *Nature* **1998**, *396*, 679–682.
- [133] Xue, L.; Rovira, X.; Scholler, P.; Zhao, H.; Liu, J.; Pin, J.-P.; Rondard, P. *Nat. Chem. Biol.* **2015**, *11*, 134–140.
- [134] Herrick-Davis, K. *Exp. Brain Res.* **2013**, *230*, 375–386.
- [135] Bayburt, T. H.; Vishnivetskiy, S. A.; McLean, M. A.; Morizumi, T.; Huang, C.-c.; Tesmer, J. J. G.; Ernst, O. P.; Sligar, S. G.; Gurevich, V. V. *J. Biol. Chem.* **2011**, *286*, 1420–1428.
- [136] Kuszak, A. J.; Pitchiaya, S.; Anand, J. P.; Mosberg, H. I.; Walter, N. G.; Sunahara, R. K. *J. Biol. Chem.* **2009**, *284*, 26732–26741.
- [137] Ferrè, S.; Casadó, V.; Devi, L. A.; Filizola, M.; Jockers, R.; Lohse, M. J.; Milligan, G.; Pin, J.-P.; Guitart, X. *Pharmacol. Rev.* **2014**, *66*, 413–434.
- [138] Teitler, M.; Klein, M. T. *Pharmacol. Ther.* **2012**, *133*, 205–217.
- [139] Teitler, M.; Herrick-Davis, K. *Curr. Pharm. Biotechnol.* *15*, 927–937.
- [140] Herrick-Davis, K.; Grinde, E.; Cowan, A.; Mazurkiewicz, J. E. *Mol. Pharmacol.* **2013**, *84*, 630–642.
- [141] Yin, X.; Xu, H.; Hanson, M.; Liu, W. *Curr. Pharm. Biotechnol.* **2014**, *15*, 971–979.
- [142] Liu, W. et al. *Science* **2013**, *342*, 1521–1524.
- [143] Stoddart, L. A.; Kilpatrick, L. E.; Briddon, S. J.; Hill, S. J. *Neuropharmacology* **2015**, *98*, 48–57.
- [144] Kasai, R. S.; Kusumi, A. *Curr. Opin. Cell Biol.* **2014**, *27*, 78–86.

- [145] Franco, R.; Martínez-Pinilla, E.; Lanciego, J. L.; Navarro, G. *Front. Pharmacol.* **2016**, *7*, year.
- [146] Manglik, A.; Kruse, A. C.; Kobilka, T. S.; Thian, F. S.; Mathiesen, J. M.; Sunahara, R. K.; Pardo, L.; Weis, W. I.; Kobilka, B. K.; Granier, S. *Nature* **2012**, *485*, 321–326.
- [147] Huang, J.; Chen, S.; Zhang, J. J.; Huang, X.-Y. *Nat. Struct. Mol. Biol.* **2013**, *20*, 419–425.
- [148] Herrick-Davis, K.; Grinde, E.; Lindsley, T.; Cowan, A.; Mazurkiewicz, J. E. *J. Biol. Chem.* **2012**, *287*, 23604–23614.
- [149] Scarselli, M.; Annibale, P.; McCormick, P. J.; Kolachalam, S.; Aringhieri, S.; Radenovic, A.; Corsini, G. U.; Maggio, R. *FEBS J.* **2016**, *283*, year.
- [150] Limbird, L. E.; De Meyts, P.; Lefkowitz, R. J. *Biochem. Biophys. Res. Comm.* **1975**, *64*, 1160–1168.
- [151] Mattera, R.; Pitts, B. J.; Entman, M. L.; Birnbaumer, L. *J. Biol. Chem.* **1985**, *260*, 7410–21.
- [152] Potter, L. T.; Ballesteros, L. A.; Bichajian, L. H.; Ferrendelli, C. A.; Fisher, A.; Hanchett, H. E.; Zhang, R. *Mol. Pharmacol.* **1991**, *39*, 211–221.
- [153] Albizu, L.; Balestre, M.-N.; Breton, C.; Pin, J.-P.; Manning, M.; Mouillac, B.; Barberis, C.; Durroux, T. *Mol. Pharmacol.* **2006**, *70*, 1783–1791.
- [154] Albizu, L. et al. *Nat. Chem. Biol.* **2010**, *6*, 587–594.
- [155] Conn, P. M.; Rogers, D. C.; Stewart, J. M.; Niedel, J.; Sheffield, T. *Nature* **1982**, *296*, 653–655.
- [156] Venter, J. C.; Horne, P.; Eddy, B.; Greguski, R.; Fraser, C. M. *Mol. Pharmacol.* **1984**, *26*, 196–205.
- [157] Conn, P. M.; Venter, J. C. *Endocrinol.* **1985**, *116*, 1324–1326.
- [158] Nimchinsky, E. A.; Hof, P. R.; Janssen, W. G. M.; Morrison, J. H.; Schmauss, C. *J. Biol. Chem.* **1997**, *272*, 29229–29237.

Bibliography

- [159] Hebert, T. E.; Moffett, S.; Morello, J.-P.; Loisel, T. P.; Bichet, D. G.; Barret, C.; Bouvier, M. *J. Biol. Chem.* **1996**, *271*, 16384–16392.
- [160] Zeng, F.-Y.; Wess, J. *J. Biol. Chem.* **1999**, *274*, 19487–19497.
- [161] Romano, C.; Yang, W.-L.; O'Malley, K. L. *J. Biol. Chem.* **1996**, *271*, 28612–28616.
- [162] Ng, G. Y.; O'Dowd, B. F.; Lee, S. P.; Chung, H. T.; Brann, M. R.; Seeman, P.; George, S. R. *Biochem. Biophys. Res. Comm.* **1996**, *227*, 200–204.
- [163] Bai, M.; Trivedi, S.; Brown, E. M. *J. Biol. Chem.* **1998**, *273*, 23605–23610.
- [164] Bai, M.; Trivedi, S.; Kifor, O.; Quinn, S. J.; Brown, E. M. *Proc. Natl. Acad. Sci.* **1999**, *96*, 2834–2839.
- [165] Monnot, C.; Bihoreau, C.; Conchon, S.; Curnow, K. M.; Corvol, P.; Clauser, E. *J. Biol. Chem.* **1996**, *271*, 1507–1513.
- [166] Maggio, R.; Vogel, Z.; Wess, J. *Proc. Natl. Acad. Sci.* **1993**, *90*, 3103–3107.
- [167] Gouldson, P. R.; Higgs, C.; Smith, R. E.; Dean, M. K.; Gkoutos, G. V.; Reynolds, C. A. *Neuropsychopharmacology* **2000**, *23*, S60–S77.
- [168] Schulz, A.; Grosse, R.; Schultz, G.; Gudermann, T.; Schöneberg, T. *J. Biol. Chem.* **2000**, *275*, 2381–2389.
- [169] Wilson, S.; Wilkinson, G.; Milligan, G. *J. Biol. Chem.* **2005**, *280*, 28663–28674.
- [170] Salahpour, A.; Angers, S.; Mercier, J.-F.; Lagacé, M.; Marullo, S.; Bouvier, M. *J. Biol. Chem.* **2004**, *279*, 33390–33397.
- [171] Dunham, J. H.; Hall, R. A. *Trends Biotechnol.* **2009**, *27*, 541–545.
- [172] Pflieger, K. D. G.; Eidne, K. A. *Biochem. J.* **2005**, *385*, 625–637.
- [173] Alvarez-Curto, E.; Padiani, J.; Milligan, G. *Analytical and Bioanalytical Chemistry* **2010**, *398*, 167–180.
- [174] Kremers, G.-J.; Gilbert, S. G.; Cranfill, P. J.; Davidson, M. W.; Piston, D. W. *J. Cell Sci.* **2011**, *124*, 157–160.

- [175] Overton, M. C.; Blumer, K. J. *Curr. Biol.* **2000**, *10*, 341–344.
- [176] Floyd, D. H.; Geva, A.; Bruinsma, S. P.; Overton, M. C.; Blumer, K. J.; Baranski, T. J. *J. Biol. Chem.* **2003**, *278*, 35354–35361.
- [177] Dinger, M. C.; Bader, J. E.; Kóbor, A. D.; Kretzschmar, A. K.; Beck-Sickinger, A. G. *J. Biol. Chem.* **2003**, *278*, 10562–10571.
- [178] Latif, R.; Graves, P.; Davies, T. F. *J. Biol. Chem.* **2001**, *276*, 45217–45224.
- [179] Kaczor, A.; Selent, J. *Curr. Med. Chem.* **2011**, *18*, 4606–4634.
- [180] Cottet, M.; Faklaris, O.; Falco, A.; Trinquet, E.; Pin, J.-P.; Mouillac, B.; Durroux, T. *Biochem. Soc. Trans.* **2013**, *41*, 148.
- [181] Rocheville, M.; Lange, D. C.; Kumar, U.; Patel, S. C.; Patel, R. C.; Patel, Y. C. *Science* **2000**, *288*, 154–157.
- [182] Rocheville, M.; Lange, D. C.; Kumar, U.; Sasi, R.; Patel, R. C.; Patel, Y. C. *J. Biol. Chem.* **2000**, *275*, 7862–7869.
- [183] Maurel, D.; Comps-Agrar, L.; Brock, C.; Rives, M.-L.; Bourrier, E.; Ayoub, M. A.; Bazin, H.; Tinel, N.; Durroux, T.; Prezeau, L.; Trinquet, E.; Pin, J.-P. *Nat. Meth.* **2008**, *5*, 561–567.
- [184] McVey, M.; Ramsay, D.; Kellett, E.; Rees, S.; Wilson, S.; Pope, A. J.; Milligan, G. *J. Biol. Chem.* **2001**, *276*, 14092–14099.
- [185] Ayoub, M. A.; Couturier, C.; Lucas-Meunier, E.; Angers, S.; Fossier, P.; Bouvier, M.; Jockers, R. *J. Biol. Chem.* **2002**, *277*, 21522–21528.
- [186] Ramsay, D.; Kellett, E.; McVey, M.; Rees, S.; Milligan, G. *Biochem. J.* **2002**, *365*, 429–440.
- [187] Gandia, J.; Galino, J.; Amaral, O. B.; Soriano, A.; Lluís, C.; Franco, R.; Ciruela, F. *FEBS Lett.* **2008**, *582*, 2979–2984.
- [188] Jensen, A. A.; Hansen, J. L.; Sheikh, S. P.; Bräuner-Osborne, H. *Eur. J. Biochem.* **2002**, *269*, 5076–5087.

Bibliography

- [189] Hern, J. A.; Baig, A. H.; Mashanov, G. I.; Birdsall, B.; Corrie, J. E. T.; Lazareno, S.; Molloy, J. E.; Birdsall, N. J. M. *Proc. Natl. Acad. Sci.* **2010**, *107*, 2693–2698.
- [190] Kasai, R. S.; Suzuki, K. G. N.; Prossnitz, E. R.; Koyama-Honda, I.; Nakada, C.; Fujiwara, T. K.; Kusumi, A. *J. Cell Biol.* **2011**, *192*, 463–480.
- [191] Barbeau, A.; Swift, J. L.; Godin, A. G.; Koninck, Y. D.; Wiseman, P. W.; Beaulieu, J.-M. Chapter 1 - Spatial Intensity Distribution Analysis (SpIDA): A New Tool for Receptor Tyrosine Kinase Activation and Transactivation Quantification. In *Receptor-Receptor Interactions*; Conn, P. M., Ed.; Academic Press, 2013; Vol. 117, pp 1–19.
- [192] Ward, R. J.; Padiani, J. D.; Godin, A. G.; Milligan, G. *J. Biol. Chem.* **2015**, *290*, 12844–12857.
- [193] Mazurkiewicz, J. E.; Herrick-Davis, K.; Barroso, M.; Ulloa-Aguirre, A.; Lindau-Shepard, B.; Thomas, R. M.; Dias, J. A. *Biol. Reprod.* **2015**, *92*, 100, 1–12.
- [194] Galbraith, C. G.; Galbraith, J. A. *J. Cell Sci.* **2011**, *124*, 1607–1611.
- [195] Jonas, K. C.; Fanelli, F.; Huhtaniemi, I. T.; Hanyaloglu, A. C. *J. Biol. Chem.* **2015**, *290*, 3875–3892.
- [196] Sydor, A. M.; Czymmek, K. J.; Puchner, E. M.; Mennella, V. *Trends Cell Biol.* **2015**, *25*, 730–748.
- [197] Park, J. H.; Scheerer, P.; Hofmann, K. P.; Choe, H.-W.; Ernst, O. P. *Nature* **2008**, *454*, 183–187.
- [198] Salom, D.; Lodowski, D. T.; Stenkamp, R. E.; Trong, I. L.; Golczak, M.; Jastrzebska, B.; Harris, T.; Ballesteros, J. A.; Palczewski, K. *Proc. Natl. Acad. Sci.* **2006**, *103*, 16123–16128.
- [199] Wu, B.; Chien, E. Y. T.; Mol, C. D.; Fenalti, G.; Liu, W.; Katritch, V.; Abagyan, R.; Brooun, A.; Wells, P.; Bi, F. C.; Hamel, D. J.; Kuhn, P.; Handel, T. M.; Cherezov, V.; Stevens, R. C. *Science* **2010**, *330*, 1066–1071.

- [200] Wu, H.; Wang, C.; Gregory, K. J.; Han, G. W.; Cho, H. P.; Xia, Y.; Niswender, C. M.; Katritch, V.; Meiler, J.; Cherezov, V.; Conn, P. J.; Stevens, R. C. *Science* **2014**, *344*, 58–64.
- [201] Fotiadis, D.; Liang, Y.; Filipek, S.; Saperstein, D. A.; Engel, A.; Palczewski, K. *Nature* **2003**, *421*, 127–128.
- [202] Liang, Y.; Fotiadis, D.; Filipek, S.; Saperstein, D. A.; Palczewski, K.; Engel, A. *J. Biol. Chem.* **2003**, *278*, 21655–21662.
- [203] George, S. R.; Lee, S. P.; Varghese, G.; Zeman, P. R.; Seeman, P.; Ng, G. Y. K.; O’Dowd, B. F. *J. Biol. Chem.* **1998**, *273*, 30244–30248.
- [204] Wang, J.; He, L.; Combs, C. A.; Roderiguez, G.; Norcross, M. A. *Mol. Cancer Ther.* **2006**, *5*, 2474–2483.
- [205] Harikumar, K. G.; Pinon, D. I.; Miller, L. J. *J. Biol. Chem.* **2007**, *282*, 30363–30372.
- [206] Harikumar, K. G.; Ball, A. M.; Sexton, P. M.; Miller, L. J. *Regul. Pept.* **2010**, *164*, 113–119.
- [207] Granier, S.; Terrillon, S.; Pascal, R.; Déméné, H.; Bouvier, M.; Guillon, G.; Mendre, C. *J. Biol. Chem.* **2004**, *279*, 50904–50914.
- [208] Carrillo, J. J.; López-Giménez, J. F.; Milligan, G. *Mol. Pharmacol.* **2004**, *66*, 1123–1137.
- [209] Thévenin, D.; Lazarova, T.; Roberts, M. F.; Robinson, C. R. *Prot. Sci.* **2005**, *14*, 2177–2186.
- [210] Gorinski, N.; Kowalsman, N.; Renner, U.; Wirth, A.; Reinartz, M. T.; Seifert, R.; Zeug, A.; Ponimaskin, E.; Niv, M. Y. *Mol. Pharmacol.* **2012**, *82*, 448–463.
- [211] Guo, W.; Shi, L.; Javitch, J. A. *J. Biol. Chem.* **2003**, *278*, 4385–4388.
- [212] Knepp, A. M.; Periole, X.; Marrink, S.-J.; Sakmar, T. P.; Huber, T. *Biochemistry* **2012**, *51*, 1819–1821.
- [213] Johnston, J. M.; Aburi, M.; Provasi, D.; Bortolato, A.; Urizar, E.; Lambert, N. A.; Javitch, J. A.; Filizola, M. *Biochemistry* **2011**, *50*, 1682–1690.

Bibliography

- [214] Uddin, M. S.; Kim, H.; Deyo, A.; Naider, F.; Becker, J. M. *J. Recept. Signal Transduct. Res.* **2012**, *32*, 65–75.
- [215] Hu, J.; Hu, K.; Liu, T.; Stern, M. K.; Mistry, R.; Challiss, R. A. J.; Costanzi, S.; Wess, J. *J. Biol. Chem.* **2013**, *288*, 34777–34790.
- [216] Schertler, G. F. *Curr. Opin. Struct. Biol.* **2005**, *15*, 408–415.
- [217] Dean, M. K.; Higgs, C.; Smith, R. E.; Bywater, R. P.; Snell, C. R.; Scott, P. D.; Upton, G. J. G.; Howe, T. J.; Reynolds, C. A. *J. Med. Chem.* **2001**, *44*, 4595–4614.
- [218] Fanelli, F. *Mol. Cell. Endocrinol.* **2007**, *260–262*, 59–64.
- [219] Nemoto, W.; Yamanishi, Y.; Limviphuvadh, V.; Saito, A.; Toh, H. *Proteins* **2016**.
- [220] Dror, R. O.; Arlow, D. H.; Maragakis, P.; Mildorf, T. J.; Pan, A. C.; Xu, H.; Borhani, D. W.; Shaw, D. E. *Proc. Natl. Acad. Sci.* **2011**, *108*, 18684–18689.
- [221] Deupi, X. *Nat. Chem.* **2014**, *6*, 7–8.
- [222] Chavent, M.; Duncan, A. L.; Sansom, M. S. *Curr. Opin. Struct. Biol.* **2016**, *40*, 8–16.
- [223] Trzaskowski, B.; Latek, D.; Yuan, S.; Ghoshdastider, U.; Debinski, A.; Filipek, S. *Curr. Med. Chem.* **2012**, *19*, 1090–1109.
- [224] Perilla, J. R.; Goh, B. C.; Cassidy, C. K.; Liu, B.; Bernardi, R. C.; Rudack, T.; Yu, H.; Wu, Z.; Schulten, K. *Curr. Opin. Struct. Biol.* **2015**, *31*, 64–74.
- [225] Dror, R. O.; Dirks, R. M.; Grossman, J.; Xu, H.; Shaw, D. E. *Annu. Rev. Biophys.* **2012**, *41*, 429–452.
- [226] Borhani, D. W.; Shaw, D. E. *J. Comput. Aided Mol. Des.* **2012**, *26*, 15–26.
- [227] van Gunsteren, W.; Weiner, P.; Wilkinson, A. *Computer Simulation of Biomolecular Systems: Theoretical and Experimental Applications*; Computer Simulations of Biomolecular Systems; Springer Netherlands, 2013.
- [228] Harvey, M. J.; Fabritiis, G. D. *Drug Discov. Today* **2012**, *17*, 1059–1062.
- [229] Cordomi, A.; Perez, J. J. *J. Biomol. Struct. Dyn.* **2009**, *27*, 127–147.

- [230] Witt, M.; Ślusarz, M. J.; Ciarkowski, J. *QSAR Comb. Sci.* **2008**, *27*, 684–693.
- [231] Latif, R.; Ali, M. R.; Mezei, M.; Davies, T. F. *Endocrinol.* **2015**, *156*, 488–498.
- [232] Marrink, S. J.; Risselada, H. J.; Yefimov, S.; Tieleman, D. P.; de Vries, A. H. *J. Phys. Chem. B* **2007**, *111*, 7812–7824.
- [233] Periole, X.; Huber, T.; Marrink, S.-J.; Sakmar, T. P. *J. Am. Chem. Soc.* **2007**, *129*, 10126–10132.
- [234] Periole, X.; Knepp, A. M.; Sakmar, T. P.; Marrink, S. J.; Huber, T. *J. Am. Chem. Soc.* **2012**, *134*, 10959–10965.
- [235] Provasi, D.; Boz, M. B.; Johnston, J. M.; Filizola, M. *PLoS Comput. Biol.* **2015**, *11*, 1–21.
- [236] Johnston, J. M.; Wang, H.; Provasi, D.; Filizola, M. *PLoS Comput. Biol.* **2012**, *8*, e1002649.
- [237] Chattopadhyay, A. *Advances in Biology* **2014**, *143023*,.
- [238] Prasanna, X.; Chattopadhyay, A.; Sengupta, D. *Biophys. J.* **2014**, *106*, 1290–1300.
- [239] Prasanna, X.; Chattopadhyay, A.; Sengupta, D. In *Role of Lipid-Mediated Effects in β_2 -Adrenergic Receptor Dimerization*; Chakrabarti, A., Surolia, A., Eds.; Springer International Publishing: Cham, 2015; pp 247–261.
- [240] Mondal, S.; Khelashvili, G.; Weinstein, H. *Biophys. J.* **2014**, *106*, 2305–2316.
- [241] Ritchie, K.; Iino, R.; Fujiwara, T.; Murase, K.; Kusumi, A. *Mol. Membr. Biol.* **2003**, *20*, 13–18.
- [242] Kusumi, A.; Koyama-Honda, I.; Suzuki, K. *Traffic* **2004**, *5*, 213–230.
- [243] Langhorst, M. F.; Solis, G. P.; Hannbeck, S.; Plattner, H.; Stuermer, C. A. *FEBS Lett.* **2007**, *581*, 4697–4703.
- [244] Head, B. P.; Patel, H. H.; Insel, P. A. *Biochim. Biophys. Acta* **2014**, *1838*, 532–545.

Bibliography

- [245] He, J.; Xu, J.; Castleberry, A. M.; Lau, A. G.; Hall, R. A. *Biochem. Biophys. Res. Comm.* **2002**, *297*, 565–572.
- [246] Michineau, S.; Alhenc-Gelas, F.; Rajerison, R. M. *Biochemistry* **2006**, *45*, 2699–2707.
- [247] Zheng, H.; Pearsall, E. A.; Hurst, D. P.; Zhang, Y.; Chu, J.; Zhou, Y.; Reggio, P. H.; Loh, H. H.; Law, P.-Y. *BMC Cell Biol.* **2012**, *13*, 1–18.
- [248] Xu, T.; Ward, R. J.; Padiani, J. D.; Milligan, G. *Biochem. J.* **2011**, *439*, 171–183.
- [249] Margeta-Mitrovic, M.; Jan, Y. N.; Jan, L. Y. *Neuron* **2000**, *27*, 97–106.
- [250] McGraw, D. W.; Mihlbachler, K. A.; Schwarb, M. R.; Rahman, F. F.; Small, K. M.; Almoosa, K. F.; Liggett, S. B. *J. Clin. Invest.* **2006**, *116*, 1400–1409.
- [251] Ciruela, F. et al. *J. Neurosci.* **2006**, *26*, 2080–2087.
- [252] Zhu, W.-Z.; Chakir, K.; Zhang, S.; Yang, D.; Lavoie, C.; Bouvier, M.; Hébert, T. E.; Lakatta, E. G.; Cheng, H.; Xiao, R.-P. *Circ. Res.* **2005**, *97*, 244–251.
- [253] Zhao, G. Q.; Zhang, Y.; Hoon, M. A.; Chandrashekar, J.; Erlenbach, I.; Ryba, N. J.; Zuker, C. S. *Cell* **2003**, *115*, 255–266.
- [254] Banéres, J.-L.; Parello, J. *J. Mol. Biol.* **2003**, *329*, 815–829.
- [255] Whorton, M. R.; Jastrzebska, B.; Park, P. S.-H.; Fotiadis, D.; Engel, A.; Palczewski, K.; Sunahara, R. K. *J. Biol. Chem.* **2008**, *283*, 4387–4394.
- [256] Arcemishéhère, L. et al. *J. Biol. Chem.* **2010**, *285*, 6337–6347.
- [257] El Moustaine, D.; Granier, S.; Doumazane, E.; Scholler, P.; Rahmeh, R.; Bron, P.; Mouillac, B.; Banéres, J.-L.; Rondard, P.; Pin, J.-P. *Proc. Natl. Acad. Sci.* **2012**, *109*, 16342–16347.
- [258] Han, Y.; Moreira, I. S.; Urizar, E.; Weinstein, H.; Javitch, J. A. *Nat. Chem. Biol.* **2009**, *5*, 688–695.
- [259] Pascal, G.; Milligan, G. *Mol. Pharmacol.* **2005**, *68*, 905–915.

- [260] Colley, N. J.; Cassill, J. A.; Baker, E. K.; Zuker, C. S. *Proc. Natl. Acad. Sci.* **1995**, *92*, 3070–3074.
- [261] Rajan, R. S.; Kopito, R. R. *J. Biol. Chem.* **2005**, *280*, 1284–1291.
- [262] Szidonya, L.; Cserző, M.; Hunyady, L. *J. Endocrinol.* **2008**, *196*, 435–453.
- [263] Johnston, J. M.; Filizola, M. In *Beyond Standard Molecular Dynamics: Investigating the Molecular Mechanisms of G Protein-Coupled Receptors with Enhanced Molecular Dynamics Methods*; Filizola, M., Ed.; Springer Netherlands: Dordrecht, 2014; pp 95–125.
- [264] Sadiq, S.; Guixa-Gonzalez, R.; Dainese, E.; Pastor, M.; Fabritiis, G. D.; Selent, J. *Curr. Med. Chem.* **2013**, *20*, 22–38.
- [265] Zhang, D.; Zhao, Q.; Wu, B. *Mol. Cells* **2015**, *38*, 836–842.
- [266] Schäfer, L. V.; de Jong, D. H.; Holt, A.; Rzepiela, A. J.; de Vries, A. H.; Poolman, B.; Killian, J. A.; Marrink, S. J. *Proc. Natl. Acad. Sci.* **2011**, *108*, 1343–1348.
- [267] Bennett, W. D.; Tieleman, D. P. *Biochim. Biophys. Acta* **2013**, *1828*, 1765–1776.
- [268] de Jong, D. H.; Lopez, C. A.; Marrink, S. J. *Faraday Discuss.* **2013**, *161*, 347–363.
- [269] Ingólfsson, H. I.; Melo, M. N.; van Eerden, F. J.; Arnarez, C.; Lopez, C. A.; Wassenaar, T. A.; Periole, X.; de Vries, A. H.; Tieleman, D. P.; Marrink, S. J. *J. Am. Chem. Soc.* **2014**, *136*, 14554–14559.
- [270] Smirnova, Y. G.; Aeffner, S.; Risselada, H. J.; Salditt, T.; Marrink, S. J.; Muller, M.; Knecht, V. *Soft Matter* **2013**, *9*, 10705–10718.
- [271] Baoukina, S.; Marrink, S.; Tieleman, D. *Biophys. J.* **2012**, *102*, 1866–1871.
- [272] Arnarez, C.; Uusitalo, J. J.; Masman, M. F.; Ingólfsson, H. I.; de Jong, D. H.; Melo, M. N.; Periole, X.; de Vries, A. H.; Marrink, S. J. *J. Chem. Theor. Comput.* **2015**, *11*, 260–275.
- [273] Koldsø, H.; Shorthouse, D.; Hélie, J.; Sansom, M. S. P. *PLoS Comput. Biol.* **2014**, *10*, 1–11.
- [274] Risselada, H. J.; Marrink, S. J. *Proc. Natl. Acad. Sci.* **2008**, *105*, 17367–17372.

Bibliography

- [275] Ollila, O. H. S.; Risselada, H. J.; Louhivuori, M.; Lindahl, E.; Vattulainen, I.; Marrink, S. J. *Phys. Rev. Lett.* **2009**, *102*, 078101.
- [276] Schäfer, L. V.; Marrink, S. J. *Biophys. J.* **2010**, *99*, L91–L93.
- [277] Daily, M. D.; Olsen, B. N.; Schlesinger, P. H.; Ory, D. S.; Baker, N. A. *J. Chem. Theory Comput.* **2014**, *10*, 2137–2150.
- [278] González, M. *JDN* **2011**, *12*, 169–200.
- [279] Leach, A. *Molecular Modelling: Principles and Applications*; Pearson Education; Prentice Hall, 2001.
- [280] Marrink, S. J.; Tieleman, D. P. *Chem. Soc. Rev.* **2013**, *42*, 6801–6822.
- [281] Marrink, S. J.; Mark, A. E. *J. Am. Chem. Soc.* **2003**, *125*, 15233–15242.
- [282] Marrink, S. J.; Mark, A. E. *J. Am. Chem. Soc.* **2003**, *125*, 11144–11145.
- [283] Monticelli, L.; Kandasamy, S. K.; Periole, X.; Larson, R. G.; Tieleman, D. P.; Marrink, S.-J. *J. Chem. Theor. Comput.* **2008**, *4*, 819–834.
- [284] Melo, M. N.; Ingólfsson, H. I.; Marrink, S. J. *J. Chem. Phys.* **2015**, *143*, 243152.
- [285] Yesylevskyy, S. O.; Schäfer, L. V.; Sengupta, D.; Marrink, S. J. *PLoS Comput. Biol.* **2010**, *6*, 1–17.
- [286] Uusitalo, J. J.; Ingólfsson, H. I.; Akhshi, P.; Tieleman, D. P.; Marrink, S. J. *J. Chem. Theor. Comput.* **2015**, *11*, 3932–3945.
- [287] López, C. A.; Sovova, Z.; van Eerden, F. J.; de Vries, A. H.; Marrink, S. J. *J. Chem. Theor. Comput.* **2013**, *9*, 1694–1708.
- [288] Bulacu, M.; Périole, X.; Marrink, S. J. *Biomacromolecules* **2012**, *13*, 196–205.
- [289] López, C. A.; Rzepiela, A. J.; de Vries, A. H.; Dijkhuizen, L.; Hünenberger, P. H.; Marrink, S. J. *J. Chem. Theor. Comput.* **2009**, *5*, 3195–3210.
- [290] Lee, H.; de Vries, A. H.; Marrink, S.-J.; Pastor, R. W. *J. Phys. Chem. B* **2009**, *113*, 13186–13194.

- [291] Gobbo, C.; Beurroies, I.; de Ridder, D.; Eelkema, R.; Marrink, S. J.; De Feyter, S.; van Esch, J. H.; de Vries, A. H. *J. Phys. Chem. C* **2013**, *117*, 15623–15631.
- [292] Panizon, E.; Bochicchio, D.; Monticelli, L.; Rossi, G. *J. Phys. Chem. B* **2015**, *119*, 8209–8216.
- [293] Tozzini, V.; McCammon, J. A. *Chem. Phys. Lett.* **2005**, *413*, 123–128.
- [294] Bayramoglu, B.; Faller, R. *Macromolecules* **2012**, *45*, 9205–9219.
- [295] Marrink, S. J.; de Vries, A. H.; Mark, A. E. *J. Phys. Chem. B* **2004**, *108*, 750–760.
- [296] Davies, K. M.; Anselmi, C.; Wittig, I.; Faraldo-Gómez, J. D.; Kühlbrandt, W. *Proc. Natl. Acad. Sci.* **2012**, *109*, 13602–13607.
- [297] Fritz, D.; Koschke, K.; Harmandaris, V. A.; van der Vegt, N. F. A.; Kremer, K. *Phys. Chem. Chem. Phys.* **2011**, *13*, 10412–10420.
- [298] Baron, R.; Trzesniak, D.; de Vries, A. H.; Elsener, A.; Marrink, S. J.; van Gunsteren, W. F. *Chem. Phys. Chem.* **2007**, *8*, 452–461.
- [299] Hadley, K. R.; McCabe, C. *Mol. Simul.* **2012**, *38*, 671–681.
- [300] Pucadyil, T. J.; Chattopadhyay, A. *Biochim. Biophys. Acta* **2007**, *1768*, 655 – 668.
- [301] Paila, Y. D.; Chattopadhyay, A. *Glycoconj. J.* **2008**, *26*, 711–720.
- [302] Liu, W.; Chun, E.; Thompson, A. A.; Chubukov, P.; Xu, F.; Katritch, V.; Han, G. W.; Roth, C. B.; Heitman, L. H.; IJzerman, A. P.; Cherezov, V.; Stevens, R. C. *Science* **2012**, *337*, 232–236.
- [303] Warne, T.; Moukhametzianov, R.; Baker, J. G.; Nehme, R.; Edwards, P. C.; Leslie, A. G. W.; Schertler, G. F. X.; Tate, C. G. *Nature* **2011**, *469*, 241–244.
- [304] Lee, J. Y.; Lyman, E. *J. Am. Chem. Soc.* **2012**, *134*, 16512–16515.
- [305] Cang, X.; Du, Y.; Mao, Y.; Wang, Y.; Yang, H.; Jiang, H. *J. Phys. Chem. B* **2013**, *117*, 1085–1094.

Bibliography

- [306] Ferro, A.; Coash, M.; Yamamoto, T.; Rob, J.; Ji, Y.; Queen, L. *Br. J. Pharmacol.* **2004**, *143*, 397–403.
- [307] Milano, C.; Allen, L.; Rockman, H.; Dolber, P.; McMinn, T.; Chien, K.; Johnson, T.; Bond, R.; Lefkowitz, R. *Science* **1994**, *264*, 582–586.
- [308] Liggett, S. B. *J. Allergy Clin. Immunol.* **2000**, *105*, S487–S492.
- [309] Sengupta, D.; Marrink, S. J. *Phys. Chem. Chem. Phys.* **2010**, *12*, 12987–12996.
- [310] Prasanna, X.; Praveen, P. J.; Sengupta, D. *Phys. Chem. Chem. Phys.* **2013**, *15*, 19031–19041.
- [311] Sengupta, D.; Rampioni, A.; Marrink, S.-J. *Mol. Membr. Biol.* **2009**, *26*, 422–434.
- [312] Sengupta, D. *J. Phys. Chem. B* **2012**, *116*, 14556–14564.
- [313] Arnold, K.; Bordoli, L.; Kopp, J.; Schwede, T. *Bioinformatics* **2006**, *22*, 195–201.
- [314] Van Der Spoel, D.; Lindahl, E.; Hess, B.; Groenhof, G.; Mark, A. E.; Berendsen, H. J. C. *J. Computat. Chem.* **2005**, *26*, 1701–1718.
- [315] Berendsen, H. J. C.; Postma, J. P. M.; van Gunsteren, W. F.; DiNola, A.; Haak, J. R. *J. Chem. Phys.* **1984**, *81*, 3684–3690.
- [316] Humphrey, W.; Dalke, A.; Schulten, K. *J. Mol. Graph.* **1996**, *14*, 33–38.
- [317] Saxena, R.; Chattopadhyay, A. *J. Neurochem.* **2011**, *116*, 726–733.
- [318] Lindahl, E.; Sansom, M. S. *Curr. Opin. Struct. Biol.* **2008**, *18*, 425–431.
- [319] Klepeis, J. L.; Lindorff-Larsen, K.; Dror, R. O.; Shaw, D. E. *Curr. Opin. Struct. Biol.* **2009**, *19*, 120–127.
- [320] Khalili-Araghi, F.; Gumbart, J.; Wen, P.-C.; Sotomayor, M.; Tajkhorshid, E.; Schulten, K. *Curr. Opin. Struct. Biol.* **2009**, *19*, 128–137.
- [321] Risselada, H. J.; Grubmüller, H. *Curr. Opin. Struct. Biol.* **2012**, *22*, 187–196.
- [322] Lemmin, T.; Soto, C. S.; Clinthorne, G.; DeGrado, W. F.; Dal Peraro, M. *PLoS Comput. Biol.* **2013**, *9*, 1–11.

- [323] Skjaerven, L.; Grant, B.; Muga, A.; Teigen, K.; McCammon, J. A.; Reuter, N.; Martinez, A. *PLoS Comput. Biol.* **2011**, *7*, 1–14.
- [324] Larsson, D. S. D.; Liljas, L.; van der Spoel, D. *PLoS Comput. Biol.* **2012**, *8*, 1–8.
- [325] Olausson, B. E. S.; Grossfield, A.; Pitman, M. C.; Brown, M. F.; Feller, S. E.; Vogel, A. *J. Am. Chem. Soc.* **2012**, *134*, 4324–4331.
- [326] Arkhipov, A.; Shan, Y.; Das, R.; Endres, N.; Eastwood, M.; Wemmer, D.; Kuriyan, J.; Shaw, D. *Cell* **2013**, *152*, 557–569.
- [327] Shan, Y.; Eastwood, M.; Zhang, X.; Kim, E.; Arkhipov, A.; Dror, R.; Jumper, J.; Kuriyan, J.; Shaw, D. *Cell* **2012**, *149*, 860–870.
- [328] Baaden, M.; Marrink, S. J. *Curr. Opin. Struct. Biol.* **2013**, *23*, 878–886.
- [329] Mim, C.; Cui, H.; Gawronski-Salerno, J.; Frost, A.; Lyman, E.; Voth, G.; Unger, V. *Cell* **2012**, *149*, 137–145.
- [330] Hall, B. A.; Armitage, J. P.; Sansom, M. S. P. *PLoS Comput. Biol.* **2012**, *8*, 1–9.
- [331] Wei, P.; Zheng, B.-K.; Guo, P.-R.; Kawakami, T.; Luo, S.-Z. *Biophys. J.* **2013**, *104*, 1435–1444.
- [332] Chng, C.-P.; Tan, S.-M. *Proteins* **2011**, *79*, 2203–2213.
- [333] Janosi, L.; Li, Z.; Hancock, J. F.; Gorfe, A. A. *Proc. Natl. Acad. Sci.* **2012**, *109*, 8097–8102.
- [334] Mondal, S.; Johnston, J. M.; Wang, H.; Khelashvili, G.; Filizola, M.; Weinstein, H. *Sci. Rep.* **2013**, *3*, 2909.
- [335] Van Gunsteren, W. F.; Daura, X.; Mark, A. E. *Helv. Chim. Acta* **2002**, *85*, 3113–3129.
- [336] Park, S.; Im, W. *J. Chem. Theor. Comput.* **2013**, *9*, 13–17.
- [337] Park, S.; Kim, T.; Im, W. *Phys. Rev. Lett.* **2012**, *108*, 108102.
- [338] Li, P.-C.; Miyashita, N.; Im, W.; Ishido, S.; Sugita, Y. *J. Comput. Chem.* **2014**, *35*, 300–308.

Bibliography

- [339] Neale, C.; Madill, C.; Rauscher, S.; Pomés, R. *J. Chem. Theor. Comput.* **2013**, *9*, 3686–3703.
- [340] Kopelevich, D. I. *J. Chem. Phys.* **2013**, *139*, 134906.
- [341] Jämbeck, J. P. M.; Lyubartsev, A. P. *J. Phys. Chem. Lett.* **2013**, *4*, 1781–1787.
- [342] Fung, J. J.; Deupi, X.; Pardo, L.; Yao, X. J.; Velez-Ruiz, G. A.; DeVree, B. T.; Sunahara, R. K.; Kobilka, B. K. *EMBO J.* **2009**, *28*, 3315–3328.
- [343] Deupi, X.; Kobilka, B. K. *Physiology* **2010**, *25*, 293–303.
- [344] Unal, H.; Karnik, S. S. *Trends in Pharmacological Sciences* **2012**, *33*, 79–88.
- [345] Khelashvili, G.; Albornoz, P. B. C.; Johnner, N.; Mondal, S.; Caffrey, M.; Weinstein, H. *J. Am. Chem. Soc.* **2012**, *134*, 15858–15868.
- [346] Jafurulla, M.; Tiwari, S.; Chattopadhyay, A. *Biochem. Biophys. Research Commun.* **2011**, *404*, 569–573.
- [347] Milligan, G. *Curr. Opin. Pharmacol.* **2010**, *10*, 23–29.
- [348] Martin, M.; Dotti, C. G.; Ledesma, M. D. *Biochim. Biophys. Acta* **2010**, *1801*, 934–944.
- [349] Stranahan, A. M.; Cutler, R. G.; Button, C.; Telljohann, R.; Mattson, M. P. *J. Neurochem.* **2011**, *118*, 611–615.
- [350] Alemany, R.; Perona, J. S.; Sánchez-Dominguez, J. M.; Montero, E.; Cañizares, J.; Bresnani, R.; Escribá, P. V.; Ruiz-Gutierrez, V. *Biochim. Biophys. Acta* **2007**, *1768*, 964–975.
- [351] Chattopadhyay, A.; Paila, Y. D. *Biochem. Biophys. Res. Commun.* **2007**, *354*, 627–633.
- [352] Grossfield, A.; Feller, S. E.; Pitman, M. C. *Proc. Natl. Acad. Sci. USA* **2006**, *103*, 4888–4893.
- [353] Grossfield, A.; Pitman, M. C.; Feller, S. E.; Soubias, O.; Gawrisch, K. *J. Mol. Biol.* **2008**, *381*, 478–486.
- [354] Dror, R. O.; Arlow, D. H.; Borhani, D. W.; Jensen, M. O.; Piana, S.; Shaw, D. E. *Proc. Natl. Acad. Sci.* **2009**, *106*, 4689–4694.

- [355] Lyman, E.; Higgs, C.; Kim, B.; Lupyan, D.; Shelley, J. C.; Farid, R.; Voth, G. A. *Structure* **2009**, *17*, 1660–1668.
- [356] Nezil, F. A.; Bloom, M. *Biophys. J.* **1992**, *61*, 1176.
- [357] Castillo, N.; Monticelli, L.; Barnoud, J.; Tieleman, D. P. *Chem. Phys. Lip.* **2013**, *169*, 95–105.
- [358] Botelho, A. V.; Huber, T.; Sakmar, T. P.; Brown, M. F. *Biophys. J.* **2006**, *91*, 4464–4477.
- [359] Alves, I. D.; Salamon, Z.; Hraby, V. J.; Tollin, G. *Biochemistry* **2005**, *44*, 9168–9178.
- [360] Wang, C. et al. *Science* **2013**, *340*, 610–614.
- [361] Nygaard, R. et al. *Cell* **2013**, *152*, 532–542.
- [362] Perez-Aguilar, J. M.; Shan, J.; LeVine, M. V.; Khelashvili, G.; Weinstein, H. *J. Am. Chem. Soc.* **2014**, *136*, 16044–16054.
- [363] Provasi, D.; Artacho, M. C.; Negri, A.; Mobarec, J. C.; Filizola, M. *PLoS Comput. Biol.* **2011**, *7*, 1–11.
- [364] Kohlhoff, K. J.; Shukla, D.; Lawrenz, M.; Bowman, G. R.; Konerding, D. E.; Belov, D.; Altman, R. B.; Pande, V. S. *Nat. Chem.* **2014**, *6*, 15–21.
- [365] Schmidt, P.; Thomas, L.; Müller, P.; Scheidt, H. A.; Huster, D. *Chemistry* **2014**, *20*, 4986–4992.
- [366] Manglik, A.; Kim, T.; Masureel, M.; Altenbach, C.; Yang, Z.; Hilger, D.; Lerch, M.; Kobilka, T.; Thian, F.; Hubbell, W.; Prosser, R.; Kobilka, B. *Cell* **2015**, *161*, 1101–1111.
- [367] Chakraborty, H.; Chattopadhyay, A. *ACS Chem. Neurosci.* **2015**, *6*, 199–206.
- [368] Goddard, A. D.; Watts, A. *Biophys. Rev.* **2012**, *4*, 291–298.
- [369] Harding, P. J.; Attrill, H.; Boehringer, J.; Ross, S.; Wadhams, G. H.; Smith, E.; Armitage, J. P.; Watts, A. *Biophys. J.* **2009**, *96*, 964 – 973.
- [370] Ganguly, S.; Pucadyil, T. J.; Chattopadhyay, A. *Biophys. J.* **2008**, *95*, 451–463.
- [371] Bellot, M. et al. *Nat. Chem. Biol.* **2015**, *11*, 271–279.

Bibliography

- [372] Dix, A. V.; Moss, S. M.; Phan, K.; Hoppe, T.; Paoletta, S.; Kozma, E.; Gao, Z.-G.; Durell, S. R.; Jacobson, K. A.; Appella, D. H. *J. Am. Chem. Soc.* **2014**, *136*, 12296–12303.
- [373] Mancia, F.; Assur, Z.; Herman, A. G.; Siegel, R.; Hendrickson, W. A. *EMBO rep.* **2008**, *9*, 363–369.
- [374] Müller, C. P.; Carey, R. J.; Huston, J. P.; Silva, M. A. D. S. *Prog. Neurobiol* **2007**, *81*, 133–178.
- [375] Samuels, B. A.; Mendez-David, I.; Faye, C.; David, S. A.; Pierz, K. A.; Gardier, A. M.; Hen, R.; David, D. J. *Neuroscientist* **2014**, *22*, 26–45.
- [376] Fiorino, F.; Severino, B.; Magli, E.; Ciano, A.; Caliendo, G.; Santagada, V.; Frecen-tese, F.; Perissutti, E. *J. Med. Chem.* **2014**, *57*, 4407–4426.
- [377] Sengupta, D.; Chattopadhyay, A. *Biochim. Biophys. Acta* **2015**, *1848*, 1775–1782.
- [378] Soubias, O.; Teague, W. J.; Hines, K.; Gawrisch, K. *Biophys. J.* **2015**, *108*, 1125–1132.
- [379] Patra, S. M.; Chakraborty, S.; Shahane, G.; Prasanna, X.; Sengupta, D.; Maiti, P. K.; Chattopadhyay, A. *Mol. Membr. Biol.* **2015**, *32*, 127–137.
- [380] Khelashvili, G.; Grossfield, A.; Feller, S. E.; Pitman, M. C.; Weinstein, H. *Proteins* **2009**, *76*, 403–417.
- [381] Shan, J.; Khelashvili, G.; Mondal, S.; Mehler, E. L.; Weinstein, H. *PLoS Comput Biol* **2012**, *8*, 1–15.
- [382] Horn, J. N.; Kao, T.-C.; Grossfield, A. In *Coarse-Grained Molecular Dynamics Provides Insight into the Interactions of Lipids and Cholesterol with Rhodopsin*; Filizola, M., Ed.; Springer Netherlands, 2014; pp 75–94.
- [383] Gater, D.; Saurel, O.; Iordanov, I.; Liu, W.; Cherezov, V.; Milon, A. *Biophys. J.* **2014**, *107*, 2305–2312.
- [384] Oates, J.; Faust, B.; Attrill, H.; Harding, P.; Orwick, M.; Watts, A. *Biochim. Biophys. Acta* **2012**, *1818*, 2228–2233.

- [385] Herrick-Davis, K.; Weaver, B. A.; Grinde, E.; Mazurkiewicz, J. E. *J. Biol. Chem.* **2006**, *281*, 27109–27116.
- [386] Herrick-Davis, K.; Grinde, E.; Lindsley, T.; Teitler, M.; Mancina, F.; Cowan, A.; Mazurkiewicz, J. E. *Mol. Pharmacol.* **2015**, *87*, 660–673.
- [387] Smiljanic, K.; Vanmierlo, T.; Djordjevic, A. M.; Perovic, M.; Loncarevic-Vasiljkovic, N.; Tesic, V.; Rakic, L.; Ruzdijic, S.; Lutjohann, D.; Kanazir, S. *Lipids* **2013**, *48*, 1069–1077.
- [388] Martí-Solano, M.; Schmidt, D.; Kolb, P.; Selent, J. *Drug Discov. Today* **2016**, *21*, 625–631.
- [389] Breitwieser, G. E. *Circ. Res.* **2004**, *94*, 17–27.
- [390] Hofsäß, C.; Lindahl, E.; Edholm, O. *Biophys. J.* **2003**, *84*, 2192–2206.
- [391] Pan, J.; Tristram-Nagle, S.; Nagle, J. F. *Phys. Rev. E* **2009**, *80*, 021931.
- [392] Vance, J. E. *Dis. Model Mech.* **2012**, *5*, 746–755.
- [393] Fantini, J.; Yah, N. *Brain Lipids in Synaptic Function and Neurological Disease: Clues to Innovative Therapeutic Strategies for Brain Disorders*; Elsevier Science, 2015.
- [394] Singh, P.; Paila, Y. D.; Chattopadhyay, A. *J. Neurochem.* **2012**, *123*, 716–724.
- [395] Jafurulla, M.; Chattopadhyay, A. *Eur. J. Pharmacol.* **2015**, *763, Part B*, 241–246.
- [396] Holthuis, J. C. M.; Pomorski, T.; Riggers, R. J.; Sprong, H.; Van Meer, G. *Physiol. Rev.* **2001**, *81*, 1689–1723.
- [397] Masserini, M.; Ravasi, D. *Biochim. Biophys. Acta* **2001**, *1532*, 149–161.
- [398] Slotte, J. P. *Prog. Lipid Res.* **2013**, *52*, 424–437.
- [399] Sjögren, B.; Svenningsson, P. *Acta Physiol.* **2007**, *190*, 47–53.
- [400] Mahfoud, R.; Garmy, N.; Maresca, M.; Yah, N.; Puigserver, A.; Fantini, J. *J. Biol. Chem.* **2002**, *277*, 11292–11296.
- [401] Fantini, J. *Cell. Mol. Life Sci.* **2003**, *60*, 1027–1032.

Bibliography

- [402] Fantini, J.; Barrantes, F. J. *Biochim. Biophys. Acta* **2009**, *1788*, 2345–2361.
- [403] Chattopadhyay, A.; Paila, Y. D.; Shrivastava, S.; Tiwari, S.; Singh, P.; Fantini, J. In *Sphingolipid-Binding Domain in the Serotonin_{1A} Receptor*; Sudhakaran, R. P., Suro-
lia, A., Eds.; Springer, New York, 2012; pp 279–293.
- [404] Bussi, G.; Donadio, D.; Parrinello, M. *J. Chem. Phys.* **2007**, *126*, 014101.
- [405] Hess, B.; Bekker, H.; Berendsen, H. J. C.; Fraaije, J. G. E. M. *J. Comput. Chem.* **1997**,
18, 1463–1472.
- [406] Basu, I.; Mukhopadhyay, C. *Phys. Chem. Chem. Phys.* **2015**, *17*, 17130–17139.
- [407] Epand, R. M. *Prog. Lipid Res.* **2006**, *45*, 279–294.
- [408] Fantini, J.; Barrantes, F. *Front. Physiol.* **2013**, *4*, 31.
- [409] Li, H.; Papadopoulos, V. *Endocrinology* **1998**, *139*, 4991–4997.
- [410] Oddi, S.; Dainese, E.; Fezza, F.; Lanuti, M.; Barcaroli, D.; De Laurenzi, V.; Centonze, D.;
Maccarrone, M. *J. Neurochem.* **2011**, *116*, 858–865.
- [411] Snook, C.; Jones, J.; Hannun, Y. *Biochim. Biophys. Acta* **2006**, *1761*, 927–946.
- [412] Mutoh, T.; Tokuda, A.; Miyadai, T.; Hamaguchi, M.; Fujiki, N. *Proc. Natl. Acad. Sci.*
1995, *92*, 5087–5091.
- [413] Contreras, F.-X.; Ernst, A. M.; Haberkant, P.; Bjorkholm, P.; Lindahl, E.; Gonen, B.;
Tischer, C.; Elofsson, A.; von Heijne, G.; Thiele, C.; Pepperkok, R.; Wieland, F.; Brug-
ger, B. *Nature* **2012**, *481*, 525–529.
- [414] Renner, U.; Glebov, K.; Lang, T.; Papusheva, E.; Balakrishnan, S.; Keller, B.;
Richter, D. W.; Jahn, R.; Ponimaskin, E. *Mol. Pharmacol.* **2007**, *72*, 502–513.
- [415] Mahfoud, R.; Mylvaganam, M.; Lingwood, C. A.; Fantini, J. *J. Lipid Res.* **2002**, *43*,
1670–1679.
- [416] Ling, H.; Boodhoo, A.; Hazes, B.; Cummings, M. D.; Armstrong, G. D.; Brunton, J. L.;
Read, R. J. *Biochemistry* **1998**, *37*, 1777–1788.

- [417] St. Hilaire, P. M.; Boyd, M. K.; Toone, E. J. *Biochemistry* **1994**, *33*, 14452–14463.
- [418] Chattopadhyay, A.; Rukmini, R.; Mukherjee, S. *Biophys. J.* **1996**, *71*, 1952–1960.
- [419] Jafurulla, M.; Pucadyil, T. J.; Chattopadhyay, A. *Biochim. Biophys. Acta* **2008**, *1778*, 2022–2025.
- [420] Paila, Y. D.; Ganguly, S.; Chattopadhyay, A. *Biochemistry* **2010**, *49*, 2389–2397.
- [421] Singh, P.; Chattopadhyay, A. *Biochem. Biophys. Res. Commun.* *419*, 321–325.
- [422] Kolter, T.; Sandhoff, K. *Biochim. Biophys. Acta* **2006**, *1758*, 2057–2079.
- [423] Wu, G.; Lu, Z.-H.; Kulkarni, N.; Amin, R.; Ledeen, R. W. *Neurochem. Res.* **2011**, *36*, 1706–1714.
- [424] Wu, G.; Lu, Z.-H.; Kulkarni, N.; Ledeen, R. W. *J. Neurosci. Res.* **2012**, *90*, 1997–2008.
- [425] Haleem, D. J. *Behav. Pharmacol.* **2015**, *26*, 45–58.
- [426] Wheatley, M.; Wootten, D.; Conner, M.; Simms, J.; Kendrick, R.; Logan, R.; Poyner, D.; Barwell, J. *Br. J. Pharmacol.* **2012**, *165*, 1688–1703.
- [427] Peeters, M. C.; van Westen, G. J. P.; Guo, D.; Wisse, L. E.; Müller, C. E.; Beukers, M. W.; IJzerman, A. P. *FASEB J.* **2011**, *25*, 632–643.
- [428] Hjorth, S. A.; Schambye, H. T.; Greenlee, W. J.; Schwartz, T. W. *J. Biol. Chem.* **1994**, *269*, 30953–30959.
- [429] Lawson, Z.; Wheatley, M. *Biochem. Soc. Trans.* **2004**, *32*, 1048–1050.
- [430] Hawtin, S. R.; Simms, J.; Conner, M.; Lawson, Z.; Parslow, R. A.; Trim, J.; Sheppard, A.; Wheatley, M. *J. Biol. Chem.* **2006**, *281*, 38478–38488.
- [431] Haldar, S.; Raghuraman, H.; Namani, T.; Rajarathnam, K.; Chattopadhyay, A. *Biochim. Biophys. Acta* **2010**, *1798*, 1056–1061.
- [432] Shahane, G.; Parsania, C.; Sengupta, D.; Joshi, M. *PLoS Comput. Biol.* **2014**, *10*, 1–10.

Bibliography

- [433] Hamilton, P. J.; Belovich, A. N.; Khelashvili, G.; Saunders, C.; Erreger, K.; Javitch, J. A.; Sitte, H. H.; Weinstein, H.; Matthies, H. J. G.; Galli, A. *Nat. Chem. Biol.* **2014**, *10*, 582–589.
- [434] Khelashvili, G.; Weinstein, H. *Biochim. Biophys. Acta* **2015**, *1848*, 1765–1774.
- [435] Gimpl, G.; Fahrenholz, F. *Biochim. Biophys. Acta* **2002**, *1564*, 384–392.
- [436] Thompson, A. A.; Liu, J. J.; Chun, E.; Wacker, D.; Wu, H.; Cherezov, V.; Stevens, R. C. *Methods* **2011**, *55*, 310–317.
- [437] Salom, D.; Padayatti, P. S.; Palczewski, K. Crystallization of G Protein-Coupled Receptors. In *Receptor-Receptor Interactions*; Conn, P. M., Ed.; Academic Press, 2013; Vol. 117, pp 451–468.
- [438] Píknová, B.; Pérochon, E.; Tocanne, J.-F. *Eur. J. Biochem.* **1993**, *218*, 385–396.
- [439] Kusumi, A.; Hyde, J. S. *Biochemistry* **1982**, *21*, 5978–5983.
- [440] Sankaram, M. B.; Thompson, T. E. *Biochemistry* **1990**, *29*, 10676–10684.
- [441] Ipsen, J.; Mouritsen, O.; Bloom, M. *Biophys. J.* **1990**, *57*, 405–412.
- [442] Hung, W.-C.; Lee, M.-T.; Chen, F.-Y.; Huang, H. W. *Biophys. J.* **2007**, *92*, 3960–3967.
- [443] Lee, A. *Biochim. Biophys. Acta* **2003**, *1612*, 1–40.
- [444] Han, Y.; Moreira, I. S.; Urizar, E.; Weinstein, H.; Javitch, J. A. *Nat. Chem. Biol.* **2009**, *5*, 688–695.
- [445] Barnett-Norris, J.; Lynch, D.; Reggio, P. H. *Life Sci.* **2005**, *77*, 1625–1639.
- [446] Hiller, C.; Kühhorn, J.; Gmeiner, P. *J. Med. Chem.* **2013**, *56*, 6542–6559.
- [447] Cvejic, S.; Devi, L. A. *J. Biol. Chem.* **1997**, *272*, 26959–26964.
- [448] Kroeger, K. M.; Hanyaloglu, A. C.; Seeber, R. M.; Miles, L. E. C.; Eidne, K. A. *J. Biol. Chem.* **2001**, *276*, 12736–12743.

- [449] Patel, R. C.; Kumar, U.; Lamb, D. C.; Eid, J. S.; Rocheville, M.; Grant, M.; Rani, A.; Hazlett, T.; Patel, S. C.; Gratton, E.; Patel, Y. C. *Proc. Natl. Acad. Sci.* **2002**, *99*, 3294–3299.
- [450] Villar, V. A. M.; Cuevas, S.; Zheng, X.; Jose, P. A. Chapter 1 - Localization and signaling of GPCRs in lipid rafts. In *G Protein-Coupled Receptors Signaling, Trafficking and Regulation*; Shukla, A. K., Ed.; Academic Press, 2016; Vol. 132, pp 3–23.
- [451] Mystek, P.; Dutka, P.; Tworzydło, M.; Dziejzicka-Wasylewska, M.; Polit, A. *Biochim. Biophys. Acta* **2016**, *1861*, 1775–1786.
- [452] Hughes, J.; Rees, S.; Kalindjian, S.; Philpott, K. *Br. J. Pharmacol.* **2011**, *162*, 1239–1249.
- [453] Schonenbach, N. S.; Hussain, S.; O'Malley, M. A. *Wiley Interdiscip. Rev. Nanomed. Nanobiotech.* **2015**, *7*, 408–427.
- [454] Rask-Andersen, M.; Masuram, S.; Schiöth, H. B. *Annu. Rev. Pharmacol. Toxicol.* **2014**, *54*, 9–26.
- [455] Mullard, A. *Nat. Rev. Drug Discov.* **2016**, *15*, 73–76.
- [456] Prezeau, L.; Rives, M.-L.; Comps-Agrar, L.; Maurel, D.; Kniazeff, J.; Pin, J.-P. *Curr. Opin. Pharmacol.* **2010**, *10*, 6–13.
- [457] Ferrè, S. *Trends Pharmacol. Sci.* **2015**, *36*, 145–152.
- [458] Hager, M. H.; Solomon, K. R.; Freeman, M. R. *Curr. Opin. Clin. Nutr. Metab. Care* **2006**, *9*, 379–385.
- [459] Escribá, P. V.; Busquets, X.; Inokuchi, J.-i.; Balogh, G.; Török, Z.; Horváth, I.; Harwood, J. L.; Vígh, L. *Prog. Lipid Res.* **2015**, *59*, 38–53.